The Return of the Queen

Final Report - DSE Fall 2018
Delfi-REAL

Group 4

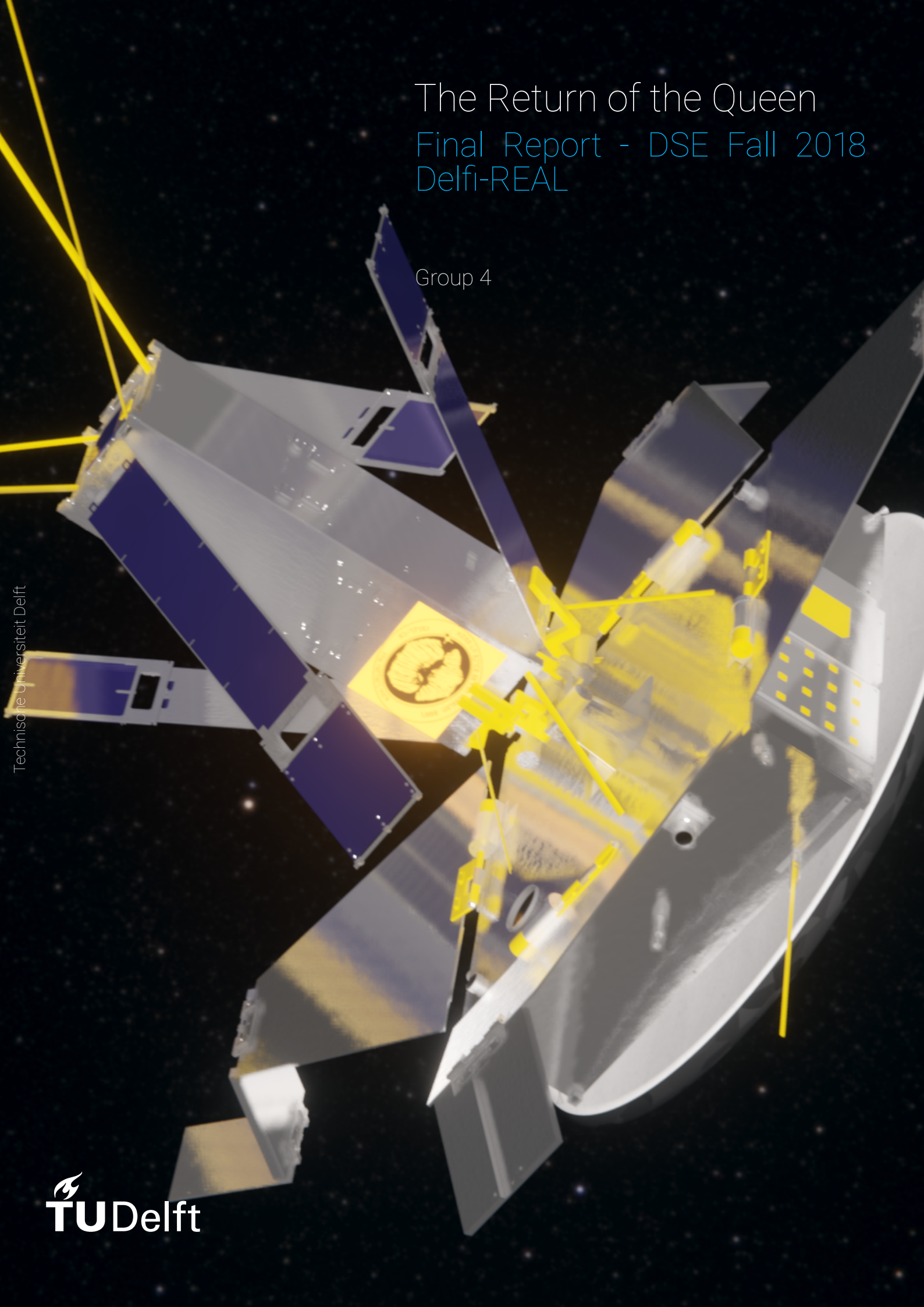

Technische Universiteit Delft

TU Delft

The Return of the Queen

Final Report - DSE Fall 2018 Delfi-REAL

by

Group 4

Bosman, Bastiaan	4430247
Fricano, Tommaso	4281608
Kraijema, Jeroen	4366980
Mikirtumov, Vladimir	4474007
Sachs, Maxim	4236262
Schild, Maarten	4158474
Schutten, Hidde	4283139
Segeren, Megan	4441893
Villé, Thomas	4269039
Vries, Joël de	4222571
Vries, Roelof Jan de	4278933

Design Synthesis Exercise (AE3200)

Project committee:

Dr. ir. C. Verhoeven,	TU Delft tutor
Dr. ir. E. Quaeghebeur,	TU Delft coach
Dr. T. Mahon,	TU Delft coach

January 29, 2019
Version 1.0

TU Delft

Executive Overview

Delfi-C3 is a student-built nano-satellite of the TU Delft which was launched in 2008. The satellite was designed to perform tests on new nano-satellite designs which would last 3 months. The satellite is still operational to this day. Some subsystems have showed signs of degradation in the mean time. The cause of failure cannot be specified with the data being sent down. To find the cause of failure, the "The Return of the Queen" mission was established.

The "The Return of the Queen" mission will attempt to retrieve Delfi-C3 non-destructively from its orbit in order perform further analysis on it. The system for this mission was designed by 11 students in 10 weeks and was given the name Delfi-REAL (Re-Entry And Landing).

Mission Profile

The mission starts with the launch. The system will be launched into a 600 km and 97.5° circular polar orbit with a 35 km and 0.2° accuracy. After this launch, the orbit matching phase starts. Delfi-REAL will burn for 10 seconds to reduce the orbit perigee. This process will repeat itself until the perigee of both satellites match. After perigee matching, the apogees will be matched in the same way. This mission phase will take 46.9 days and a delta-V of $48\,\mathrm{m\,s^{-1}}$. When Delfi-REAL and Delfi-C3 are in the same orbit and only 1 km apart, the observation and capture phase is initiated. During this phase, photos and video of Delfi-C3 will be made, which will be sent down to earth. If the situation is deemed safe, Delfi-REAL will approach to capture Delfi-C3. After capture, the combined system will initiate the return to earth.

First, the orbit altitude will be reduced to 150 km. This takes 103.4 days and a delta-V of $110\,\mathrm{m\,s^{-1}}$. After that, the re-entry phase starts by closing the payload bay doors to protect Delfi-C3 during descent. During re-entry, the heat shield will protect the system from the high temperatures. At 10 km altitude, the drogue chute deploys. At the same time, the heat shield will be dropped to decrease the area and mass. At 5 km from the ground, the main parachute is deployed, ensuring that the touchdown speed does not exceed $7\,\mathrm{m\,s^{-1}}$. The landing site chosen is in Kazakhstan, as more landings occur there so procedures are known and the area is not inhabited. After a safe landing, Delfi-REAL will send a VHF band signal. This way the system can easily be located in the desert. After the system has been located, it will be safely transported to Delft for research.

ADCS

The Attitude Determination and Control Subsystem (ADCS) is used to obtain the rotational knowledge of Delfi-REAL and to control this rotation. The reliability of this subsystem is extremely important as many other subsystems are dependent on it. For attitude determination, a magnetometer is used for a coarse accuracy of 1° and a star tracker is used for a high accuracy of 0.003°. To ensure that the star tracker is not blinded by the sun, a sun sensor is positioned next to the star tracker which has a determination accuracy of 0.1°. The magnetometer is capable of determining the attitude of Delfi-REAL with respect to the Earth. The attitude control subsystem consists of a set of magnetorquers and reaction wheels. The reaction wheels can counteract torques of up to 4.6 mN m with a maximum momentum storage of 60 mN m s. The magnetorquers are used to desaturate (de-spin) the reaction wheels. These are sized to perform full reaction wheel desaturation within the time period of one orbit. The ADCS will be controlled by a space-grade circuit board, which uses minimum power in case of emergencies.

Detection

The detection system uses three different methods for detecting the relative location to Delfi-C3 and its rotation. For rough estimates, the ground tracking data can be used. This is sufficiently accurate up to 1 km. Then, using a phased antenna array radar, both active and passive radar can find the direction and distance of Delfi-C3 up to 200 m. Finally, a zoom camera will be used to visually determine the relative position and rotation of the target. However, light is needed to be able to visually detect Delfi-C3. Therefore manoeuvres close to Delfi-C3 will only be done while in sunlight. This also implies that pictures and observations cannot be taken while Delfi-C3 is between the system and the Sun. It was estimated that an eclipse by Delfi-C3 upon the system is negligible and the batteries will able to bridge the minute power loss for the small amount of time that this situation might occur.

Capture

The capture subsystem is an essential part in the retrieval of Delfi-C3. It is therefore important that it is reliable. To be reliable it is important to have as little moving parts as possible, therefore the system should be simple with a low risk of failure. To capture Delfi-C3 the most optimal design option is to go with a clamp that clamps Delfi-C3 at the bottom on four sides. Two clamp arms first clamp the flat sides of Delfi-C3, after which two other clamp arms fold in the two solar panels that are mounted with a hinge at the bottom of Delfi-C3. The clamp arms are actuated using a stepper motor for each arm to be able to control them individually. The clamp arms are spring loaded to return to their folded position and to apply a clamping force on Delfi-C3. In this way the stepper motors only have to be turned on during the capture manoeuvre. In order to clamp Delfi-C3 before the small antennae of Delfi-C3 hit Delfi-REAL, an extendable arm is needed, which can extend more than 15 cm. This will be a telescopic arm that is spring loaded. The extension is controlled by a stepper motor through a Dyneema rope. During the whole mission, except for the capture phase, the telescopic arm is locked in place with two actuated pins.

Telemetry, Tracking & Communication

The Telemetry, Tracking & Communication (TT&C) subsystem deals with the transmission of status, housekeeping, and science data. Furthermore, the reception of telecommands is part of the subsystem. It is primarily based on the need of a high data rate for the science data. It became apparent that any frequency band below the S-band will not have a bandwidth that is capable of supporting such a high data rate. The health and status data requirements fit within the requirements for science data. The telecommands will be transmitted over a different frequency. This will eliminate the noise created by the simultaneous transmission and reception of data over the same frequency. For the frequency range, it should be noted that the space path loss will increase with increasing frequency. For this reason, the downlink frequency range is chosen to be within the S band range. The uplink frequency range can be both Very High Frequency (VHF) or Ultra High Frequency (UHF). In order to increase the strength of the beacon signal, VHF will be used to transmit when Delfi-REAL has landed. UHF will be used for telecommands.

The components selected for the subsystem are all designed specifically for space. The components for downlink consists of a high data rate transmitter and an S band patch antenna. The components for uplink and the beacon are combined. The VHF/UHF transceiver will be used for receiving telecommands over the UHF frequency range and transmitting after landing over the VHF frequency range. Furthermore, two UHF antennas are included which will be deployed while Delfi-REAL is in orbit. The antenna for the beacon will be the body of Delfi-REAL itself.

A link budget has been created to ensure the subsystem will function properly. The link budget consists of both a downlink and uplink part. The most important items are stated in Table 1. The model is verified with unit tests and is validated using actual satellite data. Finally, the subsystem should be validated during further development.

Table 1: Link budget for Delfi-REAL. Values are based on an orbital altitude of 550 km and an elevation angle of 0°.

Item	**Symbol**	**Unit**	**Downlink**	**Uplink**
Frequency	f	MHz	2450	438
Data Rate	R	$\mathrm{kbit\,s^{-1}}$	3400	9.6
E_b/N_o	E_b/N_o	dB	9.6	38
Margin	-	dB	3.6	24

Command and Data Handling

The Command and Data-Handling System (CDHS) is responsible for the internal command handling; meaning the distribution of tasks and data being sent between different subsystems. It was also determined that this subsystem will compress the data delivered by the payload to reduce its transmission size. To accomplish this, a highly reliable On-Board-Computer OBC will be used, delivered by Innovative Solutions In Space. Furthermore, a dedicated device will be used specifically for video recording, video analysis, and live-streaming applications.

Power

The Electrical Power System (EPS) is composed of solar arrays which are the main source of power for Delfi-REAL. These are located on the payload bay doors that have an area of 1328 $\mathrm{cm^2}$, generate 77.02 W at peak power and 24.70 W average power during one orbit. Provided that the solar arrays are only functional under sunlight, batteries

are required to make the system functional during eclipse. Two lithium-polymer batteries perform this task which provides the EPS sufficient battery capacity as well as redundancy. This stored and collected power is distributed to three different busses of 3.3 V, 5 V and 12 V using direct current via a decentralised approach to the respective components of the spacecraft. This design choice also implies an unregulated bus voltage control.

Thermal Control

The thermal control of Delfi-REAL only consists of passive control. The main body will be protected by anodising the aluminium body panels, which results in a maximum operating temperature of 24.4 °C and a minimum of 11.1 °C. In addition, the payload bay doors, which are holding the solar panels, are thermally insulated from the main body. This is done because the solar cells have a larger operating range than most other subsystems and have a high absorption ratio, which leads to a high temperature. The maximum and minimum operating temperature of the solar arrays are 55.0 °C and −16.4 °C respectively.

Propulsion

The Propulsion System is used to change the orbit of Delfi-REAL and rendezvous with Delfi-C3. After a brief period of taking video footage and images, it will be used to capture Delfi-C3 by matching its rotation and slowly decreasing the distance. This procedure will be done fully autonomous and was validated using a simulation.

A total Delta-V of 236 m s^{-1} is required to complete the mission. Electric thrusters were discarded as they would use too much power and provide insufficient thrust. Since mass and volume were critical parameters, it was decided that only one single type of chemical propellant could be used, as using multiple would require multiple propellant tanks, valves and pipes. Cold gas thrusters did not have a high enough specific impulse and would therefore require too much propellant. Solid fuel thrusters could not provide the required control. Therefore this Delta-V will be provided by a total of nine 100 mN high performance thrusters developed by Bradford Engineering. These thrusters will use a total of 1.05 liter LMS-103S, a non-toxic high density propellant.

As the final de-orbit manoeuvre makes up almost half of the total required Delta-V, the use of passive propulsion systems such as tethers and drag sails were analysed. These systems look promising in possible future iterations but as of now they are not yet developed enough and are too big of a risk during the re-entry phase of the mission.

Re-Entry

The re-entry design can be split up into two interrelated parts, being the flight path and the Thermal Protection System (TPS). The chosen flight path requires an initial angle of −3.5° relative to the horizon. This optimises the relation between the maximum deceleration and the heat loading. With this flight path, maximum deceleration is 8.5 g, ensuring no damage is caused to Delfi-C3 due to compression loading during re-entry. The ablative TPS is designed using a phenolic novolac resin impregnated 3D fine-woven pierced carbon fabric composite. This material is chosen because for this material the most knowledge is publicly available with respect to re-entry applications. The 18.2 mm thick layer of TPS has a blunt shape with a diameter of 500 mm and a curvature radius of 2 m. This design ensures the system is protected from the heat loading, and that the bondline temperature does not exceed 80 °C to prevent overheating of Delfi-REAL and Delfi-C3. The ablative part of the TPS weighs 1.2 kg and the structural support weighs 1.8 kg, which brings the total TPS mass to 3 kg.

Recovery

The recovery subsystem can be split up into two components; the parachute, and the deployment system. Due to the large packing size of a parachute that could handle the the combined weight of Delfi-C3, Delfi-REAL, and the heat shield, it was decided to remove the heat shield after re-entry. In order to decelerate 7 m s^{-1}, it was found that an annular parachute with an area of 4.5 m, and a line length of 3 m was required. Furthermore, a rotafoil pilot chute with area of 0.1 m and line length of 2.7 m are required. The parachutes are deployed at 10 km, and 5 km respectively. In the chosen configuration, the impact speed of Delfi-REAL is 6.7 m s^{-1}. It is chosen to use Nylon for both parachutes, due to its high strength, low mass, and small packing volume. Nylon has also been used for several other space applications. The parachutes are stored in a UV-resistant canister to limit the effects of UV-radiation on the parachute fabric. The deployment system is designed to use a drogue gun which shoots out a slug and the pilot chute. This is activated by an altimeter when the deployment altitude is reached. At 5 km an electrically actuated

pin is released, and the main parachute will be deployed from the canister. The overall cost of the system will be approximately EUR 16 k, and will weigh 1.2 kg.

Structures

The Structure system is composed of a custom 9 U cubesat structure of dimensions 340.5 mm × 342 mm × 100 mm with a mass of 1.9 kg, which will be acquired form Innovative Solutions In Space (ISIS). The second component of the structure subsystem are the payload bay doors, which will act as solar panels, mechanism to fold Delfi-C3 solar panels, protective cover for Delfi-C3 and restrainment structure for Delfi-C3 after locking in place. The doors are composed of a large panel actuated by a stepper motor and smaller panels folded upon each other that when released through spring loaded hinges will cover, restrain Delfi-C3's Thin Film Solar Cells (TFSC)'s and cover the top of Delfi-C3. The total mass of the current structure subsystem design is 4 kg and the total cost is 103 kEUR .

Layout

The selected components from all the subsystems were successfully integrated with the structure. The components were placed in a manner that allows for each subsystem to fulfill its requirements. The resulting total mass of Delfi-REAL is 14.7 kg. The layout is shown in Figure 1 and Figure 2.

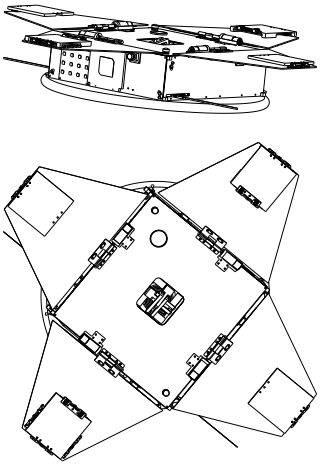

Figure 1: Side and top view of Delfi-REAL with open doors

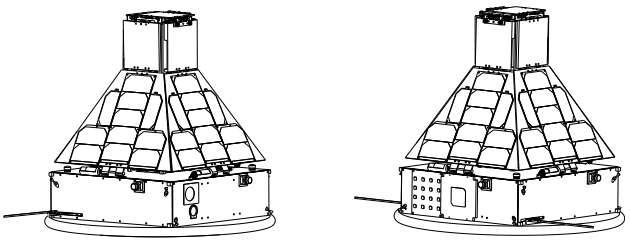

Figure 2: Front and side view of Delfi-REAL with closed doors

Simulation

To prove the feasibility of the propulsion concept, a simulation was created. This simulation models the final part of approaching Delfi-C3 and matching its angular velocity. This is done by modelling the thrusters on the spacecraft and calculating a pulsing sequence for each individual thruster. The simulation modelled the spacecraft as a point mass and calculated its movement based on the resultant force from the thrusters. The simulation showed that the tracking error in steady state rotation matching was between 0.38 mm to 0.43 mm.

Technical Risk Assessment

When considering Delfi-REAL at a subsystem level, it is possible to identify different components and interfaces that could produce undesirable risks for the mission. The risks were considered with respect to their likelihood of occurrence as well as their impact on the system in case they happen. Given that it is desirable for the design team to control, avoid or transfer these risks, three mitigation procedures were established. To eliminate the risk, the following mitigation's were considered:

1. **Mitigation 1-**Early initiation of development activities
2. **Mitigation 2-**Initiation of parallel developments
3. **Mitigation 3-**Implementation of extensive analysis and testing

The subsystem that required the most resources in terms of time and cost are the Structures subsystem, followed by Re-entry and Landing subsystem and lastly, the Command and Data Handling subsystem. Risk mitigation for these include vibrational and heat analysis for Structures and testing of the heat shield during re-entry. The parachute deployment testing and integration testing for the On Board Computer are also required. After mitigation, there are no very likely or likely risks carrying critical or catastrophic consequences for Delfi-REAL.

Technical Performance Measurement

During the entire design four important parameters were tracked in order to end up with a design that fulfils the top level and stakeholder requirements. These parameters were total spacecraft mass, cost, size and power usage. For each of these parameters the actual, current, target and specification values were tracked. With a contingency percentage that decreases as the design matured, starting from 20 % to 5 % in the end.

Besides these four main parameters, some secondary parameters were tracked as well. These were the Delta-V and Link budgets as well as the propellant mass and spacecraft pointing accuracy. These were tracked as they have significant impact on the design. However, they have no directly imposed high level or stakeholder requirements.

The actual values for each subsystem as well as for the total design are shown in Table 2. The size unit 1 U refers to a standard nano-satellite size of 10 cm × 10 cm × 10 cm.

Table 2: Delfi-REAL actual budget breakdown

Subsystem	**Mass [kg]**	**Cost in thousands [EUR]**	**Size [U]**	**Operating Power [W]**
Structure	3.8	103	2.29	0
Comms+CDH	0.68	55.6	0.75	10.7
Parachute	1.9	16	0.34	0
Heat Shield	3.0	194	2.4	0
Capture	0.57	23	1.0	3.6
Propulsion	2	86	1.24	10.2
ADCS	1.3	76	0.79	6.2
Sensors	0.42	15	0.38	2.4
Power	1.0	57	1.4	0.51
Total	14.7	621	10	35.9

Market Analysis

A market analysis was performed to establish the possible volume of the market and to determine the competitive cost of a product. The past years the space market and the nano-satellite industry in particular have seen immense growth. With multiple companies planning to launch constellations it is predicted that this growth will only increase in the coming years.

Currently there are no competitors providing a system with the same or even similar capabilities to Delfi-REAL. Multiple institutions and companies are however developing technology to prevent or remove space debris.

With a spacecraft cost of EUR 621 thousand, a launch cost of EUR 800 thousand and operational cost of EUR 550 thousand the total mission cost would be EUR 2 million as shown in Table 3.

Table 3: Total Mission Cost [EUR]

Type	**Cost in thousands [EUR]**
Spacecraft	621
Launch	800
Operational	550
Total	2021

The return on investment was estimated. Since this is a unique mission, not only monetary return was looked at but educational, marketing and brand value as well. In summary, it was concluded that companies involved with the development of Delfi-C3 would have incentive to sponsor this product. If successfull, they could study what effect on performance of their product the effects of being in space for ten years would have. The rest of the required

money would come from grants from the government or research institutions. Finally there was a lot of value found in the development of the required software and hardware for Delfi-REAL. Providing a great research and learning opportunity for students and staff of multiple faculties at TU Delft.

Finally three possible future iterations were created that would generate a commercially viable product with only a few alterations. Together with the original design this leads to four different products as shown in Figure 3 to 6. These products are the current system, capable of observing, capturing and landing of nano satellites. Concept 1 and 2; both aimed at removing space debris, either small by capturing it with a clamp or big debris by using a net. Finally Concept 3, the observation satellite, would be the cheapest and most lightweight variant. This concept is aimed at observing satellites in-orbit.

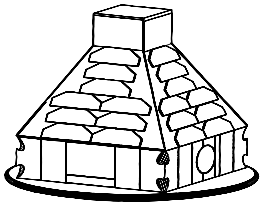

Figure 3: Delfi-REAL: Clamp, capture, and landing

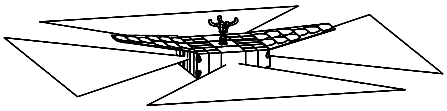

Figure 4: Concept 1: Clamp, capture and de-orbit

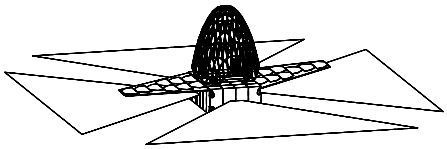

Figure 5: Concept 2: Net, capture, and de-orbit

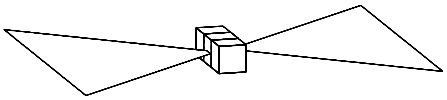

Figure 6: Concept 3: Observation satellite

List of Abbreviations

ADCS	Attitude Determination & Control System
AWSS	Autonomous Wireless Sun Sensor
BER	Bit Error Rate
BOL	Beginning-Of-Life
CAD	Computer Assisted Design
CATIA	Computer-Aided Three-dimensional Interactive Application
CDHS	Command and Data Handling System
CES	Capture and Enclosing System
CFRP	Carbon Fibre Reinforced Polymer
c.g.	Centre-of-Gravity
CNC	Computer Numerical Control
COTS	Commercial-Off-The-Shelf
DARE	Delft Aerospace Rocket Engineering
DOD	Depth of Discharge
DOT	Design Option Tree
DRS	De-orbit and Recovery System
ECSS	European Cooperation for Space Standardisation
EOL	End-Of-Life
EO/RS	Earth Observation & Remote Sensing
EPS	Electric Power System
ESA	European Space Agency
FBS	Functional Breakdown Structure
FFD	Functional Flow Diagram
FTA	Fault Tree Analysis
GE	General Electric
GFRP	Glass Fibre Reinforced Polymers
GNC	Guidance, Navigation, and Control
GPS	Global Positioning System
GTO	Geostationary Transfer Orbit
I2C	Inter-Integrated Circuit
IP	Internet Protocol
ISA	International Standard Atmosphere
ISIS	Innovative Solutions in Space
ISS	International Space Station
LEO	Low Earth Orbit
Li-Ion	Lithium-Ion
Li-Po	Lithium-Polymer
MIB	Minimum Impulse Bit
NASA	National Aeronautic and Space Administration
OBC	On Board Computer
OQPSK	Offset Quadrature Phase Shift Keying
PCM	Protection Circuit Module
PICA	Phenolic-Impregnated Carbon Ablator
PSLV	Polar Satellite Launch Vehicle
PTFE	Polytetrafluoroethylene
RAAN	Right Ascension of the Ascending Node
RAS	Reliability, Availability and Safety
REN	Re-entry
RPM	Rotations Per Minute
RQ	Requirement
SBC	Single-board computers
SMAD	Space Mission Analysis and Design
SNR	Sound to Noise Ratio
SSO	Sun Synchronous Orbit
TFSC	Thin Film Solar Cell
THER	Thermal
TPM	Technical Performance Measurement
TPS	Thermal Protection System
TRL	Technological Readiness Level
TT&C	Telemetry Tracking & Command
TU Delft	Delft University of Technology
UHF	Ultra High Frequency
UTIAS	University of Toronto Institute for Aerospace Studies
VHF	Very High Frequency
WBS	Work Breakdown Structure
WFD	Work Flow Diagram

List of Units

°	Degree
AU	Astronomical Unit
bit	Bit
B	Byte
dB	Decibel
EUR	Euro
fps	Frames per second
K	Kelvin
kg	Kilogram
m	Meter
mils	Milli inch
N	Newton
s	Second
V	Volt
W	Watt
U	Standard cube-sat unit of $10\,\text{cm} \times 10\,\text{cm} \times 10\,\text{cm}$

List of Constants

k	Boltzmann constant $1.380 \times 10^{-23}\,\text{J K}^{-1}$
μ	Earth gravitation parameter $3.986 \times 10^{14}\,\text{m}^3\,\text{s}^{-2}$
π	Pi 3.1415
σ	Stefan-Boltzmann constant $5.670 \times 10^{-8}\,\text{J m}^{-2}\,\text{s}^{-1}\,\text{K}^{-4}$

List of Symbols

A	Area	[m^2]
A_{sa}	Solar array area	[m^2]
A_0	Available solar array area	[m^2]
a	Semi-major axis	[m]
a_{atmdr}	Deceleration by atmospheric drag	[$m\,s^{-2}$]
B	Bandwidth	[Hz]
BER	Bit error rate	[–]
c	Specific heat	[$J\,K^{-1}$]
c	Speed of light	[$m\,s^{-1}$]
C	Data Rate	[$bit\,s^{-1}$]
C_d	Drag coefficient	[–]
d	Thermal protection system thickness	[mm]
d_{abl}	Total ablation thickness	[mm]
$\dot{d_{abl}}$	Ablation rate	[$mm\,s^{-1}$]
DOD	Depth of Discharge	[–]
e	Eccentricity	[–]
e	Pointing error	[°]
e_r	Pointing error receiver	[°]
e_t	Pointing error transmitter	[°]
E_b	Energy per bit received	[$J\,bit^{-1}$]
$EIRP$	Effective Isotropic Radiated Power	[W]
f	Frequency	[Hz]
F_t	Total Force	[N]
g	Acceleration due to Earth's gravity	[$m\,s^{-2}$]
g_0	Acceleration due to Earth's gravity at the earth's surface	[$m\,s^{-2}$]
G	Antenna gain	[dB]
G_c	Coding gain	[dB]
G_p	Peak gain	[dB]
G_{pr}	Peak receiver gain	[dB]
G_{pt}	Peak transmitter gain	[dB]
G_r	Receiver gain	[dB]
G_t	Transmitter gain	[dB]
h	Altitude	[m]
i	Inclination angle	[°]
I_d	Inherent degradation	[–]
I_{sp}	Specific impulse	[s]
L_a	Propagation and polarisation loss	[dB]
L_l	Line loss	[dB]
L_s	Space loss	[dB]
m	Mass	[kg]
M_{dry}	Dry mass	[kg]
M_{wiring}	Wire mass	[kg]
n	Radial velocity	[$°\,s^{-1}$]
n_e	Power transmission efficiency	[–]
N	Noise	[dB]
N_i	Number of bits	[–]
N_o	Noise spectral density	[dB]
P	Power	[W]
p_c	Internal pressure	[MPa]
P_d	Daylight power consumption	[W]
P_e	Eclipse power consumption	[W]
P_{EOL}	Power per unit area at EOL	[$W\,m^{-2}$]
$P_\odot$	Solar irradiance	[$W\,m^{-2}$]
P_r	Probability	[–]
P_{sa}	Solar array power provision	[W]
q	Heat flux	[$W\,cm^{-2}$]
Q	Thermal energy	[W]
R	Radiation intensity	[$W\,m^{-1}$]
R_E	Earth radius	[m]
r	Radius	[m]
r_a	Apogee radius	[m]
r_{opt}	Optimal radius	[m]
r_p	Perigee radius	[m]
S	Sound	[dB]
S_d	Propagation path length	[m]
t	Time	[s]
t_t	Tank wall thickness	[m]
T	Temperature	[K]
T_b	Bondline temperature	[°C]
T_d	Daylight period	[min]
T_e	Eclipse period	[min]
$T_{fly-over}$	Fly-over duration	[s]
T_o	Orbit period	[s]
T_s	System noise temperature	[K]
X_d	Path efficiency during daylight	[–]
X_e	Path efficiency during eclipse	[–]
V	Velocity	[$m\,s^{-1}$]
V_{bat}	Average battery voltage	[V]
α	Thermal energy absorbence ratio	[–]
γ	Flight path angle	[°]
ϵ	Thermal energy emittence ratio	[–]
ϵ_{min}	Minimum visibility angle	[°]
η_{max}	Maximum nadir angle	[°]
η_{SC}	Solar cell efficiency	[%]
Δa_{rev}	Change of a per revolution	[m]
ΔV	Delta-V	[$m\,s^{-1}$]
Δt	time impulse	[s]
$\Delta\Omega$	Change in Longitude of the ascending node	[°]
θ	Half power beam width	[°]
θ_r	Half power beam width receiver	[°]
θ_t	Half power beam width transmitter	[°]
ν	True anomaly	[°]
ρ	Density	[$kg\,m^{-3}$]
σ_x	Axial stress	[MPa]
σ_y	Circumferential stress	[MPa]
Ω	Longitude of the ascending node	[°]

Contents

1 Introduction

On the 28th of April 2008, the student-built nano-satellite Delfi-C3 was launched and it is still operational to this day. The primary mission objectives of Delfi-C3 were in-orbit testing of the Thin Film Solar Cell (TFSC) technique and Autonomous Wireless Sun Sensors (AWSS). The satellite has experienced issues in multiple components, but the causes remain unknown. The issues faced include a "deaf" radio receiver, the potential ablation of the experimental thin film solar cells, and an apparent tenfold increase in current consumption of the On-Board Computer (OBC). Currently, there is no technology to further analyse the state of the satellite and for this reason, the "Return of the Queen" mission was established.

The goal of the mission is to design a nano-satellite system which is capable of collecting information about the state of Delfi-C3 by means of live images and videos, and returning it back to Earth intact. The name of the system designed to accomplish this mission is Delfi-REAL (Delfi-Re-Entry-And-Landing). In order to fully complete the mission, Delfi-REAL has been designed to be launched, inserted into orbit, reach Delfi-C3, observe and capture the satellite, and finally return it back to Earth.

The purpose of this report is to present the final design of Delfi-REAL. This report follows the midterm report where the system design trade-off was performed and the subsystem requirements were determined. Using the previously established requirements, the subsystems were sized and a final configuration of Delfi-REAL was established. The system design was then analysed for sustainability, reliability, risk, technical performance and sensitivity. With this, the final design could be presented with recommendations for the future development.

The structure of the report is as follows. The project objectives, including the mission statement, the scope and stakeholders, are found in Chapter 2. The system concept trade-off and mission profile are in Chapter 3 and Chapter 4 respectively. Chapter 5 describes Delfi-REAL's functions and hardware. This is followed by Chapter 6 through Chapter 17 which include all subsystems of Delfi-REAL. Each subsystem chapter explains the function of the system, requirements, trade-off, final design, and future recommendations where applicable. After the subsystems, the configuration and layout of Delfi-REAL is presented in Chapter 18. Once the system design is presented, the sustainability, reliability, availability and safety, and the technical risk assessment are found in Chapter 19, 20 and 21. The technical performance measurement is in Chapter 22 followed by the market analysis in Chapter 23. Finally, the sensitivity analysis and recommendations for future development are found in Chapter 24 and Chapter 25 respectively.

2

Project Objectives

This chapter describes the goals that the project team has established for the system. The mission statement is presented in Section 2.1 which directly influences the project objectives shown in Section 2.2. The functionality of the system scope is defined in Section 2.3 and lastly, the primary stakeholders are summarised in Section 2.4.

2.1. Mission Statement

The mission statement presented below describes the goal of the project.

> *Observing the TU-Delft nano-satellite Delfi-C3 and returning it safely back to Delft, without causing excessive damage.*

2.2. Project Objective Statement

From the mission statement presented above, the primary and secondary project objectives can be established. These are broad goals the system must achieve in order for the mission to be deemed successful.

> ***Primary objective***
> *Design a system capable of observing 3U CubeSats in orbit and return them back to Earth safely without causing excessive damage during the retrieval process, with 11 students in 10 weeks.*

> *Secondary objectives*
> - Collect data and gain experience on de-orbiting space debris.
> - Develop procedures and tools for designing reconnaissance missions in a structured way.
> - Expand the areas of study of the TU Delft space program.

2.3. Scope Definition

The scope of the project describes the different tasks the system is required to perform. Inherently, time is an important variable to consider as it directly relates to the mission. Thus, the description provided below briefly presents the five main stages of the mission for which the project team will develop a technical solution.

> ***Scope***
> 1. Launch and Orbit Insertion
> 2. Reconnaissance and Rendezvous with Delfi-C3
> 3. Capture
> 4. Altitude Reduction
> 5. Re-entry and Landing

2.4. Primary Stakeholders

The project has a number of stakeholders with interest in the success of the system. These are briefly summarised in Table 2.1.

Table 2.1: Project Stakeholders.

Stakeholder Name	Interests
Delft University of Technology (TU Delft)	• Scientific value for future space development by the TU Delft. • Safety of staff and assets during the development and construction of the system on the TU Delft premises. • Good PR for the TU Delft in case of success.
Chris Verhoeven and Delfi-C3 Development Team	• Scientific research and hypothesis check regarding operational issues. • Emotional value.
European Space Agency (ESA)	• ESA has expressed interest in becoming a leading entity in Space Debris Removal.[1]
Launch and Transportation Service Providers	• These companies will want a guarantee that the system does not harm their launch and transportation vehicle. • In the case of a piggyback launch, the safety of the other space-systems on board needs to be ensured.
Other companies with assets in Low Earth Orbit (LEO)	• Do not produce more space debris which could endanger other satellites.
Cubesat component manufacturers	• Validate and flight test newly designed equipment
The International Space Community	• Potential for debris removal and satellite return. • Motivates the community for future development.

2.5. Design Compatibility

Some critical main stakeholder requirements were obtained that define the design on a system level. All subsystems have to be integrated to meet these requirements.

RQ-COM-01 The system shall be compatible with nano-satellite standards.
RQ-COM-01.02 The system shall be launched from a nano-satellite cassette.
RQ-COM-01.03 The system shall be able to withstand the load as specified in the launcher manual.
RQ-COM-01.04 The system shall operate on a standard nano-satellite I^2C bus.
RQ-COM-02 The system shall be compatible with nano-satellite procedures.
RQ-COM-02.01 The system shall be launched as a secondary payload.
RQ-COM-03 The system shall be able to withstand the environmental conditions for the mission lifetime.

[1] http://www.esa.int/Our_Activities/Space_Engineering_Technology/Clean_Space/e.Deorbit accessed on 19 Nov. 2018

3
System Concept Trade-Off

In this chapter the concept trade-off and design description will be shown. First, the trade-off criteria will be stated in Section 3.1. Then the concepts produced in the previous design phase [1] will be described in Section 3.2 and will then be compared in a trade-off in Section 3.3. After which a sensitivity analysis of the trade-off is presented in Section 3.4. The final concept selection is made in Section 3.5. Finally the concept sketches are presented in Section 3.6.

3.1. Trade-off Criteria

The trade-off criteria chosen by the design team as well as an explanation for the chosen relative weights are presented below.

- **Mass 5/10** -The system mass is a typical parameter for estimation and in this particular instance, directly impacts launch cost. This is a stakeholder requirement which needs to be complied with. However, exceeding the launch costs requirement does not have a catastrophic impact on the mission objective.
- **System Cost 8/10** - The cost of the mission is one of the main driving requirements. If the product exceeds the set limit, the provided service will no longer be worth the investment for the stakeholders. The cost of the system was selected as a trade-off criterion due to its great influence on if the product is realisable. It is also relevant to note that this parameter excludes launch cost.
- **Complexity 7/10** - This criterion regards the complexity of the design process. Complexity commonly increases the risk of completing the project as well. The weighting considered the limited cost, time and resources available to complete the project.
- **Reliability 9/10** - The reliability of the system describes the chance of failure or success of the concept. This covers the reliability of certain components such as actuators and spring loaded devices, the number of manoeuvres during rendezvous and the reliability of the re-entry protection method. Since mission success is highly dependant on this criterion, it is given the highest weight in the trade-off.
- **Volume 2/10** - The system volume is constrained by the launching system. Therefore, the design options are subjected to the size of the structure. However, due to the fact that mass has a bigger impact on the launch cost, the criterion weight is deemed as the least important for this trade-off

The values for the weights were established through a survey among the group members. Every group member was instructed to give each criterion a weight out of 10 based on their engineering knowledge and intuition. The results of the survey were then averaged to result in the assigned weights. This method was chosen as it would assimilate the engineering knowledge and intuition of 10 engineers and so improve the objectivity of the weight selection.

These five trade-off criteria, and their weights, are also used in for the subsystem trade-off, unless stated otherwise.

3.2. Concept Description

After using a Design Option Tree (DOT) and eliminating some unfeasible options. The design options left, are described in this section. The DOT and option elimination is further explained in the previous report [1]. Each of the concepts is provided with a brief description followed by an illustration of the concept as well as its mission profile.

1. **Expanding Foam** - This concept relies on protecting Delfi-C3 during re-entry by covering it with foam either directly or within a rigid or flexible structure. During the application of the foam, Delfi-C3 shall be held in place by a robotic arm. Different stages of the capture and deployment mechanism are displayed in Figure 3.1. The three different variations of this concept are shown in Figure 3.2, the *flexible shell*, *no shell* and *rigid shell*.
2. **Tightening Rails** - Using two different modules connected by a structure, Delfi-C3 can be caught and secured. These modules can include parachutes or heat shields needed to protect the spacecraft on re-entry and landing. This procedure is shown in Figure 3.3.
3. **Direct Attachment** - A direct attachment approach uses a physical bond to attach the system to Delfi-C3. This can be done by using a clamping system or a net. The net concepts will also include a clamping system to secure

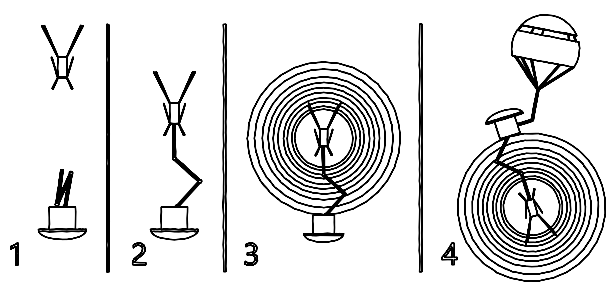

Figure 3.1: Expanding foam mission profile

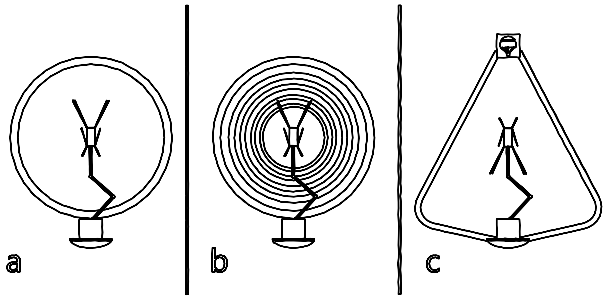

Figure 3.2: Expanding foam variations

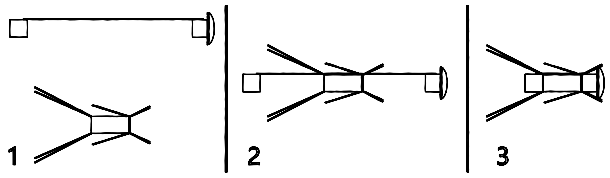

Figure 3.3: Tightening Rails mission profile

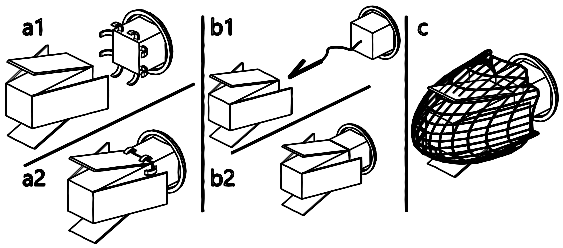

Figure 3.4: Direct attachment variations and mission profile

Delfi-C3 during the remainder of the mission. These different capture mechanisms and the configurations for different mission stages are shown in Figure 3.4.

4. **Swarm**- The last concept enables us to explore simple systems that work together forming a swarm. Using two modules to dock with Delfi-C3, shown in Figure 3.7 or using a swarm of modules with a net in between to encapsulate Delfi-C3, shown in Figure 3.6.

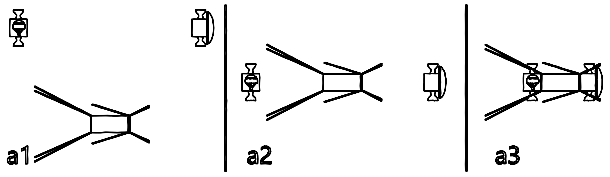

Figure 3.5: Swarm clamping

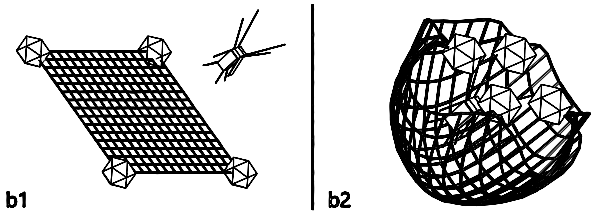

Figure 3.6: Swarm Net

Figure 3.7: Swarm Modular mission overview

3.3. Concept Trade-off

At the given stage, the concepts stated in Section 3.2, can be inserted in the trade-off method. First, a more detailed manner to characterise the score of each criteria is presented. For reliability and complexity, which are more subjective criteria, a custom explanation is provided. This procedure then culminates in the trade-off table.

In order to perform a consistent trade-off, thresholds need to be established as to define what is excellent, what meets expectations (Nominal), what has correctable deficiencies (Violates Requirements) and what is unacceptable. For the criteria which possess a numerical input, it was decided to use the boundaries as depicted in Table 3.1. For the requirements, the Technical Performance Measurement (TPM) margins are also considered. This resulted in a system cost requirement of EUR 1.67 million, since a specification value of EUR 2 million was given and a TPM margin of 20 % is applied at this stage of the design. A mass requirement of 20.8 kg applies, which is calculated from a launch budget requirement of EUR 1 million divided by a launch cost of EUR 40 $\mathrm{k\,kg^{-1}}$ and a TPM margin of 20 % [2]. Furthermore, a volume requirement of 10 U is derived from the 12 U requirement on nano-satellites, combined with the same 20 % TPM margin [3].

For criteria without a numerical value, it is more difficult to identify an appropriate quality level. Using the research information obtained in the previous report [1] and the engineering judgement of the team, a description of the reasoning process is provided:

Table 3.1: Trade-off boundaries.

Criterion	Excellent	Nominal	Exceeds Requirements	Unacceptable
Percentage of Requirement	< 80	80-100	100-110	> 110

- The complexity of the *Flexible Shell* concept relies heavily on the capturing mechanism. Encapsulation of Delfi-C3 with a flexible shell will be very challenging. Therefore, it is established that it has correctable deficiencies. The reliability will be nominal, since protection during re-entry will be good and no overly complex manoeuvres need to be performed, but no redundancies are included either.
- After research on using foam for heat protection during re-entry, it was established that the *No Shell* concept will be overly complex to design. This is partially because the act of applying the foam will be difficult to perform accurately. Furthermore, the foam will need to perform under very high re-entry temperatures and no such foam was found during literature research. Therefore, the complexity of the concept was deemed unacceptable. The reliability of the *No Shell* is nominal because if the right foam would be available, re-entry and capture would not pose a high risk.
- The complexity of the *Rigid Shell* concept is nominal because the rigid shell (box) is considerably straightforward with regards to resource consumption. At the same time, it will most likely need to be an unfolding mechanism to ensure the fact that it doesn't exceed a the limited launch volume. The reliability is very high, because Delfi-C3 will be protected from all sides during re-entry. Therefore, a rating of excellent is given for this criterion.
- For the *Tightening Rails* concept, the complexity is nominal, since the rail system requires considerable resources to develop the connecting structure. The rest of the system is rather simple. The reliability of the rail system is low, because precise docking with Delfi-C3 will be a very complicated and risky manoeuvre. The interference with the solar arrays that are on its sides deemed this concept as possessing correctable deficiencies.
- The *Clamp* concept scores nominal on both reliability and complexity. This is because the docking manoeuvre is deemed straightforward and reliable. This is counter-balanced with the re-entry mission phase, for which the regarded concept is complex and less reliable. Thus, design complexity contains different considerations which still require a considerable amount of resources and the reliability for the concept success is considered nominal.
- The *Net* concept has the same design complexity as the *Clamp* concept, since the docking is made easier with the net, but the re-entry will be even more complex. The reliability of the net however is very low. This is due to the fact that the shot needs to be very precise and if it fails, a second try will be impossible. Therefore, the complexity is set on nominal and the reliability of the concept is set to contain correctable deficiencies.
- Both complexity and reliability for the *Swarm Clamp* concept have correctable deficiencies. The fact that the concept includes two separate satellites makes it a more complex concept than the *Rails* concept and the *Clamp* concepts. Furthermore, because the docking manoeuvre needs to be performed twice, the reliability of the concept is also below nominal.

Taking into account all of the consideration previously provided, the quality levels for each concept are presented in Table 3.2.

Table 3.2: Design concept trade-off table. excellent: exel, nominal: nom, exceeds requirement: exreq, unacceptable: unacc

Criterion / Option	Mass	System cost	Complexity	Reliability	Volume
Flexible Shell	nom	exel	exreq	nom	nom
No Shell	nom	exel	unacc	nom	exreq
Rigid Shell	nom	nom	nom	exel	nom
Tightening Rails	exel	exel	nom	exreq	exel
Clamp	exel	exel	nom	nom	exel
Net	nom	nom	nom	exreq	nom
Swarm Net	exel	nom	exreq	exreq	exel

Table 3.3: Design concept trade-off table with 30% mass increase. excellent: exel, nominal: nom, exceeds requirement: exreq, unacceptable: unacc

Criterion / Option	Mass	System cost	Compl-exity	Relia-bility	Vol-ume
Option *Flexible Shell*	exreq	exel	exreq	nom	nom
Option *No Shell*	unacc	exel	unacc	nom	exreq
Option *Rigid Shell*	unacc	nom	nom	exel	nom
Option *Tightening Rails*	exel	exel	nom	exreq	exel
Option *Clamp*	exel	exel	nom	nom	exel
Option *Net*	nom	nom	nom	exreq	nom
Option *Swarm clamp*	unacc	nom	exreq	exreq	exel

Table 3.4: Design concept trade-off table with 30% cost increase. excellent: exel, nominal: nom, exceeds requirement: exreq, unacceptable: unacc

Criterion / Option	Mass	System cost	Compl-exity	Relia-bility	Vol-ume
Option *Flexible Shell*	nom	nom	exreq	nom	nom
Option *No Shell*	nom	exreq	unacc	nom	exreq
Option *Rigid Shell*	nom	exreq	nom	exel	nom
Option *Tightening Rails*	exel	nom	nom	exreq	exel
Option *Clamp*	exel	nom	nom	nom	exel
Option *Net*	nom	exreq	nom	exreq	nom
Option *Swarm clamp*	exel	exreq	exreq	exreq	exel

3.4. Sensitivity Analysis

The trade-off table presented in Section 3.3 showed that the *Rigid Shell* and *Clamp* concepts were the winning concepts, but it did not show a clear winner between the two. These results are only valid if the sensitivity of the outcome, with respect to the inputs, is low. Therefore, a sensitivity analysis is needed to see the change in outcome for slight changes in the input. This is done for the mass, system cost and volume by adding 30% of the total and analysing whether the change influences the overall outcome of the trade-off. The limit, 30%, was chosen as it would give an adequate contingency for the development team to ensure that the requirements are met. The trade-off tables after the implementation of the mass and cost increase are shown in Table 3.3 and 3.4 respectively.

When implementing this 30% increase in the mass, a few significant changes are observed. The mass of the *No Shell*, *Rigid Shell* and *Swarm Clamp* concept will be unacceptable. This means that if one of these concepts is chosen, extra attention needs to be paid to the mass during the design process.

For the system cost, a 30% increase will not lead to a significant change, since every concepts shifts one level, except for the *No Shell* concept, which shifts 2 levels. None of the concept costs become unacceptable.

For the size, the sensitivity analysis shows only one significant change after a 30% increase. This is a shift of the *No Shell* concept, which will have an unacceptable size. This sensitivity analysis is not visualised, because the *No Shell* concept already had an unacceptable complexity.

This type of sensitivity analysis can not be performed for complexity and reliability, since there are no concrete values for these criteria. Instead, a qualitative sensitivity analysis was performed. During this qualitative analysis, the weight of the criteria was adjusted to see whether it influenced the trade-off in a significant way. For both criteria, the sensitivity analysis looked at changing the weight of the criteria and removing it all together. Halving or doubling the weight of complexity shows no major changes in the trade-off table. Changing the weight of complexity doesn't cause major changes as the two winning concepts have the same score. Removing it causes the *Flexible Shell* and *No Shell* concepts to improve relative to the other concepts. However, both are still not the optimal concepts.

Halving, doubling or removing reliability does have a significant influence on the trade-off table, since it brings most options closer together. Especially removing the criteria, causes the *Tightening Rails* concept to become the best option together with the *Clamp* concept and causes *Rigid Shell* concept to become a less attractive.

3.5. Final Concept Selection

Provided that the previous trade-off procedure determined a similar result for the *Rigid Shell* and *Clamp* concepts, further analysis was deemed necessary in order to determine a unique design concept. Given that such a trade-off is commonly performed to output a single solution, the design team could not consider both concepts again with respect to the weight criteria. As a high-level study had already been conducted, evaluating the two concepts in further detail could already be considered starting the conceptual design before finishing the trade-off.

Hence, in order to accomplish a similar level of analysis, it was decided that the two concepts should be investigated against each other with respect to critical mission phases. These were considered to be the rendezvous approach as well as the system re-entry, due to their importance to achieve the primary mission objective. A list of beneficial and detrimental aspects symbolised by the + and - signs respectively is presented in Table 3.5.

Table 3.5: Critical mission phase performance of *Rigid Shell* and *Clamp* concepts.

Mission phase	**Rigid Shell**	**Clamp**
Rendezvous	+ Encapsulation of Delfi-C3 - Higher number of mechanical manoeuvres - Higher power usage	+ Simpler to attach + Redundancy of clamping mechanism + Faster procedure (daylight time provides 45 minute window for the rendezvous procedure) - Antennas will be in the way
Re-entry	+ Vibration tolerant + Buoyant + Less risk of damaging during recovery	- No protection - Complexity and cost of recovery system

As seen in Table 3.5, the *Rigid Shell* and *Clamp* concepts perform best at different critical mission stages. Their defining subsystems are not incompatible with each other, enabling the possibility to combine their respective strengths. To reduce compromises, the benefits of both concepts are combined into a new design concept.

This new concept uses a clamp to secure Delfi-C3 and encapsulates it with four rigid walls. The inside of these walls are lined with an inflatable device. With this system, Delfi-C3 shall be protected from vibrations, heat and impact during re-entry. The inflation system also increases buoyancy, contributing to the ability of the system to float on water for easy retrieval. A sketch of the new concept design is shown in Figure 3.8. This design is denoted as concept **VI - Encapsulating Clamp**.

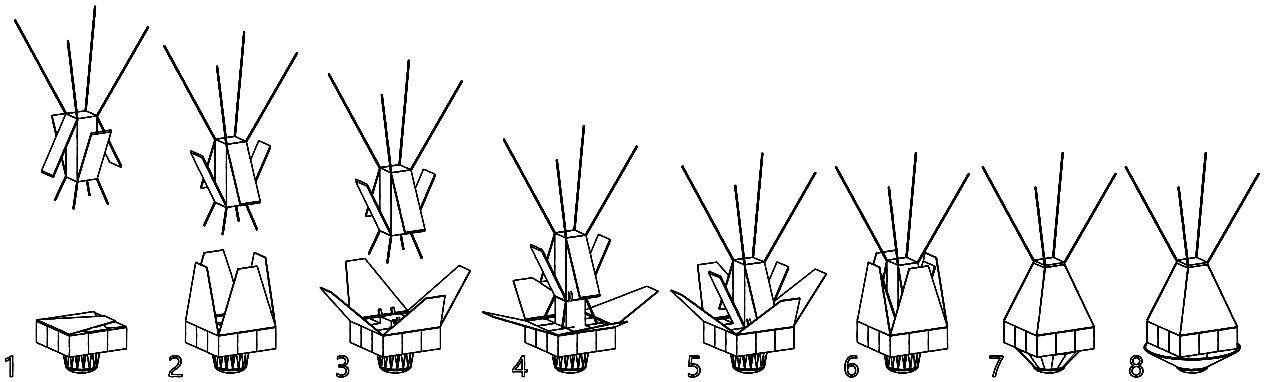

Figure 3.8: Sketch for concept *Encapsulating Clamp*

To ensure that this new concept is indeed the best, it is entered in a trade-off, together with the *Rigid Shell* and *Clamp* concept, as shown in Table 3.6. From this table, it can be seen that the *Encapsulating Clamp* concept scores equal to the *Rigid Shell* on reliability, but performs better with regards to system cost and mass. This is because the *Rigid Shell* would make use of a large rigid shell, which also acts as an heat shield compared to rigid shell walls not responsible for heat shielding. Furthermore, the *Rigid Shell* makes use of a robotic arm compared to smaller and simpler clamp. The *Clamp* concept also performs better with regards to system cost and mass compared to the *Rigid Shell* concept. When comparing the new concept with the *Clamp*, it is possible to observe a switch in the volume and reliability columns, while all else is unchanged. As discussed in Section 3.1, reliability possesses a higher weight consideration for the design team. Furthermore, as the design is more lightweight and reliable than both other single designs, it will be more sustainable. From this it was concluded that the *Encapsulating Clamp* is the best option overall. Therefore, this concept is designated to fulfil the mission.

A preliminary sizing was performed on this concept, using the same standards as those used on the other concepts. The results of this sizing can be found in Table 3.7 and present very rough estimations for the criteria of importance considered during the trade-off.

Table 3.6: Iterated design concept trade-off table. excellent: exel, nominal: nom, exceeds requirement: exreq, unacceptable: unacc

Criterion / Option	Mass	System cost	Complexity	Reliability	Volume
Rigid Shell	nom	nom	nom	exel	nom
Clamp	exel	exel	nom	nom	exel
Encapsulating Clap	exel	exel	nom	exel	nom

Table 3.7: Concept sizing for encapsulating clamp concept.

Concept	Mass [kg]	Power [W]	Volume [U]	System Cost [kEUR]	Complexity	Reliability
Encapsulating Clamp	12	60	10	1261.0	nom	high

3.6. Detailed Concept

In order to continue with subsystem requirements, an analysis of the integration of the subsystems into the system was needed. During this analysis, the goal was to decide the location of the main propulsion system, due to the fixed locations of both the heat shield and clamping systems. It is important to note that a trade-off for each of the subsystems will happen at a later point in the project.

In the concept shown in Figure 3.8 on Page 8, a design with a deployable heat shield is shown. This heat shield idea is based on a 2U system from NASA which would be added to the 9U base, making it 11U in total [4]. In this option, the propulsion system would have to be integrated into two corners of the 9U base. This can be seen in Figure 3.9. This concept was modified for three reasons. First, the placement of the main thrusters has the potential of adding complexity to the system, and lower performance, especially during the capture phase of the mission. This is because placing thrusters off centred will create moments. Second, the heat shield technology is new, thus it is not prudent to design the system architecture around a concept with insufficient technology readiness. The exact form the heat shield will take will be decided when the subsystem trade-off is completed. Third, the structure of the system has the potential to be simplified, which will also decrease complexity for the structural design. It is for these three reasons that a modified configuration was determined.

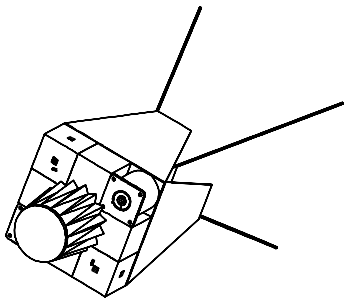

Figure 3.9: Detailed sketch of the *Encapsulating Clamp* concept

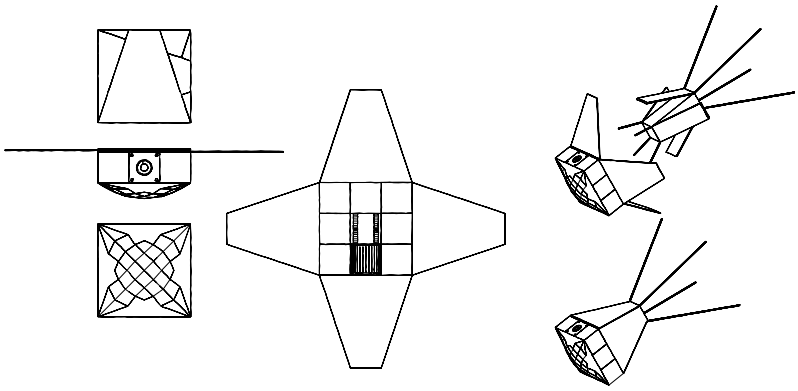

Figure 3.10: Detailed sketch for the *Encapsulating Clamp* concept

In the modified configuration, the spacecraft uses an integrated heat shield and the main propulsion system is located on the side of the system. The use of Attitude Determination and Control System (ADCS) thrusters on each corner allows for manoeuvrability, and the centre of the spacecraft is available for the clamp system. This system solves the previously mentioned issues, while leaving adequate space for the payload, Delfi-C3, and other subsystems to be integrated. The modified design sketch can be found in Figure 3.10. The placement of the propulsion system will still allow for the use of the deployable heat shield if it is deemed favourable in the subsystem trade-off.

Using the modified configuration of the *Encapsulating Clamp* concept, the basic architecture of the system is known, and subsystem requirements can be formulated.

4
Mission Profile

This chapter discusses the mission profile in order to determine an orbit plan. First, in Section 4.1 the different launch vehicle options are discussed. In the second section, Section 4.2, a basic overview of the terms used within the section are displayed. In the next section, Section 4.3, the Delfi-C3 orbital characteristics are discussed and determined. In Section 4.4, the Delta-V required to change from the drop-off orbit to the Delfi-C3 orbit is calculated. In Section 4.5, the visibility and coverage of the satellite trajectory is discussed. In Section 4.6, the options for de-orbiting the satellite are shown. Finally, in Section 4.7, an overview of the different mission phase time stamps is given.

4.1. Launch Vehicle

The mission will begin at launch, which will bring Delfi-REAL to a 600 km altitude orbit. This orbit is higher than the orbit of Delfi-C3. It was found that 80 % of nano-satellites are expected to launch to Sun-Synchronous Orbit (SSO) or Polar orbit in the next years. It was also found that piggy-backing[1] is possible with many launchers to the required orbit [5]. In order to allow for piggy-backing, the spacecraft must be designed to comply with all possible launchers. The most used launchers for nano-satellites were found to be the Polar Satellite Launch Vehicle (PSLV), Soyuz, Atlas V, Antares and Falcon 9 [5]. Some recently developed small satellite launchers were considered as well. The most relevant of these are the Vector-R[2], Firefly-alpha[3] and Rocketlabs Electron[4]. Delfi-REAL is designed to withstand worst case scenario laucnh loads so that all launch vehicles remain as valid options.

4.2. Orbital Mechanics Terms

This section discusses the parameters used to describe an orbit. In the first figure, Figure 4.1, the relationship between the apogee (the highest orbital altitude), the perigee (the lowest orbital altitude), and the semi-major axis (the average of the apogee and perigee) is shown.

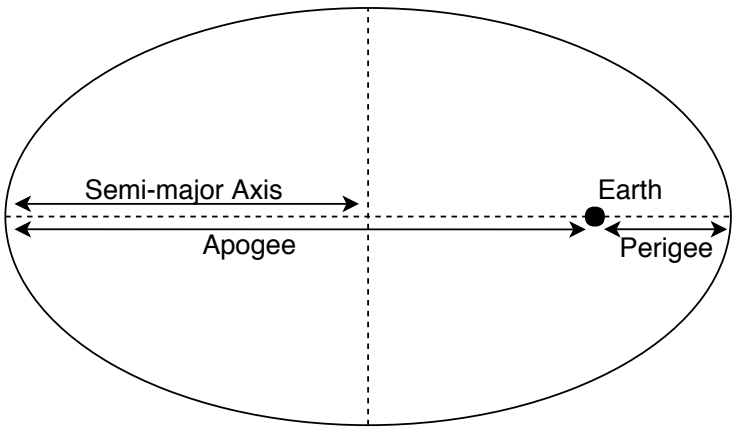

Figure 4.1: Depiction of apogee, perigee, and semi-major axis

In Figure 4.2[5], more orbital parameters are depicted. Ω is the Right Ascension of the Ascending Node (RAAN), which is the angle at which the satellite passes over the equator, with respect to the direction of movement of the Earth. The argument of the perigee, ω, is the angle that denotes the location of the perigee with respect to the RAAN. The inclination angle i is the angle between the orbit ground track and the equator. The zenith is the pointing vector following P and the nadir is the same vector but in the opposite direction.

[1] `http://spaceflight.com/schedule-pricing/` accessed 5 December 2018
[2] `https://www.vector-launch.com/vector-r/` accessed on 29 Jan. 2019
[3] `https://fireflyspace.com/` accessed on 29 Jan. 2019
[4] `https://www.rocketlabusa.com/vehicle/electron/` accessed on 29 Jan. 2019
[5] `http://orbitertutorials.tripod.com/orbital_mechanics.htm`, accessed on 20, Dec. 2018

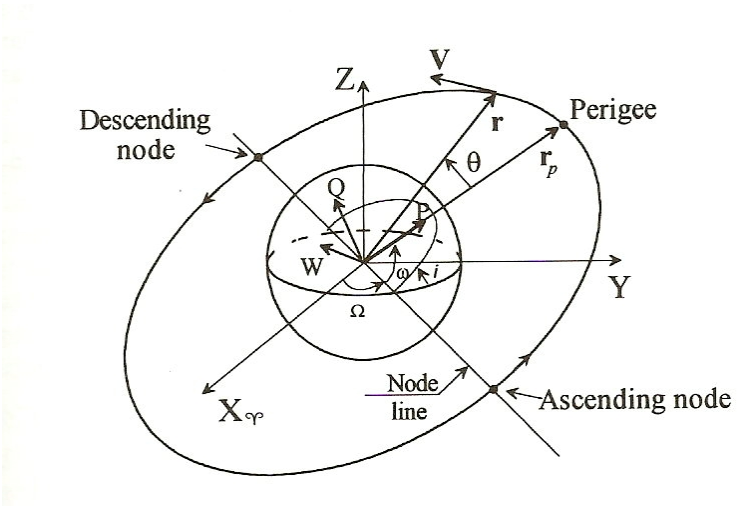

Figure 4.2: Orbital reference frame of an orbit with respect to Earth

4.3. Delfi-C3: Orbital Characteristics

In order to determine the position of Delfi-C3, ground station estimates[6] are taken. This source states that it estimates the position of Delfi-C3 with an accuracy of approximately 1 km. Delfi-C3 is estimated to have an apogee altitude of 556 km, a perigee altitude of 537 km, and an inclination of 97.49°.

4.4. Orbit Matching

To capture Delfi-C3, the satellite should be able to match its orbit with that of Delfi-C3. The starting orbit of the satellite is assumed to be at a 600 km circular SSO with a 35 km accuracy [6].

Initially, multiple engine thrust levels were considered. It was deduced, through market research, that the commercial off-the-shelf Attitude Determination and Control System (ADCS) would not be able to compensate enough for large thrusts. It was found that engines with a nominal thrust of 0.1 N are manageable by the ADCS. This means that the burn time of the engines, that have to produce a specific Delta-V, would be too long to be considered instantaneous. To compensate for this, while maintaining the efficiency of the Delta-V budget from a Hohmann transfer, it was decided to perform an orbit transfer composed of a range of smaller velocity changes, each performed at the apogee.

To determine the Delta-V induced by the propulsion system, Equation 4.1 was used:

$$\Delta V = \frac{F_t \Delta t}{m} \tag{4.1}$$

Where F_t is the total force exerted by the thrusters, m is the mass of the satellite, Δt is the burn time, and ΔV is the velocity change experienced during the burn time.

In order to calculate the new orbit parameters, such as the apogee, the perigee, and the semi-major axis, the vis-viva equation was re-arranged. The original equation is seen in Equation 4.2, and the manipulated equation to determine the new semi-major axis is written in Equation 4.3 [7]. The third equation is used to determine the new perigee, Equation 4.4 [7].

$$V^2 = \mu\left(\frac{2}{r} - \frac{1}{a}\right) \tag{4.2}$$

$$a = \left(\frac{2}{r} - \frac{V^2}{\mu}\right)^{-1} \tag{4.3}$$

$$r_p = 2a - r_a \tag{4.4}$$

μ = standard gravitational parameter
a = semi-major axis
r = current radial position
V = velocity at radial position
r_p = orbit radius at perigee
r_a = orbit radius at apogee

As stated before, to optimise the Delta-V budget, Delfi-REAL will perform an engine burn for a specific time. This time was chosen to be 10 seconds. This burn is performed when the system is at apogee. The burn starts 5 seconds

[6] https://heavens-above.com/orbit.aspx?satid=32789&lat=0&lng=0&loc=Unspecified&alt=0&tz=UCT&cul=en, accessed on 4 Dec. 2018

before and stops 5 seconds after reaching apogee. This step is repeated until Delfi-REAL's orbit perigee is reduced to that of Delfi-C3. This entire process is repeated to match the orbit apogees of Delfi-REAL and Delfi-C3. Another benefit of this method, as opposed to a continuous burn, is that the argument of the perigee does not shift, making it easier to determine when these burns must be performed. In the case that the inclination of the orbits do not match, a burn will be performed to align the orbits into one plane.

For a specific total engine thrust of 0.1 N, an initial system mass of 14.5 kg, and an engine burn time per orbit of 10 s, the following mission parameters were deduced. The Delta-V was approximated at $48\,\mathrm{m\,s^{-1}}$, the total number of burns required was 698, leading to a total orbit matching time of 46.9 days. This would be an orbit transfer from a 635 km circular orbit to the Delfi-C3 orbit, with an apogee altitude of 557 km and a perigee altitude of 536 km.

4.5. Coverage and Visibility

The coverage time of a satellite is the time that a satellite is visible from a single point on Earth. In order to predict the satellite's coverage time, the maximum nadir angle needs to be determined. Using this nadir angle, the visibility radius of the Delft ground station can be determined, shown in Figure 4.3. A single orbit is displayed to fly directly over the ground station. The time required to perform this fly-over is then calculated; this is indicated on Figure 4.3 as $T_{fly-over}$ The next step is calculating the shift per orbit. As the Earth rotates, the tracking line of the satellite on the ground moves in the opposite direction. This shift is called the shift in the Right Ascension of the Ascending Node (RAAN), indicated as $\Delta\Omega$ on Figure 4.3. The orbital shift is then used to calculate how many times a satellite flies in the visibility radius per day. The average of different orbits is then taken to estimate the average coverage time for the entire mission duration.

Nadir Angle

The visibility of the satellite was calculated for the situation that only the telemetry station in Delft is usable. In the case that a global array of antennae is employed, these values have to be revised. From Space Mission Analysis and Design (SMAD) [7], the equation for this angle is shown below, in Equation 4.5:

$$\sin\eta_{\max} = \frac{R_{\mathrm{E}}}{R_{\mathrm{E}}+h}\cos\epsilon_{\min} \tag{4.5}$$

here R_{E} is the Earth's radius, h is the altitude of the satellite, $\epsilon_{\min}$ is the minimum angle of visibility, and $\eta_{\max}$ is the maximum nadir angle. This angle denotes how much the satellite can see of the Earth at a specific altitude. This angle is corrected by the minimum angle an object has to be above the horizon before it is visible by the ground system. Using this maximum nadir angle, the maximum angle that the fly-over covers is calculated. Given that the nadir angle is dependent on the system's altitude, the calculation should be made with the semi-major axis of the orbit as the radius. From all these equations, a maximum angle λ of 37° is deduced.

Fly-over Duration

To determine the duration of the fly-over, the ratio of the fly-over angle and total angle is multiplied by the total orbital period. The duration of this fly-over is depicted by the center line in Figure 4.3 as $T_{fly-over}$ where the satellite flies directly over Delft. This equation is shown in Equation 4.6:

$$T_{fly-over} = \left(\frac{\lambda}{2\pi}\right)2\pi\sqrt{\frac{a^3}{\mu}} \tag{4.6}$$

Where λ is the fly-over angle, a the semi-major axis, μ the standard gravitational parameter of Earth, and $T_{fly-over}$ the fly-over time period. This method obtains a mean value for the fly-over duration as the semi-major axis is the mean orbital radius.

This value on its own does not provide a satisfactory estimate, as it depicts the time period during a single perfect fly-over. $T_{fly-over2}$ is an alternate orbit that does not fly over Delft directly; this is shown in Figure 4.3. The difference between $T_{fly-over}$ and $T_{fly-over2}$ can be seen on Figure 4.3. The satellite will not always orbit straight over the ground station. To calculate the average total fly-over duration per day, first, the amount of orbits that fly-over per day were calculated. It can be seen in Figure 4.3 that under certain conditions, the satellite only flies over once per day. Then, the actual fly-over time for each of these orbits was calculated. To obtain a full data set, the initial fly-over angle was shifted over an increment. Finally, an average of all these durations results in an estimate of the total fly-over period per day.

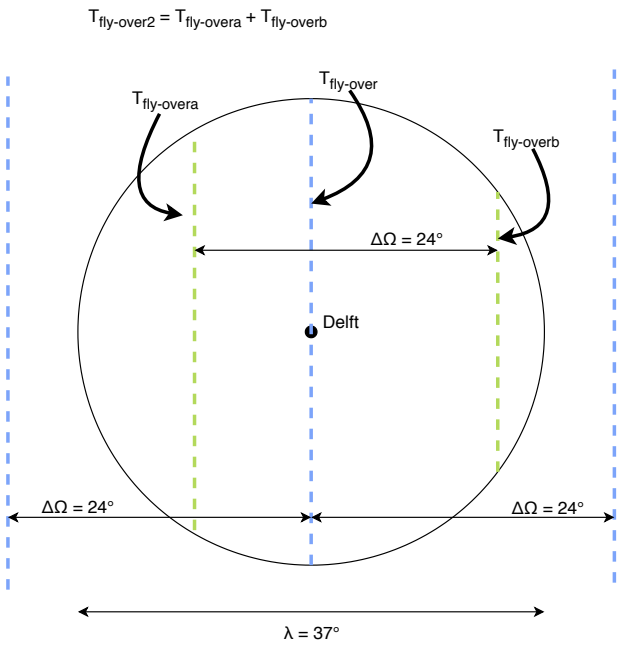

Figure 4.3: Orbital shift example. The circle denotes the visibility of the Delft ground station

To calculate the amount of fly-overs per day, the change in the RAAN per orbit, $\Delta\Omega$, has to be calculated. This shift[7] is depicted in Figure 4.3. There are two contributions to this change: the rotation of the Earth, and the shift due to higher gravity around the equator, the J_2 effect.

To calculate the Earth's rotation for the duration of one orbit, the Earth's rotation per second was multiplied by the orbital period, shown in Equation 4.7.

$$\Delta\Omega = \mathrm{P}\frac{2\pi}{86400} \tag{4.7}$$

In the above equation, P is the orbital period, and $\Delta\Omega$ is the change in the RAAN during this period. This resulted in a shift of the RAAN of 24° per orbit.

Right Ascension of the Ascending Node

Another parameter that effects the rate of change of the ascending node is the J_2 effect. This effect is caused by the variations in the gravitational field; more specifically, the J_2 effect is caused by the gravitational bulge along the equator. The equation used to calculate this is shown below, in Equation 4.8 [7]:

$$\Delta\Omega_{J_2} = -1.5nJ_2\left(\frac{R_\mathrm{E}}{a}\right)^2(\cos i)(1-e^2)^{-2} \tag{4.8}$$

Where n is the mean motion, J_2 is the geopotential expansion term, R_E is the Earth's radius, a is the semi-major axis, i is the orbit inclination, and e is the orbit eccentricity.

Due to the orbital inclination of the Delfi-C3 orbit, the $\cos i$ is very close to 0. This causes the J_2 effect to be negligible in comparison to the Earth's rotation. Hence, the shift in the ascension node per orbit is 24°.

Given that the change in RAAN per orbit is determined, the duration of the fly-overs can be calculated. This was done by calculating the length of each fly-over at its respective off-set from the perfect line.

Furthermore, to deduce the fly-over duration for many different situations, the previous step has to be iterated over multiple small increments in the ascension node. One such increment is shown in Figure 4.3, where the new total fly-over time is depicted by $T_{fly-over2}$. With all these data points, an average was taken to estimate the total fly-over duration of the satellite per day, which was estimated to be 600 seconds.

[7] `https://www.quora.com/How-long-does-it-take-to-photograph-the-surface-of-earth-with-one-satellite-at-a-resolution-similar-to-that-used-in-Google-maps-satellite-view`, accessed on 12, Dec. 2018

4.6. Satellite De-orbit

One of the ways in which the orbit altitude can be lowered, is by using passive systems. To determine the time this would take, a program was made in Python. This program has the characteristics such as mass, effective area and altitude of Delfi-C3 and the system as inputs. As output it has the orbital decay time. Assuming Delfi-C3 has been captured, a total mass of 16.8 kg and an effective area of 0.15 m^2 was estimated. Using the yearly average atmospheric density values provided by the National Aeronautics and Space Administration (NASA)[8] and a C_d of 0.8 , the natural orbital decay was calculated [7]. Equation 4.9 shows the change in semi major axis per revolution where A is the effective area, a is the semi major axis and m the combined system mass.

$$\Delta a_{\text{rev}} = \frac{-2\pi C_d A \rho a^2}{m} \tag{4.9}$$

The density in space varies highly every day. To take this into account in the de-orbit estimation, 5 different density measurements were used. These are the maximum, minimum, mean, mean plus 15 % and mean minus 15 %. The altitude-time graph of the satellite for these 5 densities can be seen in Figure 4.4. The leftmost line has the maximum density measured from 2008 till 2017 per altitude. The line on the right represents the decay in the case that the lowest density in the same time span is used. The middle line uses the average densities per altitude. As the densities vary a lot, a safety factor of 15 % was introduced. The lines left and right of the middle line represent the decay rate with this safety factor.

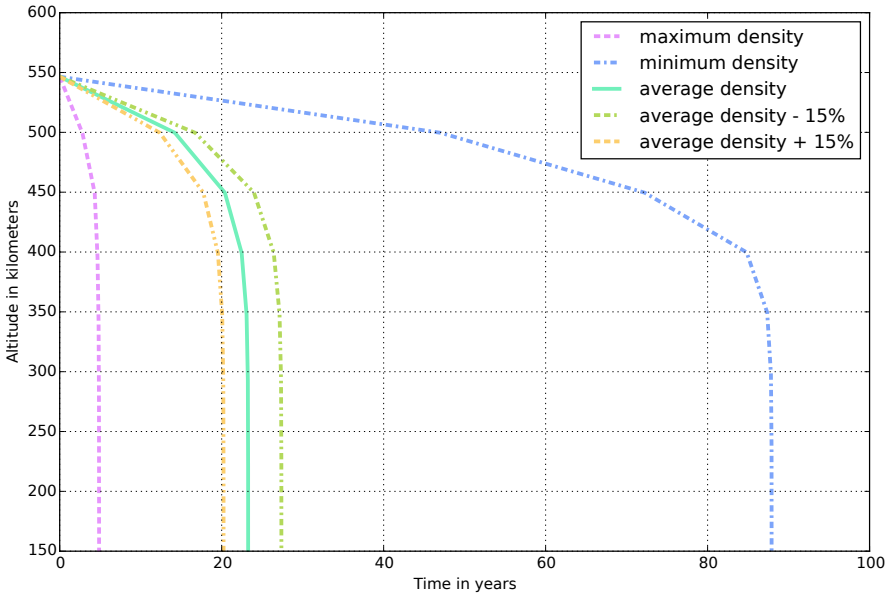

Figure 4.4: Altitude in km vs time in years

Using the method described in Section 4.4, a similar calculation can be made to calculate the Delta-V required to lower the perigee of the Delfi-C3 orbit to 150 km. This results in a Delta-V of 110 m s^{-1}, as shown in Equation 4.10.

$$\begin{aligned}\Delta V &= \sqrt{\mu\left(\frac{2}{r_{apo}} - \frac{1}{a_1}\right)} - \sqrt{\mu\left(\frac{2}{r_{apo}} - \frac{1}{a_2}\right)} \\ &= \sqrt{3.98\times10^{14}\,\text{m}^3\,\text{s}^{-2}\left(\frac{2}{6920\,\text{km}} - \frac{1}{6910\,\text{km}}\right)} - \sqrt{3.98\times10^{14}\,\text{m}^3\,\text{s}^{-2}\left(\frac{2}{6920\,\text{km}} - \frac{1}{6720\,\text{km}}\right)} = 110\,\text{m}\,\text{s}^{-1}\end{aligned} \tag{4.10}$$

4.7. Mission Time Stamps

From the calculations previously mentioned, a preliminary set of mission phase time stamps can be made. The mission will begin at launch, after which our satellite is inserted in an estimated circular orbit of 600 km. The inaccuracies of these launches are further discussed in Chapter 13. The duration of a launch varies widely between

[8] `https://ccmc.gsfc.nasa.gov/modelweb/models/nrlmsise00.php` accessed on 4 Dec. 2018

different launch vehicles. An example of a launch is given by the Ariane 5G User Manual [8], which states a duration of 60 minutes to insert a satellite into a Geostationary Transfer Orbit (GTO). Due to the relatively small duration of the launch in comparison to the other mission phases, the variations between the launch vehicles are negligible.

The next mission phase is orbit matching, explained in Section 4.4. The duration of this mission phase was approximated at 46.9 days. Once the satellite has reduced the orbital difference, the reconnaissance and capture procedure commences. The duration of this stage was estimated at 3 months, as this was deemed to be long enough to gather the required data and capture Delfi-C3.

Finally, the de-orbit and re-entry phase begins. The orbital altitude will be reduced from 550 km to 150 km by the use of the main thruster. This manoeuvre will take 103.4 days. When the system is at 150 km the atmospheric drag will be enough to reduce the altitude enough to return to earth in 25 minutes.

Adding up the different mission phases makes the total mission duration 242.3 days.

4.8. Landing Site

To meet landing requirements, a safe area has to be chosen. This area has to be clear of people and buildings at the time of landing. With an entry angle accuracy of 0.1°, the landing site diameter has to be 180 km. The site chosen is in Kazakhstan as found in Subsection 16.3.3 (page 83). This site was chosen as it is frequently used for the landing of the Soyuz module, so the required procedures are known. The area is also not inhabited, which decreases the risk of endangering anyone. The centre of the landing site can be seen in Figure 4.5[9]. As the heat shield is decoupled before landing, it will be ensured that it also lands in the designated area.

Figure 4.5: Landing site location in Kazakhstan

4.9. Verification & Validation

The Delta-V verification procedure comprises of performing a numerical simulation for the Hohmann transfer using instantaneous impulses. Furthermore, to verify the orbit decay model, a specific altitude and density is to be chosen and thus the deceleration of a space system can be found. Both parameters are to be checked for coding mistakes, separating it into different blocks to analyse the different outputs, and combining it into the final result.

For the validation of the orbit decay calculations, the International Space Station (ISS) presents an acceptable example on which the numerical model can be tested. The ISS was selected as the orbit decay rate is known with a high degree of accuracy. For the validation of the orbital velocity and period, Delfi-C3 itself can be used due to the wide access to its data and contact with participants in the project.

To validate the coverage and visibility calculations, the coverage and visibility of Delfi-C3 were used as they are well known.

[9] https://www.nasa.gov/mission_pages/station/expeditions/expedition34/e34_031513.html

5

Satellite Functions and Hardware Integration

Delfi-REAL will need to perform multiple essential functions during its lifetime. If these functions are to be executed properly, all subsystem hardware will need to be integrated with each other in a correct way. In order to reach this goal, first, all operational and logistical functions together with the system functions will need to be identified. To help identifying the functions, certain tools can be used. During the design process two tools were used: the Functional Flow Diagram (FFD) and the Functional Breakdown Structure (FBS). In this chapter the FBS and FFD will be presented and explained in Section 5.1 and 5.2. Then, the hardware integration is addressed with a hardware diagram in Section 5.3.

5.1. Functional Breakdown Structure

The FBS shows all functions Delfi-REAL is able to perform, with all functions grouped together in logical categories. It is depicted in Figure 5.1 on Page 17 and Figure 5.2 on Page 18. All functions were grouped in five high level functions Delfi-REAL is able to perform: the launch, adjusting the orbit (which includes re-entry and landing), approaching Delfi-C3, capturing Delfi-C3, and housekeeping functions. These high level functions are then divided in the subtasks that need to be performed for the high level function to succeed. This tool is useful to visualise the functions Delfi-REAL is able to perform and was used to identify further functions it needs to perform.

5.2. Functional Flow Diagram

The FFD shows the functions as they are performed during the mission in chronological order. These functions are derived from breaking down general mission steps into system or subsystem functions. It is shown in Figure 5.3 on Page 19 and Figure 5.4 on Page 20. In the first part of the FFD, shown in Figure 5.3, the first three main phases are shown. This part ends with a choice of either ending the mission after collecting image/video data, or continuing the mission. This specific choice was asked for by the main stakeholder and will be made by the client.

The FFD is less detailed then the FBS. However, due to the chronological order of the visualisation, a clear time line of all functions is shown. This will be an aid for further software development to identify the order of the software execution.

5.3. Hardware interface

In order to perform all functions described in Section 5.2, all hardware components need to be able to properly communicate with each other. Therefore, a Hardware interface is presented in Figure 5.5 on Page 21. This Hardware interface shows all links between the multiple subsystems and subsystem components. As can be seen in Figure 5.5, most links between subsystems go through the On Board Computer (OBC). There are two OBCs in Delfi-REAL for redundancy. In the hardware diagram they are shown as one OBC because they can be seen as one component as they can perform the same functions and are both connected to all the subsystems.

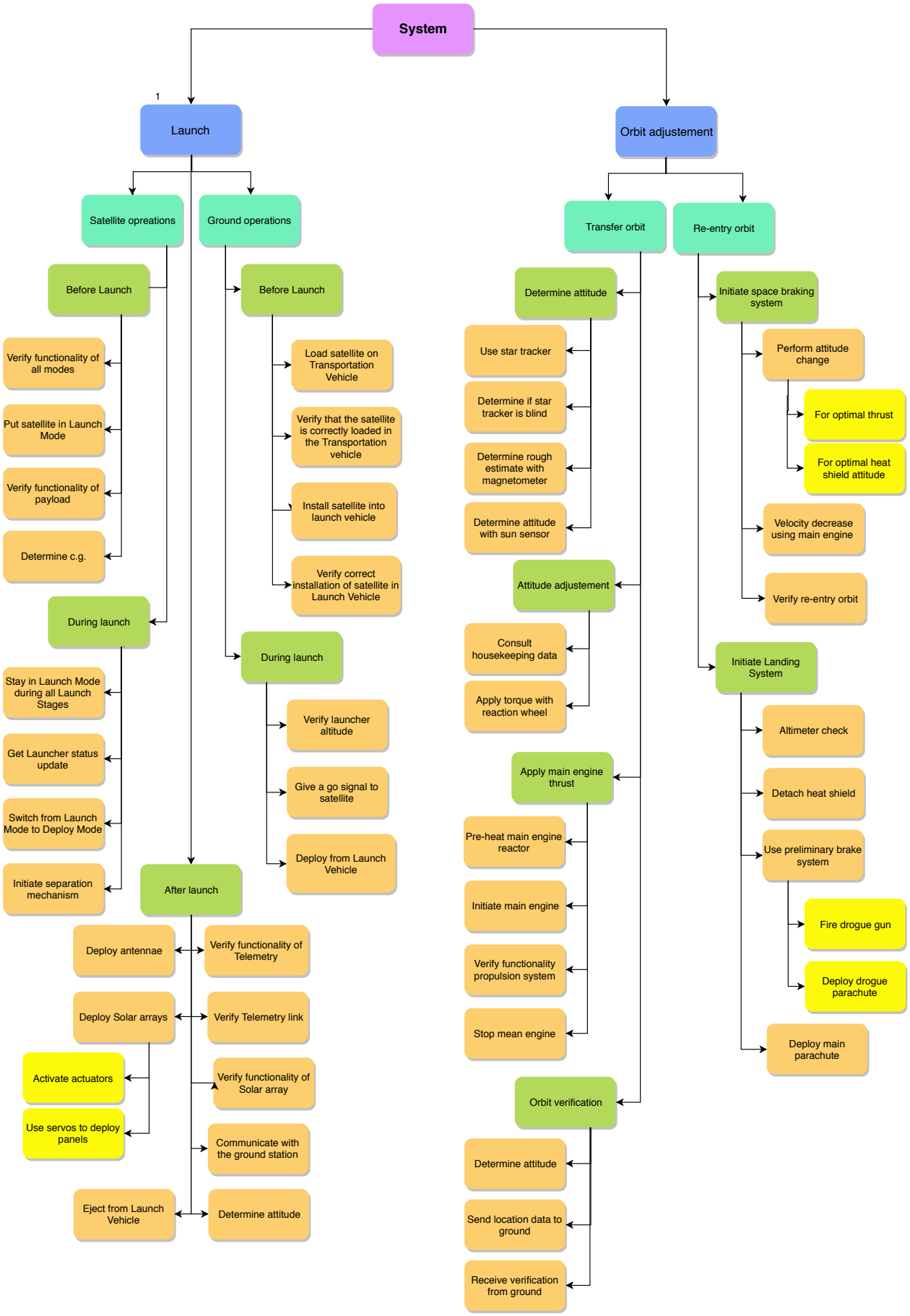

Figure 5.1: Functional Breakdown Structure part 1

Figure 5.2: Functional Breakdown Structure part 2

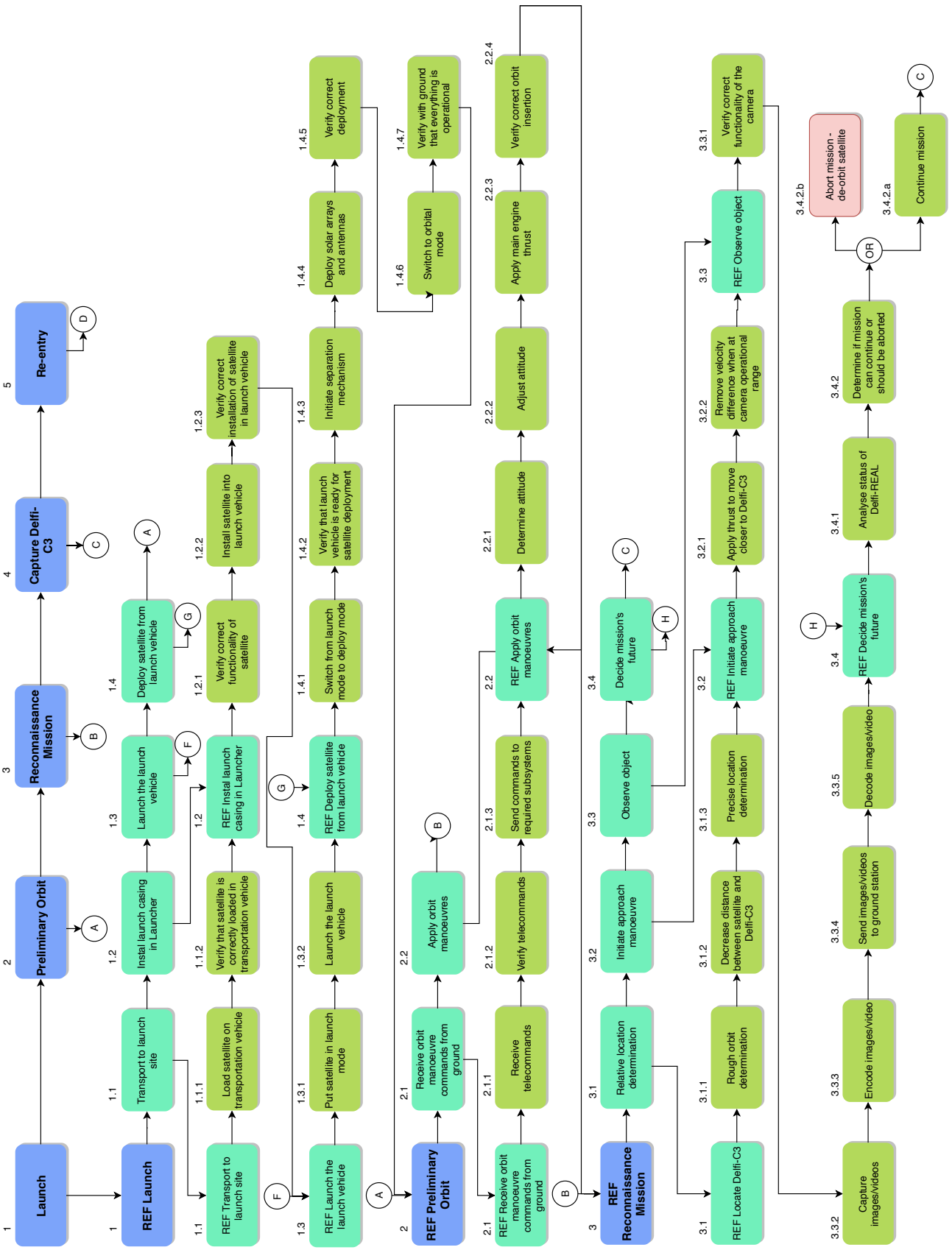

Figure 5.3: Functional Flow Diagram part 1

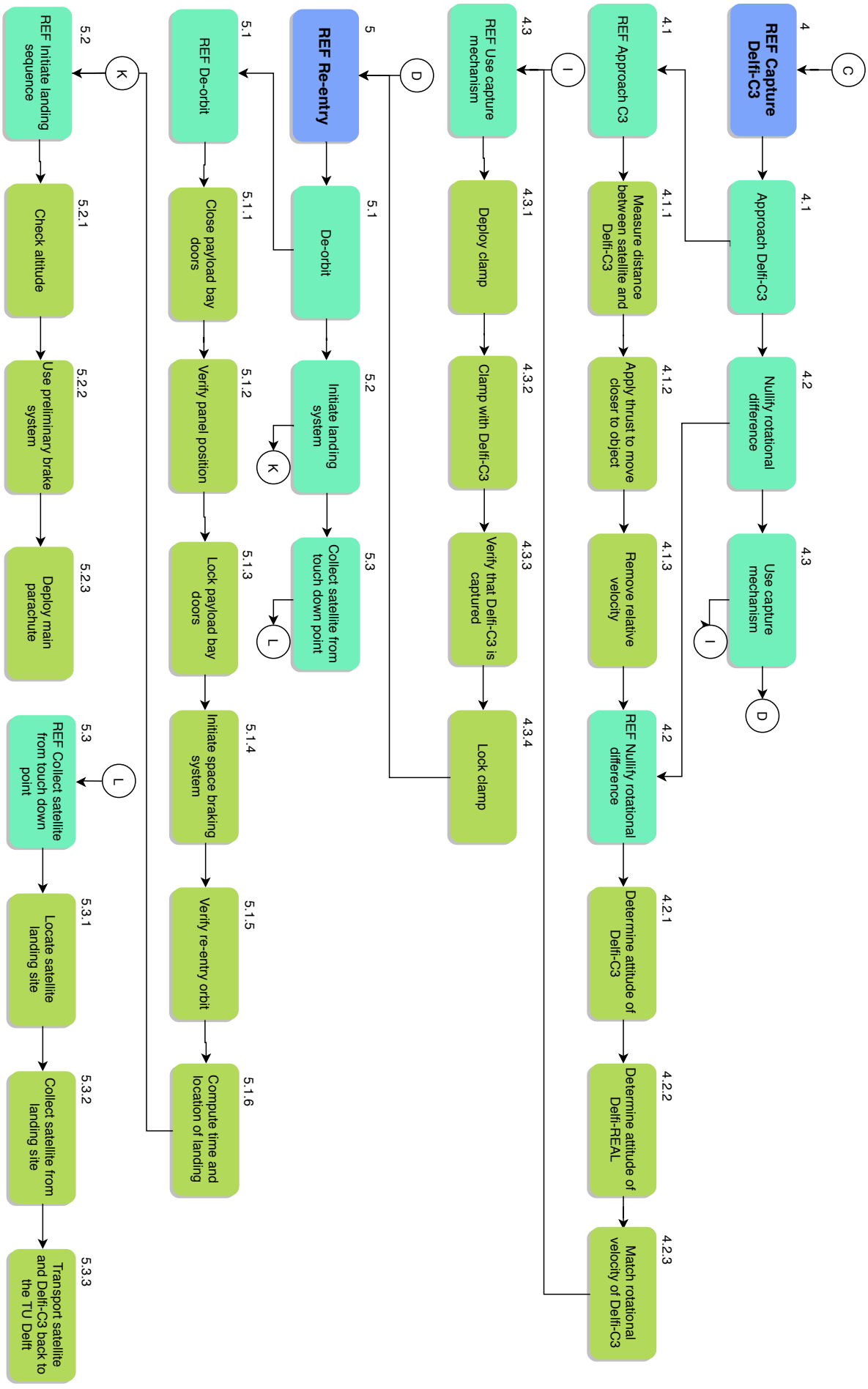

Figure 5.4: Functional Flow Diagram part 2

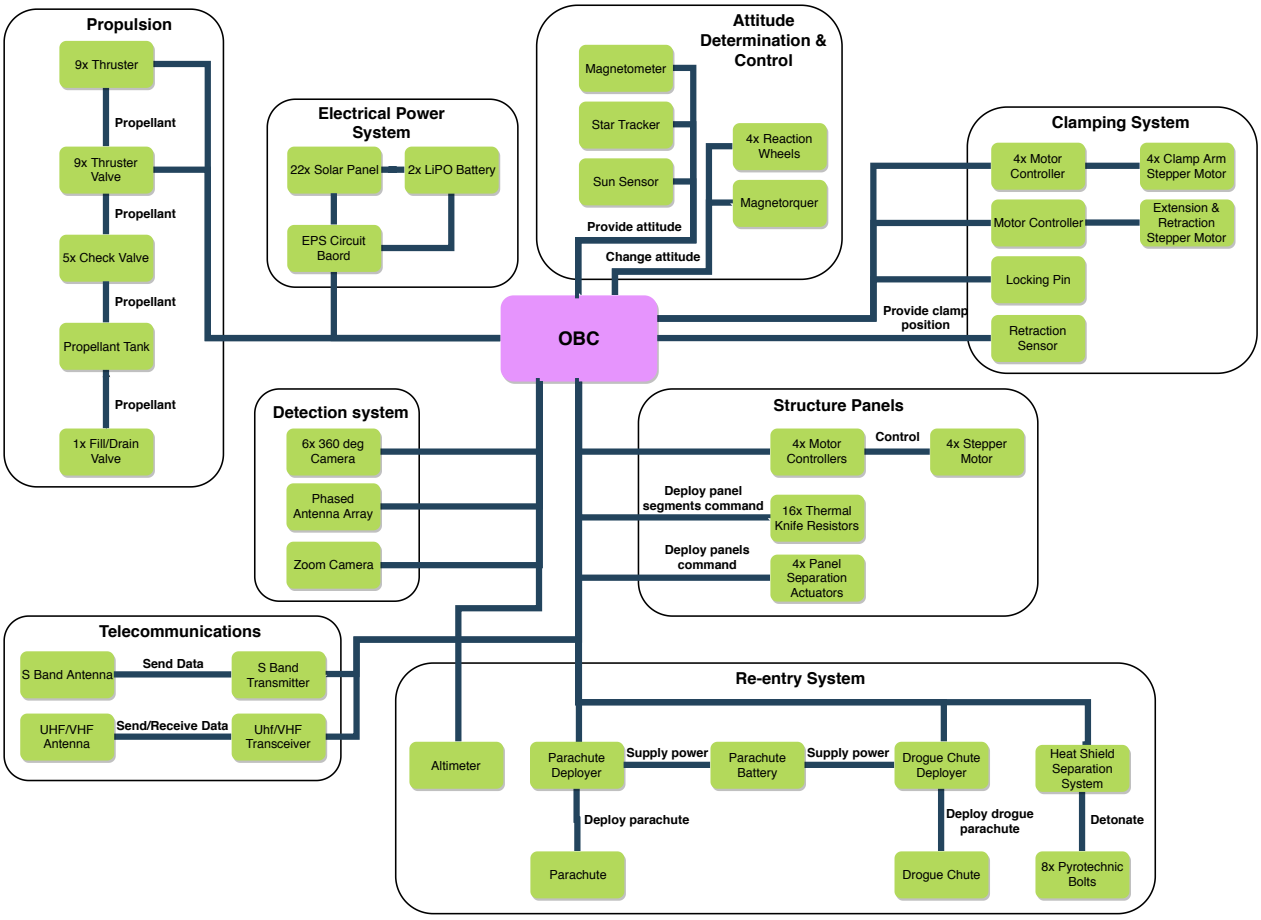

Figure 5.5: Hardware diagram

6
Attitude Determination and Control Subsystem

This section discusses the final design of the Attitude Determination and Control Subsystem (ADCS). First, a small explanation is given as to what the ADCS is and what its functions are, which is given in Section 6.1. In Section 6.2, the requirements are stated. In Section 6.3, the possible components are identified through a Design Option Tree (DOT) and concepts are sized to meet the requirements. Following this, a concept trade-off is performed, including criteria and weight determination, as well as a sensitivity analysis. The final design of the Attitude Determination and Control Subsystem is shown in Section 6.4. Finally, the verification and validation of the ADCS is discussed in Section 6.5.

6.1. Subsystem Function

The Attitude Determination and Control Subsystem (ADCS) is responsible for obtaining and controlling the orientation of the spacecraft. The ability of a spacecraft to control its orientation is important for a variety of subsystems such as propulsion, power, and telecommunication. The mission of Delfi-REAL also requires the capture of Delfi-C3. The design of the ADCS is divided into two sections: attitude determination and attitude control as these can be viewed independently as all components for each are compatible with one another.

Off-set Center-of-Gravity

The aim of the mission is to capture Delfi-C3. This means that an extra structure will be added during the mission, which results in an inevitable shift in the center-of-gravity (c.g.) of the total system. Doing so causes the moment arm of the main thruster to change, thus changing the moment. This moment has to be counteracted by the ADCS whenever the main engine is firing. This adds a minimum torque and momentum storage requirement on the subsystem.

In Chapter 17, the center-of-gravity (c.g.) of the initial subsystem is calculated to be 58 mm above the bottom of the structure. The c.g. of Delfi-C3 was estimated to be in the center of the rectangular body. Using these two values as well as the respective masses of Delfi-REAL and Delfi-C3, a new c.g. can be calculated. This causes a shift in the c.g. of 31 mm.

6.2. ADCS Requirements

The requirements were refined by analysing the mission phases and determining minimum condition for the ADCS.

Furthermore, the mass, cost, size, and power were estimated in the Technical Performance Measurement (TPM) in Chapter 22 on page 111. Although these values are allowed to vary, they will be used as a baseline to compare the different components.

RQ-ADCS-01	The ADCS shall be able to determine the attitude of Delfi-REAL.
RQ-ADCS-01.01	The ADCS shall have a determination accuracy of 0.1° during daylight.
RQ-ADCS-01.02	The ADCS shall have a determination accuracy of 1° during eclipse.
RQ-ADCS-01.03	The ADCS shall have a determination range in all directions.
RQ-ADCS-02	The ADCS shall be able to control the attitude of Delfi-REAL.
RQ-ADCS-02.01	The ADCS shall have a control accuracy of 0.1°.
RQ-ADCS-02.02	The ADCS shall have a control range in all directions.
RQ-ADCS-03	The ADCS shall have a mass no larger than 1.5 kg.
RQ-ADCS-04	The ADCS shall cost less than EUR 190 k.
RQ-ADCS-05	The ADCS shall have a volume no larger than 1.2 U.
RQ-ADCS-06	The ADCS shall have a maximum power consumption of less than 2.7 W.

6.3. Component Trade-Off

As stated before, the design of the ADCS can be divided into two parts; attitude determination and attitude control. These can be viewed independently as all components for each are compatible with one another.

6.3.1. Design Option Tree

The attitude determination subsystem is responsible for measuring the orientation of the spacecraft. There are two key mission phases during a Low Earth Orbit (LEO): daylight and eclipse. The possible components can be seen in the Design Option Tree (DOT) in Figure 6.1.

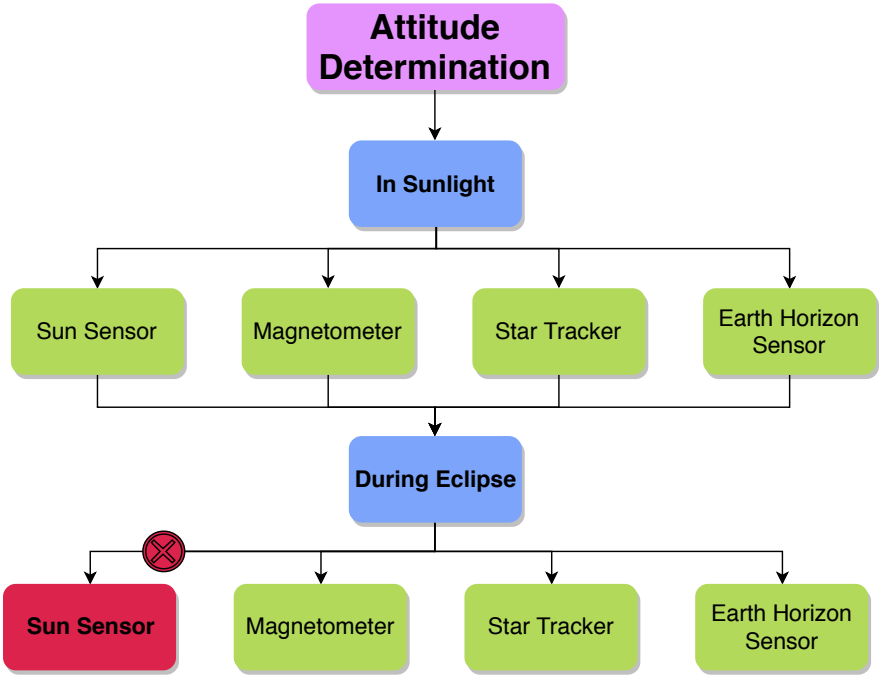

Figure 6.1: Attitude Determination Design option tree.

There are four different attitude determination subsystems available for nano-satellites: a sun sensor, a magnetometer, a star tracker, and an Earth horizon sensor.

A sun sensor determines the angle of the sun with respect to the satellite. This requires the sensor to have the Sun within its Field Of View (F.O.V.) to be functional.

A magnetometer determines the satellite's orientation with respect to a magnetic field; in this case, Earth's magnetic field. Even though this only requires the satellite to stay within the Earth's magnetic field, magnetic components within the satellite can off-set this measurement. A full pre-flight test should be performed to measure the full effects of the shape of Delfi-REAL and subsystems on the magnetometer measurements.

A star sensor determines the orientation of a satellite by comparing a taken image with an entire star library. This sensor does not work if it faces the Sun or the Earth.

An Earth horizon sensor scans a line within its field of view (F.O.V.) to detect a difference in infrared radiation. Similarly to the previous sensor, if this sensor does not have its target, the Earth, within its field of view (F.O.V.), it is incapable of determining the orientation. Two Earth horizon sensors are required for full orientation knowledge.

There are only two electronically powered options available for attitude control for nano-satellites. These are reaction wheels and magnetorquers. Reaction wheels are capable of providing a larger torque than magnetorquers, but require desaturation after a certain time period as reaction wheels have a maximum rotations per minute (RPM). For this reason, it was decided that both reaction wheels as well as magnetorquers would be used. The magnetorquers will be capable of desaturating (de-spinning) the reaction wheels.

Attitude control using micro-thrusters should be avoided as the limited propellant should be used exclusively for small positional changes.

6.3.2. Component Sizing

Using the requirements stated in Section 6.2, the ADCS components was sized for each concept. The sizing of the the components for both the attitude determination and the attitude control subsystems was performed using data of Commercial Off-The-Shelf (COTS) components. Concepts that undergo the trade-off are designed to meet the requirements for both daylight and eclipse. The concepts are therefore more detailed than the DOT and can include combinations of different components. The cost, power, accuracy, volume, and mass are taken from the component documentation[1] available.

Attitude Determination

A list of the different attitude determination components and their relevant parameters are shown in Table 6.1. The parameters may vary slightly depending on the specific product but they are similar enough to provide a baseline for a trade-off.

Table 6.1: Attitude Determination Subsystem Components

Component name	**Mass** [g]	**Cost** [EUR]	**Size** [mm]	**Accuracy** [°]	**Power** [mW]
Magnetometer	196	8000	95.9 × 90.1 × 17	1	1200
Sun Sensor	120	300	34 × 32 × 20	0.1	210
Star Tracker	250	30 000	45 × 50 × 95	0.003	2000
Earth Horizon Sensor	66	14 900	43.3 × 31.8 × 31.8	0.25	132

Different combinations of the aforementioned attitude determination components were made to create the following concepts.

- **Magnetometer Only:** A 3 axis magnetometer has an accuracy of 1°, a total maximum power of 750 mW and a total mass of 85 g.
- **Sun Sensors + Magnetometer:** The sun sensors are incapable of determining the attitude during eclipse. For this reason, a magnetometer has to be included. A single sun sensor has an F.O.V. of 140°, an accuracy of 0.1°, a maximum power of 130 mW, and a mass of 35 g. Under ideal circumstances, only four sun sensors are required for full attitude determination in daylight. However, due to the shape of Delfi-REAL and the use of payload doors, shown in Figure 3.8 on page 8, multiple blindspots are present. To compensate for these blindspots, seven sun sensors are required. This results in a total maximum power of 1660 mW and a total mass of 330 g. The volume required for this design is 0.15 U and the cost is EUR 84 k.
- **Star Trackers Only:** A star tracker can identify the orientation in all three axes whenever it faces the stars. A single star tracker has a maximum power of 1000 mW, a mass of 250 g, and an accuracy of 0.003°. A star tracker, however, has two blind spots: the Sun and the Earth. To compensate for these blindspots, three star trackers are required, as two star trackers could still be alligned to face the Sun and Earth simultaneously. The total maximum power for this design is 3000 mW, the total mass is 750 g, the volume is 0.64 U, and a cost of EUR 90 k.
- **Earth Horizon Sensors Only:** This design is similar to that of the "Sun Sensors + Magnetometer" design as Earth horizon sensors also require a specific target to be in range. An Earth horizon sensor has an F.O.V. of 60°, an accuracy of 1°, and is capable of determining the attitude during eclipse, due to its infrared vision. A single Earth horizon sensor has a maximum power of 132 mW and a mass of 33 g. Due to the complex shape of Delfi-REAL and all the blindspots, ten Earth horizon sensors are required to cover all angles. This design requires a total maximum power of 1320 mW and a total mass of 330 g. The volume required for this design is 0.43 U and the cost is EUR 149 k.
- **Star Trackers + Sun Sensors:** For this design two star trackers and two sun sensors, forming pairs, are used. The pairs are positioned at 180° from one another. The sun sensors are used in the case the star tracker is blinded by the Sun, and two star trackers are used to ensure that at least one star tracker is facing away from the Earth. This design requires a total maximum power of 2260 mW and a total mass of 570 g. The volume required for this design is 0.47 U and the cost is EUR 84 k.
- **Star Tracker + Magnetometer:** This design utilises a single star tracker and magnetometer. The magnetometer's measurements are used to determine the attitude of Delfi-REAL with respect to the Earth. With this knowledge, Delfi-REAL can be rotated to ensure that the star tracker does not face the Earth. This results in

[1] `https://www.cubesatshop.com/` accessed on 14 Jan. 2019

a single blindspot, the Sun. This design has a total power of 1750 mW and a total mass of 335 g. The volume required for this design is 0.47 U and the cost is EUR 84 k.

- **Star Tracker + Sun Sensor + Magnetometer:** This design is the same as the one above except that it removes the blindspot of the star tracker by pairing it with a sun sensor. This design requires a total maximum power of 1880 mW and a total mass of 370 g. The volume required for this design is 0.23 U and the cost is EUR 42 k.
- **Earth Horizon Sensors + Magnetometer:** This design utilises a set of Earth horizon sensors for precise measurements, with an accuracy of 0.25° for an F.O.V. of 7°, and a magnetometer for coarse attitude determination, with and accuracy of 1°. This coarse measurement is used to rotate Delfi-REAL so that the Earth is within the F.O.V. of the Earth horizon sensors. This design requires a total maximum power of 885 mW and a total mass of 118 g. The volume required for this design is 0.45 U and the cost is EUR 112 k.

Note that for normal operations or main engine use, a single degree of freedom is present; this is the axis about the thrust vector from the main engine. This grants the possibility to "un-blind" certain sensors prior to firing the engine by rotating about this vector.

Attitude Control

After calculating the c.g. shift in Section 6.1, the torque generated by an off-set thruster can be calculated. For a thruster of 0.125 N, a torque of 2.75 mN m is applied to Delfi-REAL. It was found that two COTS reaction wheels, which each produce 2.3 mN m of torque would suffice. Furthermore, given the variability in the c.g. in the other axes due to the movable parts of Delfi-REAL, it was determined that a similar c.g. off-set should be considered. Therefore, one reaction wheel of 2.3 mN m should be placed for each other axes. As stated in Section 6.6, the design can be optimised further once the true center-of-gravity of Delfi-REAL is known.

These four reaction wheels have a total mass of 800 g, a peak power of 8800 mW, a volume of 0.4 U, and a cost of EUR 26 k.

The magnetorquers are sized so that the reaction wheels can be desaturated completely over a duration of 90 % of the orbit. This means that for a maximum momentum storage of 30 mN m s and a duration of 5700 s, a minimum torque (T) of 5 µN m is required. Using Equation 6.1, from SMAD [7], and a worst-case magnetic field strength (B) of 45 µT, the minimum magnetic dipole (D) was calculated.

$$D = \frac{T}{B} = \frac{5 \times 10^{-6}\,\mathrm{N\,m}}{45 \times 10^{-6}\,\mathrm{T}} = 0.11\,\mathrm{A\,m^2} \tag{6.1}$$

A standard nano-satellite magnetorquer has a magnetic dipole of 0.2 $\mathrm{A\,m^2}$, which delivers enough redundancy allowing the reaction wheels to be desaturated within a smaller time period. Using available COTS components, a magnetorquer board capable of 3 axis control is chosen. This specific component includes a magnetometer. Therefore, any concepts including a magnetometer will not include the mass of the magnetometer during the trade-off, since it is already included in the mass of the magnetorquer. This component has a maximum power of 1200 mW, a maximum mass of 196 g, a maximum volume of 0.15 U and a cost of EUR 8 k.

The attitude control subsystem therefore has a total maximum power of 10 W, a total maximum mass of 996 g, a total maximum volume of 0.55 U, and a total cost of EUR 34 k. The maximum power required for the attitude control subsystem alone is higher than the original TPM. After discussing this issue with the electrical power subsystem engineer, the maximum power budget for the ADCS was expanded to 11 W.

6.3.3. Trade-Off

To perform a trade-off, three steps have to be performed; the criteria have to be stated, the trade-off has to be performed, and a sensitivity analysis of this trade-off has to be made. It should be noted that only attitude determination concepts are traded off.

Criteria

The criteria used to evaluate the different attitude determination components are listed below. The individual requirements for the attitude determination subsystem are stated within these criteria. The standard criteria: mass, cost, complexity, reliability, and volume are explained in-depth in Chapter 3 on page 4.

- **Mass 5/10** - The requirement on the maximum mass of the attitude determination subsystem is 500 g.

Table 6.2: Design concept trade-off table for the ADCS. excellent: excel, nominal: nom, exceeds requirement: exreq, unacceptable: unacc

Option \ Criterion	Mass	System cost	Complexity	Reliability	Vol	Accuracy	Power
Magneto-meter Only	excel	excel	excel	excel	exce	unacc	excel
Sun Sensors + Magnetometer	excel	excel	unacc	exreq	nom	nom	nom
Star Trackers Only	unacc	excel	excel	excel	nom	excel	unacc
Star Trackers + Sun sensors	unacc	excel	unacc	nom	exce	nom	unacc
Star Tracker + Magnetometer	excel	excel	nom	excel	exce	excel	nom
Star Tracker + Sun Sensor + Magnetometer	excel	excel	excel	excel	exce	excel	exreq
Earth Horizon Sensors Only	excel	excel	unacc	unacc	exce	unacc	exreq
Earth Horizon Sensors + Magnetometer	excel	excel	nom	excel	exce	unacc	excel

- **System Cost 8/10** - The requirement on the maximum cost of the attitude determination subsystem is EUR 160 k.
- **Complexity 7/10** - The complexity of the attitude determination subsystem is defined by the amount of potential issues arising from blindspots due to the variable shape of Delfi-REAL. Delfi-REAL should always be capable of determining its attitude. If a concept has no blindspots, it will be graded as excellent. If a concept has a known blindspot it will be graded as nominal. If a concept has an unpredictable blindspot, it will be graded as unacceptable.
- **Reliability 9/10** - The reliability of the subsystem is dependent on the amount of failure points; more components is more failure points. Concepts with two or less components are graded as excellent. Concepts with 3 to 5 components are graded as nominal. Concepts with 6 to 9 components are graded as exceeds requirements. Concepts with ten or more components will be graded as unacceptable.
- **Volume 2/10** - The requirement on the maximum volume of the attitude determination subsystem is 0.65 U.
- **Accuracy 9/10** - The accuracy of the attitude determination subsystem is essential for the mission to be successful. If the accuracy of the subsystem is not good enough it could mean that orbit matching with Delfi-C3 is not possible which leads to a mission failure. For this reason, the accuracy was weighted at 9/10. The accuracy required during daylight is 0.1° and during eclipse is 1°.
- **Power 6/10** - The maximum power requirement for the attitude determination subsystem is 1000 mW. This criterion is weighted at 6/10 because the power requirement for the ADCS is small in comparison to the maximum power generation by the electrical power system.

From the trade-off shown in Table 6.2, there are only two concepts available which do not contain any criteria deemed unacceptable. These concepts are the "Star Tracker + Magnetometer" and the "Star Tracker + Sun Sensor + Magnetometer".

6.3.4. Sensitivity Analysis

The two feasible concepts only differ by a single component; a sun sensor. This means that the mass, cost, and volume differ only slightly which is visualised in the trade-off, Figure 6.2. Adjusting the values for these criteria by 30 % does not change the trade-off result.

The only criterion that changes is Power. If the power of each concept is increased by 30 %, both concepts will become unacceptable for the Power criterion. The adjusted trade-off table is show in Table 6.3. Due to the lack of changes, it can be concluded that the result of the trade-off was correct. It is important to note that with proper engine management, the reaction wheels do not have to be actuated simultaneously, which reduces the power consumption significantly.

Given that the minimal difference in power required by the two concepts and the additional functionality of the extra sun sensor, the second concept was chosen to be the final design for the attitude determination subsystem.

The magnetometer can easily deduce the relative orientation with the Earth but extra information is required to determine the position of the Sun, in the case that the star tracker is blinded.

Table 6.3: Trade-off sensitivity for Power for the ADCS. excellent: excel, nominal: nom, exceeds requirement: exreq, unacceptable: unacc

Option \ Criterion	Mass	System cost	Complexity	Reliability	Vol	Accuracy	Power
Star Tracker + Magnetometer	excel	excel	nom	excel	exce	excel	unacc
Star Tracker + Sun Sensor + Magnetometer	excel	excel	excel	excel	exce	excel	unacc

6.4. Final Design

Using the analysis performed in Section 6.3, the final design of the ADCS was determined. The total mass is 1300 g, the total peak power is 11.8 W, the total volume is 0.79 U, and the system cost is EUR 76 k.

The different components are discussed in their individual sections. In Section 6.4.1 and Section 6.4.2, the costs and sizings of the components for attitude determination and attitude control are discussed, respectively. The c.g. range of Delfi-REAL and stability characteristics are discussed in Section 6.4.3.

6.4.1. Attitude Determination

The attitude determination subsystem was designed so that the highest accuracy can be provided during daylight. During daylight, all the payload measurements are made, and eventually Delfi-C3 will be captured. For this reason, it was determined that an accuracy of less than 0.1° was required.

It was determined that the most optimal solution is composed of a magnetometer, a star tracker, and a sun sensor. A three step attitude determination process is utilised. Firstly, it is determined if the star tracker is blinded. Secondly, if the star tracker is blinded by the Earth, the magnetometer determines the coarse orientation of Delfi-REAL and adjusts the attitude to un-blind the star tracker. Finally, the star tracker determines the orientation of Delfi-REAL in an un-blinded position. If the star sensor is still blinded by the Sun, the sun sensor, which is placed facing the same direction, determines the attitude. This design provides a coarse accuracy of 1°, a sun-blinded accuracy of 0.1°, and an optimal accuracy of 0.003°.

During the eclipse period however, visual contact with Delfi-C3 is lost and no measurements can be made. During this period, it was decided that communication downlink would still be possible. To perform the communication downlink, it was determined that an accuracy of 1° was enough. The design's performance, however, does not vary between daylight or eclipse and the same process stipulated above can be used to determine the attitude.

The suggested star tracker is the KU Leuven Star Tracker [9] and the suggested sun sensor is the NSS Fine Sun Sensor [10]. The magnetometer, as stated earlier, is a component of the ISIS Magnetorquer board [11]. These components are available on the CubeSatShop.[2]

The positions of the sensors is shown in Chapter 18 on page 101. It is important to note that all the attitude determination sensors deliver a relative orientation. This means that if the sensors are mounted to the satellite at a different angle than intended, they will also determine the orientation at a different angle. A pre-flight calibration test should be used to mitigate this issue.

Further accuracy in pointing knowledge is determined by the main mission phase, capturing Delfi-C3. This mission phase, however, is dependent on the relative position with Delfi-C3 for which a specific set of sensors will be used. This is discussed in depth in Chapter 10 on page 47.

6.4.2. Attitude Control

The attitude control subsystem comprises of four large reaction wheels and a magnetorquer board. The coordinate system is described in Section 14.3 on page 71. This provides a maximum torque of 2.3 mN m about the x-axis, 4.6 mN m about the y-axis, and 2.3 mN m about the z-axis. The reaction wheels on these axes have a maximum

[2] `https://www.cubesatshop.com/` accessed on 14 Jan. 2019

momentum storage of 30 mN m s, 60 mN m s, and 30 mN m s respectively. The magnetorquer board, with a magnetic dipole of 0.2 A m^2 is used to desaturate these reaction wheels.

The suggested reaction wheels are the CubeWheel Large [12] and the suggest magnetorquer is the ISIS Magnetorquer board [11]. These components are available on the CubeSatShop.[3]

Since all attitude determination sensors have an update frequency, a discrepancy between real and measured rotation will always be present. To minimise this issue, all manoeuvres and thrust commands should be simulated prior to initiation to predict the effects on the attitude, thus allowing the attitude control subsystems to fire simultaneously.

Before manoeuvres, reaction wheel housekeeping data should be consulted. This is required to ensure that the reaction wheels do not reach their maximum rotations per minute (RPM) during the manoeuvre.

6.4.3. System Stability and Controllability

Due to the symmetrical shape of Delfi-REAL and the relatively large surface area of the payload bay doors, the center of pressure is determined to be behind the center-of-gravity, if the bottom of the heatshield is seen as the front. This stabilising force is negligible in comparison to the control forces, but will naturally cause Delfi-REAL to be stable in the direction of the resultant drag force.

The attitude control subsystem is designed to deliver a maximum torque of 4.6 mN m about the y-axis and 2.3 mN m about the x- and z-axis. Given these limitations, the maximum c.g. range can be determined as a function of thrust. This is show in Figure 6.2. The c.g. shifts due to production accuracies, propellant use, payload bay door movement, and capturing Delfi-C3.

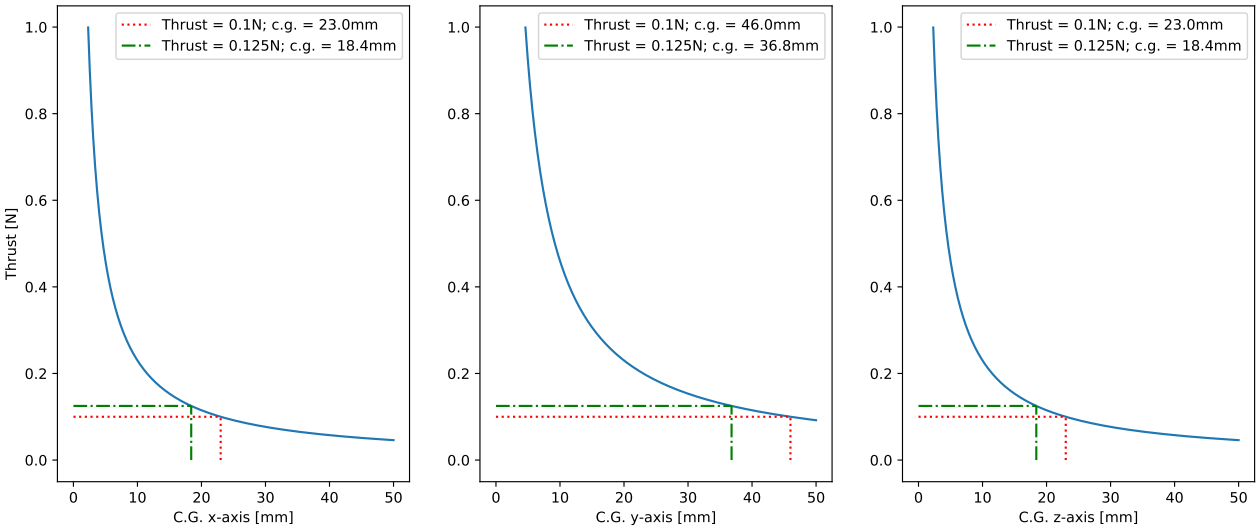

Figure 6.2: C.G. limit per Thrust about positive x-, y-, z-axis. The same limit applies in the negative direction.

For example, as long as the thrust vector for a thrust of 0.1 N goes through a point which lies in between the origin and the red dashed line, the ADCS will be able to control the attitude.

The actual center-of-gravity (c.g.) of the satellite should be measured before the flight, preferably in all positions of the payload doors.

6.5. Verification and Validation

The ADCS design will be verified through the use of a simulation. The ADCS components available on the CubeSatShop[3] are verified and validated by their individual supplier through official certifications.

The ADCS components will be validated through individual tests to ensure correct functionality post delivery before assembly. The Attitude Determination and Control Subsystem will be validated through a full-scale test where multiple sensor inputs are used to test the attitude determination subsystems and external forces are applied to Delfi-REAL to test the attitude control subsystem. These inputs will be representative of those encountered during the mission, therefore showing that the customer needs are met.

[3] `https://www.cubesatshop.com/` accessed on 14 Jan. 2019

6.6. Future Recommendations

To improve the ADCS even further, special care can be taken during assembly to reduce the variance in the center-of-gravity of Delfi-REAL and the pointing vector of the main engine. This would allow for the reduction of the size of the x-axis and z-axis reaction wheels. This can potentially save a total mass, cost, volume, and peak power of 280 g, EUR 4.4 k, 0.16 U, and 3.2 W respectively.

7
Detection Subsystem

In this section the process of detecting the system's position and rotation relative to Delfi-C3 at different distances is elaborated upon. The requirements from previous analysis are given below.

Delfi-C3 Detection

RQ-DTCT-01	The system shall not fully eclipse Delfi-C3.
RQ-DTCT-02	The system shall be able detect Delfi-C3 visually using cameras when closer than 200 m.
RQ-DTCT-03	The system shall be able to detect Delfi-C3 still when eclipsed.
RQ-DTCT-04	The system shall do docking only when Delfi-C3 is illuminated to allow high accuracy visual position detection.
RQ-DTCT-05	The system shall match a 3d model to the picture of Delfi-C3 to determine both distance and rotation by camera.
RQ-DTCT-06	The system shall use the combination of the individual camera measurements and known camera position to triangulate position with increased accuracy.
RQ-DTCT-07	The system shall interpolate position measurements over time to create an iteratively refined position estimation.
RQ-DTCT-08	The OBC needs to perform real-time analysis and object detection using up to 4 4k 360° camera feeds with at least 20 fps.
RQ-DTCT-09	The capture procedure shall only be executed while Delfi-C3 is illuminated by the Sun.

7.1. Detection at Large Distance

The orbit tracking from the ground station is accurate to within 1 km of Delfi-C3 position.[1] The system needs to align with the same orbit by matching the inclination and altitude to be able to rendezvous with Delfi-C3. From the position of the system relative to Delfi-C3 it can be determined if it is in front or behind Delfi-C3 along the orbit. From this the general direction to approach Delfi-C3 can be found.

Next, radar is used to determine the direction of Delfi-C3. Most radar systems in space are created to detect objects on earth and vastly exceed the size and mass constraints for this mission. A better approach without moving parts is using a phased antenna array patch[2] to determine the direction of Delfi-C3 more accurately.

When Delfi-C3 is transmitting, the antenna array can be used as passive radar. The signal will arrive at the patches on the antenna array at different times causing slight phase shifts, which results into a distinct interference pattern. The analysis of this pattern allows the direction of signal origin to be determined. When the target is not able to transmit by itself, the antenna array can be used as an active array by using the S-Band antenna (normally used for data down link, see Section 9.3.1 on page 43) as a signal source. This requires the antenna array patch to be directed the same as the S-Band antenna on the system. A good choice of array patch antenna for this purpose is sold by Endurosat[3].

7.2. Detection at Medium Distance

Once the system has acquired the position of Delfi-C3 using the phase antenna array radar it can begin moving towards Delfi-C3. A zoom camera can optically detect Delfi-C3. For this an object detection algorithm is run on the on-board computer (OBC). When Delfi-C3 is eclipsed, the cameras will not be able to detect it. Therefore, all relative velocity of Delfi-REAL should be removed when approaching eclipse while being near Delfi-C3. To be able to detect Delfi-C3 with a height of 15 px at a distance of 200 m using a resolution of 3840 px × 2160 px, a field of view of 12.4° is required.

[1] `https://heavens-above.com/orbit.aspx?satid=32789&lat=0&lng=0&loc=Unspecified&alt=0&tz=UCT&cul=en`, accessed on 4 December 2018
[2] `http://rfmicrotech.com/products-smart-solutions/antennas-and-phased-arrays/` accessed on 7 December 2018
[3] `https://www.endurosat.com/products/cubesat-x-band-4x4-patch-array/#scroll-to` accessed on 17 Jan. 2019

7.3. Detection at Close Distance

Once much closer to Delfi-C3, 360° fish-eye cameras can be used to visually cover all directions around the system such that Delfi-C3 can be tracked at all possible relative rotations. This positioning method can only be used while illuminated by the Sun. Therefore, it is recommended to only move relative to Delfi-C3 in that case. The 360° cameras need to be able to accurately detect Delfi-C3 during the process of capturing. Assuming the camera to be placed on top of an unfolded side panel with a height of 30 cm then the distance to the point of contact of the clamp would be approximately 35 cm. For a camera resolution of 3840 px × 2160 px and field of view of 220°, the spatial resolution is 0.62 mm. This spatial resolution is therefore the expected tracking error from a single frame. A more accurate measurement can be taken by sampling the position frequently, for example at 20 fps, and then interpolating between the measured positions.

7.4. Commercial Camera Hardware in Space

The cameras selected are Commercial Off-The-Shelf components. However while there have been examples of many commercial cameras in space, for example with high altitude weather balloons or on the ISS, care needs to be taken to select an appropriate camera. It needs to be tested to confirm the camera can function in vacuum. Especially there may be no air trapped in the lens assembly. Multiple cameras can be employed to increase reliability and accuracy of the system by combining multiple measurements.

7.5. Camera Selection

The system will have seven cameras in total. The first camera is the high definition zoom camera with a resolution of 3840 px × 2160 px and a field of view of 12.4°. This camera[4] will have a size of about 110 mm × 50 mm × 65 mm and a mass less than 300 g. The other six cameras will be fish-eye lens wide angle cameras. These cameras will be smaller than 30 mm × 20 mm × 20 mm and will have a mass below 20 g each. The total power required for the six wide angle cameras shall stay below 210 mW[5]. Two of the 360° cameras are placed facing the same direction as the clamp. If one of them fails the other will be sufficient for the problem, however with the penalty of reduced accuracy.

7.6. Detection System Components

The discussed solutions are the only approaches found applicable to solve the detection problem. The phased antenna array is insufficient as a standalone solution, due to its low accuracy. Especially when close to Delfi-C3 accuracy is very important as the relative location and rotation information is used by the propulsion system to align the clamp. Further to ensure that there is a large range of relative rotations at which Delfi-C3 can be detected the field of view of the cameras needs to be large, which is why the 360° cameras were chosen.

The chosen components for the detection system are summarised in Table 7.1.

Table 7.1: Detection System Components

Component name	**Mass** [g]	**Cost** [EUR]	**Size** [mm]	**Power** [mW]
Zoom camera	300	200	110 × 50 × 65	1000
6x 360° camera	120	300	30 × 10 × 10	210
Phased Antenna Array	100	6500	98 × 82 × 7	2000
Testing		8000		
Total	520	15 000		3210

[4] `https://nl.aliexpress.com/item/Free-shipping-FPV-36X-Zoom-700TTL-HD-Camera-Module-For-1-2G-5-8G-Telemetry/32460828649.html` accessed on 16 Jan. 2019

[5] `https://www.aliexpress.com/i/32960324779.html` accessed on 16 Jan. 2019

8

Clamping and Enclosing Subsystem

In this Chapter the clamp that will capture Delfi-C3 is discussed. In Section 8.1 the outer dimensions and constraints of the clamp are set. In Section 8.2 the requirements for the clamp are stated. In Section 8.3 the Design Option Tree is set up together with the trade-off criteria. In Section 8.4 the elimination of obviously in feasible design options is done. In Section 8.5 the trade-off table is made and the most optimal design options are selected from the trade-off table. In Section 8.6 the sensitivity analysis which was done on the trade-off table is discussed. In Section 8.7 the final design is presented. First an overview of the final clamp design is given. After this the components are sized and selected. At last the cost of the different components is estimated and determined and presented in Table 8.2 together with the mass and power usage. In the last Section, Section 8.8, the Verification and Validation is described. The two figures at the end of the chapter show an overview of the clamp and how it works.

8.1. Overall sizing

The force the clamp has to exert on Delfi-C3 is calculated using statics equations. It was assumed that the force the main thruster applies to Delfi-REAL is at most 1 N. It is assumed that the ADCS keeps Delfi-REAL from rotating and that the force from the main thruster only creates a lateral force. Delfi-C3 is connected to Delfi-REAL through the clamp, which means that the clamp has to transfer this force onto Delfi-C3. This implies that the clamp has to apply a force of at least 1 N onto Delfi-C3 in order not to open during manoeuvring.

The maximum length of the clamp arms is 8 cm because the clamp has to extend through the structure which has a hole of 8 cm × 8 cm. To account for some margin the maximum length of the clamp arm is set at 7.5 cm. The same constraint of 7.5 cm holds for the width and length of the clamp base. The total height of the clamp in folded position is set at a maximum of 10.6 cm. This is a bit more than the height of the structure. This is because the folding panels are not flat onto the structure in folded position, they are about 1 cm higher, the clamp can extend 8 mm above the structure as long as this part stays within 8 cm × 8 cm.

Due to the structure of Delfi-REAL, the maximal size of the clamp is not 1 U, 10 cm × 10 cm × 10 cm, but 8.9 cm × 8.9 cm × 9.8 cm. However, due to the payload bay doors which are not flat onto the structure of Delfi-REAL, there is a space of 10 mm between the structure and the payload bay doors, the maximal size is 8.9 cm × 8.9 cm × 10.6 cm

8.2. Clamp Requirements

The requirements found from the analysis are stated below. CES stands for Clamp and Enclosing System.

RQ-CES-01	The clamp shall exert a minimal force on the side of Delfi-C3 of 1 N.
RQ-CES-02	The clamp shall be able to extend itself in the direction of Delfi-C3 by a minimum of 15 cm.
RQ-CES-03	The clamp shall be locked into it's lowest position after capturing Delfi-C3.
RQ-CES-06	The clamp shall exert a minimal force on the solar panels of Delfi-C3 of 2.26 N at 45 mm from the hinge.
RQ-CES-07	The clamp arms shall have a maximal length in folded position of 7.5 cm.
RQ-CES-08	The clamp shall have a maximal height in folded position of 10.6 cm.
RQ-CES-08-01	The clamp extension base plus arms shall be lower than 4.6 cm in folded position.
RQ-CES-08-02	The extendable arm of the clamp shall have a maximal height of 6 cm.
RQ-CES-09	The clamp shall not use more than 10 W during operation.
RQ-CES-10	The clamp shall be locked into it's lowest position during the mission phases before capture.
RQ-CES-11	The clamp shall be less than 8.9 cm wide.
RQ-CES-12	The clamp shall be less than 8.9 cm long.
RQ-CES-13	The extending part of the clamp shall not be larger than 8 cm × 8 cm.

8.3. Trade-off criteria

This section discusses the different trade-off criteria and their respective weights. The weight for System Cost and Volume differs from the weight used in the System Design Option Trade-off. System Cost is changed from 8/10 to

5/10 and Volume is changed from 2/10 to 7/10.

- **Mass 5/10** - Even though the clamp should not be to heavy and exceed the estimated TPM mass, the mass for the clamp is not of great importance to the design of the clamp.
- **System Cost 5/10** - The cost of the clamp is not more important than the mass of the clamp. The clamp is a complicated system, however the components do not cost a lot. Therefore, it is assumed the clamp options are not influencing the total cost of Delfi-REAL significantly. For this reason the System Cost for the clamp is not as important.
- **Complexity 7/10** - Complexity is important for the clamp. It should be as simple as possible. This also adds to the reliability of the design.
- **Reliability 9/10** - The reliability of the clamp is of great importance because it is a crucial phase of the mission. If the clamp fails the mission also fails.
- **Volume 7/10** - The volume is important for the clamp . Since it cannot exceed the dimensions of 10 cm × 10 cm × 10 cm it is important to keep the components as small as possible.
- **Accuracy 9/10** - The accuracy of the clamp is essential for the mission to be successful. If the accuracy of the clamp is not good enough it could mean that the clamp is not able to attach to Delfi-C3 which leads to a mission failure. Also, if the accuracy is too low it could mean the clamp unintentionally hits Delfi-C3 before it is grabbed properly which will propel Delfi-C3 away which also leads to a mission failure. For these reasons the accuracy is given the same weight as reliability.
- **Power usage 8/10** - The power usage of the different parts of the clamp is very important to be as low as possible. Since there are multiple components that work at once or right after each other, the power consumption during this phase can become quite substantial. This would lead to heavy batteries and more solar panels, which leads to more mass and cost. Therefore it is important to take the power consumption of the different options into account in the trade-off.

8.4. Design option elimination

This section elaborates on why the design options that are marked red in the Clamp Design Option Tree are eliminated. The Clamp Design Option Tree can be found in Figure 8.1.

- **Wait for good alignment** - Waiting for Delfi-C3 and Delfi-REAL to align is not a good option by itself, because it can take a very long time before Delfi-C3 is in exact the right orientation to capture it. However waiting for Delfi-C3 to be in an adequate orientation to start the capture phase will be used for all the other attitude matching options since this will make the capture manoeuvre easier.
- **Linear Actuators** - The downside of the linear actuator is that they are quite big in comparison to how far they can extend. Another downside is that they are quite expensive and are not easily found in the small size needed. The force they can deliver is quite large. However, since there is no gravitational force on Delfi-REAL, the forces don't need to be that large. For these reasons the linear actuator is discarded.
- **Hydraulic Telescopic Arm** - Hydraulics do work in space but there are a couple of challenges to it. The operating temperature of the fluid, pumps and actuators should be kept within their working temperature range in order to precisely control the movement of the actuator. This requires heaters that consume a lot of power. Another downside is that the efficiency of hydraulic systems is a lot less compared to DC servo motors and stepper motors. For these reasons hydraulics to actuate the telescopic arm are discarded.[1]
- **Locking spring** - The locking spring is discarded because the spring has to apply a lot of force to keep the clamp and Delfi-C3 down during re-entry. And even if this force is applied it can still happen that Delfi-C3 will move a little bit up and down during re-entry which means it will start vibrating. Another difficulty is that this stiff spring has to be deployed after the clamp captured Delfi-C3 and moved down. This requires a strong mechanism which adds mass. For these reasons the locking spring is discarded and a locking pin is deemed more rigid and suitable.
- **Constant clamping force hydraulically actuated** - This is discarded for the same reasons as the Linear Actuators.

[1] `https://www.engineeringclicks.com/hydraulics-in-space/` accessed 8 Jan 2019

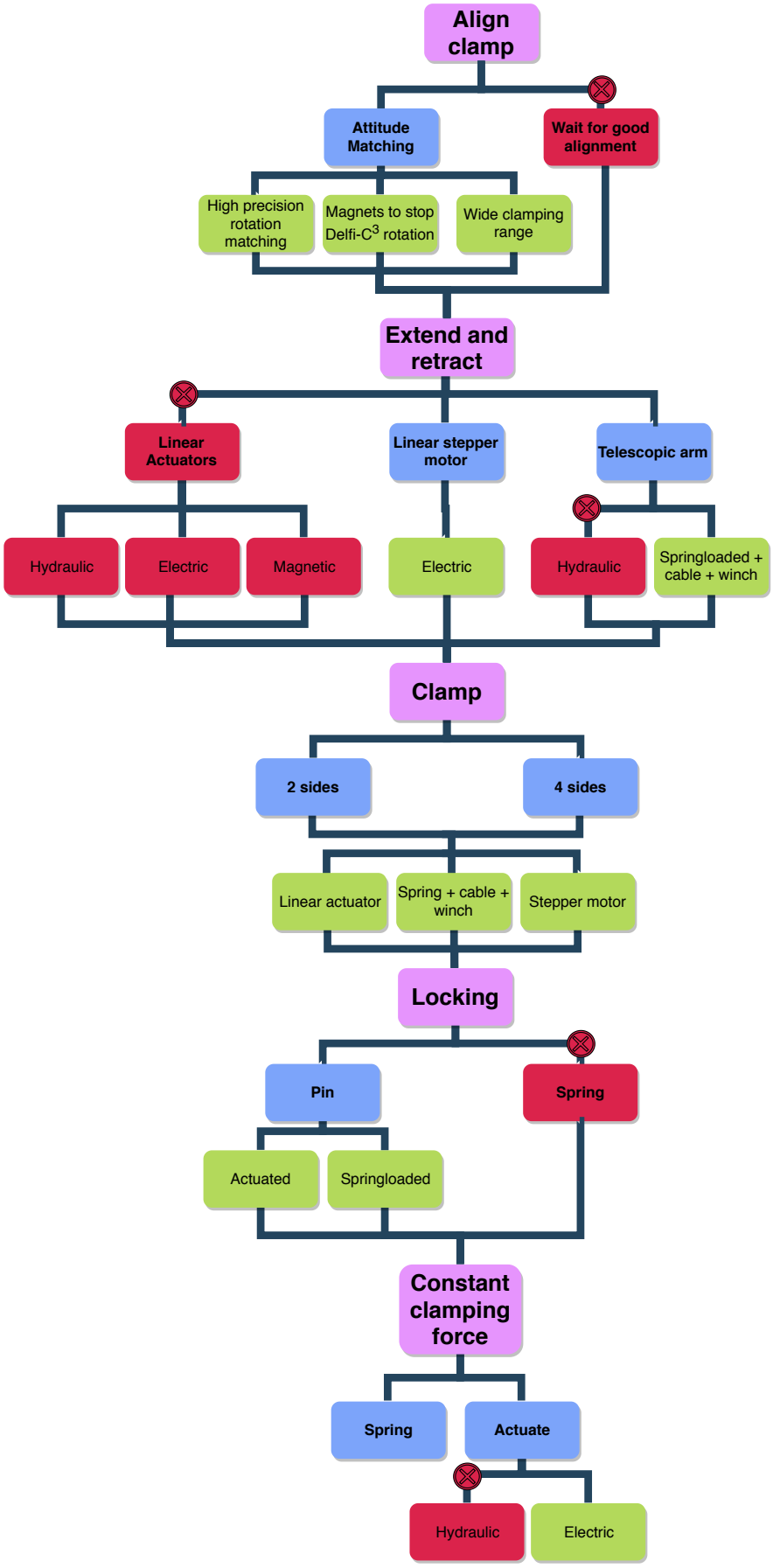

Figure 8.1: Clamping System Design Option Tree

8.5. Concept Selection

Table 8.1: Design concept trade-off table for the Clamping and Enclosing System. excellent: excel, nominal: nom, exceeds requirement: exreq, unacceptable: unacc.

Option \ Criterion	Mass	System cost	Complexity	Reliability	Vol	Accuracy	Power usage
Align clamp							
High precision rotation matching	excel	nom	nom	nom	excel	excel	nom
Magnets to stop Delfi-C3 rotation	exreq	nom	exreq	exreq	exreq	exreq	exreq
Wide clamping range	nom	nom	nom	excel	nom	nom	excel
Extend and Retract							
Linear stepper motor	nom	excel	nom	nom	exreq	excel	nom
Telescopic arm	excel	excel	nom	excel	excel	nom	excel
Clamp							
2 sides	excel	nom	excel	nom	excel	nom	nom
4 sides	nom	nom	nom	excel	nom	excel	nom
Clamp actuation							
Linear actuator	exreq	nom	excel	excel	exreq	excel	exreq
Cable, spring, winch	excel	nom	nom	nom	nom	nom	excel
Stepper motor	nom	nom	excel	excel	nom	excel	nom
Locking							
Actuated pin	nom	nom	nom	excel	nom	excel	nom
Springloaded pin	excel	excel	excel	nom	excel	nom	excel
Constant clamping force							
Spring	excel	excel	excel	excel	excel	nom	excel
Actuated	nom	nom	nom	nom	nom	nom	nom

From the Design Option Tree, found in Figure 8.1, it is clear that a spring is the better option to provide constant clamping force. This would still require a stepper motor to open the clamp. However, since this is only a short period that the clamp has to be kept open, it requires less power than actuated clamping force, which uses power during the remainder of the mission after capture.

For the aligning of the clamp, the magnets to stop Delfi-C3 from rotating exceed the requirements on multiple criteria. The idea behind this would be to capture Delfi-C3 using magnets to attach the antennae of Delfi-C3 to Delfi-REAL. However it would be too heavy, too complex, less reliable, less accurate and it would use a lot of power. It would also mean an extra system has to be added, while for the clamp a wide clamping ratio would only mean a different design and for the high precision rotation matching an extra task for the thrusters, which are already present. Therefore the magnets to stop Delfi-C3 from rotating are discarded as suitable option.

The high precision rotation matching scores better on mass, volume and accuracy while the wide clamping range scores better on reliability and power usage. The high precision rotation matching was determined to be the better choice. The reason for this is that the volume of a wide clamping range would be difficult to fit within the 1 U size constraint and that it would be heavier. It would also mean that the clamp can be relatively simple if the clamping range does not have to be large. The clamp is already difficult to fit within the 1 U due to the requirement of extending 15 cm.

For the trade-off between clamping two sides and four sides it can be seen that clamping Delfi-C3 on four sides scores better in reliability and accuracy. Clamping two sides scores better in mass, complexity and volume. Even though for the size and mass it would be better to go with clamping on two sides, it is more important to have a good reliability and accuracy because this part of the mission is crucial. Furthermore, it was determined that the payload bay doors are not able to close the two bottom hinged solar panels of Delfi-C3 without damaging the experimental solar panel at the end. Therefore the clamp has to close the solar panels at the bottom. The option of clamping only 2 sides would then already be almost impossible. The solar panels are under an angle due to which the clamp would most likely propel Delfi-C3 away before it could properly clamp Delfi-C3. It is therefore chosen to go with clamping four sides.

For the locking of the clamp in its lowest position there are two options; an actuated pin and a spring loaded pin. The

spring loaded pin performs better in mass, system cost, complexity, volume and power usage. The actuated pin is better in reliability and accuracy because it can be controlled. The spring loaded pin will be deployed with a thermal knife burning through a wire, which means it can only be deployed once. When the spring loaded pin and hole are not exactly aligned the locking will fail. The actuated pin is therefore deemed the better option. Another reason is that the clamp has to be locked during launch and the first part of the mission, after which it has to be unlocked for the capture manoeuvre. When the capture manoeuvre is done, the clamp has to be locked again. A spring loaded pin cannot perform both tasks, it would require two different pins. Therefore, an actuated pin is chosen to perform both of these manoeuvres and to make sure the locking system is reliable and accurate.

For the extension and retraction of the clamp there are two options, a linear stepper motor and a telescopic arm. The telescopic arm performs better in mass, reliability, volume and power usage. The linear stepper motors rotate a threaded rod to push something up or to push itself up. The maximum height of the threaded rod would be 10 cm, due to the height constraint of 1 U. The height of a stepper motor is around 2 cm.[2] This would mean that one linear stepper motor can push itself up by 8 cm. To acquire the extension of 15 cm, on top of the height of Delfi-REAL, multiple stepper motors need to be placed on top of each other. To fit this within the 1U box is very difficult and the linear stepper motor tower would not be very stable. Moreover, the linear stepper motor uses a lot of power; one linear stepper motor uses 5.7 W of power[2] while a stepper motor, as used in the telescopic arm, uses only 1.5 W.[3] For these reasons the telescopic arm is determined to be more suitable and viable.

For the clamp actuation the linear actuator is not a good option. They use a lot of power, around 2.5 W[4] versus around 1 W for a stepper motor[5], and are quite heavy and large. The option which performs the best in the trade-off is the stepper motor. It is better in complexity, reliability and accuracy than the cable, spring and winch although the cable, spring and winch is better in mass and power usage. Since the stepper motor is a lot better in complexity, reliability and accuracy the little difference in mass and power usage with the cable, spring and winch can be neglected. Therefore the cable, spring, winch concept is eliminated and the stepper motors for the clamp actuation are chosen.

8.6. Sensitivity analyses

For the sensitivity analyses the different parameters are increased and decreased by 11 %. The 11 % is taken because according to the TPM this is the contingency for this phase, as discussed in Section 22.1. Also the trade-off criteria were altered by 1 point to see if this changed the outcome of the trade-off. For none of the design options these changes influenced the outcome of the trade-off. The high precision rotation matching, telescopic arm, clamping 4 sides, clamp actuation by stepper motor, actuated locking and a constant clamping force with a spring are the most optimal design options.

8.7. Final Design

This section first provides a subsystem overview of the clamp. Next, the different components for the clamp to function are selected. After this, the cost of the components is discussed and the mass, cost and power are presented.

8.7.1. Subsystem Overview

The dimensions for the clamp are constrained to 8.9 cm × 8.9 cm × 10.6 cm. In order to be able to extend the clamp at least 15 cm above Delfi-REAL, the telescopic arm needs the space from the bottom till 6 cm height. The last 4.6 cm are used for the clamp.

The telescopic arm will consist of multiple segments that extend. The force delivered to extend these segments is provided by a spring, which will be in compressed state when the clamp is not deployed and in almost extended position when the clamp is extended. An actuated pin will lock the telescopic arm when it is not deployed.

To control the extension and retraction, a stepper motor will be used which controls the extension through a wire. The clamp arms will be spring loaded in the folded direction. These springs will make sure the arms stay folded and apply the clamping force on Delfi-C3. Stepper motors will open the arms and close them. When Delfi-C3 is clamped by the arms the stepper motors can be turned off and the springs make sure Delfi-C3 stays clamped.

[2] https://www.distrelec.nl/Web/Downloads/60/18/05446018.pdf accessed 16 Jan 2019
[3] https://www.faulhaber.com/fileadmin/Import/Media/EN_AM2224_FPS.pdf accessed 16 Jan 2019
[4] https://s3.amazonaws.com/actuonix/Actuonix+L12+Datasheet.pdfaccessed 16 Jan 2019
[5] https://www.faulhaber.com/fileadmin/Import/Media/EN_AM2224_FPS.pdfaccessed 16 Jan 2019

After Delfi-C3 is clamped the extension stepper motor will retract the telescopic arm again. Once the telescopic arm is at the lowest position the clamp arms will rest on top of Delfi-REAL. The actuated pin will then lock the telescopic arm after which the extension stepper motor can be turned off. Schematics of the extension and opening of the clamp are shown in Figure 8.2 on page 40.

8.7.2. Component selection

There are two different arms in the clamp. The reason for this is that in this way the arms can fold together in a more compact way. The two lower arms are used to clamp the sides of Delfi-C3 where no solar panels are present. The two top arms are used to clamp Delfi-C3 at the solar panel sides and to fold in the solar panels. The reason for this division is that the top arms clamp Delfi-C3 at a higher point than the lower arms, at 45 mm and 30 mm from the bottom of Delfi-C3 respectively. This means that the top arms have to apply a lower force on the solar panels to close them which means a lower torque delivered by the motor.

The clamp arms are folded over each other to make the height as small as possible. They are shaped in such a way that when the clamp has captured Delfi-C3 and is retracted the arms are resting on the top surface of Delfi-REAL when the clamp is retracted to its lowest position. They are furthermore shaped with an angle of 2° at the side where they touch Delfi-C3. This is done to make sure that the top of the arm touches Delfi-C3 first.

In order to provide the required clamping force of 1 N, the spring needs to have a torque of at least 0.067 N m. This is calculated by multiplying the distance from the hinge to the point where the clamp touches Delfi-C3, which is 0.067 m, by the clamping force of 1 N. To make sure the motor is able to rotate the clamp enough, a safety factor of 1.3 is used, which leads to a torque of 0.087 N m. To achieve this the AM1524 stepper motor of Faulhaber is selected.[6] This motor is small enough to be fitted inside the clamp with a gearbox attached. It can drive one clamp arm using a gearbox with a ratio of 28 to 1.[7] It is able to generate 6 mN m of torque, after the gearbox 0.131 N m. For each arm there will be a separate motor and gearbox. To control these two motors two Motion Controllers of Faulhaber are used, the MCST 3601.[8] The motor weighs 12 g and the gearbox weighs 5 g, which amounts to 34 g for the two sides of Delfi-C3 with no solar panels. The Motion Controller weighs 22 g.

For the sides with the solar panels a higher clamping force is needed. The spring force in the hinge of the solar panels is found to be 101.5 mN m in Section 17.4.3. The force to be delivered at 45 mm is 2.26 N. The torque the spring has to deliver is than 0.152 N m. For the motor torque a safety factor of 1.3 is used again which leads to 0.198 N m. If a gearbox ratio of 28 to 1 is used again the motor would not be strong enough to open and close the arm, a higher ratio gearbox would be an option, however due to size constraints a higher ratio gearbox cannot be fitted. A stronger motor will also not fit in the given space. However, the motor can operate safely at double the current if this is less than 5 % of the duty cycle, according to Faulhaber. This results in a torque of 0.218 N m, which is enough to operate the arm. For these two motors again MCST 3601 Motion Controllers are used.

The clamp arms are designed in such a way, that when they have Delfi-C3 clamped and they are in retracted position that they are against the walls of the structure and rest on top of the structure. In this way, the loads introduced in the clamp due to Delfi-C3 during re-entry are going straight into the structure. On the structure of Delfi-REAL are furthermore 4 blocks at the corners where Delfi-C3 will rest onto the structure. This makes sure that the loads introduced during re-entry are going through the 4 struts of Delfi-C3, as it is designed to carry the loads through these struts. The clamp arms can also not open anymore since they are stuck between the structure of Delfi-REAL. Therefore Delfi-C3 cannot move sideways anymore.

The telescopic arm consists of six extendable parts. The base part is 6 cm high and has a diameter of 65 mm. The extendable parts are 36 mm high each. The walls and flanges are 2 mm thick. The flanges make the extension stop from extending beyond the previous extension. Due to these flanges each extension adds 32 mm. This makes the total length of the telescopic arm 252 mm in extended position. Subtracting the height of Delfi-REAL leads to an extension of 15.2 cm in the direction of Delfi-C3, which is in accordance with the requirement.

The diameter of the telescopic base is chosen such that the inner diameter of the last extension is slightly bigger than the spring. The chosen spring for the extension is the DR5990 from Alcomex.[9] This spring has a compressed length of 55.6 mm, a spring force at compressed length of 87.5 N, an extended length of 262.5 mm and an outside diameter of 24.3 mm. When the clamp is retracted the spring is in compressed state delivering a force of 87.5 N. When the clamp is extended the spring will be at a length of 247.6 mm, delivering a force of 6.9 N to make sure the telescopic arm stays extended.

[6] `https://www.faulhaber.com/nl/producten/serie/am1524/` accessed 16 Jan 2019
[7] `https://www.faulhaber.com/nl/producten/serie/15a/` accessed 16 Jan 2019
[8] `https://www.faulhaber.com/nl/producten/serie/mcst-3601/` accessed 17 Jan 2019
[9] `https://webshop.alcomex.nl/producten/drukveren/compression-stainless-2451.html` accessed 15 Jan 2019

The stepper motor to control the extension is also a motor from Faulhaber, the AM2224 motor.[10] This motor is able to deliver 22 mN m, using a gearbox with a ratio of 69 to 1 it delivers a torque of 1.03 N m.[11] If a winch with a radius of 10 mm is used this leads to a force in the wire of 103 N. The spring delivers a force of 87.5 N when the telescopic arm is retracted, hence the force in the wire is sufficient to retract the telescopic arm. For this motor the same motion controller as for the AM1524 is used.

The wire will be a rope made from Dyneema. The rope has to be thin, strong and cut resistant. Therefore a Dyneema rope is very suitable. The rope selected for the design is a 1 mm SK99 Kiteline.[12] The rope has a tensile strength of 280 kg, which amounts to 2747 N. This is way more than the maximum spring force of 87.5 N and the maximum force the stepper motor can put on the rope, which makes the thin rope very suitable for the application. The mass of the rope is not specified, but can be determined from comparable ropes. The mass of the SK99 Kiteline is determined to be 0.6 kg per 100 m using D-CORE 99 data[13] and converting it to a diameter of 1 mm.

In order to lock the telescopic arm when it is not deployed, an actuated pin is used. This pin needs to withstand 87.5 N of shear force which is created by the spring in the telescopic arm. Steel is commonly used for locking pins, it has a good strength and the friction coefficient of steel on aluminium is only 0.45.[14] The pin will therefore be made out of steel. The shear stress can be calculated using $\tau = \frac{F}{A}$. This can be rewritten into $A = \frac{F}{\tau}$. Using a value for τ of 345 N mm^{-1}[15] for Low Carbor HR Steel, a minimum area of 0.26 mm^2 is needed. This leads to a minimum diameter of 0.58 mm. If a safety factor of 2 is used the diameter of the pin is 1.2 mm. The length of the pin needs to be 20 mm to lock all the telescopic segments. This leads to a mass of 0.15 g. For redundancy and to prevent the telescopic arm from getting skewed there are two locking pins used, one on either side of the telescopic arm.

To actuate the pin, the AM0820 stepper motor of Faulhaber is selected. This motor is capable of delivering 0.65 mN m. This is sufficient to actuate the pin since there is no force on the pin when it is put in place.[16] This motor is selected because it only weighs 3.3 g, 8 mm in diameter, 13.9 mm long and uses 0.4 W.

The materials considered for the clamp arms and base and the telescopic arm are aluminium, titanium, carbon fibre and plastics. More details about the materials can be found in Section 17.5. The material chosen for these applications is aluminium. The reason for this is that it is not as expensive as titanium and it is easy to manufacture. Titanium could be a good option, however it is very expensive and difficult to manufacture. The production cost of the arm would go up drastically when titanium is used. Carbon fibre is strong and light, however for the clamp and telescopic arm multiple different moulds would be needed which are very expensive. This would drive the cost of the clamp up drastically. Plastics would be suitable for some parts of the clamp and telescopic arm as they are not expensive and provide low friction. However it is less strong than aluminium. Since the clamp has to withstand launch and re-entry loads aluminium is favoured over plastics for the structural parts of the clamp. Plastics could be used for the winch and pulleys.

8.7.3. Cost

The cost for the different components can be found in Table 8.2. The cost of the motors and motor controllers was inquired at Faulhaber. The cost of the spring and rope was found from their website.

The cost of the telescopic arm was estimated at EUR 1000 , this amounts to roughly EUR 140 per telescopic segment. These parts have to be lathed from an aluminium tube. This would not require more than an hour of work at a rate of EUR 80 per hour. Including material and a margin of 50 % this leads to an estimation of EUR 140 . The winch can be lathed or 3D printed. 3D printing would be cheaper than the estimated EUR 100 . Lathing the part would take roughly one hour of work, which amounts to EUR 140 again. The pulleys can be 3D printed and are estimated to cost around EUR 30 per pulley.

The clamp extension base has to be milled using a CNC milling machine, CNC stands for Computer Numerical Control. CNC machining costs around EUR 80 per hour. The part has to be made out of one block, therefore a lot of material has to be taken away. It furthermore requires multiple fixtures, for these reasons the machining time is quite long and the total cost is estimated to be EUR 1000 . The clamp arms also have to be CNC milled. Although

[10] https://www.faulhaber.com/nl/producten/serie/am2224/ accessed 16 Jan 2019
[11] https://www.faulhaber.com/nl/producten/serie/22e/ accessed 16 Jan 2019
[12] http://www.lijnenspecialist.nl/touwwerk-lijnen/dyneema-lijnen-vallen-schoten-en-trimlijnen/kaal-dyneema/sk99-powerline-kite accessed 15 Jan 2019
[13] http://www.lijnenspecialist.nl/touwwerk-lijnen/dyneema-lijnen-vallen-schoten-en-trimlijnen/kaal-dyneema/d-core-99 accessed 15 Jan 2019
[14] https://www.engineeringtoolbox.com/friction-coefficients-d_778.html accessed 21 Jan 2019
[15] https://www.unipunch.com/support/charts/material-specifications/ accessed 21 Jan 2019
[16] https://www.faulhaber.com/nl/producten/serie/am0820/ accessed 21 Jan 2019

Table 8.2: Mass and cost of the different parts of the clamp

Part	Needed	Mass [g]	Total Mass [g]	Cost [€]	Total Cost [€]	Total Power [W]
Telescopic arm	1	250	250	1000	1000	-
Winch	1	20	20	140	100	-
Pulleys	2	2	4	30	60	-
Clamp extension base	1	20	20	1000	1000	-
Clamp extension arms	4	20	80	750	3000	-
DR5990 spring	1	50	50	5	5	-
AM1524 + 15AK	4	17	68	400	1600	3.5
AM2224 + 22EK	1	60	60	400	400	1.5
MCST 3601	7	22	154	260	1820	-
Rope	1	1	1	1	1	-
AM1020	2	3.3	6.6	400	800	0.8
Locking pin	2	0.15	0.3	10	20	-
Assembly & Testing	80			150	12 000	-
			703.9		21 806	6.1

they also have multiple fixtures a lot less material has to be taken away. Therefore the machining time is less and they are estimated to cost around EUR 750 each.

The assembly and testing are estimated to take 80 h, 1 person two weeks, at an hourly wage of EUR 150 . This amounts to EUR 12 000 .

8.8. Verification & Validation

The forces the clamp has to apply on Delfi-C3 were calculated and verified by hand. The dimensions and initial sizing was done by hand. After which the available space was created in CATIA, short for Computer-Aided Three-dimensional Interactive Application, and it was verified if everything would fit. At this point some dimensions had to be changed to fit exactly in the given space. From this detailed sizing in CATIA the available space for the motors was retrieved. From this the motors were chosen and were verified by hand calculations if they could deliver the needed torque. The dimensions retrieved from CATIA were verified by hand drawings and calculations if they were correct. A drawing of the most important dimensions can be found in Figure 8.3 on page 40. The hand calculated values are tracked using an Excel file to be able to change them quickly.

The working of the clamp needs to be validated using a model of Delfi-C3. First the clamp should be assembled and tested if it performs the right actions and if everything works together. After this a test with a model of Delfi-C3 needs to be performed to see if it grabs properly onto Delfi-C3 and is able to hold on to it. After this test, a test in vacuum conditions should be performed to validate that the clamp operates normally in vacuum conditions. The cost for vacuum testing is not accounted for in the clamp system but is accounted for in the system integration testing.

Figure 8.2: Schematics of how the clamp extends and unfolds

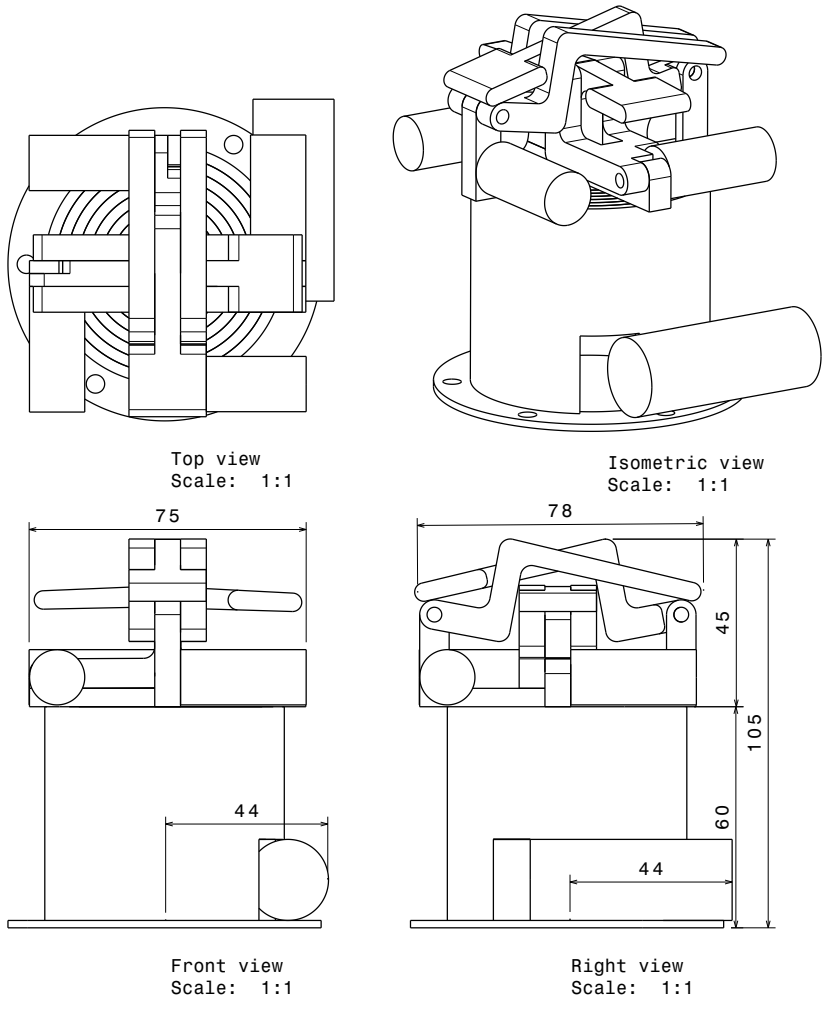

Figure 8.3: Drawings of the clamp in folded position

9 Telemetry, Tracking and Communication Subsystem

The Telemetry, Tracking and Communication subsystem (TT&C) is used to send health and status telemetry, and science data which consists of the images and video footage. Furthermore, TT&C is used to receive telecommands from the ground station. In order to ensure the subsystem functions properly, it is designed according to a list of requirements. These are formulated in Section 9.1. Furthermore, Section 9.2 describes the design considerations and shows the Design Option Tree (DOT). In Section 9.3, the final design is described. Finally, Section 9.4 lists the actions taken to verify and validate the subsystem.

9.1. Requirements

The requirements for the TT&C subsystem comes primarily from the data that needs to be transmitted or received, the time in which the data can be transmitted or received, and the chance that an error occurs during the transmission or reception of the data. These requirements are based on top level requirements, system level requirements, and from other subsystems.

RQ-TTC-01	The TT&C subsystem shall have an antenna to transmit payload data to amateur ground stations and the Delft University of Technology (TU Delft) ground station.
RQ-TTC-01.01	The TT&C subsystem shall be able to transmit payload data with a minimum bit rate of $3\,\mathrm{Mbit\,s^{-1}}$.
RQ-TTC-01.02	The TT&C subsystem shall have a maximal bit error rate of 8×10^{-9} during the transmission of payload data.
RQ-TTC-02	The TT&C subsystem shall have an antenna to transmit health and status telemetry to the TU Delft ground station.
RQ-TTC-02.01	The TT&C subsystem shall be able to transmit health and status telemetry with a minimum bit rate of $80\,\mathrm{kbit\,s^{-1}}$.
RQ-TTC-02.02	The TT&C subsystem shall have a maximal bit error rate of 10^{-7} during the transmission of health and status telemetry.
RQ-TTC-03	The TT&C subsystem shall have an antenna to receive telecommands from the TU Delft ground station.
RQ-TTC-03.01	The TT&C subsystem shall be able to receive telecommands with a minimum bit rate of $16\,\mathrm{kbit\,s^{-1}}$.
RQ-TTC-03.02	The TT&C subsystem shall have a maximal bit error rate of10^{-7} while receiving telecommands.
RQ-TTC-04	The TT&C subsystem shall transmit a signal after landing back on Earth.

9.2. Concept

For the TT&C subsystem, the design considerations are as follows. The science data to be sent to Earth consists of large amounts of data. Since, the time Delfi-REAL will be able to transmit data to the ground station at the Delft University of Technology (TU Delft) is limited, a high data rate is required for the science data. The data rate, frequency, and other parameters given by hardware, determines the computed ratio of energy per bit and noise spectral density (E_b/N_o). This ratio is used to quantify how well a signal is received. Furthermore, the Bit Error Rate (BER), which depends on the modulation used and the probability of an error occurring, determines the required E_b/N_o. For both the uplink and the downlink, a required and computed E_b/N_o is determined and compared. Whenever the required E_B/N_o is lower than the computed, a stable connection is possible.

The downlink of health and status data, and the uplink of telecommands are also part of the TT&C subsystem. The health and status data will have requirements all below the requirements for science data. Therefore, the downlink part of the TT&C will be designed based on the requirements set by the science data. The uplink can both be integrated in the hardware used for downlink, or designed separately. However, the uplink should also be used to track Delfi-REAL. This raises the need for the uplink antenna to not be blocked by the satellite itself. When Delfi-REAL has landed, it needs to be located. For fast and reliable tracking of Delfi-REAL after landing, a beacon signal will be broadcast.

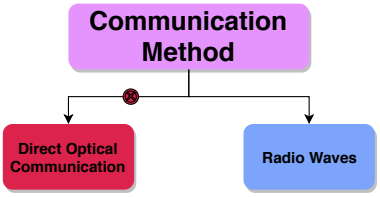

Figure 9.1: Design option tree of different modes of communication

The different design options for the method of communication are listed in the DOT in Figure 9.1. The optical communication method was discarded since this would require a high pointing accuracy of the system at all times. In practice this is not possible, especially during the clamping procedure. The second option is the use of radio waves. This is a viable option used widely in the space industry.

For the chosen method of communication, a frequency will have to be chosen over which data will be transmitted. There is an option to both transmit and receive over the same bandwidth (crosslink). This has the advantage of potentially reducing the amount of required hardware components. The downside however, is the added noise due to interference.

The first consideration for the frequency is given by the fact that a lower frequency means lower bandwidth allocation [13]. Furthermore, according to the Shannon-Hartley equation, the lower the bandwidth, the higher the Sound to Noise Ratio SNR needs to be for the same data rate.[1] The equation is given by

$$C = B \log_2 \left(1 + \frac{S}{N}\right), \tag{9.1}$$

where C is the data rate, B is the bandwidth and $\frac{S}{N}$ is the SNR. For the downlink, a minimum data rate of 3 Mbit s^{-1} has to be achieved. The Very High Frequency (VHF) and Ultra High Frequency (UHF) maximal bandwidth is 25 kHz and 50 kHz respectively [13]. This means that the SNR should be at least 10^{20} dB, to adhere to the data rate requirement. This is not achievable with any hardware that exists today. For the uplink, any frequency can be chosen to meet the telecommand data rate requirement.

The second consideration for the frequency is the space loss. The equation is described in Space Mission Analysis and Design (SMAD) as

$$L_s = \left(\frac{c}{4\pi S_d f}\right)^2, \tag{9.2}$$

where L_s is the space loss, c is the speed of light, S_d is the range to the ground station, and f the frequency. If the frequency increases, the space loss value will become lower. This means that a low frequency is desirable to minimise the effects of space loss.

Figure 9.2 shows the DOT for the frequency options. The VHF band is the lowest frequency band while the Ka band is the highest frequency band. Since data has to be transmitted to the TU Delft ground station, the X, Ka, K, Ku bands are not available since the ground station is not capable of receiving or transmitting these signals.

Finally, the only viable option is transmission within the S band frequency. This band has a channel size of 1 MHz which means that an SNR is needed of about 10 dB. For the uplink, the TU Delft ground station is capable of transmitting in the VHF and UHF frequency range [14]. This means that crosslink communication is eliminated as an option.

[1] https://www.gaussianwaves.com/2008/04/channel-capacity/ accessed on 14 Jan. 2019

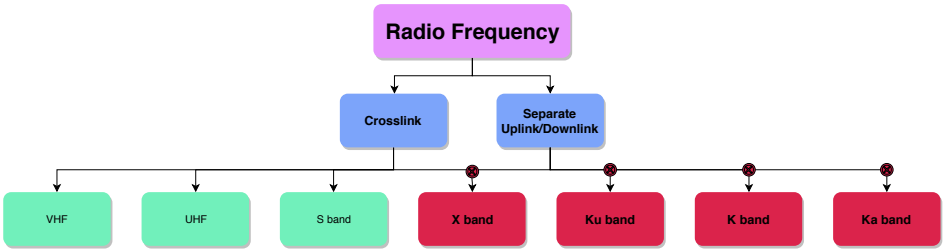

Figure 9.2: Design option tree of different radio wave frequencies.

9.3. Final Design

Based on the elimination done in Section 9.2, the components can be selected and a link budget can be set up. A link budget is created for both the downlink of science data and the uplink of telecommands. The housekeeping data is assumed to fit within the budget created for the downlink. Furthermore, the beacon which will be used to find Delfi-REAL after successful landing back on Earth will be discussed.

9.3.1. Component Selection

For the transmission of data, a transmitter is required and an antenna has to be used. For receiving telecommands, a receiver is needed and an antenna. There is also the possibility of using a transceiver, which combines the functionality of the transmitter and the receiver. The components used will be commercial off-the-shelf. Endurosat and Innovative Solutions In Space (ISIS) have components available for downlink and uplink.

- **Downlink antenna-** The S band antenna, has to meet the high data rate requirement. Endurosat has an S band antenna built for cubesats, while ISIS has an S band antenna designed for nano and pico satellites. ISIS's antenna will not comply with the data rate requirements.
- **Downlink transmitter-** ISIS has an S band transmitter which includes both modulation and coding. The modulation and coding is required to have a stable connection whenever Delfi-REAL is in view. Endurosat does not have such a transmitter.
- **Uplink antenna-** ISIS has transceiver components for the VHF/UHF frequency range, while Endurosat only has options for the UHF frequency range. The ISIS transceiver could both function for uplink and whenever Delfi-REAL has landed as a beacon.
- **Uplink receiver-** ISIS has both VHF and UHF antenna's. Endurosat only has a UHF antenna.

The way that the components are used for downlink, uplink and the beacon are described in the list below. Furthermore, Table 9.1 shows the details of the components.

- **Downlink-** The TT&C subsystem will be designed such that it will be able to communicate to the ground station at the TU Delft. However, the subsystem will also transmit live video whenever it is not within range of the ground station. This will enable the use of the amateur frequency range of 2400-2450 MHz. During the live video transmission, the data rate will be reduced such that the transmitted signal will be receivable for amateur ground stations.
- **Uplink-** The uplink frequency will be within the UHF spectrum. The frequency range is between 435-438 MHz. Normally, data sent over amateur frequencies cannot be encrypted. However, the telecommands can be encrypted, this will ensure that Delfi-REAL cannot be hijacked. The data rate of the telecommands will be 9.6 kbit s^{-1}. This is lower than stated in the requirements. However, the telecommands will not be more than a few hundred kbit. The time window where a signal is possible, will suffice to uplink all the telecommands.
- **Beacon-** The VHF downlink functionality of the ISIS transceiver will be used in conjunction with the body of Delfi-REAL as antenna to function as a beacon after landing.

Table 9.1: TT&C subsystem components

Component name	Number	Cost [EUR]	Mass [g]	Power [W]	Size [mm]
S band antenna	1	2500	64	0	98 × 98 × 12
S band transmitter	1	30 000	300	9.2	90 × 96 × 33
UHF/VHF antenna	1	5500	85	2 (During deployment)	98 × 98 × 7
UHF/VHF transceiver	1	8500	85	0.2 (Receiver only) 1.7 (Transmitter on)	90 × 96 × 15

9.3.2. Link Budget

The TT&C subsystem needs to transmit video and high quality images to the ground station. This is done within a certain time window. In order to maximise the time window, the range over which a stable connection is possible should be as large as possible. The range can be expressed in term of the altitude of the orbit and the elevation angle. This can be seen in Figure 9.3. In general, the smaller the elevation angle, the longer the range.

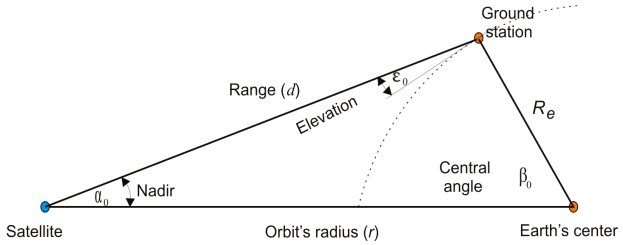

Figure 9.3: Relation between range and elevation angle [15].

In order to establish for what range a stable connection is possible, a link budget is created. The link budget compares the required and computed E_b/N_o. The required E_b/N_o is obtained by setting requirements to the probability that no errors occur in a certain amount of bits

$$BER = 1 - P_r^{\frac{1}{N_i}}, \tag{9.3}$$

where P is the probability of no error occurring and N_i is the amount of bits. With the required BER and the modulation used we can find the ratio of energy per bit and spectral noise density. For the transmitter from ISIS, Offset Quadrature Phase Shift Keying (OQPSK) modulation is used. For the ground station transmitter, Binary Phase Shift Keying (BPSK) is used. The equation for these modulations [16] is given by

$$\left(\frac{E_b}{N_o}\right)_{req} = \left(erfc^{-1}(2BER)\right)^2. \tag{9.4}$$

Furthermore, the required E_b/N_o will be lowered due to the fact that the transmitter has gain due to coding. The coding gain used by the transmitter is Concatenated Reed Solomon and Convolutional coding. According to the lecture by S. Speretta [13], the data rate is halved and the coding gain is approximately 8 dB for downlink. Uplink does not use coding.

For the computed E_b/N_o, the ground station and satellite characteristics are used. The energy per bit is computed with

$$E_b = S/C = \frac{PL_lG_tL_sL_aG_r}{R}, \tag{9.5}$$

where P is the transmission power, G_t the gains of the transmitter antenna, G_r the receiver antenna, L_l the losses due to the cables, L_a the transmission path loss, L_s the space loss, and R the data rate. The transmission path loss is neglected since this is only of influence for frequencies below 200 MHz and above 50 GHz [17]. The gain of an antenna is determined from the peak gain by

$$G = G_p - 12 \cdot \left(\frac{e}{\theta}\right)^2, \tag{9.6}$$

where G_p is the peak gain, e the pointing error and θ the half-power beam width. The equation can be found in SMAD [17] on page 525. The noise spectral density is given by

$$N_o = kT_s, \tag{9.7}$$

where k is the Boltzmann constant, and T_s the system noise temperature which can be found in SMAD [17] on page 526.

With the required and computed E_b/N_o, the margin can be found. If the margin is positive, the link budget is closed and a stable connection is possible. However, a margin of 3 dB is used as a safety factor. Finally, with the computed E_b/N_o, the SNR can be found with

$$\frac{S}{N} = \frac{E_b}{N_o}\frac{C}{B}, \tag{9.8}$$

where R is the data rate and B is the bandwidth. With the computed SNR, the maximal data rate, based on the Shannon-Hartley Equation 9.1, can be found to ensure the data rate in the link budget does not exceed this maximum. Table 9.2 shows all parameters for the link budget, Figure 9.4 shows the margins for uplink and downlink compared to the elevation angle.

Table 9.2: Link budget for Delfi-REAL. Values are based on an orbital altitude of 550 km and an elevation angle of 0°.

Item	Symbol	Unit	Downlink	Uplink
Frequency	f	MHz	2450	146
Transmitter Power	P	W	2	120
Transmitter Line Loss	L_l	dB	−1	−1
Peak Transmit Antenna Gain	G_{pt}	dBi	8.3	15.5
Half Power Beam Width Transmitter	θ_t	°	71	30
Transmit Antenna Pointing Offset	e_t	°	10	0.1
Transmit Antenna Gain	G_t	dB	8.1	15.5
Equivalent Isotropic Radiated Power	$EIRP$	dBW	10.1	35.3
Propagation Path Length	S_d	km	2700	2700
Space Loss	L_s	dB	−169	−154
Propagation and Polarisation Loss	L_a	dB	0	0
Gain and Noise Temperature Ratio	G/T	dB	4.9	-
System Noise Temperature	T_s	K	719	1590
Spectral Noise Density	N_o	dB	−200	−197
Peak Receive Antenna Gain	G_{pr}	dB	33.5	-
Half Power Beam Width Receiver	θ_r	°	5.1	-
Receive Antenna Pointing Offset	e_r	°	0.1	-
Receive Antenna Gain	G_r	dB	32.0	0
Data Rate	C	kbit s^{-1}	3400	9.6
E_b/N_o (1)	E_b/N_o	dB	9.6	38
Bandwidth	B	MHz	1	0.05
Sound to Noise Ratio	SNR	dB	15	68.0
Maximal Data Rate	C_{max}	kbit s^{-1}	3990	305
Bit Error Rate	BER	-	8.55×10^{-9}	1.00×10^{-9}
Coding Gain	G_c	dB	8	0
Required E_b/N_o (2)	$(E_b/N_o)_{req}$	dB	4.0	13
Implementation Loss (3)	-	dB	2	2
Margin (1) - (2) - (3)	-	dB	3.4	23

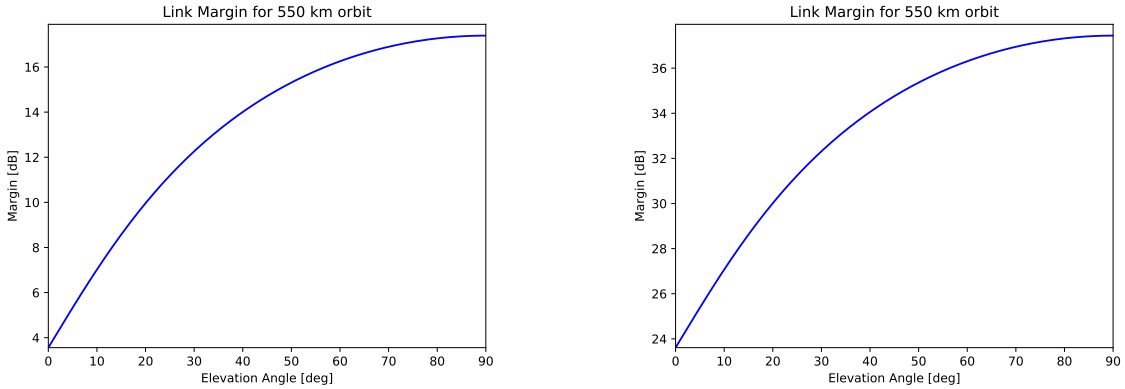

(a) Downlink

(b) Uplink

Figure 9.4: E_b/N_o margin compared to elevation angle for the TT&C subsystem

9.3.3. Beacon

The beacon is required to enable the location finding of Delfi-REAL after landing. Due to the harsh conditions of re-entry, it has to be assumed that no external components, such as antennae, will survive. For this reason, the beacon is connected to the metal body of Delfi-REAL which will act as a no-gain omni-directional antenna.

The beacon signal is optimised to use minimum power to decrease battery drain, therefore increasing duration. The beacon will be transmitted on the frequency range of 145.8 MHz to 146 MHz, using the VHF transmitter, with a power of 1.7 W for a 0.2 s impulse and a period of 2 s. With these specifications, the beacon is expected to transmit for 370 hours before the battery is completely drained. Using the landing site estimation range of 80 km, see Chapter

15, it is assumed that Delfi-REAL will be found within a day.

To ensure that the beacon is only turned on during landing and that the satellite body does not become electrically charged during flight, a two-gate relay system will be implemented. The use of two relays, facing the opposite direction, ensures that the beacon is not accidentally switched on due to vibrational forces.

9.4. Verification & Validation

The TT&C subsystem is designed with the use of the link budget model as described in Section 9.3. The model is used to ensure the signal transmitted will reach the receiver. The equations used in the model, have been verified with the use of unit testing. The model has been validated with the use of actual satellite data. For the physical subsystem, the components that have been selected for the subsystem, have already been verified. Finally, by building the subsystem it can be validated.

10 Command and Data Handling Subsystem

During approach and capturing of Delfi-C3 an optical detection method is used to determine the relative position and rotation. For this, analysis software is used and executed on the on-board computer (OBC). Processing of video is computationally expensive and is the driving requirement for the sizing of the OBC.

This chapter discusses the selection and configuration to deliver the needed functionality. The requirements from previous analysis are listed below.

In Section 10.1 the role of the OBC in the target detection process is explained. Followed by a review of the capability required for video encoding in Section 10.2. The storage device and boards are selected in Sections 10.3, 10.4 and 10.5. Finally the system overview is shown in Section 10.6.

Command and Data handling

RQ-CMS-01 Commands shall be encrypted during uplink.

RQ-CMS-02 The system shall be commandable to start recording a video.

RQ-CMS-03 The OBC shall be able to encode video in real-time at 20 fps.

RQ-CMS-04 The capture manoeuvre shall be recorded on video.

RQ-CMS-05 The compression encoding and bit-rate settings shall be changeable from the ground station using commands.

RQ-CMS-06 Each video frame shall have a time stamp associated with it.

RQ-CMS-08 Any electronic devices currently not needed shall not be powered.

RQ-CMS-09 Over-current protection shall be added to protect critical hardware from exceeding their design voltage.

RQ-CMS-10 The OBC shall have a storage memory size of 128 GB.

10.1. Target Detection

The amount of performance required to do optical detection of an object using multiple camera feeds is difficult to predict without the detection software being available.

The feasibility of this operation is however demonstrated by numerous applications of similar software in, for example, self driving cars[1], autonomous drones and surveillance systems. Companies like NanoNets[2] specialise in the development of object detection abilities for light performance devices like drones. Compared to examples on earth, the problem simplifies when located in space, as there are fewer objects (Delfi-C3, Earth and Moon) to differentiate between and most of the picture will be filled by the blackness of space.

The ability to perform optical object detection with widely available mobile phone hardware is demonstrated using a Samsung Galaxy S8 smartphone. Using an app created by Febin Mathew[3] the S8 is able to differentiate multiple objects using its built in camera. An example of this program in action can be seen in Figure 10.1.

Single-board computers (SBC) with similar performance to the Galaxy S8 are available and could be used as OBC. The optical object detection process becomes more demanding with the number of pixels to be processed and with increasing refresh rate.

10.2. Video Encoding

Aside from object detection, the OBC also performs video encoding. From a benchmark performed on the Raspberry Pi 3 it was observed that hardware encoding is the only usable option (50 fps) as encoding in software (0.8 fps)

[1] `https://www.hackerearth.com/blog/machine-learning/object-detection-for-self-driving-cars/` accessed on 11 January 2019

[2] `https://nanonets.com/object-detection-api/` accessed on 11 January 2019

[3] `https://github.com/febinmathew/TensorFlow-Object-Detection-and-Classification-Android-Example` accessed on 11 January 2019

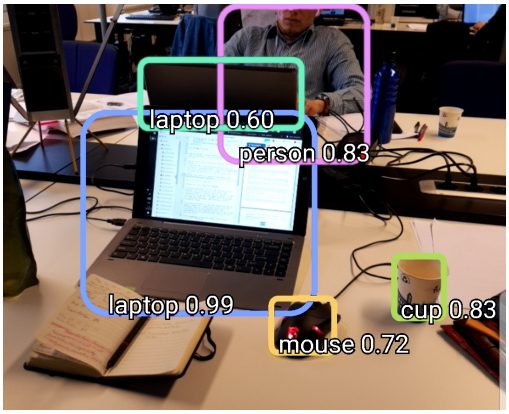

Figure 10.1: Object Detection example created using Galaxy s8 android

requires very high CPU performance and with it comes a high power consumption, while still only achieving relatively low frame rates.

Using hardware encoding will allow for real time encoding for live streaming or recording video to disk without re-encoding. Internet Protocol (IP) cameras, developed originally for Closed-Circuit Television (CCTV) applications, with built in encoding could be useful to reduce the filesize of video while allowing the OBC to focus its resources primarily on video analysis and re-encoding for transmission. The OBC video encoding capability is useful to cut or combine multiple video streams into a single output. Maximising the information density per bit transmitted is beneficial due to the limited time available for downlink. Many encoding algorithms are available, with h.264 and HVEC (h.265) most widespread in hardware implementations. The choice of encoding for transmission shall be configurable in flight. The chosen cameras provide interfaces to easily adjust their settings.

10.3. File Storage

Some SBC already have storage on board, but most require storage to be attached in form of an external device or a Secure Digital (SD) card.

Hard Disk Drives (HDD) and Solid State Drives (SSD) are not feasible choices due to mass, size and power requirements. SD cards have comparatively much smaller mass and size, with a different storage capacity having negligible impact on physical size, mass and power requirements. Therefore a high performance SD card is the best choice for this application with the MicroSDXC PRO+ Memory Card 128GB[4] being widely used in terrestrial applications.

10.4. SBC Selection

Many different SBC's are available, however only very few are used for space applications, and of those none provide the amount of processing power required. While optimisation of the software might make these boards usable, an alternative approach is to use Commercial Off-The-Shelf (COTS) and test it for space application. The Raspberry Pi has for example been used in weather balloons[5]. However, has not been used for a prolonged period of time in space (except inside of the ISS[6]). Therefore, testing of the SBC is required to evaluate its ability to function in space.

The driving requirement for the SBC are the ability for video encoding using a hardware encoder, sufficient performance for optical object detection, and a SD card slot to make use of the chosen card for storage. A selection of usable SBC's is given in Table 10.1.

The Raspberry Pi 3 Model B+ has already been used by hobbyists for object recognition using neural networks[10] however they also report low performance in terms of refresh rate. The Hikey-960 makes use of an Cortex A73 CPU which is approximately twice as powerful as a Cortex A53, resulting in the Hikey-960 being about three times as powerful as the Raspberry Pi 3 Model B+. Requirement RQ-CMS-03 requires to perform the object detection process

[4] `https://www.samsung.com/us/computing/memory-storage/memory-cards/micro-sd-pro-128gb-memory-card-w-adapter-mb-md128da-am/` accessed on 14 January 2019
[5] `https://www.raspberrypi.org/blog/pi-in-the-sky-2/` accessed on 11 January 2019
[6] `https://www.raspberrypi.org/blog/astro-pi-upgrades/` accessed on 11 January 2019
[10] `https://medium.com/nanonets/how-to-easily-detect-objects-with-deep-learning-on-raspberrypi-225f29635c74` accessed on 14 January 2019

Table 10.1: Single Board Computers

Board name	**CPU**	**GPU**	**Mass** [g]	**Power** [W]	**HW Encoding**
Raspberry Pi 3 Model B+[7]	Quad ARM Cortex A53	-	50	10	h.264
Rock64 Media Board[8]	Quad ARM Cortex A53	ARM Mali 450	46	10	h.264
Hikey-960[9]	Quad ARM Cortex A73 + Quad ARM Cortex A53	ARM Mali G71 MP8	60	20	HVEC (h.265) + h.264

cycle at a frame rate of at least 20 fps. To prove that the chosen board is sufficient it is recommended to develop the software and test it with the SBCs. The CPU of the Hikey-960 is in use in the Galaxy S8 smartphone, which is able to run a similar workload as demonstrated in Section 10.1. Therefore the Hikey-960 was chosen for Delfi-REAL as the exact performance requirement is unknown and the Hikey-960 is currently the most powerful option in this small form factor. It is recommended to reiterate this SBC selection at a later point in the project. Considering the fast pace of performance improvements in low energy CPUs and GPUs there might be superior choices available in a few years with improved computational and thermal performance and reduce power usage.

10.5. OBC Selection

The downside of using COTS hardware like the Hikey-960 is the compatibility to other sub-systems on board the spacecraft, primarily limited by the low number of general-purpose input/output (GPIO) pins available on the board. Further pins are required to interface with other controlled systems like the thrusters or ADCS. An additional board to provide these extra pins is therefore required. This board can also provide redundancy in case of an SBC failure. A low performance and power OBC with flight heritage would be an ideal choice. The cubesatshop provides just such a board, the Innovation Solutions In Space (ISIS) OBC[11].

This ISIS OBC could be dedicated to operating Delfi-REAL and controlling mission critical functions, while the high performance SBC is dedicated to the process intensive tasks of object detection and video processing. This separation further allows SBC to only be used and drawing power whenever it is really required, while the ISIS OBC is on at all times resulting in a lower power consumption of the combined system.

The properties of the complete system is summarised in Table 10.2.

Table 10.2: OBC Components

Component name	**CPU**	**GPU**	**Cost** [EUR]	**Mass** [g]	**Power** [W]	**Size** [mm]
Hikey-960	Quad Cortex A73 + Quad Cortex A53	ARM Mali G71 MP8	230	60	20	$85 \times 55 \times 10$
ISIS OBC	ARM9 CPU	-	4400	94	0.55	$96 \times 90 \times 12.4$
Testing			4000			
Total			8630	154	20.55	

10.6. Software and Communication Flow

The OBC needs to continuously be processing housekeeping tasks, mission planning, observations, and data for transmission. The way this can be structured is conceptualised by the software block diagram Figure 10.2.

Within the components different types of data will be exchanged. The functional separation of recording cameras, storing and processing video is nicely visible in the data handling diagram Figure 10.3.

In the high level visualisation of the communications flow diagram, Figure 10.4, the interaction between the OBC, the Delfi-C3 and the ground station is visualised.

[11] `https://www.cubesatshop.com/product/isis-on-board-computer/` accessed on 10 January 2019

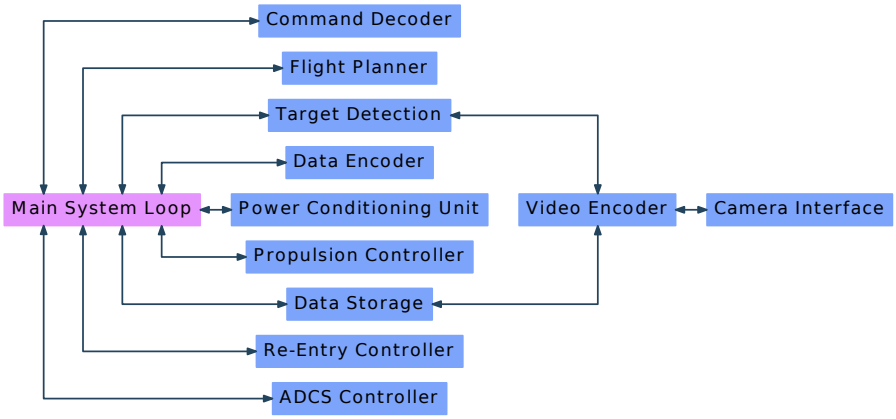

Figure 10.2: Software Block Diagram

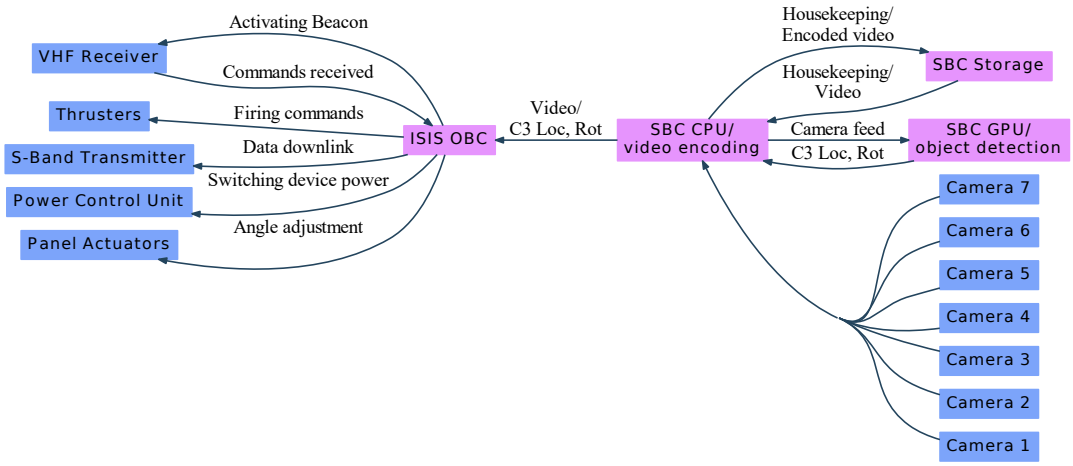

Figure 10.3: Data Handling Diagram

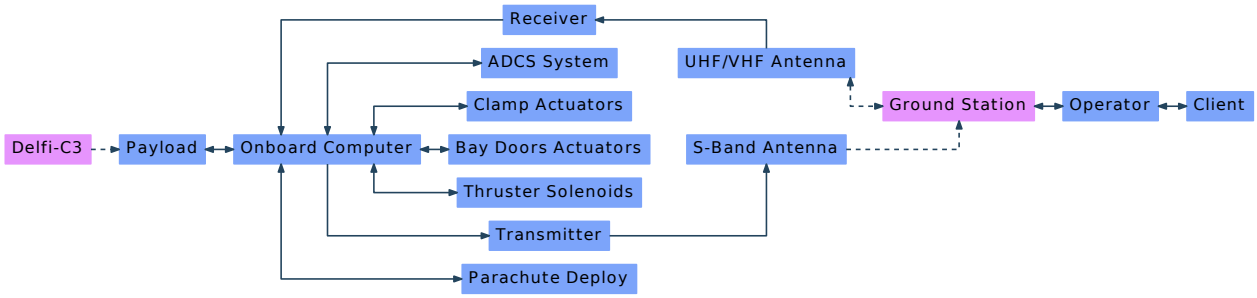

Figure 10.4: Communications Diagram

11 Electrical Power Subsystem

The Electrical Power System (EPS) provides, stores, distributes and controls the electrical power of Delfi-REAL. This section provides an overview of a typical EPS in Section 11.1, providing the subsystem requirements in Section 11.2. All of the components and design options of the subsystem are performed in Section 11.3, displaying the final layout in Section 11.4 and sizing the components in Section 11.5. Verification and validation procedures of the EPS are laid out in Section 11.6.

11.1. System Description

The size of the EPS is dependent on the power required by the subsystems throughout the mission as well as the orbital profile of the spacecraft. The EPS is comprised of a power source, power storage unit and a system responsible for its distribution and control. The main power source for a satellite demanding a power output that lies in the 1 W to 100 W range and a mission duration of a few months to years, are photovoltaic solar cells. These convert solar to electrical energy when the spacecraft is located under direct sunlight, also referred to as daylight period.

Whenever there is no sunlight because of the occlusion of the Earth, the spacecraft is found in eclipse where the solar cells will not be able to generate any power. Thus, a power storage unit in the form of batteries is required. These supply power to Delfi-REAL during eclipse and peak power demands and are recharged once the spacecraft is under direct sunlight again.

These two components are linked to the power distribution and control unit, which provides stabilised voltages via converters to the remaining subsystems. Protection circuits on the EPS are also included to prevent over-currents and battery overcharge and discharge conditions. Lastly, housekeeping parameters such as solar panel current, battery voltage and temperature require a measurement system. The data is later sent to the ground station.

11.2. Subsystem Requirements

The requirements found from the subsystem analysis are presented below.

RQ-EPS-01	The EPS shall distribute power for all spacecraft components, their duty cycles and special operating modes.
RQ-EPS-02	The EPS shall generate power via solar arrays.
RQ-EPS-02.01	The solar arrays shall use a maximum area of 1328 cm^2.
RQ-EPS-02.02	Solar array configuration shall be body-mounted.
RQ-EPS-02.03	The peak power shall be 50 W minimum.
RQ-EPS-03	The system shall use at least two batteries for energy storage and sufficient redundancy.
RQ-EPS-03.01	The batteries shall provide a stable voltage for all operating conditions during the mission life.
RQ-EPS-03.02	The number of duty cycles (discharge and charge cycles) shall be 5510 times per year.
RQ-EPS-03.03	The secondary battery shall have a maximal depth-of-discharge of 25 %.
RQ-EPS-04	The EPS shall distribute power within the specified voltage band to all bus and payload equipment.
RQ-EPS-04.01	Power distribution shall be provided to busses of different voltages using direct current.

11.3. Concept

The following section presents the different considerations taken in order to achieve the most optimal EPS design. These range from a primary concept elimination to the analysis of the Commercial-Off-The-Shelf (COTS) components for the solar cells and batteries. Design options for distribution and control of the collected power are also evaluated as shown in Figure 11.1.

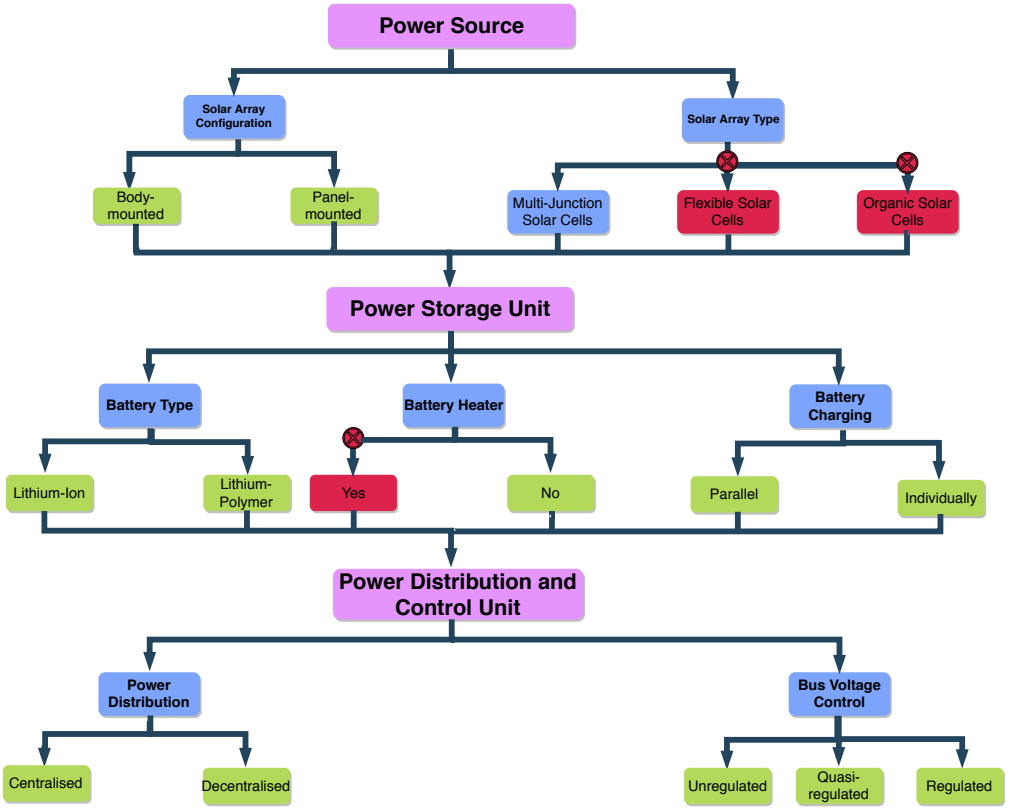

Figure 11.1: Power subsystem design option tree

11.3.1. Concept Elimination

- **Flexible Solar Cells-** As the name suggests, the flexibility of the solar cells could provide more options when regarding its placement on the spacecraft. In comparison to standard solar cells, this option has the potential to decrease the cost of the solar cell production whilst increasing its durability.[1] At the same time, current models possess an efficiency of 8 % which is deemed too low to consider for further steps.
- **Organic Solar Cells-** Organic polymers are another option that was quickly dismissed due to the low Technological Readiness Level (TRL).[2] Additional testing is required to study their behaviour in a space environment and current models have an efficiency of 4 %.
- **Battery Heater-** Batteries are the most temperature sensitive component of the EPS, requiring a temperature above 0 °C to operate properly [18]. Due to the passive thermal control selected in Chapter 12 which is able to keep the system above this temperature, the battery heater is not required.

11.3.2. Main Component Selection

The power source generates electrical power for Delfi-REAL. Photovoltaic multi-junction solar cells have been selected to perform this function. The efficiency as well as the average weight per unit area of different models have been considered as shown in Table 11.1. Only the most recent solar cells are examined due to the objective of obtaining as much power as possible per unit area with sufficient reliability.

As one can observe, current solar cell efficiencies are found just below or at 30 % efficiency. The Triple Junction Solar Cell 3G30C-Advanced (80 µm) by Azurspace is an outlier regarding average weight. Thus, this solar cell type was selected as the power source of the EPS. These are available in standard 30.18 cm^2 units however the company also offers customised sizes based on customer needs.[3]

In either instance, it is assumed that the solar cells will be connected in series to form a solar array, fulfilling the power requirements of the system. These solar arrays could either be located on the structure itself or be extended from it. Due to the importance of the observation of Delfi-C3 for the mission and avoiding additional components

[1] `https://sst-soa.arc.nasa.gov/03-power` accessed 8 Jan. 2019
[2] `https://sst-soa.arc.nasa.gov/03-power` accessed 8 Jan. 2019
[3] `http://www.azurspace.com/index.php/en/products/products-space/space-solar-cells` accessed 12 Jan. 2019

Table 11.1: State-of-the-art solar cells

Solar Cell Type	Efficiency [%]	Average Weight [mg cm^{-2}]
Spectrolab NeXt Triple Junction (XTJ)	29.5	84
Spectrolab Ultra Triple Junction (UTJ)	28.4	84
Azurspace Triple Junction Solar Cell 3G30C-Advanced	30	86
Azurspace Triple Junction Solar Cell 3G30C-Advanced (80 µm)	30	50
Endurosat Triple Junction (InGaP/GaAs/Ge)	29.5	85

sticking out of the spacecraft during re-entry that could impact aerodynamic properties, it was decided that the arrays will be located on the outside of payload bay doors of the structure. These are actuated surface areas that enable to position the solar panels efficiently relative to the sun.

Furthermore, in order to remain operational during eclipse and peak power demands, the EPS requires a power storage unit. The most optimal choices would be lithium-ion (Li-Ion) or lithium-polymer (Li-Po) batteries which are compared in Table 11.2.

Table 11.2: Battery technology comparison [19]

Battery Type	Lithium-Ion	Lithium-Polymer
Gravimetric Energy [Wh kg^{-1}]	100-200	130-250
Volumetric Energy [Wh L^{-1}]	150-250	150-300
Operational Temperature [°C]	-20 to 60	0 to 60

As one can conclude, lithium-polymer batteries have a better gravimetric energy (energy density) which is a criterion of primary importance. This happens due to the fact that they do not need metal packaging. As previously mentioned, the operational temperature is not a killer requirement as the Thermal subsystem is able to provide a satisfactory temperature for both cases. Lastly, Li-Po batteries are not flammable, in contrary to the organic solvent found in lithium-ion batteries [18]. Hence, lithium-polymer batteries are selected, in particular the 40Whr CubeSat Battery model from Clyde Space.[4] These are going to be recharged during daylight in parallel due to the short duration of the mission and easier assembly. Individual battery charging is typically considered for missions longer than five years, when the degradation of the batteries becomes an issue [7].

11.3.3. Secondary Design Choices

Assuming that the EPS is able to collect electrical energy to a sufficient degree, it is relevant to consider the manner in which that power is distributed throughout the spacecraft. In short, power distribution is dependent on the location of converters which rely on individual component requirements. As can be observed in Table 11.3, Delfi-REAL includes components operating at 3.3 V, 5 V and 12 V and their respective power consumption during daylight and eclipse periods which adds up to 29.9 W during daylight and 7.2 W during eclipse.

Thus, provided that there are three groups of components requiring different voltages on-board, it was determined to choose a decentralised approach. This means the converters are put at each component separately. Distributed design contains a similar efficiency to a centralised power distribution and enables to optimise the EPS at a lower level [20]. This design choice also implies that the bus voltage control is unregulated. Because these distributed converters regulate power, it means that the voltage of the bus is the same as the voltage of the batteries, which varies during their charge/discharge cycle.

Protection circuits are placed on user boards, saving space on the EPS card. This configuration also allows the On-Board Computer (OBC) to turn the power of each subsystem on and off individually [18]. Batteries are also delivered with a Protection Circuit Module (PCM), which protects the batteries against over and under charge as well as over current conditions. Several circuits for housekeeping parameter measurement are included on the EPS and communicated to the OBC. Lastly, Table 11.3 shows the parachute does not require any power however that is not completely true; a switch controlling the flow of current is located on the EPS card which allows the component to be deployed via an OBC command. Due to the relatively sudden power required for this one-off mode, the circuit is supplied directly from the batteries. A similar approach is taken for the antenna deployment in the initial stage of the mission.

[4] `https://www.clyde.space/products/49-40whr-cubesat-battery` accessed 12 Jan. 2019

Table 11.3: Power usage of Delfi-REAL during daylight and eclipse

Main Mode		Daylight			Eclipse		
Subsystem/Component	Voltage [V]	Mode	Duty [%]	Power [mW]	Mode	Duty [%]	Power [mW]
On Board Computer	-	on	-	15655	passive	-	556
Data processing OBC	12	on	75	15150	off	0	0
Primary OBC	12	on	100	505	on	100	556
Radio Transceiver	-	receive	-	691	receive	-	691
Telecommand Receiver	12	on	100	505	on	100	505
Transmitter	12	on	2	186	on	2	186
ADCS	-	on	-	6595	passive	-	5454
ADCS Main Board	3.3	on	100	404	on	100	404
Sun sensor	5	on	100	131	off	0	0
Star tracker	5	on	100	1010	off	0	0
Magneto(meter/torquer	5	on	50	606	on	50	606
Reaction wheels	3.3	on	50	4444	on	50	4444
Payload	-	on	-	6446	off	-	0
Detection cameras	3.3	on	75	2651	off	0	0
Non-detection cameras	3.3	on	75	159	off	0	0
Propulsion	12/3.3	off	0	0	off	0	0
Clamp	12	off	0	0	off	0	0
Structures	3.3	on	100	3636	off	0	0
Parachute	0	off	0	0	off	0	0
Electrical Power System	3.3	on	100	505	on	100	505
Total				29892			7206

11.4. Electrical Block Diagram

All of the design options presented above combine into the electrical block diagram shown in Figure 11.2. The power source and the power storage unit are linked to the power distribution and control whose converters ensure that all the users get their required voltage. The deployment of the antenna and the parachute are one-off circuits which are switched during a pre-set time during the mission and housekeeping measurements occur at a voltage of 3.3 W [18]. Within the users, every component found in Table 11.3 is linked to the OBC (both primary and data processing) as shown in Figure 5.5 (Page 21). Besides the power provision supplied at three different voltages, the components communicate with the OBC via the Inter-Integrated Circuit (I2C-bus) protocol. The I2C-bus is a bidirectional interface which uses a controller (known as a master) to communicate with the remaining components (slaves) via a data and clock lines [21].

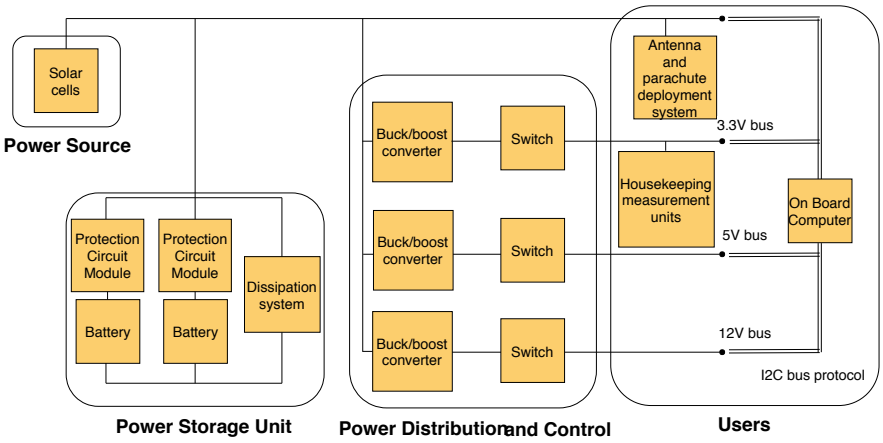

Figure 11.2: Electrical Block Diagram

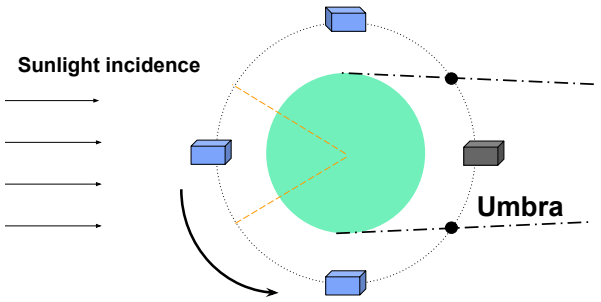

Figure 11.3: 2D orbit simplification with daylight and eclipse.

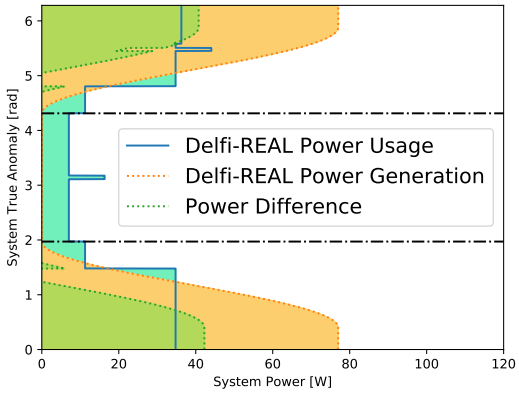

Figure 11.4: System power profile during an average Delfi-C3 study orbit.

11.5. Final Design

In order to size the EPS, first the orbital period was computed. The orbital altitude was taken to be 547 km, an average between the perigee and apogee altitudes.[5] Hence, the orbital period can be found using Equation 11.1 where a is the semi-major axis and μ is Earth's gravitational constant.

$$T_o = 2 \cdot \pi \cdot \sqrt{\frac{a^3}{\mu}} \tag{11.1}$$

This equation outputs an orbital period of 95.4 minutes which translates to 5510 orbits per year, meaning that there is an equal number of charge and discharge cycles for the batteries. The orbital period is split into daylight and eclipse periods which is depicted in Figure 11.3. As can be observed, the orbit contains periods where the satellite is under direct impact of sunlight and others where it is found in Earth's shadow. The fractional time of daylight was computed using

$$\frac{T_s}{T_o} = \frac{\pi + 2 \cdot \arccos(\frac{R_E}{a})}{2 \cdot \pi} \tag{11.2}$$

where R_E is the equatorial radius of the Earth [22]. It was found that the satellite daylight period fraction is 0.627 , which translates into 59.9 min in sunlight and 35.5 min in eclipse. Due to the body-mounted design, the payload bay doors offer 0.1328 m^2 as seen in Chapter 17 on page 95. This value is taken for A_0 in Equation 11.3 where ν is the true anomaly of the satellite [22]. The equation was then used as input for Equation 11.4 where $P_\odot$ is the solar irradiance (1367 $W m^{-2}$) and n_{SC} is the solar cell efficiency.

$$A = 2 \cdot A_0 \cdot \cos(45°) \cdot \sin^2(\nu) \tag{11.3}$$

$$P = P_\odot \cdot \eta_{SC} \cdot A \tag{11.4}$$

This outputs the power generation of Delfi-REAL as presented in Figure 11.4. The peak power is found to be 77.02 W and was assumed to stay constant during a 45° range where the spacecraft is fully aligned with the solar flux, displayed by the orange dotted lines in Figure 11.3 which is matched by levelling at the edges of the graph. Integrating Equation 11.3 yields an average power of 24.70 W, assuming an additional EPS efficiency factor of 85 % due to design inefficiencies, shadowing and temperature variation [7]. Due to the short mission duration, physical degradation of the solar cells was neglected, making the array's performance the same at Beginning-Of-Life (BOL) and End-Of-Life (EOL) [22].

The power usage of Delfi-REAL during eclipse found in Table 11.3 is used to design the energy storage unit. It enables to compute the capacity of the batteries using Equation 11.5 and thus the number of units required onboard. The equation takes T_e as the eclipse time duration in hours, 7.2 V as an average of the lithium-polymer battery voltage[6], a depth of discharge (DOD) of 20 % and n_e, the transmission efficiency between the battery and the component of 0.9 [7]. This outputs a required battery capacity of 3.29 Ah. Provided that one singular battery has a typical capacity

[5] `https://heavens-above.com/orbit.aspx?satid=32789&lat=0&lng=0&loc=Unspecified&alt=0&tz=UCT&cul=en` accessed 10 Dec. 2018

[6] `https://www.clyde.space/products/49-40whr-cubesat-battery` accessed 15 Jan. 2019

of 5.2 Ah[7], one battery would suffice, however for redundancy purposes two lithium-polymer batteries will be part of the power storage unit.

$$C = \frac{P_e \cdot T_e}{V_{bat} \cdot DOD \cdot n_e} \tag{11.5}$$

The most power demanding stage of the mission is the transmission of live video during observation of Delfi-C3, requiring 36.7 W of instant power consumption, with the capture stage requiring 35.6 W both during daylight. As it is arguably observable from the power difference in Figure 11.4 and was confirmed using the model, the EPS is able to withstand such power loads, using additional charge available from the batteries. This EPS configuration makes the power production for Delfi-REAL sustainable as it enables it to function properly for the mission duration as well as potentially longer periods of time in case unforeseen circumstances extend the mission duration.

The selected solar arrays and batteries possess a mass of 66.4 g and respectively.[8] 670 g[9] Additional mass is taken by the EPS circuit board[10] with 292 g, including two battery packs, totalling 1.028 kg for the EPS. The total cost of the subsystem is EUR 57 k breaking down into EUR 44 k, EUR 10 k and EUR 3 k for the considered components respectively.

11.6. Verification and Validation

Provided that the sizing of the solar arrays was taken from the available area on the payload bay doors, it is valuable to estimate the required area in case the power source was independent from the rest of Delfi-REAL. A raw area estimation is provided by finding how much available power the EPS needs to collect during one orbit and dividing it by the solar array performance at EOL as shown in Equation 11.8.

$$P_{sa} = \frac{\frac{P_e \cdot T_e}{X_e} + \frac{P_d \cdot T_d}{X_d}}{T_d} \tag{11.6}$$

$$P_{EOL} = P_{\odot} \cdot \eta_{SC} \cdot I_d \tag{11.7}$$

$$A_{sa} = \frac{P_{sa}}{P_{EOL}} \tag{11.8}$$

Equation 11.6 requires the power usage as well as the duration of eclipse and daylight period, taking into consideration the efficiency of the path from the solar array to the individual users taken to be 0.85 and 0.65 for X_e and X_d respectively, yielding 41.8 W for P_{sa}. Equation 11.7 presents similar considerations seen in Section 11.5 and introduces inherent degradation, I_d with a value of 0.77 , outputting 315.8 $\mathrm{W\,m^{-2}}$. Thus, A_{sa} was found to be 0.1322 $\mathrm{m^2}$, closely matching with the area provided by the payload bay doors taken to be 0.1328 $\mathrm{m^2}$ [7].

Provided that all of the components are COTS, it is insightful to validate the system via integration testing and mission phase simulations. The first one could be done by performing a full power system analysis. Analysing the power performance of every components found before the user, enables the design team to identify where the power is dissipating. Battery charge and discharge currents are also an important factor when testing the final EPS layout. Mission phase simulations have been examined in order to size the EPS properly by considering the cumulative power demands of all components. At the same time, further modelling of the solar array and batteries could be used to perform full mission simulations for the power system where bus voltages and bus switches could be implemented based on mission scenarios. Such a model could be developed in MatLab Simulink [20].

[7] `https://www.clyde.space/products/49-40whr-cubesat-battery` accessed 15 Jan. 2019
[8] `http://www.azurspace.com/images/products/0004148-00-01_DB_GBK_80%C2%B5m.pdf` accessed 16 Jan. 2019
[9] `https://www.clyde.space/products/49-40whr-cubesat-battery` accessed 16 Jan. 2019
[10] `https://www.endurosat.com/cubesat-store/cubesat-power-modules/power-module/` accessed 16 Jan. 2019

12
Thermal Control Subsystem

In order to ensure that all subsystems perform satisfactory in the harsh environment of space, the operating temperature of Delfi-REAL needs to be analysed and, if necessary, controlled. For this purpose, the thermal control subsystem is introduced. In this chapter, the requirements on the thermal control system will be discussed in Section 12.1, then the thermal analysis will be described in Section 12.2. Afterwards, the trade-off of the Thermal control system is performed in Section 12.3. Finally, the design of the thermal control system is summarised in Section 12.4.

12.1. Requirements

The requirements on the thermal control subsystem are given by the maximum and minimum operating temperatures of all other subsystems. These give an operating range in which Delfi-REAL will function as required. For some of the subsystems, no exact components are known at this stage of the design process. For these subsystems, a value for the operating temperature range is taken from the Space Mission Analysis and Design (SMAD) book [17]. In Table 12.1 the operating temperature range of all relevant subsystems are stated.

From Table 12.1, an operating range requirement for Delfi-REAL of 0 °C to 50 °C is deduced.

12.2. Thermal analysis

In this section, the calculation methods applied for the thermal analysis will be explained. The analysis itself is an iterative process, using the same calculation methods. Every time a design change in the thermal control is made, a new iteration in the calculation is performed, eventually leading to a final design that satisfies the requirements.

The fundamental equations for the thermal analysis are the equations for the absorption, Equation 12.1, and emittance, Equation 12.2, of thermal energy by a flat plate.

$$Q_{absorbed} = (\alpha \text{ or } \epsilon) \cdot A \cdot R \cdot sin(i) \tag{12.1}$$

In Equation 12.1 α and ϵ are the absorptivity and emissivity of the material respectively, A is the surface area of the plate, R is the radiation intensity and i is the incidence angle of the plate with the radiation source. α is used when the radiation source is the sun and ϵ is used when the radiation concerns infrared (IR) radiation.

$$Q_{emitted} = \epsilon \cdot \sigma \cdot A \cdot T^4 \tag{12.2}$$

In Equation 12.2, ϵ is the emissivity, σ is the Stefan–Boltzmann constant, A is the surface area and T is the material temperature.

In order to calculate the total absorbed and emitted energy by Delfi-REAL, the satellite will be divided into multiple panels, for which the incidence angle with both Earth and the Sun as well as the surface area need to be determined. Looking at the structure of Delfi-REAL as described in Chapter 17 on page 89, Delfi-REAL is divided in 14 panels, six for the main body and eight for the payload bay doors (4 doors with an inside and an outside). The payload bay doors are two panels each, since both sides of the panels are subjected to different radiation conditions. They might have different material properties due to coatings that may be applied during the design phase. In Table 12.2 the surface areas of all panels are given.

Subsystem	**Low** °C	**High** °C
Battery (see chapter 11)	0	50
Communication system [17]	−20	60
Solar panels [17]	−120	150
OBC	−25	50
Structures [1]	−40	80
Propulsion[23]	−5	60

Table 12.1: Critical operating temperature

Plate	surface Area [m^2]
Main body	
Nadir	0.09
Zenith	0.09
4 Sides	0.03
Payload bay doors	
4 Insides	0.0776
4 outsides	0.0776

Table 12.2: Surface areas plates, calculated from dimensions stated in Chapter 17

Now that the panels have been defined, the radiation sources need to be analysed. There are three radiation sources Delfi-REAL is subjected to: solar radiation (R_{solar}), albedo radiation (R_{albedo}) and earth infrared radiation (R_{IR}). R_{solar} is the direct radiation from the sun, which in orbit around Earth is equal to 1358 $\mathrm{W m^{-2}}$[17]. For the absorption of this radiation α should be used. R_{albedo} is the solar radiation reflected by Earth, which is 30% of the direct solar radiation, 407.4 $\mathrm{W m^{-2}}$. For the albedo radiation also α is used. R_{IR} is the infrared radiation emitted by Earth. The intensity of this radiation is dependent on the orbital altitude. At an orbital altitude of 547 km, which is the same as Delfi-C3, the R_{IR} intensity was calculated to be 201 $\mathrm{W m^{-2}}$[17]. For the absorption of this radiation, ϵ was used, since this defines the absorption ratio of the IR spectrum.

Both the temperature of the system and incidence angle of the panels varies throughout the orbit. Since the analysis is focused on the extreme values of the temperature, the orbital locations where these extreme values occur have to be determined. The maximum temperature will occur at the point where Delfi-REAL has the most exposed area to the solar, albedo and IR radiation. This is the situation where Delfi-REAL is in between the sun and Earth and has a pitch angle of 90° and roll angle of zero. At this point, the payload bay doors and the large panels of the main body are most exposed. This leads to an incidence angle for the nadir and zenith panels of 90° with Earth and the sun respectively. The side panels have an incidence angle of 0°.

The α and ϵ are dependent on the outside material of the panels. These materials can be chosen during the design process, by applying a coating to the panel. This is further discussed in Section 12.3.

Since all variables in the absorbed and emitted energy equations are known except for the temperature, the energy balance can be computed. Since emitted energy increases with increasing temperature, an equilibrium temperature will be achieved, which can be formulated in an equilibrium Equation 12.3.

$$\sum_{i=0}^{n=14} Q_{absorbed_i} + P_{used} = \sum_{i=0}^{n=14} Q_{emitted_i} \tag{12.3}$$

In Equation 12.3 the i is the i^{th} panel and P_{used} is the power used by Delfi-REAL, since this will also be converted into heat . In this equation the only unknown is the temperature, which will be the same for every panel in this equation and can therefore be calculated. During the design process it can be chosen to thermally separate parts of Delfi-REAL, keeping them at different temperatures. This is further discussed in Section 12.3.

This equilibrium temperature calculation can be done for both the maximum and the minimum temperature. However, this equilibrium temperature will only occur if the satellite stays in the equilibrium conditions for a sufficient amount of time. Since Delfi-REAL will stay in sunlight longer than it will stay in eclipse, the maximum equilibrium will be achieved. Due to the short eclipse time of the Delfi-C3 orbit, the minimum equilibrium conditions might not be achieved. To analyse the minimum temperature of the orbit, Equations 12.4, 12.5 and 12.6 are derived from the thermal analysis concepts as described in SMAD [17].

$$\dot{Q} = \sum_{i=0}^{n=14} Q_{absorbed_i} + P_{used} - \sum_{i=0}^{n=14} Q_{emitted_i} \tag{12.4}$$

$$\Delta T = \int_0^{t_{eclipse}} \frac{\dot{Q}}{m \cdot c} dt \tag{12.5}$$

$$T_{minimum} = T_{maximum} + \Delta T \tag{12.6}$$

Equation 12.4 gives the energy flux at every point in the orbit; $Q_{emitted}$ depends on the temperature. As an initial value, the maximum temperature was used. Equation 12.5 calculates the change in temperature due to an energy flux; m is the mass of the system, c is the average specific heat of the system and $t_{eclipse}$ is the total eclipse time. Finally, Equation 12.6 gives the minimum temperature of the system.

The Electric Power System (EPS) uses one side of the payload bay doors as solar arrays. For the solar cells used, the absorptivity and emissivity are known to be approximately 0.9 and 0.85 respectively [17]. When for all other panels a white paint coating is assumed, for which α is 0.3 and ϵ is 0.8 [17], the maximum and minimum temperature of the entire system become 77.5 °C and 13.4 °C respectively. The maximum temperature is well above the maximum allowable temperature according to the requirements stated in Section 12.1. Therefore, some form of thermal needed implemented.

During this entire analysis, the heat dissipated by Delfi-C3 was neglected. This was due to the low Power usage of Delfi-C3, this was assumed not to be an issue. Also the it was assumed that all components within the main body have a uniform temperature, this assumption's validity should be investigated using further analysis of all components, their power usage and their placement within the system.

12.3. Trade-off Thermal control

For the design of the Thermal control system, some design choices need to be made. In order to find all possible options, a Design Option Tree (DOT) is presented in Subsection 12.3.1. Then all concepts are analysed in Subsection 12.3.2. Finally, the trade-off itself is performed in Subsection 12.3.3.

12.3.1. DOT and concept elimination

In order to get the maximum temperature within the allowable range, multiple design options are possible. To find all design options for the thermal control, a DOT is used, which is shown in Figure 12.1.

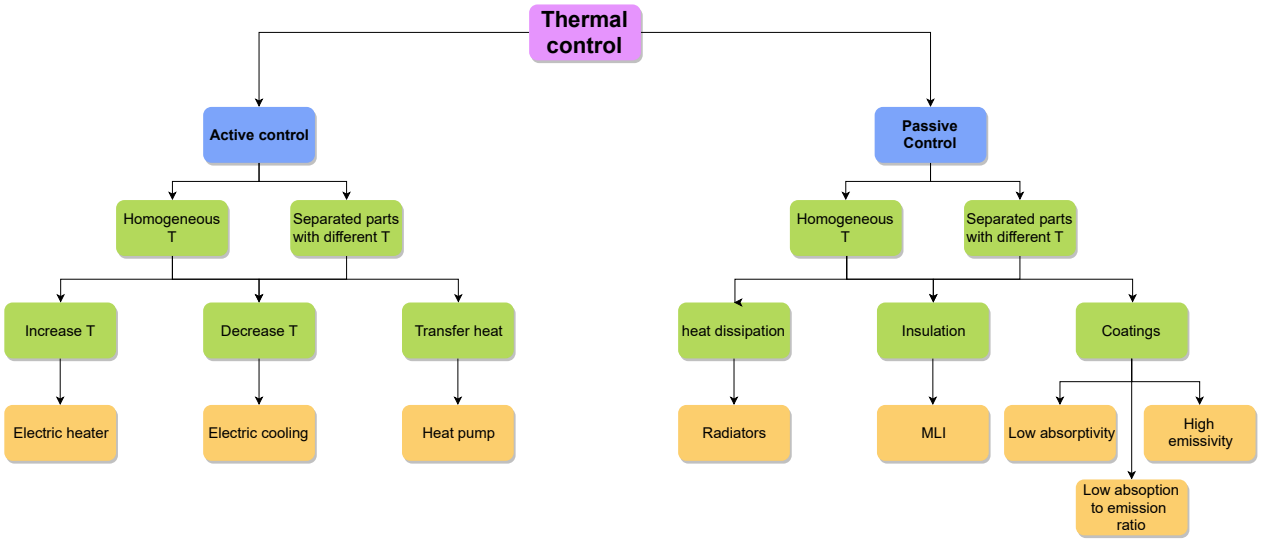

Figure 12.1: Thermal DOT

In the DOT, the first choice is between active and passive thermal control. Active thermal control is when power is used to actively heat or cool the entire system or parts of it. Passive control does not use any power to influence the systems temperature. Active thermal control is something that is best avoided if possible. It increases the power budget in a significant way, which in turn influences the heat balance, as explained in Section 12.2. A higher power requirement also increases the mass. Finally, active thermal control leads to more complexity and contains less reliable parts. Therefore, this design concept was discarded early in the process.

The next design choice is whether the system will have one homogeneous temperature, or whether it will be split up into two or more parts, which will be kept at different temperatures. This division of the system is best suitable if there is a significant difference in operating temperature requirements for subsystems that are not placed together. This makes it easier to thermally separate the compartments. Furthermore, it is also possible to insulate a specific subsystem within the main body, such as the batteries. This ensures less temperature fluctuations for that subsystem.

For both homogeneous and separated temperature, there are three ways to passively influence the thermal energy flow: Heat dissipation, insulation and coatings. Heat dissipation uses surface areas (radiators) with high ϵ characteristics to dump excess thermal energy to space. Insulation decreases the heat transfer within the system or the

heat transfer to space. Coatings can be applied on the outside surface areas to change the thermal absorption and emission properties to obtain the desired energy flux. Of these three concepts, a combination can be used.

Heat dissipation through radiators was discarded early on, since mounting radiation panels on the spacecraft would increase the weight significantly, which should be avoided if possible.

12.3.2. Concept analysis

The concepts that are left after elimination of active thermal control and dissipating heat through radiators, are homogeneous or separate temperatures using coatings, insulation or a combination of both.

If possible, homogeneous temperature is preferred over separation, since it introduces less complexity to the design. However, homogeneous temperature is not always possible. To analyse the feasibility of a homogeneous temperature, a simple calculation is done using the calculation method described in Section 12.2, assuming the main body to have an α of zero, an ϵ of one and the payload bay doors to consist of the solar cells with α and ϵ of 0.9 and 0.85 respectively. This is a theoretical exercise since there are no coatings or materials with an absorptivity of zero or emissivity of one. However, when the maximum temperature in this theoretical case is still exceeding the requirement, no passive thermal control can be implemented without multiple temperatures, since no coatings with better properties can exist. Performing this calculation, a maximum temperature of 68.5 °C and a minimum temperature of 10.7 °C is obtained. Therefore, the system must be separated into two or more compartments operating at different temperatures.

Since the solar panels have a significantly larger operating range than all other subsystems and since they are mounted on the payload bay doors, thermally separating the payload bay doors from the main body is the most logical and least complex design.

The only design option left is the application of coatings. To perform a trade-off between different coatings, the characteristics of some commonly applied thermal coatings for space are stated in Table 12.3.

Coating	α	ϵ
Catalac white paint	0.24	0.9
Z9SC55 white paint	0.14	0.94
Polished aluminium	0.14	0.03
Clear anodised aluminium	0.44	0.85
ITO coated silver FEP10 [24]	0.15	0.85
Anodize black paint	0.88	0.88

Table 12.3: Coating characteristics

The coatings in Table 12.3 are just a small selection of coatings. However, all major types of coatings are represented in the table. White paint is the most commonly used, since it is cheap (negligible cost) and has low α/ϵ values. Polished and clear anodised aluminium are also easy choices, since most structural panels are made from aluminium, where anodising or polish treatments are possible. Moreover, polished aluminium has very low ϵ values and is therefore preferable when low heat emission is required or when low IR radiation absorption is needed. Furthermore, the ITO coated silver is a Multi Layer Insulation (MLI) sheet, which is very effective and often used for spacecraft, but is more expensive. Black paint is for situations where the temperature needs to be increased, due to its high α value.

Since the temperature needs to be decreased, not increased, the black paint can not be used. The other four coatings will be analysed further. In Table 12.4 the outcome of the calculations for all coatings are given. Here it can be seen that clear anodised aluminium is the only coating that provides a minimum and maximum temperature that is within the requirements for the main body. All other coatings give either too low or too high minimum or maximum temperatures. Therefore, a coating with similar characteristics as clear anodised aluminium needs to be applied. In Table 12.5, four suitable coatings are stated. All of these coatings result in an acceptable operating temperature. These coatings will enter a trade-off.

In Table 12.5, four suitable coatings are stated. All of these coatings result in an acceptable operating temperature. These coatings will enter a trade-off.

12.3.3. Trade-off

In order to perform a trade-off, first the trade-off criteria need to be established. Since mass and volume for all possible coatings are negligible, these will not be entered in the trade-off as trade-off criteria.

Coating	Max. T	Min T
Catalac white paint	7	-4
Z9SC55 white paint	-7	-15
Polished aluminium	320	311
Clear anodised aluminium	32	15
ITO coated silver FEP10 [24]	0	-9

Table 12.4: Coating characteristics

Coating	α	ϵ
Clear anodised aluminium	0.32	0.75
Aeroglaze A971 yellow paint	0.43	0.89
Beta cloth/VDA sheldahl	0.38	0.85
Tedlar white plastic	0.39	0.87

Table 12.5: Coating characteristics

Reliability (9/10) - The reliability of the coating is mostly related to the Technological Readiness Level (TRL) and on the chance of damage. Since all four coatings have been used on numerous space missions and are collected from a NASA reference book from 2005 [25], the TRL is assumed to be high. The vulnerability however differs. The Tedlar plastic and Beta cloth have the risk of damage and in the worst case scenario rupture, when hit by micro meteorites. Therefore, they are ranked “exceeds requirements” for reliability. The yellow paint can also be damaged, but in a less severe way. Therefore it is ranked nominal. And finally, the anodised aluminium is ranked excellent, since the thermal properties of it will only drastically change when the satellite it self is damaged as well.

Cost (8/10) - No exact costs are known for any of the coatings. However, a division can be made in the coatings to make an estimation on their cost relative to each other. The paint will most likely be cheaper than the other coatings, since applying the paint is not a complex process and testing on it can be minimal. Therefore, it is ranked as excellent. The testing on the anodised aluminium can be minimal as well, however, its application is more expensive since it requires expert knowledge and therefore needs to be performed by an outside company. It is therefore ranked as nominal. The Tedlar and Beta cloth both have significant material cost, will need to be applied by experts and will need thorough testing to verify whether it will hold during procedures such as launch.

Complexity (7/10) - The complexity of a coating is mostly due to the additional handling requirements it causes, since the design of the coatings is not different. Therefore, the paint and anodised aluminium are both low in complexity, since once the coating is applied, the satellite does not need to be handled more careful than it already did. The Tedlar and Beta cloth however, are more fragile and need more delicate handling after application. Therefore, they are marked nominal, since they are still widely used techniques.

Table 12.6: Design concept trade-off table for the Thermal Control. excellent: excel, nominal: nom, exceeds requirement: exreq, unacceptable: unacc.

Criterion / **Option**	**Reliability**	System **cost**	**Complexity**
Anodised aluminium	excel	nom	excel
Aeroglaze yellow paint	nom	excel	excel
Beta cloth/VDA Sheldahl	exreq	exreq	nom
White Tedlar	exreq	exreq	nom

As can be seen in Table 12.6, the anodised aluminium is the best option for the thermal control coating of the main body.

12.4. Final design

After analysis and calculation of the operating temperature of multiple coatings and performing the aforementioned trade-off, the thermal control of Delfi-REAL will consist of the following: a thermal separations of the main body and the payload bay doors, and a clear anodised 7075 aluminium layer of 0.001 mils thickness. This leads to a minimum and maximum operating temperatures 11.1 °C and 24.4 °C respectively for the main body. The payload bay doors have a minimum temperature of −16.4 °C and a maximum temperature of 55.0 °C.

13
Propulsion Subsystem

This section discusses the final design process of the Propulsion Subsystem. A brief description of this subsystem is given in Section 13.1. Section 13.2 gives an overview of the requirements and how they were discovered. The trade-off process going from concept creation to final selection can be found in Section 13.3, in this section the Design Option Tree (DOT) can be found as well. Finally, in Section 13.4 the architecture and parameters of the final design are discussed as well as some future recommendations.

13.1. System Description

In order to accomplish the mission objectives, Delfi-REAL should be able to change its orbit and rendezvous with Delfi-C3. After taking pictures and video footage it should capture Delfi-C3 and finally it needs to decrease its altitude to re-enter in to the atmosphere.

The capture of Delfi-C3 is the most critical phase of the mission for the propulsion system. During this phase it needs to deliver high accuracy movement control. The capture will be done fully autonomous and will be controlled by the on-board computer. The capture manoeuvre will be done by flying close to Delfi-C3 and start following the rotation and position of the short antenna side on the longitudinal axis of Delfi-C3. During this rotation matching, it will slowly decrease the distance and relative velocity.

In Chapter 8, a more in-depth description of the capture manoeuvre is given. In order to analyse the feasibility as well as the required Delta-V of this manoeuvre a simulation was made. This simulation is discussed in Chapter 14.

13.2. Requirements

This section describes the requirements of the Propulsion subsystem. The requirements were established by analysing the specific individual functions. These different functions require different performances consisting of providing a certain Delta-V, using a thrust with a certain accuracy, frequency and a minimum amount of duty cycles.

13.2.1. Delta-V requirements

The primary purpose of the propulsion system is to provide velocity changes to the spacecraft throughout the mission. An overview of the Delta-V requirements for each of the functions is given in Table 13.1.

Table 13.1: Delta-V requirements for the propulsion subsystem.

Propulsion Function		**Delta-V [m/s]**
Insertion inaccuracy compensation	Altitude inaccuracy	16
	Inclination inaccuracy	10
Rendezvous with Delfi-C3	Perigee burn	16
	Apogee burn	16
Reconnaissance	Stationkeeping	0.3
	Manoeuvring	5
Capture	Close distance	39.2
	Perform Capture	12
De-Orbit	Apogee burn	110
	Total	225
	5% Margin	236

Delfi-REAL was designed to be able to be launched by the most commonly used launch vehicles. This was done to increase the chance of being able to piggy-back and therefore allowing Delfi-REAL to be launched as soon as possible. The insertion inaccuracy compensation was derived by looking at the insertion inaccuracies of these most commonly used launchers, comparing them and taking the worst case scenario. As can be seen in Table 13.2 the maximum altitude and inclination inaccuracy is 35 km and 0.2°. This results in a required Delta-V of $16\,\mathrm{m\,s^{-1}}$ and $10\,\mathrm{m\,s^{-1}}$ respectively.

Table 13.2: Insertion inaccuracy of common used launchers [8] [26] [6] [27] [28].

Launcher	Altitude inaccuracy [km]	Inclination inaccuracy [deg]
Ariane 5G	40	0.02
Falcon9	15	0.1
PSLV	35	0.2
Soyuz IKAR	25	0.2
Soyuz Fregat	10	0.1
Soyuz ST	10	0.1

To allow capture of Delfi-C3, it was decided that Delfi-REAL should match the rotation of Delfi-C3 by rotation on one axis and translation on the two others, while slowly getting closer to it, ending at a final distance of 0.15 m. From the simulation it was seen that closing this distance plus rotation matching would take 0.013 $\mathrm{m\,s^{-1}}$ while after it closed the distance it only needs 0.0066 $\mathrm{m\,s^{-1}}$.

Furthermore it was shown that closing the distance takes 25 min, while the final rotation matching for capture will take 15 min. The total Delta-V required for both these phases are shown in Table 13.3. For the sizing this was multiplied by a factor of two to account for sub-optimal conditions and multiple attempts.

Table 13.3: Delta-V required for the capture of Delfi-C3.

Phase	Delta-V per second	Time [s]	Delta-V [m/s]	Safety Factor	Total Delta-V [m/s]
Distance closing	0.013	1500	19.6	2	39
Rotation matching	0.0066	900	6.0	2	12
Final Delta-V					51

13.2.2. Thrust

In order to achieve the required velocity changes within the established mission duration a minimal required thrust of the propulsion system was determined. This was done using small Hohmann transfers to lower the perigee to 150 km. A maximum burn time per orbit of 10 seconds was used in order to maximise fuel efficiency.

Table 13.4 shows the total mission duration in days for different thrust values. The minimum thrust required is 0.1 N in order to keep the total mission duration around half a year.

Table 13.4: Mission duration by provided thrust. Determined using a frontal area of 0.14 $\mathrm{m^2}$, a C_D of 2.2 and a reconnaissance duration of 90 days.

Thrust [N]	Total mission duration in days
1	103
0.1	242
0.01	1222

13.2.3. Accuracy

Besides total Delta-V and thrust, there are requirements on the accuracy of the propulsion system as well. Both the reconnaissance and the capture require high precision manoeuvring. The Minimum Impulse Bit (MIB) is the smallest impulse a thruster is able to deliver to the satellite. For these manoeuvres, an accuracy of 1 $\mathrm{mm\,s^{-1}}$ is required. This results in a MIB of 0.0121 N s, as shown in Equation 13.1.

$$MIB = m \cdot V_{Accuracy} = 12.1\,\mathrm{kg} \cdot 0.001\,\mathrm{m\,s^{-1}} = 0.012\,\mathrm{N\,s} \tag{13.1}$$

Furthermore in order to have precise movement control during the capture phase, a high impulse frequency is preferred. This will allow the spacecraft to quickly adapt to changing circumstances or correct for errors. For this, a minimum frequency of 10 Hz is required.

13.2.4. Duty Cycles

Duty cycles in thrusters define how many times the thruster can be turned on and off. As stated earlier, the propulsion system will use multiple burns to get in the correct orbit. For this a minimum number of duty cycles of 2000 is

required. The propulsion system will also have to do multiple pulses during both reconnaissance and capture. A simulation was made to determine the amount of pulses needed during these phases. In total a minimum number of duty cycles of 10 000 is expected.

13.2.5. List of requirements

The requirements found from the analysis are presented below. The PRO label stands for propulsion.

RQ-PRO-01	The propulsion system shall provide all required Delta-V and thrust as needed for insertion inaccuracy compensation, rendezvous, reconnaissance, capture and de-orbit.
RQ-PRO-01.01	The propulsion system shall provide a minimum total Delta-V of 225 $m\,s^{-1}$.
RQ-PRO-01.02	The propulsion system shall have a minimal thrust of 0.1 N to complete the mission in the required mission time.
RQ-PRO-01.03	The propulsion system shall have a duty cycle of at least 10 000 cycles.
RQ-PRO-01.04	The propulsion system shall have a minimum impulse bit of at least 0.012 Ns.
RQ-PRO-01.05	The propulsion system shall have a minimum impulse frequency of 10 Hz.
RQ-PRO-01.06	The propulsion system shall have a 3-axis thruster system to control translational movement.
RQ-PRO-02.01	A failure of one component of the propulsion system shall not cause failure of the entire system.
RQ-PRO-02.02	A failure of one component of the propulsion system shall not cause failure of another component.
RQ-PRO-03	The propulsion system mass shall not exceed 2.6 kg.
RQ-PRO-04	The propulsion system shall have a nominal power usage lower or equal to 19 W.
RQ-PRO-05	The propulsion system shall have a total volume lower or equal to 1.7 U.

13.3. Trade-Off

This section describes the trade-off method used to finalise the design of the Propulsion subsystem. First an overview of all the possible options is given, afterwards these concepts are analysed and eventually compared. Finally a design is chosen and analysed in more detail.

13.3.1. Design Option Tree

From the requirements as described in the previous section certain design options were created. These options are shown in a Design Option Tree in Figure 13.1.

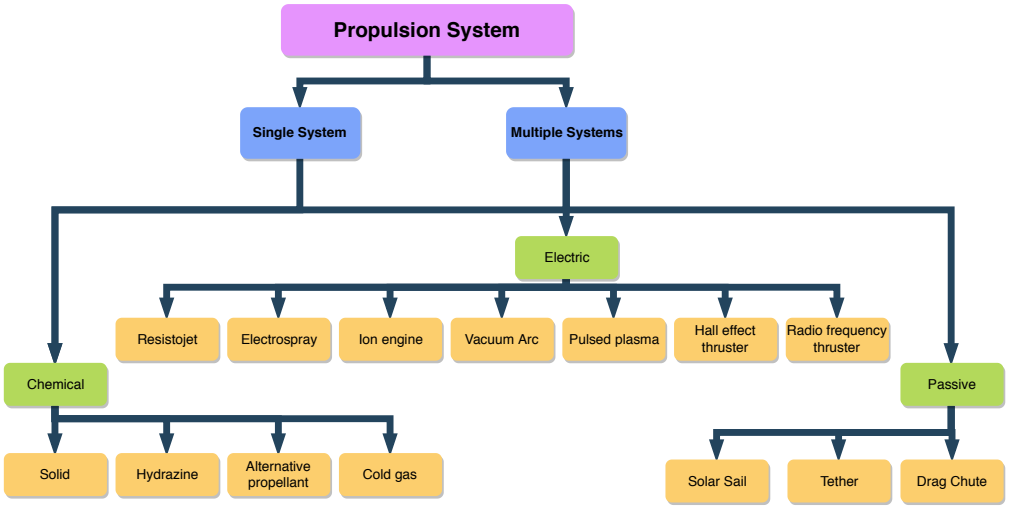

Figure 13.1: Propulsion subsystem design option tree.

First a decision should be made on using either a single system or to combine two or more systems. Both volume and mass are limited in the design of a nano-satellite. Therefore it was decided that having multiple different active propulsion systems was not possible as this would require multiple propellant tanks, valves and piping. However combining an active and a passive system together was not ruled out at this stage and was analysed in more detail.

The available propulsion systems can be separated in three different categories; chemical, electric and passive propulsion.

Chemical propulsion system

Chemical propulsion systems have the highest thrust to power ratio of all three categories. Based on the used propellant four different types of chemical propulsion can be distinguished; solid, hydrazine, cold gas and alternative green (non-toxic) propellants.

A small overview of the current state of the art of the different types of chemical propulsion systems for nano satellites is given in Table 13.5.

Table 13.5: Chemical propulsion overview [29].

Type	Name	Manufacturer	Mass [g]	Thrust [N]	Specific Impulse [s]	Power [W]
Solid	MAP	PacSci EMC	Custom	Custom	210	1
Solid	CAPS-3	DSSP	755	0.3	300	2
Hydrazine	Airbus	1N	290	1	220	N/A
Hydrazine	MOOG	MONARC-1	380	1	227.5	18
N2O + Propane	PM200	Hyperion	1400	0.5	285	6
LMP-103S	100mN HPGP	ECAPS	40	0.1	209	8
Cold Gas	Nanoprop 6U	GomSpace	900	0.01	110	2
Cold Gas	Mips Cold Gas	VACCO	542	0.01	40	10

Electric propulsion system

Electric propulsion systems generally have very high specific impulses and low impulse bits. However they provide low thrust meaning long orbital manoeuvre times and also require a lot of power to operate. An overview of available flight ready electric propulsion systems is shown in Table 13.6.

Table 13.6: Electric propulsion overview[29].

Type	Name	Manufacturer	Mass [g]	Thrust [N]	Specific Impulse [s]	Power [W]
Resistojet	Resistojet	SSTL	N/A	0.1	99	40
Electrospray	1mN	Busek	1150	0.001	800	15
Ion Engine	IFM Nano Thruster	Enpulsion	900	0.0004	4000	40
Pulsed Plasma	MPACS	Busek	550	0.00002	827	10
Vacuum Arc	u-CAT	GWU	200	0.00005	3000	0.1
Hall Effect	HT100	SITAEL	440	0.015	1300	200
RF Thruster	Phase Four	Maxwell	N/A	0.018	1300	400

Passive propulsion system

Since mass and volume are limited on nano satellites, systems that do not have to carry propellants have their advantages. However, they generally do not provide high thrust and are difficult in controlling the direction and magnitude of the orbital manoeuvre. All current systems are not retractable either. Furthermore, since these systems can not provide translational movement control, it should always be combined with either a chemical or electric propulsion system. This passive propulsion system will be deployed after the capture of Delfi-C3 and used to lower the altitude of the perigee of Delfi-REAL in order to re-enter into the atmosphere. In Table 13.7 three different types of these passive de-orbit systems can be found.

Table 13.7: Passive propulsion overview[29].

Type	Name	Manufacturer	Mass [g]
Solar Sail	NanoSail	NASA	4200
Drag sail	DragSail	UTIAS	500
Tether	Terminator Tape	Tethers	83

Although similar, the drag sail and solar sail have different approaches. The solar sail uses the radiation pressure of the sun, exchanging of momentum between the spacecraft and the electromagnetic field. By active controlling

the orientation of this sail with respect to the sun this can be used to both increase and decrease the velocity of the spacecraft. The drag sail uses the low but non-zero density of space. However, since this acceleration is always opposite to the velocity of the spacecraft this can only be used to reduce its velocity.

13.3.2. Concept Elimination

Further analysis was done to reduce the possible design options. Electric propulsion systems were deemed not viable since their power usage was too high and their delivered thrust was too low. Furthermore, the solid chemical thrusters were eliminated as they would not be able to deliver the high duty cycle required during the capture manoeuvre.

In Figure 13.2 it can be seen that the acceleration due to atmospheric drag dominates in the lower altitudes compared to the radiation pressure due to the Sun. Since the majority of the de-orbit phase will take place below 500 km altitude it was concluded that a drag sail would be more effective than a solar sail.

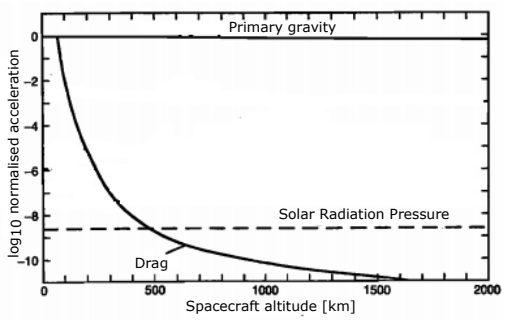

Figure 13.2: Solar radiation and atmospheric drag as function of spacecraft altitude. (Adapted from [30])

Finally the tethers, although fully developed for larger satellites, have yet to achieve Technological Readiness Level 9 for nano satellite applications and were therefore not usable for this mission.

13.3.3. Feasible Concepts

After the elimination of some of the design options, the remaining possibilities were used to create different feasible concepts. The three remaining chemical propulsion options can be used as a single system or combined with a drag sail, resulting in six different concepts.

- Hydrazine MONARC-1 Thrusters
- Hydrazine MONARC-1 Thrusters + DragSail
- 100mN HPGP Thrusters
- 100mN HPGP Thrusters + DragSail
- Nanoprop 6U Thrusters
- Nanoprop 6U Thrusters + DragSail

In order to determine the optimal design these concepts were analysed in more detail. This was done by looking at the DragSail, the layout and properties of the thrusters, and determining the required propellant and tank size.

DragSail

The use of a drag sail for the de-orbit manoeuvre would greatly reduce the required propellant. As this $110\,\mathrm{m\,s^{-1}}$ manoeuvre is almost half of the total required Delta-V. With growing interest and coming regulations to reduce and prevent space debris, multiple companies and institutions are developing these drag sails. One of them is the DragSail, developed by the University of Toronto Institute for Aerospace Studies. This sail was successfully deployed on the CanX-7 mission [31].

In Figure 13.3 a sketch is given of the Delfi-REAL with the DragSail deployed. It consists of four deployable trapezoids each with an area of $1.06\,\mathrm{m}^2$ bringing the total frontal area including the main body to $4.34\,\mathrm{m}^2$. Thereby increasing the aerodynamic drag substantially and reducing the de-orbit time. The difference of this de-orbit time for the

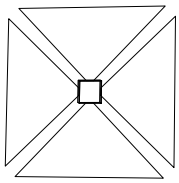

Figure 13.3: Delfi-REAL with deployed DragSail, increasing the frontal area to 4.34 m^2

spacecraft with or without DragSail is shown in 13.4. As can be seen the days it takes to reach an altitude of 200 km decreases from 1350 to only 60.

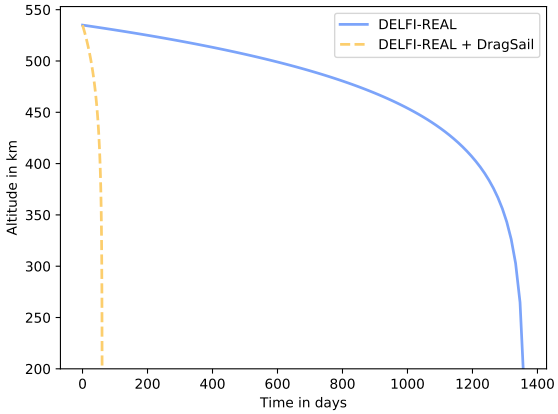

Figure 13.4: Altitude decrease over time in days due to atmospheric drag. Determined using a C_D of 2.2

The current iteration of the DragSail is uncontrollable and not retractable. As can be found in Chapter 15, the allowable re-entry flight path angle deviation can only be 0.1°. Using only these sails and the Attitude Determination and Control System this re-entry angle can be controlled somewhat but not with that precision. Furthermore, since these sails are not retractable they create a risk of destabilising the spacecraft when they inevitably burn up during re-entry.

Thrusters

To be able to have 3-axis translational control of the spacecraft, at least two thrusters on each axis are needed, for a total of six thrusters. However, this would mean no redundancy and if one of the thrusters is unable to fire, it would completely disable the movement in that specific direction. Therefore a configuration was chosen to use eight thrusters, one on each corner of Delfi-REAL orientated diagonally. Since these thrusters are not pointed through the centre of gravity they will cause a small moment when firing. This will be counteracted by the attitude control system and is discussed in more detail in Chapter 6.

Finally for the three concepts that do not use a DragSail for the de-orbit manoeuvre a ninth thruster is added on one of the sides. This thruster is orientated towards the centre of gravity of Delfi-REAL after it captures Delfi-C3. In this way the large de-orbit Delta-V manoeuvre can be performed with a high propellant efficiency.

Propellant

The propellant required was calculated using the Tsiolkovsky rocket equation. This equation links propellant mass to the velocity change it can produce.

$$\Delta V = g_0 \cdot I_{sp} \ln\left(\frac{m_0}{m_f}\right) \tag{13.2}$$

$$m_f = m_0 - m_p \tag{13.3}$$

$$m_p = m_0(1 - e^{-(\Delta V / \mathrm{I_{sp}} \cdot \mathrm{g_0})}) \tag{13.4}$$

Here, ΔV is the required velocity change and g_0 is the acceleration due to gravity at sea level which is $9.806\,65\,\mathrm{m\,s^{-2}}$. The specific impulse is a ratio of the thrust produced compared to the mass flow of the propellant and is thus a measure of how efficient a thruster uses its propellant. The initial total mass is m_0, m_f is the final total mass and m_p is the propellant mass used. Using this and the density of the propellant the required tank volume was calculated as well. The results are shown in Table 13.8.

Table 13.8: Propellant mass and volume overview per concept

Concept	**Delta-V [m/s]**	I_{sp} **[s]**	m_p **[kg]**	**Type**	**Density [kg/m3]**	**Volume [L]**
Monarc-1	236	227.5	1.2	Hydrazine	1.021	1.18
100mN HPGP	236	209	1.3	LMS-103S	1.24	1.05
NanoProp6U	236	110	2.4	Butane	2.48	0.91
Monarc-1+DragSail	115	227.5	0.60	Hydrazine	1.021	0.59
100mN HPGP+DragSail	115	209	0.65	LMS-103S	1.24	0.53
NanoProp6U+DragSail	115	110	1.21	Butane	2.48	0.49

With the required tank volume, the tanks can be sized. A pill-shaped propellant tank was chosen as this would allow maximising usable volume while still being able to withstand the stresses caused by the pressure difference. Two primary stresses act on the tank, one in the circumferential, σ_y, and one in the axial, σ_x, direction. The tank consists of a cylinder with a length L_t and diameter D_t, capped with two semi-spherical caps also with a diameter D_t. The circumferential stress is the limiting stress and therefore the tank wall thickness, t_t, will be sized accordingly. It was assumed that the wall thickness is much less than the diameter, $t_t < D_t$.

The circumferential stress can be found using 13.5, where p_c is the pressure inside the tank.

$$\sigma_y = \frac{p_c \cdot D_t}{2 \cdot t_t} \tag{13.5}$$

The propellant tank material was chosen to be TiAlV4, a widely used high strength to weight titanium alloy. The material properties together with the internal pressure obtained from the manufacturer and required tank volume were used to calculate the propellant tank mass. The results are shown in Table 13.9.

Table 13.9: Propellant tank mass overview per concept

Concept	**Volume [L]**	**Yield Stress [MPa]**	**Internal Pressure [MPa]**	**Tank Mass [kg]**
Monarc-1	1.18	880	2.76	0.052
100mN HPGP	1.05	880	0.45	0.047
NanoProp6U	0.91	880	0.50	0.043
Monarc-1+DragSail	0.59	880	2.76	0.030
100mN HPGP+DragSail	0.53	880	0.45	0.028
NanoProp6U+DragSail	0.49	880	0.50	0.026

LMS-103S is a propellant based on Ammonium DiNitrimide and is considerably less toxic than Hydrazine. It is also stable, has a higher density and is allowed on commercial passenger aircraft. Therefore reducing cost on transportation, handling and fueling.

13.3.4. Trade-Off Criteria

The following eight criteria were used for the trade-off. These criteria were discussed before, their application and relative weight is given. The justification of these weights are given as well.

- **Mass 7/10** - The propulsion system mass is a combination of the mass of the thrusters, propellant and all the necessary architecture hardware such as valves and piping. As the performance of the propulsion system and other subsystems depend heavily on the total mass this was weighted relatively high.
- **Cost 5/10** - The cost of the system is an important parameter to track mission feasibility. However since this is a highly specialised mission and the propulsion system is an essential part to achieve mission success, it was not weighted as heavily as the mass, reliability and power parameters.

- **Complexity 6/10** - As the development time of the propulsion system was limited the complexity should be kept as low as possible.
- **Reliability 9/10** - Since the propulsion system is essential to the reconnaissance phase, the capture and the final de-orbit, reliability was considered to be the most important trade-off parameter.
- **Volume 3/10** - Volume was seen as the least important trade-off parameter as it does not decrease performance as long as it remains within specification values.
- **Power usage 8/10** - Especially during capture a lot of subsystems have to work simultaneously. Therefore a low power usage is preferred as this would allow other subsystems such as the cameras and the on-board computer to use more. Resulting in a less riskier capture manoeuvre.
- **Sustainability 6/10** - Sustainability topics such as space debris and climate change are becoming increasingly important. Therefore the impact of the design of the propulsion subsystem was taken into consideration during the trade-off.

13.3.5. Trade-Off Table

The values found were used together with the specification values to create a graphical trade-off table. These specification values were found using the technical performance measurement technique as described in Chapter 22.

Table 13.10: Propulsion Trade-Off Table. excellent: exel, nominal: nom, exceeds requirement: exreq, unacceptable: unacc

Criterion / Option	**Mass**	**Cost**	**Complexity**	**Reliability**	**Volume**	**Power**	**Sustainability**
Monarc-1	unacc	nom	exel	exel	exreq	exreq	nom
100mN HPGP	nom	nom	exel	exel	nom	nom	exel
NanoProp6U	unacc	nom	exel	exel	unacc	exel	exel
Monarc-1 +DragSail	exreq	nom	nom	unacc	nom	exreq	nom
100mN HPGP +DragSail	exel	nom	nom	unacc	nom	nom	exel
NanoProp6U +DragSail	nom	nom	nom	unacc	nom	exel	exel

From the Trade-Off in Table 13.10 it can clearly be seen that using option two, the 100mN HPGP thrusters is the only viable option. However if the reliability problems during re-entry using a DragSail would be solved it would allow for significant mass reduction and make the Cold Gas NanoProp6U viable and the 100mN HPGP an even better option.

Sensitivity Analysis

A sensitivity analysis was done in order to verify the trade-off process and results. This was done by increasing and decreasing the found parameters by 11 % which was the contingency margin at that phase of the design, as discussed in Section 22.1. Furthermore the weights of the criteria were changed by one point to see if that would change the outcome of the trade-off.

For all these changes the result remained the same, the 100mN HPGP thrusters were the most optimal design option.

13.4. Final Design

Now that a concept was chosen the propulsion subsystem design was finalised. The final architecture as well as the most important parameters are discussed in this section.

13.4.1. Propulsion Architecture

The chosen thrusters were connected to the propellant tank through valves and piping. For all main pipelines, a redundant parallel pipe and valve were added. This was done to maintain the ability to use the thruster if one of these components were to fail. A schematic of the propulsion subsystem is shown in Figure 13.5.

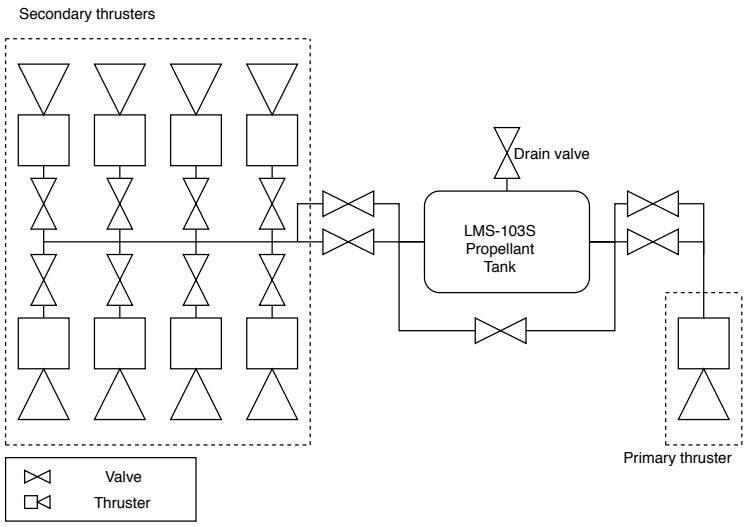

Figure 13.5: Propulsion System Schematic

13.4.2. Parameters

With the design finalised the subsystem parameters were established. This was done by looking at the mass, cost, power usage and volume of all the individual components. This is shown in Table 13.11.

Table 13.11: Propulsion System Parameters

Component	**Quantity**	**Mass [g]**	**Total Cost in thousands [EUR]**	**Volume [U]**	**Operating Power [W]**
100mN HPGP	9	360	72	0.04	10.2
Propellant tank	1	47	2	1.05	
Pipes	2m	50	1	0.08	
Thruster Valve	9	225	4.5	0.05	
Latch Valve	6	30	1	0.01	
Fill/Drain Valve	1	50	0.25	0.003	
Propellant	1.05L	1300	5	-	
Propulsion Total		2062	85.8	1.2	10.2

13.4.3. Final Remarks

The propulsion system was verified with analytical models and compared to reference missions such as the JPLMarCO and the CanX series. Furthermore it was validated using a simulation of the approach and capture procedure, a description of that simulation can be found in Chapter 14.

The current iteration of the flight controller is not optimised and gives a very conservative estimation of the Delta-V required for the capture manoeuvre. Refining this controller would result in less propellant needed and a lighter propulsion system and spacecraft mass.

Future development of the propulsion system should be done on the implementation of the propellant pipes in the CAD model and looking into pressurisation methods. Finally research and development could be done on the use of drag sails. To either make them retractable, controllable or ensuring they will not cause stability issues during re-entry.

14 Simulation

The objective of this simulation was to prove active rotation matching using small thrusters with high frequency pulsing is possible. The simulation models the movement of Delfi-REAL relative to Delfi-C3 in low earth orbit. This simulation is applicable when the distance between the two is less than 1000 m.

14.1. Assumptions

It was assumed that no gravity influences from other objects or the spacecraft are present. Approximating the mass of Delfi-REAL at 12 kg and the mass of Delfi-C3 at 3 kg. Then at a distance of 0.5 m they exert a gravitational force of $\approx 9.7 \times 10^{-9}$ N onto each other.

$$F = \frac{Gm_1 m_2}{r} = \frac{6.67 \times 10^{-11}\,\mathrm{N\,m^2\,kg^{-2}} \cdot 12\,\mathrm{kg} \cdot 3\,\mathrm{kg}}{0.5\,\mathrm{m}} \approx 9.7 \times 10^{-9}\,\mathrm{N} \tag{14.1}$$

Furthermore it was assumed that no disturbances or any other external forces are acting on the spacecraft. Due to their short distance between each other any force that might be present will affect both spacecraft similarly. The solar radiation pressure at 1 astronomical unit (AU) is 4.5 µPa [32]. Delfi-REAL has a surface area of 0.248 $\mathrm{m^2}$ and is experiencing a disturbance force of 0.11×10^{-6} N. Delfi-C3 has a surface area of 0.033 $\mathrm{m^2}$ and is experiencing a disturbance force of 0.81×10^{-8} N. These forces are considered negligible.

At an altitude difference of 10 m the orbital velocity differs by 0.55 $\mathrm{mm\,s^{-1}}$, which is three orders of magnitude smaller than the approach speed used of 0.5 $\mathrm{m\,s^{-1}}$. This result was obtained using the vis-viva equation.

$$v2 - v1 = \sqrt{\frac{\mu}{r2}} - \sqrt{\frac{\mu}{r1}} = \sqrt{\frac{3.986 \cdot 10^{14}}{6921010}} - \sqrt{\frac{3.986 \cdot 10^{14}}{6921000}} \tag{14.2}$$

14.2. Software Description

The software is structured into three main components. The primary class contains the world itself and has perfect knowledge of the objects it contains. The world is able to populate itself with spacecraft. These can be given initial values for state vectors. In this case Delfi-C3 gets initialised with a random angular velocity, and Delfi-REAL is given a starting location about 1000 m away from Delfi-C3.

The second component is the simulation loop that is executed for each time step. Within it each spacecraft can receive and execute commands, execute movements and update its state vector describing its properties, location and rotation in the world.

The last primary component is the flight controller which is only used by Delfi-REAL as Delfi-C3 does not have an active propulsion system. The flight controller determines the actions that should be taken by the spacecraft to approach Delfi-C3 and to match its rotational rate.

A class diagram showing the simulation software is shown in Figure 14.1.

14.3. Coordinate Systems

For the world a Cartesian coordinate system is being used. Each spacecraft has a body fixed coordinate system. For Delfi-REAL the x axis is pointing in the direction of travel (opposite of main thruster), and the z axis in the direction of the heatshield. For Delfi-C3 the z axis points towards the side with the shorter antenna, the x and y are arbitrary. Both spacecraft are modelled as point masses. Their actual shape is not taken into account for the purposes of this simulation.

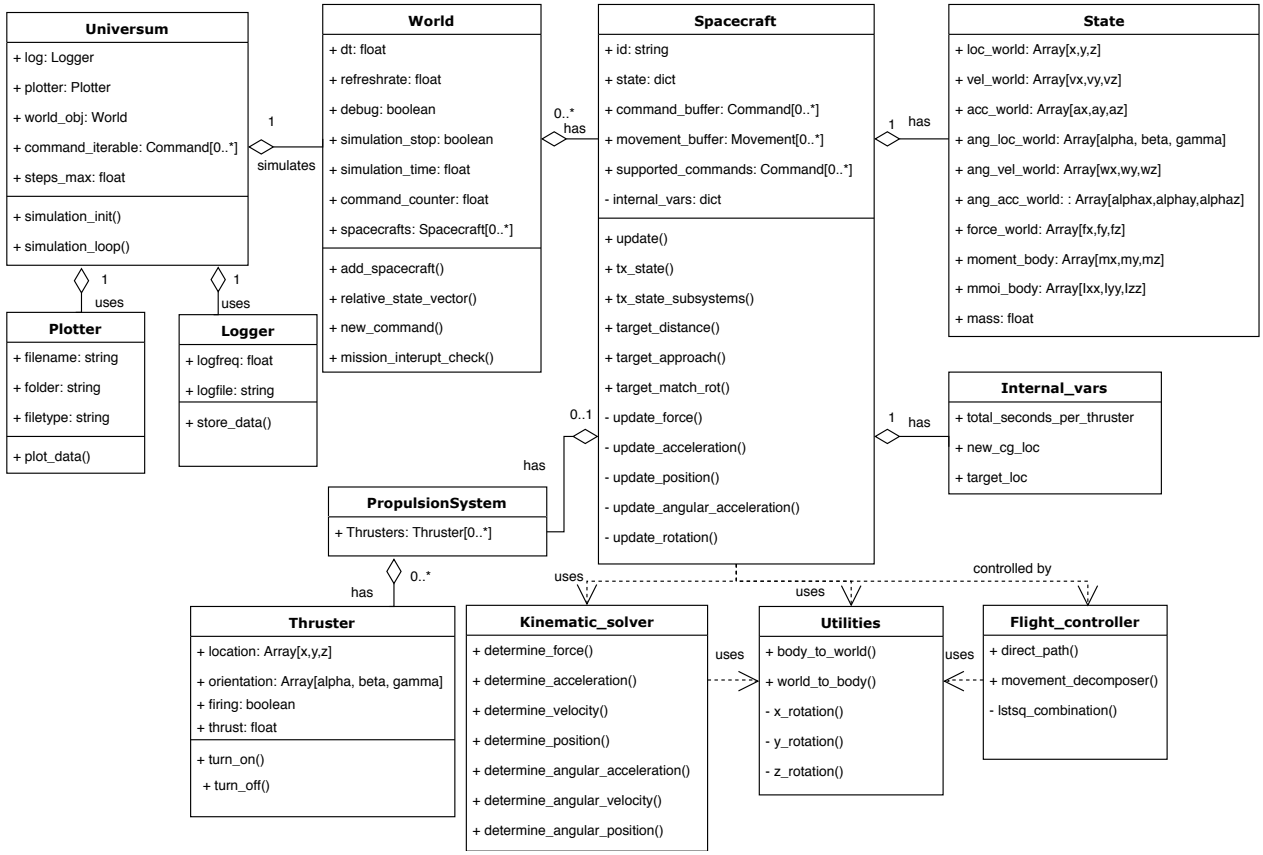

Figure 14.1: Diagram of the simulation software variables and functions

14.4. Spacecraft State

Delfi-REAL and Delfi-C3 are instances of the spacecraft class. Each spacecraft has a state dictionary containing its location, velocity and acceleration in the world, its angular location, velocity and acceleration of the body fixed coordinate system to the world world coordinate system, the resultant force and moment acting on the center of gravity (c.g.) of the spacecraft, and the properties of mass moment of inertia and mass.

14.5. Rotation Matching

For a successful capture with a clamp the relative rotational rate and velocity need to be zero between Delfi-C3 and Delfi-REAL. If there is still a residual relative velocity there is a risk of hitting Delfi-C3 and imparting enough force onto it such that it exceeds the maximum angular rate at which capture is possible or in the worst case causes space debris.

In the first step Delfi-REAL approaches Delfi-C3 to a preset distance, in this simulation 40 m. At this distance it begins to match the rotational rate of Delfi-C3 by estimating the location of a target that is rotating about the c.g. of Delfi-C3 at a fixed distance and the same rotational rate as Delfi-C3. As this target is iteratively approached by Delfi-REAL the distance of it is slowly reduced until the target is 0.35 m away from the c.g. of Delfi-C3. The path that Delfi-REAL travels during this manoeuvre is shown in Figure 14.2.

On each iteration of the simulation loop Delfi-REAL determines the distance and direction it has to travel to bring its own c.g. to the location of the target. Internally this vector gets used to obtain a resultant ΔV requirement. Which is then internally decomposed using a non-negative least square approximation into thruster firings using the known location and direction of the thrusters on Delfi-REAL. From this a sequence of firings is obtained which is then converted back into a sequence of forces by adding the force contribution of all currently firing thrusters and simulated to obtain the the motion of Delfi-REAL. By simulating many steps of this process it was observed that given the propulsion system proposed in Chapter 13 it is possible to approach to and track the rotational motion of Delfi-C3 at a distance of 0.35 m. This is shown by the blue path in Figure 14.3.

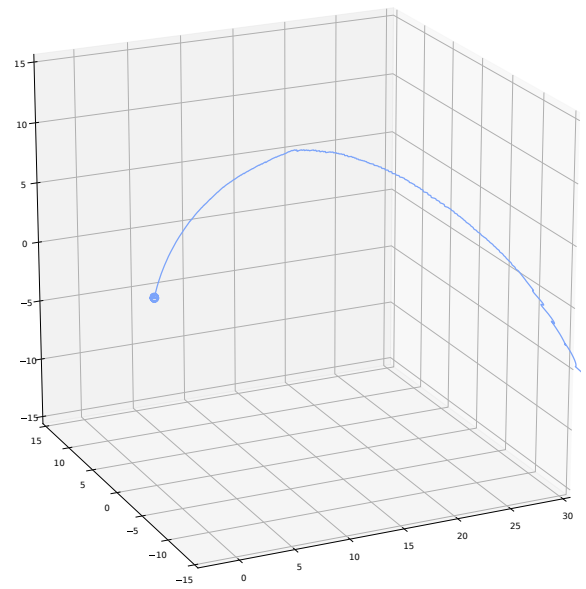

Figure 14.2: Approach path to Delfi-C3 [m]

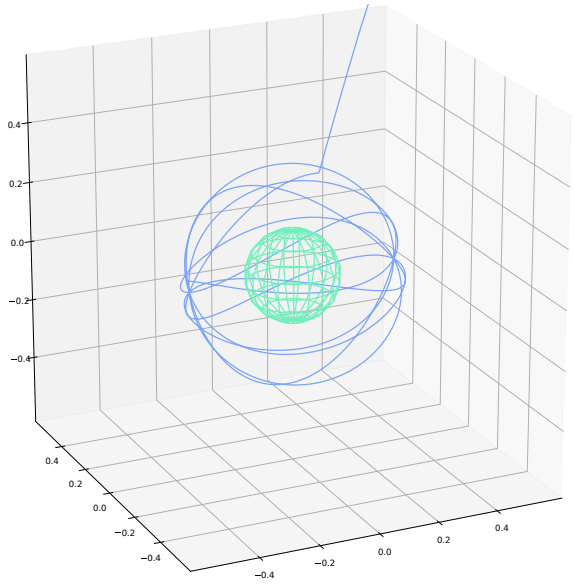

Figure 14.3: Rotation matching Delfi-C3 (represented by green sphere) [m]

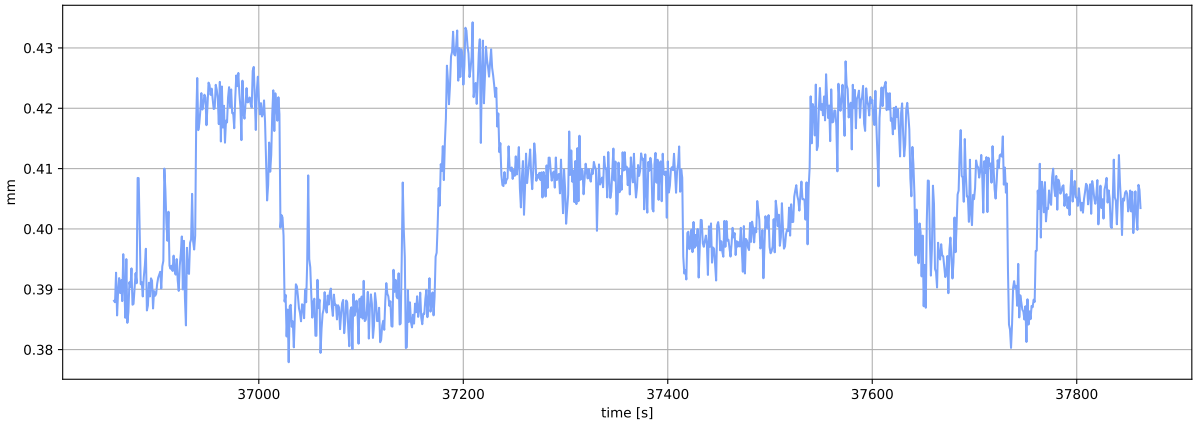

Figure 14.4: Positioning error when orbit matching

14.6. Tracking Error

After matching the rotational rate of Delfi-C3 a steady state is reached. During this rotation matching Delfi-REAL needs to actively recalculate and correct its relative position. The quicker this can be done the more accurate the tracking will be. Figure 14.4 shows the magnitude of the relative error over 1000 s in the simulation. The error varies from about 0.38 mm to 0.43 mm. This variance is acceptably low, however the average error should ideally be 0 mm. This discrepancy is attributed to the flight controller used not being perfectly tuned to the application.

14.7. Recommendations

During the development of the simulation it was discovered that some approaches to solve this problem were not ideal. Especially attempting to mimic the behaviour of the On Board Computer (OBC) in the way it handles command execution and flight controller input added an unnecessary layer of complexity especially as the simulation grew in capability and complexity.

For the real flight hardware it is recommended to build a new flight controller from scratch that determines the target location for the next iteration in a smoother and more accurate way. Furthermore, to decompose the ΔV requirement into thruster firings a least squares optimisation was used to determine the firing duration for each thruster. However, this could lead to large truncation errors when very short or long firings were required. In actual flight hardware the controller should only determine the actions taken for the next timestep instead of trying to estimate multiple steps in advance.

15
Re-Entry Subsystem

In this chapter the re-entry subsystem is presented. Section 15.1 describes the function of this subsystem. The governing requirements are shown in Section 15.2. Section 15.3 shows the used design trade-off. The final design is presented in Section 15.4.

15.1. System Description

To get Delfi-REAL including Delfi-C3 safely back to Earth, the re-entry subsystem is needed to protect both spacecraft from the associated loads and heat. The load on Delfi-REAL and Delfi-C3 can be optimised with a good flight path design. Protection from the heat during re-entry is provided by the Thermal Protection System (TPS). The leading requirements for this design are the maximum deceleration load Delfi-C3 can withstand, and the maximum allowed temperature on the leeward side of the TPS.

15.2. Requirements

The requirements found from the subsystem analysis are presented below. The REN label stands for re-entry.

RQ-REN-05	The deceleration during re-entry shall not exceed 15 g.
RQ-REN-06	The system shall have a thermal protection system.
RQ-REN-07	The thermal protection system shall be able to protect the system from the total heat load experienced during re-entry.
RQ-REN-12	The leeward side of the thermal protection system shall have a maximum temperature of 80 °C.
RQ-REN-13	The thermal protection system mass shall not exceed 3 kg.

15.3. Trade-Off

In this section the design trade-off is shown. First the design option tree is described. Then the concept elimination is explained, after which the feasible concepts are discussed.

15.3.1. Design Option Tree

The re-entry subsystem Design Option Tree (DOT) is shown in Figure 15.1. In this figure, the subsystem is categorised into three main parts.

Flight Path - The initial re-entry angle can be either steep or shallow. A steeper re-entry results in a shorter, more accurate flight path, but increases the maximum loads on the spacecraft. A more shallow re-entry decreases the maximum load, but also increases the trajectory uncertainty due to a longer flight path. If the initial re-entry angle is shallow enough, the flight path can be described as a skipping motion[1]. This decreases the maximum load even further, but further increases the flight path uncertainty.

Spacecraft Shape - The shape of the spacecraft greatly influences the aerothermodynamic properties of Delfi-REAL. A sharp body penetrates deeper into the atmosphere before maximum deceleration, while a blunt body hits maximum deceleration at a higher altitude.

Thermal Protection System - The TPS can be passive, active or ablative. Passive reusable systems include insulating heat tiles as used on the Space Shuttle [33], and a heat sink. An active reusable system can be made using liquid cooling[2]. Ablative systems absorb energy put into the system by pyrolysis, which is decomposition into char and gases due to the heat [34], these can be flexible or rigid. Flexible ablative heat shields can be produced from Kevlar

[1] `http://blogs.esa.int/rocketscience/2015/02/05/the-facts-on-reentry-accurate-navigation-is-everything/` accessed on 19 Dec. 2018

[2] `https://arstechnica.com/science/2019/01/elon-musk-is-really-really-excited-about-his-starship/` accessed on 9 Jan. 2019

or Nextel fibres. Rigid heat shields can be produced with Kevlar, Nextel or carbon fibres with a resin-based medium, or a phenolic novolac resin in a supporting structure[3][4][5].

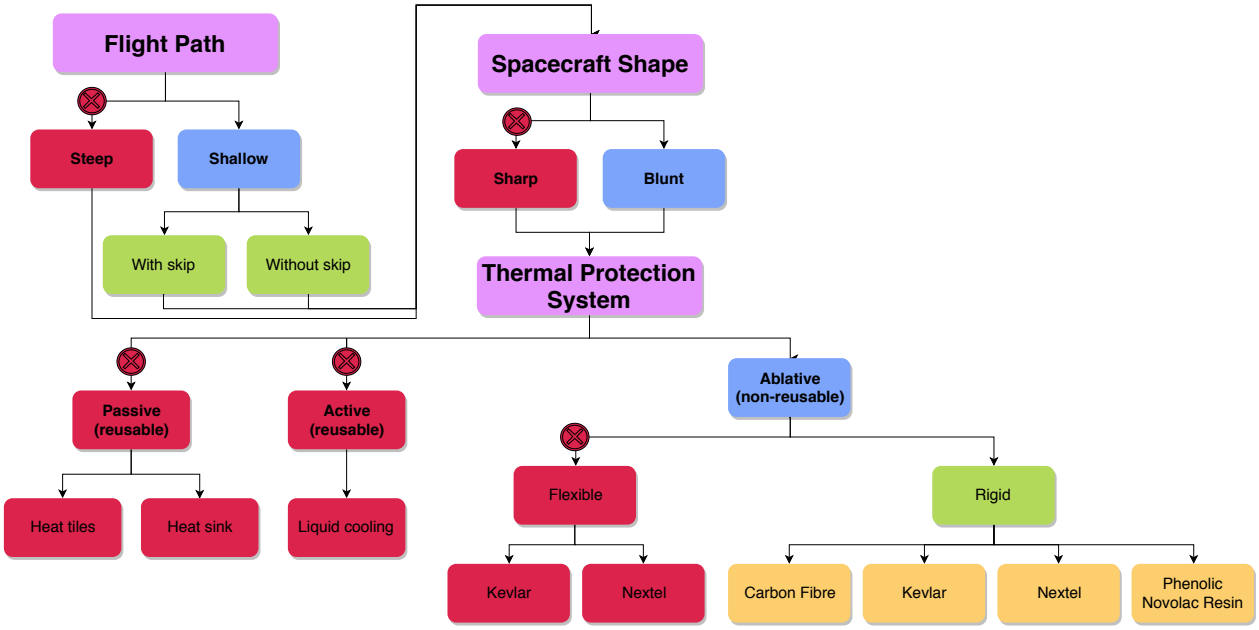

Figure 15.1: Re-entry Design Option Tree

15.3.2. Concept Elimination

When the options in the DOT are evaluated, some prove to be unfeasible or not suited for the mission. These options are explained below and then eliminated from the DOT.

Flight Path - A steep descent results in a more accurate flight path due to a shorter period through the atmosphere. The flight path angle γ is defined as positive up, measured from the local horizon. The difference between an initial flight path angle of $-3°$ and $-2°$ can increase the relative range deviation 1.7 times [35]. The maximum deceleration due to a steep descent is however a magnitude higher than with a shallow descent. Requirement RQ-REN-05 on maximum deceleration can not be met with a steep descent and this is therefore eliminated.

Spacecraft Shape - A sharp spacecraft shape increases the maximum heat flux on the TPS of Delfi-REAL. As a relatively low heat flux is essential for a functioning TPS, a sharp spacecraft shape is eliminated.

Thermal Protection System - The use of isolating heat tiles as produced for the Space Shuttle require the use of special materials, not on the market for consumers. It is therefore eliminated. A heat sink to absorb the energy from re-entry would make Delfi-REAL significantly heavier. This would make re-entry harder and increase launch cost, which is why this option is eliminated. An active re-entry TPS with liquid cooling does not have the maximum Technology Readiness Level (TRL) [36] and would require pumps, piping and radiators, increasing complexity and mass significantly. It is therefore eliminated. A flexible ablative TPS was tested by NASA as well as ESA, with Hypersonic Inflatable Aerodynamic Decelerator[6] and Inflatable Re-entry Demonstrator Technology[7] respectively. These tests seemed promising but were experimental and therefore not TRL 9, eliminating them as an option for Delfi-REAL.

15.3.3. Feasible Concepts

After the initial concept elimination, two flight path options remain. After simulation, the shallow option with skip is chosen to have an initial flight path angle of $-3.0°$. In this case, Delfi-REAL skips on Earth's atmosphere as a stone

[3] https://www.smithsonianmag.com/science-nature/nasa-successfully-tests-inflatable-heat-shield-for-descending-spacecraft-6534080/ accessed on 29 Jan. 2019
[4] https://spinoff.nasa.gov/spinoff2003/ip_3.html accessed on 29 Jan. 2019
[5] https://www.nasa.gov/centers/johnson/pdf/584728main_Wings-ch4b-pgs182-199.pdf accessed on 29 Jan. 2019
[6] https://www.nasa.gov/feature/langley/nasa-tests-inflatable-heat-shield-technology-for-deep-space-missions accessed on 21 Dec. 2018
[7] http://www.spaceflight.esa.int/irdt/factsheet.pdf accessed on 21 Dec. 2018

on water, reducing the velocity significantly for a second dive into the atmosphere. This method was also used during the Apollo capsule re-entry [37]. For the shallow option without skip, the initial flight path angle is chosen as −3.5°. For the rigid ablative TPS, the only material that has enough available information to accurately calculate the needed protection is a phenolic novolac resin impregnated 3-D fine-woven pierced carbon fabric composite. Further explanation on this material is given in Section 15.4. Lack of available information on the other materials eliminates them as design options.

Delfi-REAL shall thus have a blunt shape on one side, which is pointed in the direction of the velocity during re-entry. This will be coated with a rigid ablative heat shield based on a phenolic novolac composite. A trade-off will determine if the definitive flight path has a skip in it or not.

15.3.4. Trade-Off Criteria

The design of Delfi-REAL does not alter significantly with either of the initial flight path angle options. The mass difference is less than 4 %, resulting in a maximum mass difference of approximately 50 g. For this reason, mass is not included in the trade-off. The significant differences of interest between both options are the maximum deceleration and the range deviation, explained below.

Deceleration 9/10 - Maximum deceleration is of great importance to keep Delfi-C3 intact. For this reason, it is rated a 9/10. With the values from initial sizing put into the simulation, the maximum deceleration with $\gamma = -3.5°$ is 8.51 g. This falls within requirement RQ-REN-05 on maximum deceleration with a safety factor of 1.76. Keeping in mind that a safety factor is required to account for unforeseen circumstances, this is scored nominal. With $\gamma = -3.0°$ the maximum deceleration is 5.40 g, adhering to requirement RQ-REN-05 with a safety factor of 2.78. As the safety factor is exceptionally high, this is scored excellent.

Range Deviation 6/10 - To be able to select a suitable landing site, the range deviation must be as small as possible. The exact deviation is however not of great importance, as long as the site is large enough. For this reason, the range deviation criterion is rated a 6/10. Again with the values from initial sizing, the range difference due to the initial angle deviating by one tenth of a degree is 84 km for $\gamma = -3.5°$. This is scored nominal, considering there are no options to control the flight path after re-entry has been initiated. For $\gamma = -3.0°$, the deviation is 625 km. This will make it extremely hard to find a suitable landing site, which is why this is scored unacceptable.

15.3.5. Trade-Off

The concept scores based on the criteria as described earlier are implemented in the trade-off, seen in Table 15.1. Since the trade-off table eliminates the option where $\gamma = -3.5°$ because of unacceptable range deviation, only the option where $\gamma = -3.0°$ remains and is thus selected as the design option.

Table 15.1: Design concept trade-off table for the re-entry subsystem. excellent: excel, nominal: nom, unacceptable: unacc

Option \ Criterion	Deceleration	Range Deviation
$\gamma = -3.0°$	nom	nom
$\gamma = -3.5°$	excel	unacc

15.3.6. Sensitivity Analysis

Since only one option proves to be suitable for the mission, the chosen design is not susceptible to the weight of the trade-off criteria. If problems arise that also prove the chosen concept to be unfeasible, the option where $\gamma = -3.0°$ can be improved by adding an active flight path control system to Delfi-REAL. For now this has been deemed unacceptable because it would significantly increase complexity.

15.4. Final Design

This section presents the final design of the re-entry subsystem. First the simulation is explained, after which the aerodynamic characteristics are described. Then the flight path and thermal protection system are presented, followed by the subsystem integration. This section is concluded with final remarks for further development.

15.4.1. Simulation

For initial sizing and preliminary calculations a simulation model was created assuming ballistic re-entry starting at 150 km altitude in the International Standard Atmosphere (ISA) [38]. The initial calculations for heat flux were performed using the Chapman heat equation. For further simulation Delft Aerospace Rocket Engineering (DARE) assisted by making their flight path and parachute software ParSim available for use. This software is verified and validated by DARE using data from their Stratos II+ mission, Vorticity Inc's Supermax mission and the NASA Aspire mission [39]. The Supermax mission's MAXUS rocket had an apogee of 679 km[8], thus validating the MAXUS flight path also validates that ParSim is accurate for altitudes over 150 km.

For trajectory dynamics and heat loading, the following assumptions are made in ParSim:

- The body follows a two dimensional trajectory.
- ISA atmospheric model, no wind.
- The body is treated as a point-mass.
- The body has a 0° angle of attack.

The ParSim program asks for the initial conditions and body definition parameters as presented in Table 15.2. The nose radius is defined as the curvature radius of the forward facing side of the satellite. A small nose radius is thus coherent with a sharp body, and a large nose radius with a blunt body. The actual frontal size of the body is defined by the diameter.

Table 15.2: ParSim Body Initial Input Parameters

Initial conditions	Unit	Body definition	Unit
Altitude	km	Diameter	mm
Velocity	$m\,s^{-1}$	Mass	kg
Flight path angle	°	Nose radius	mm
relative to local horizon, positive up		Drag coefficient	-

15.4.2. Aerodynamic Characteristics

The body mass and shape of Delfi-REAL influences both flight path and heat loading. This indicates that the definition of aerodynamic characteristics is an iterative proces. After several iterations, the spacecraft wet mass converged to 14.5 kg. After initiation of re-entry, Delfi-REAL will have burned all 1.2 kg of its propellant, leaving a dry mass of 13.3 kg. Then the 2.2 kg mass of Delfi-C3 is added to the mass of Delfi-REAL, leaving a total re-entry mass of 15.5 kg.

The body definition of the TPS of Delfi-REAL converged to a diameter of 500 mm. With the diagonal of the main structure of 483 mm using the dimensions given in Table 17.1 this verifies that the TPS covers the entire base of the satellite. The circular shape divides the heat load equally to prevent burnouts on the corners of Delfi-REAL. To load the TPS as equally as possible, a nose radius of 2 m has been selected for the frontal area of the heat shield. This results in a very blunt shape, which will create a bow shock during re-entry. The more blunt an object is, the more distance between the body and the bow shock. This increases the isolating layer of low pressure air in front of the body, optimal for heat protection [40]. A sketch of the designed TPS shape is shown in Figure 15.2.

The drag coefficient of Delfi-REAL is designed to be 1.2, derived from the drag coefficient of the similar shaped Apollo capsule [37]. This needs to be validated with a wind tunnel test in a following stage of development. If the actual drag coefficient deviated form the predicted value, the shape of Delfi-REAL can be adjusted and the initial flight path angle and TPS design iterated.

15.4.3. Flight Path

As initial conditions, the altitude is chosen to be 150 km, at which point the orbital velocity is $7.8\,km\,s^{-1}$, as calculated with Equation 15.1[9].

$$V = \sqrt{\frac{g \cdot R_e^2}{Re + h}} \tag{15.1}$$

[8] `https://www.vorticity-systems.com/case-studies/esa-supermax/` accessed on 10 Jan. 2019
[9] `https://www.grc.nasa.gov/www/k-12/rocket/rktrflght.html` accessed on 10 Jan. 2019

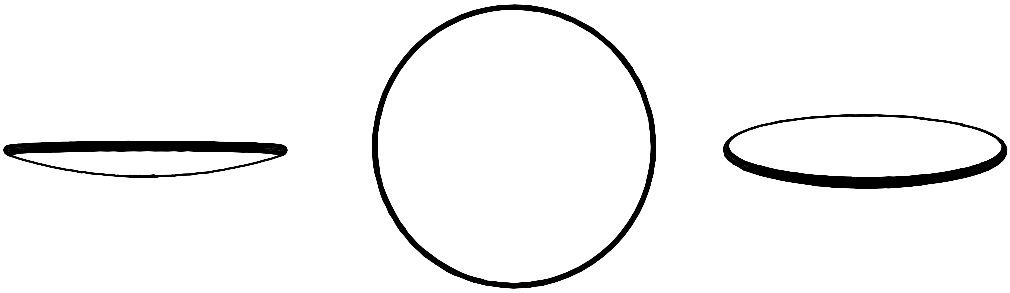

Figure 15.2: Thermal Protection System

This velocity is redirected with the propulsion system to create the initial flight path angle of −3.5°. During this procedure, the propulsion system burns its remaining propellant after validation of the correct flight path angle to reduce the mass of the spacecraft. Requirement RQ-ADCS-02.01 guarantees the needed accuracy of 0.1° for re-entry initiation is available. Figure 15.3 shows the flight path on the left. The centre graph shows the altitude decrease over time, and the right graph shows the body loading, peaking at 1.3 kN, 244 s into the re-entry phase. This load is recalculated to the maximum deceleration loading with $a = \frac{F}{m} \cdot \frac{g}{g} = \frac{1300}{15.5} \cdot \frac{g}{9.81} = 8.5\,\mathrm{g}$.This means the re-entry loading fulfils the deceleration requirement RQ-REN-05 with a safety factor of 1.76, accounting for deviations with respect to the ISA atmospheric model and flight path accuracy deviations.

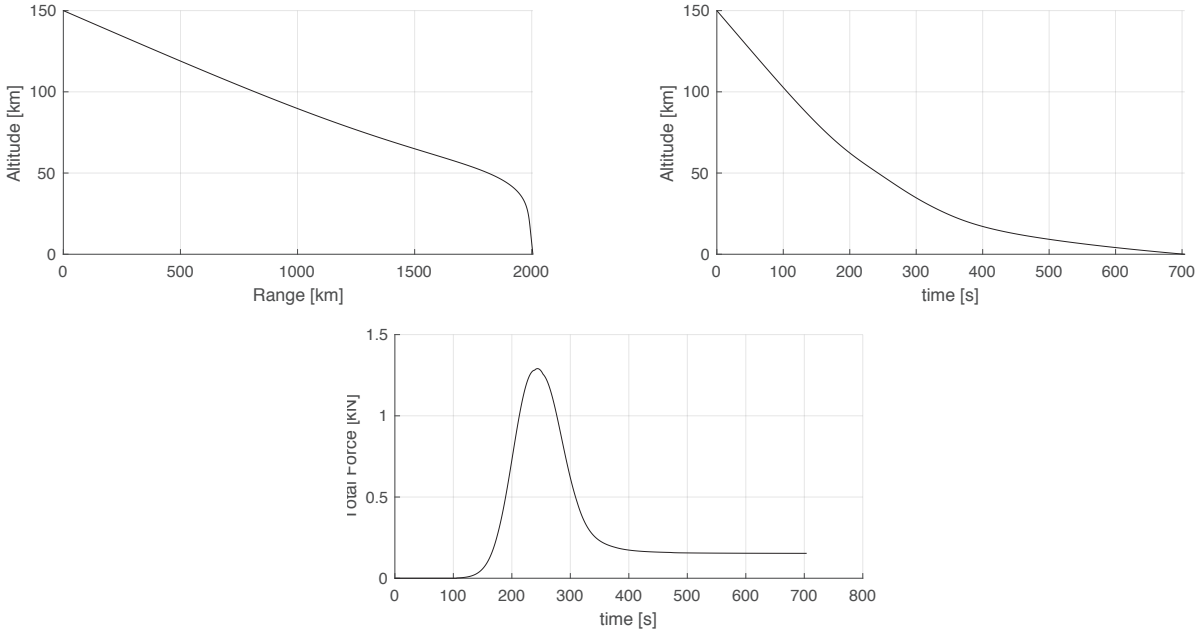

Figure 15.3: Flight Path and Spacecraft Body Force Simulation

15.4.4. Thermal Protection System

The heat flux and total heat load Delfi-REAL is subjected to during re-entry is shown in Figure 15.4. On the left, the heat flux is calculated with six different heat equations, each resulting in a slightly different heat flux. For this reason, the minimum, maximum, mean and standard deviation of all six methods are displayed in the centre graph. The same approach is used for the total heat load as shown in the right graph. The mean plus one standard deviation for the heat flux as well as the heat load is the design case for the TPS. This method results in a maximum heat flux of 103 $\mathrm{W\,cm^{-2}}$ and a total heat load of 9200 $\mathrm{J\,cm^{-2}}$.

Heat shields used in previous re-entry missions all used classified and specific purpose designed materials. As mentioned in Section 15.3, the only material of which research values are available is NASA's Phenolic-Impregnated Carbon Ablator (PICA). In a study by Hong C. et al [41], several samples of PICA were tested on ablation characteristics. In this study, a PICA sample of 40x40x20 mm was subjected to an oxyacetylene torch generating a heat flux of 450 $\mathrm{W\,cm^{-2}}$ for 200 s, resulting in a total heat load of 90 $\mathrm{kJ\,cm^{-2}}$. The PICA sample had a density of 0.352 $\mathrm{g\,cm^{-3}}$, with a phenolic resin volume content of 11.1 % and a carbon fibre volume content of 12.5 %. During testing, the ablation

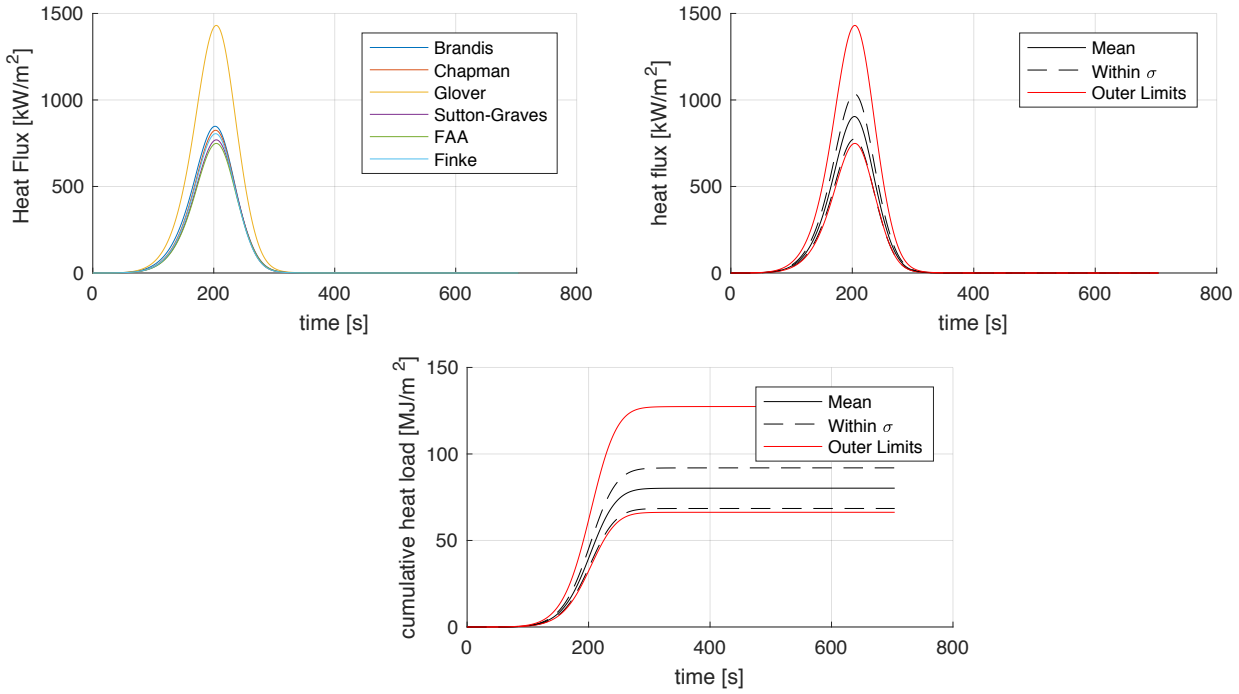

Figure 15.4: Heat Loading Simulation

rate $\dot{d_{abl}}$ proved to be linear with 0.019 mm s^{-1}.

Comparing the heat flux and loading of Delfi-REAL with that of the test, the heat flux acting on Delfi-REAL is 23 % of the test case heat flux. If PICA can withstand the test heat flux, it will also be able to withstand a heat flux almost one fifth of that. Due to a lack of more available information, the ablation due to heat load is assumed to be scaled linear with varying heat load. In the test case, the total ablation was $d_{abl} = 0.019\,\text{mm}\,\text{s}^{-1} \cdot 200\,\text{s} = 3.8\,\text{mm}$. If this is linearly scaled to the total heat load of Delfi-REAL, the ablation is $d_{abl} = 3.8\,\text{mm} \cdot \frac{9.2\,\text{kJ}\,\text{cm}^{-2}}{90\,\text{kJ}\,\text{cm}^{-2}} = 0.39\,\text{mm}$. Since PICA is a material enhanced by NASA for the specific purpose of thermal protection, and for Delfi-REAL only commercially available materials are used, the performance of the phenolic novolac resin and carbon fibre weave will be less than that of PICA. For this reason, a safety factor of five has been chosen, bringing the total calculated ablation to $d_{abl} = 1.94\,\text{mm}$.

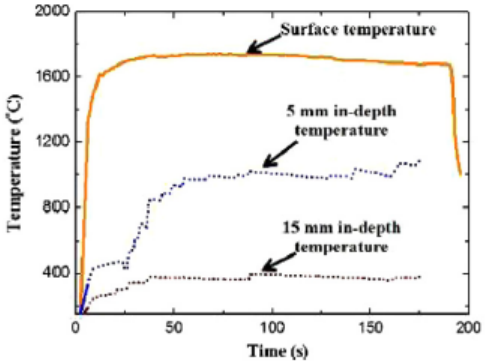

Figure 15.5: Measured Surface and In-Depth Temperatures Under Oxyacetylene Torch [41]

Figure 15.5 shows the temperature of the PICA sample at different depths from the surface during testing. The temperature decrease is exponentially related to the depth. Defining the bondline temperature T_b as the temperature at the back of the TPS and d as the TPS thickness, we get $T_b = 1665.2e^{-0.096d}$. To fulfil requirement RQ-REN-12, T_b must be below 80 °C. This is calculated with the initial thickness minus the total ablation. The temperature relation derived from literature is then linearly related to the ratio of the heat flux between the test and the Delfi-REAL case, defined as $q_{frac} = \frac{q_{system}}{q_{test}} = \frac{103}{450} = 0.23$. Keeping the bondline temperature within the requirement, the initial

thickness needed is then calculated in Equation 15.2 using the rearranged relation given above.

$$d = \frac{-\ln(\frac{T_b}{1665.2 \cdot q_{frac}})}{0.096} + d_{abl} = \frac{-\ln(\frac{80}{1665.2 \cdot 0.23})}{0.096} + 1.94 = 18.2\,\text{mm} \tag{15.2}$$

With a diameter of 500 mm, a curvature radius of 2 m and a thickness of 18.2 mm, the total volume of the TPS is 3431 cm^3. With a density of 0.352 g cm^{-3} this results in a mass of 1.2 kg, of which 0.13 kg is lost due to ablation during re-entry. This leaves 1.8 kg for the supporting structure to stay within the maximum mass of 3 kg as stated in requirement RQ-REN-13.

15.4.5. Subsystem Integration

The supporting structure of the TPS is attached using pyrotechnic bolts for easy ejection. The reason for this is further explained in Section 16.4.

The main heat shield is now designed, but the main body of Delfi-REAL also might need additional thermal protection. There are cavities, slits and sensors penetrating the main satellite body on the leeward side of the TPS. A possible solution to this is either to actively cover these parts during re-entry with thermal protection, or to sacrifice the sensors in question and apply the thermal protection behind them. The extent to which this additional thermal protection is needed can only be determined after testing of the main TPS.

15.4.6. Final Remarks

Since no commercial heat shields for re-entry are available, this design is experimental. This has been accounted for by having an exceptionally large safety factor of five. The commercially available materials chosen in this design have not yet been applied in re-entry vehicles. For this reason, thorough testing is needed to validate the design and guarantee reliability. One month of testing has been taken into account in the development budget of Delfi-REAL. The drag coefficient of the complete system, the ablation under heat loading and the aerothermodynamic flow around the system need to be measured and analysed during tests. This can validate drag, mass loss due to ablation, bondline temperature and heat protection of the system leeward of the TPS. After testing and validation, the design can be iterated for optimisation.

In this analysis, vibration loads during re-entry have not been calculated due to time constraints. For further development, these loads need to be calculated. If the addition of these loads would make the re-entry exceed the requirement, the design has to be iterated. If that case causes the re-entry to be unfeasible with a ballistic flight path, the shape of Delfi-REAL should be altered to generate lift. This method was also used on the Apollo spacecraft, drastically decreasing the re-entry loads [37]. This method also increases complexity significantly, which is why it was not used in this design.

16
Recovery Subsystem

In this section, the design of the Recovery Subsystem is discussed. In Section 16.1 the role of the subsystem is explained, and the previously set requirements are mentioned in Section 16.2. In Section 16.3 the trade-off for the subsystem is performed. This section includes the Design Option Tree (DOT), concept elimination, trade-off criteria, and the trade-off. In Section 16.4 the parachute system is designed, and in Section 16.4.3 the deployment system is discussed. Lastly, future recommendations for the system are discussed in Section 16.5.

16.1. System Description

In order to ensure that Delfi-C3 can safely return to Earth after re-entry, a recovery system is needed. The recovery system must be able to support Delfi-REAL in two landing modes: a) landing with Delfi-C3 on board after a completed mission; and b) after a failed capture of Delfi-C3 as a lone spacecraft. A failure during launch will not be designed for as Delfi-REAL is not the primary load and it is assumed that a failure system is integrated into the launching spacecraft. The recovery system must be able to decelerate Delfi-REAL from the speed after re-entry of $7800\,\mathrm{m\,s^{-1}}$ to $7\,\mathrm{m\,s^{-1}}$ [1]. The leading design mode for the system design will be with Delfi-C3 on board, and the system will be tested to ensure it will still perform in the second mode.

16.2. Requirements

In the conceptual design phase, the following requirements were found in a subsystem analysis [1]. The REN label stands for re-entry.

RQ-REN-09	The parachute shall be deployed when the system's velocity is subsonic.
RQ-REN-10	The impact acceleration of the system shall not exceed 15 g.
RQ-REN-11	The impact velocity of the system shall not exceed $7\,\mathrm{m\,s^{-1}}$.

16.3. Trade-off

In the following section the trade-off for the Recovery Subsystem is presented. This starts with the design option tree, followed by the elimination of concepts. Then the trade-off criteria are presented and the trade-off is performed.

16.3.1. Design Option Tree

In Figure 16.1 on page 82, the design option tree for the subsystem is presented. As seen in the DOT, several options were eliminated immediately. The following will explain the reasoning for all eliminated options:

Parachute- In the DOT supersonic and sub-sonic options are presented. Due to its Technology Readiness Level (TRL), the supersonic parachute option has been discarded.

Deployment Method- For the deployment method, three options were explored. Uncontrolled deployment was ruled out due to its high opening forces[1] and the possibility of canopy inflation before the lines are fully stretched. Furthermore, semi-controlled deployment was ruled out because of its low effectiveness at high velocities [42]. This means the parachute system will have to be deployed with a controlled method. Of the three controlled methods, two were ruled out. The canopy first method was ruled out due to its unpredictable behaviour, and high snatch forces. Furthermore, due to the size of Delfi-REAL the mortar deployment method would be too heavy, and over-engineered. Thus the parachute must be controlled using a drogue gun which fires a slug. This method is effective for small parachutes, and simple.

Configuration- Both options in the DOT for the configuration of the parachutes are viable options, thus will be included in the sub-system trade-off.

[1] `https://www.pcprg.com/sym01out.htm` accessed on 18 Jan. 2019

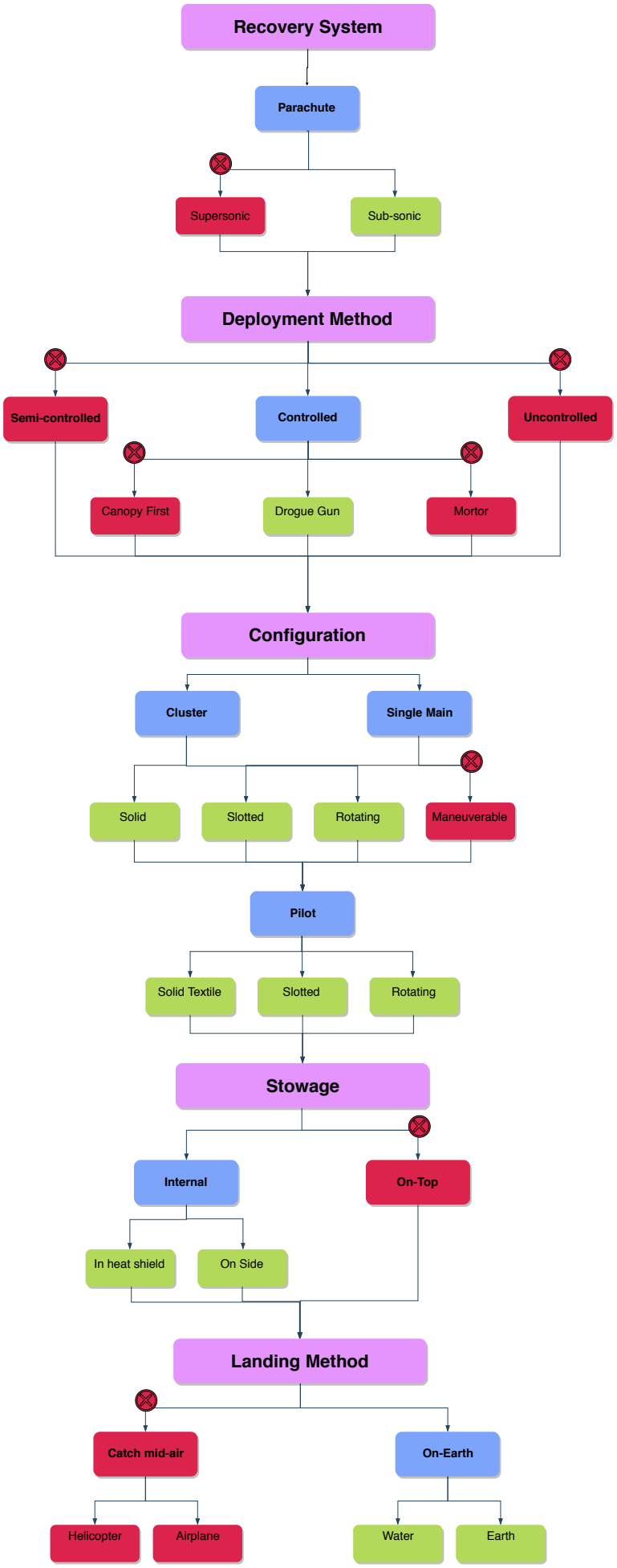

Figure 16.1: Descent and landing design option tree

Main Chute- For the main chute, four types of parachutes were considered. Manoeuvrable parachutes, or gliding parachutes, such as those used for skydiving were immediately discarded as they are not applicable for space re-entry applications.

Pilot Chute- All pilot parachute options are currently viable, and will be looked into in further detail during the final design.

Stowage- Due to the placement of Delfi-C3 in Delfi-REAL, stowing the parachute system on top of Delfi-REAL will not be possible. This leaves the options of storing in the heat shield or storing it within the main 9U system.

Landing Method- Two options for the landing system were considered. Due to its TRL and the size of Delfi-REAL catching mid-air was ruled out. This means the parachute will be designed to bring Delfi-REAL to the required speed to land on Earth.

16.3.2. Trade-off Criteria

For parachute design for spacecraft landing applications, the performance characteristics, with their respective importance in Table 16.1, were taken from the Parachute Recovery Systems Design Guide [42]. Characteristics ranked with a 3 have high importance, those with a 2 have medium importance, a 1 indicates low importance and 0 means it is not applicable.

Table 16.1: Parachute performance characteristics for spacecraft applications [42].

Performance Characteristics			
Reliability of Operation	3	High Drag	2
Repeatability of Performance	2	Low Opening Forces	1
Reuse	0	Low Maintenance/Service	1
Low Mass and Volume	3	Cost	1
Stability	2		

Due to the unique circumstances of Delfi-REAL's mission including the high re-entry speeds, strict mass and size restrictions, and Delfi-C3's loading restrictions, the drag performance will be high in importance. To trade-off the parachute configuration and types, the mass, complexity and drag performance will be compared. It is important to note that reliability is not included in the trade-off because all parachute designs that are being considered have been used and can already be considered reliable.

16.3.3. Trade-off

With these trade-off criteria it is possible to determine which design option will be optimal for Delfi-REAL. The following design choices were made for the remaining branches of the DOT:

Configuration- When comparing the parachute configuration, having a single main parachute outperforms the cluster option for all criteria. Due to the drag loss of having the parachutes in a cluster, the mass of the parachute will be higher to perform equally. Furthermore, a pilot chute for each parachute in the cluster would be necessary [42]. This also adds complexity to the system. Thus, a single main chute was chosen for the system.

Main Parachute- During concept elimination, one option for the main parachute was discarded, leaving three viable options; solid, slotted, and rotating. Slotted parachutes have low drag performance resulting in more mass and a high complexity. Therefore slotted parachutes were immediately discarded. Rotating parachutes have exceptional drag performance, ranging from a drag coefficient of 0.85-1.8 depending on the chosen type [42]. These parachutes are also low in mass. Unfortunately, the parachutes are more complex, and their general application is usually for use as a pilot parachute. Solid chutes have a drag coefficient range from 0.28-0.95 [42]. This is a high drag capability, and they have low complexity. Due to the fact that solid parachutes are often used as main chutes, and they are strong in all 3 criteria, solid chutes have been chosen for the main chute.

Pilot Chute- After the DOT, all forms of pilot parachutes were still considered for the design. Due to the fact that the design of the pilot chute design is very dependent on the sizing of the main chute, and will have a very small impact on the final design. The choice of the most appropriate type chute will occur after the main chute has been sized.

Landing Method- After the option elimination, the options of landing in water and on land remained. When compared against these three criteria, it was clear that landing on land will be a more optimal choice. Landing the

system on land will require lower speeds than a water landing, thus a larger parachute. This mass difference however is much smaller than the necessary additions to Delfi-REAL to ensure buoyancy, and to seal it from water. A water landing will also cause additional complexity to Delfi-REAL's design.

Thus, the decent and landing system will be a sub-sonic solid textile parachute which is deployed by a drogue gun. It will be stowed inside Delfi-REAL on one of the sides that does not contain the propulsion system. Delfi-REAL's parachute will be designed for deceleration for a landing on land.

16.4. Final Design

In order to properly size the parachute, it was necessary to determine the mass of Delfi-REAL and Delfi-C3 after re-entry. The wet mass of Delfi-REAL is 14.5 kg. After capture, the mass of Delfi-C3 is also included in the mass, resulting in an additional 2.2 kg. Furthermore, the mass of propellant, 1.2 kg, can be subtracted from the system. This leaves a system mass of 15.5 kg.

After performing the initial sizing of the parachute, as explained in the next Subsection 16.4.2, it was determined that the required parachute packing volume for a mass of 15.5 kg was too large for the size of Delfi-REAL. This meant it was necessary to decrease the system mass in some way to lower the parachute size, thus lowering its packing volume.

A heavy component which has a low interaction to the rest of the system is the heat shield. The heat shield has a mass of 3 kg and is located outside of the main 9U structure. This means it is possible to detach it from the rest of Delfi-REAL. It was decided that the heat shield would be released from the system when the drogue gun was deployed.

A further look into deceleration mechanisms for the heat shield will be a recommendation for the future, and not included in the following sizing section.

16.4.1. ParSim Simulation

In order to calculate the parachute system for Delfi-REAL, the simulation tool ParSim was used. This program, and the rocket definition data are further explained in Section 15.4.1. For parachute analysis, the user is able to input the parameters shown in Table 16.2. Furthermore, the user is able to input the envelope for the specific parachute

Table 16.2: ParSim parachute parameters

Characteristic	Unit	Characteristic	Unit
Area	m^2	Drag Coefficient	-
Deployment Altitude	m	Deployment Time	s
Line Length	m	Shock Load Factor	-

type. The envelope includes the dynamic pressure range and the Mach range. The program also makes the following assumptions related to the parachute:

- Linear opening time for parachutes.
- Constant C_D with opening of parachute.
- No mass spring system for deployment of the parachute lines.

The program outputs plots with forces such as the total, body, line and clean parachute forces over time. It also outputs plots of the altitude and velocity over time. Furthermore it plots the deployment of each parachute with relation to the Mach and pressure envelope, which makes it easy for the user to see if the chosen parachute will perform for the mission. The program has already been verified and validated by Delft Aerospace Rocket Engineering DARE. The principles applied to the software come from the "Parachute Recovery Systems: Design Manual", which gives a step by step instruction of the sizing of parachute systems [39]. The design guide has been used by the American government for military and space applications [42].

16.4.2. Parachute Sizing

Main Chute

For the main chute, an annular parachute design was chosen because it had the highest drag coefficient related to canopy surface area. Parameters for the annular parachute design can be found in Table 16.3.

Thus, using the values, it was determined that a parachute area, S_o, equal to 4.5 m^2 was needed to decelerate Delfi-REAL from the re-entry speed to an impact speed of 7 $m\,s^{-1}$. The necessary diameter of the parachute, D_o, is determined by:

$$D_o = 1.1284 \cdot \sqrt{S_o} \tag{16.1}$$

and the line length is determined by:

$$L = 1.250 \cdot D_o \tag{16.2}$$

resulting in a D_o of 2.4 m and line length of 3 m [42]. These values result in a main parachute drag area, C_dS_o of 4.3. The number of gores, the number of attachment lines to the canopy, N_g, is 12 [42].

Table 16.3: Annular parachute parameters

Type	Drag Coefficient Range (-)	Opening Force Coefficient (-)	General Applications
Annular	0.85-0.95	1.4	Descent, Mach<0.5
Rotafoil	0.85-0.99	1.1	Drogue, D_o<7

A similarly sized annular parachute on the market was found by an American parachute manufacturer, Fruity Chutes. Their parachute has an area of 4.4 m^2, and a packing shape of 6.2 cm diameter by 9.9 cm length in a cylindrical shape.[2] The material is made of rip-stop nylon. The company says that the parachute has a C_d equal to 2.2. As this number was much higher than those found in the literature, thus the parachute system will be designed with the value from Table 16.3 [42][43]. The parachute mass is 310 g, and it costs EUR 270 .

Pilot Chute

To size the pilot chute, the main criteria to ensure is that it will not squid[3] the main chute. Squidding is when the sides of a parachute flutter when a parachute is not properly inflated. Thus the pilot chute's drag area must be less than 6 % of the main chute drag area [42]. Furthermore, the line length of the pilot chute must be at least 6 times the diameter of the spacecraft diameter. This means the maximum C_dS_o of the pilot chute is 0.26, and the line length must be at least 2.8 m.

To choose the type of pilot chute the system should use, the pressure and Mach envelope was used. Before adding the pilot chute, the envelope indicates that a high drag parachute option must be used. The Rotafoil parachute is a high drag drogue parachute with a low opening force coefficient. This parachute will provide enough lift with a small enough opening force to ensure the main parachute opens within the envelope. The characteristics of the rotafoil parachute can be found in Table 16.3.

Thus with a line length of 2.7 m, and a drag coefficient of 0.99, a parachute area of 0.1 m^2 must be used.

Looking at similarly sized pilot chutes on the market, it was estimated that the pilot chute will cost roughly EUR 100 , and weigh 30 g.[4] The specific size of Rotafoil parachute is not on the market, but could be easily manufactured with one of the companies, or free pattern guides available.[5]

Results

When deployed at 10 000 m and 5000 m, it can be seen from Figure 16.2 that the pilot and main parachute both deploy within their respective altitude, pressure and Mach requirements. The resulting loading, trajectory and envelope can be seen on Page 86 in Figure 16.3 and 87 Figure 16.4 respectively. The combination of this drogue parachute and main parachute brings Delfi-REAL to a final impact speed of 6.7 $m\,s^{-1}$.

In order to choose the materials used for the parachute system, previous space missions were compared. It was found that a commonly used material for space missions is Nylon or a Nylon blend, as used in the Mars Rover Mission, for Orion, and Apollo [44].[6][7] When compared to Kevlar, Nylon has a better performance under UV-radiation

[2] `https://www.apogeerockets.com/Building_Supplies/Parachutes_Recovery_Equipment` accessed on 16 Jan. 2019
[3] `http://www.newworldencyclopedia.org/entry/Parachute` accessed on Jan. 29 2019
[4] `https://www.apogeerockets.com/Building_Supplies/Parachutes_Recovery_Equipment`accessed on 16 Jan. 2019
[5] `https://www.apogeerockets.com/education/downloads/Newsletter194.` accessed on 16 Jan. 2019
[6] `https://mars.nasa.gov/mer/mission/spacecraft_edl_parachute.html` accessed on 18 Jan. 2019
[7] `https://airandspace.si.edu/collection-objects/parachute-main-apollo-0` accessed on 18 Jan. 2019

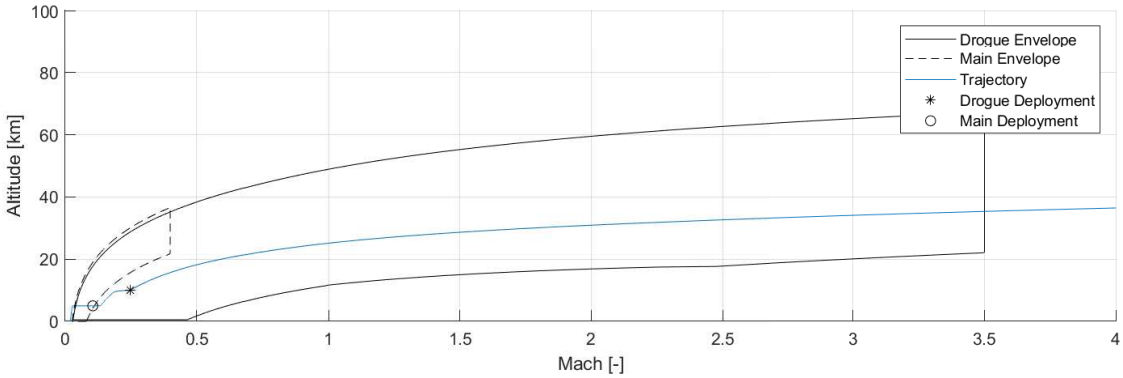

Figure 16.2: Parachute Deployment Envelope

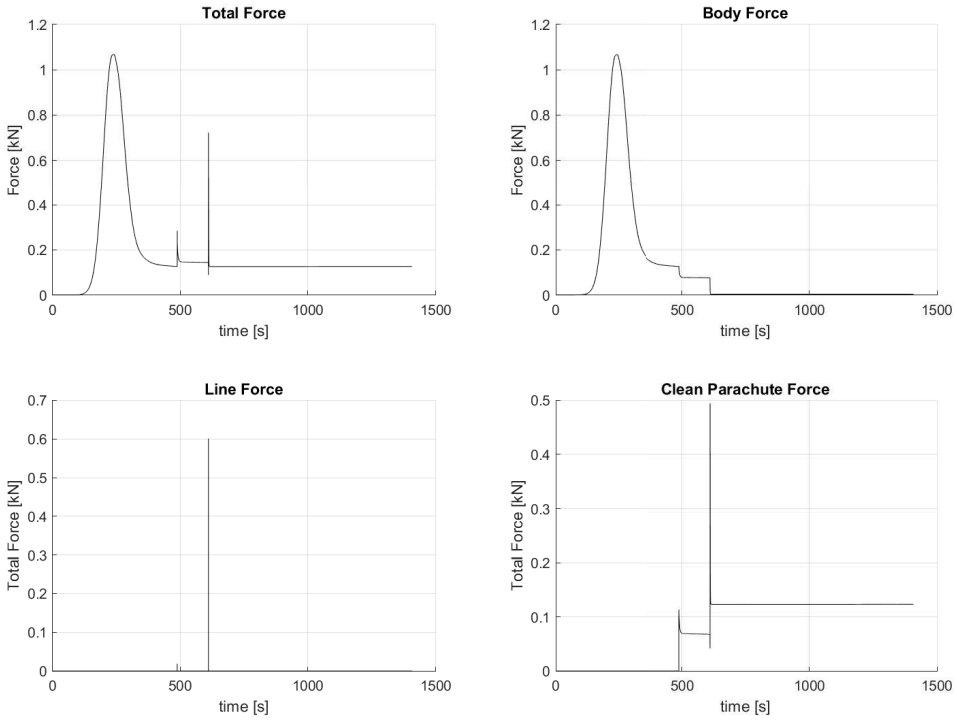

Figure 16.3: Final parachute forces

and a lower parachute mass and packing size [42]. Kevlar outperforms Nylon for its temperature limit, however since the parachutes will be stored internally until an altitude of 10 km, the temperature will be sufficiently controlled. This means that the parachutes will use the same material as the off-the-shelf product from FruityChutes.

16.4.3. Deployment Mechanism

In order to deploy the parachute, multiple mechanisms must be used. Due to the placement of Delfi-C3 on top of Delfi-REAL, the parachute must be stored internally, as explained in Section 16.3.1. The parachutes will be stored inside of a UV-resistant canister, to protect them from any space degradation during the mission.

As stated previously, in the introduction of Section 16.4, the heat shield will be dropped before parachute deployment to reduce mass. Pyrotechnic fasteners will be used to destroy the bolts connecting Delfi-REAL and the heat shield in a controlled manner. Pyrotechnic charges will be activated by an electrical charge which can be delivered by the batteries. This method of detaching satellite parts is commonly used in the space industry.

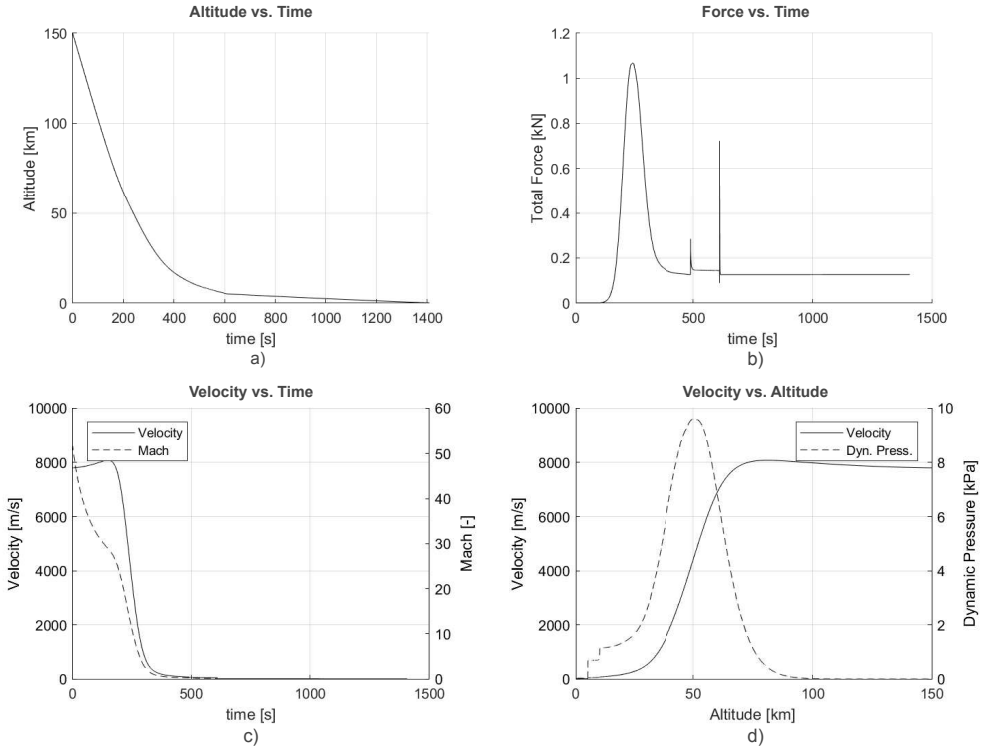

Figure 16.4: Final parachute trajectory

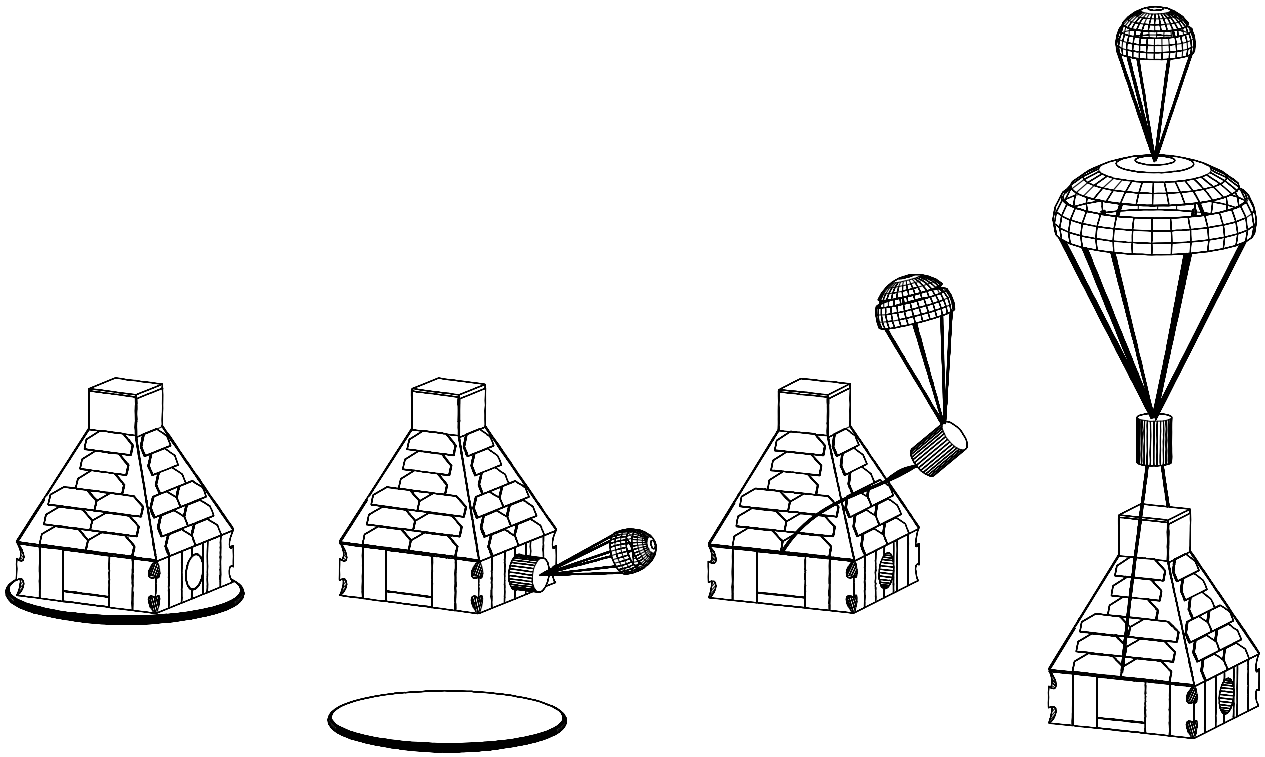

Figure 16.5: Parachute deployment sequence

Similarly, the side panel of the Delfi-REAL will also be released with Pyrotechnic fasteners, combined with over-pressure. The parachute itself will be deployed with the use of a drogue gun, as reasoned in Section 16.3.1. The drogue gun uses a pressure based mechanism that shoots a slug which is attached to the drogue chute into free-flowing air.

Once the drogue chute is deployed, it will release the canister containing the main chute from the hold. The canister is attached via two external cables which can withstand the heat of re-entry and the forces from the parachute. The mass of the cables is included in the mass of the parachutes. These cables are attached on opposite sides on the outside of the body. The placement of the cables ensures that the canister is situated above Delfi-REAL when the main chute is deployed.

The main chute, stored in the canister is held back with a pin. This will allow for a controlled deployment of the main chute at the desired altitude. Once the desired altitude is reached, this pin is removed via an electrical activation which then allows the force from the drogue chute to deploy the main chute. A timer, which is attached to the canister, controls the electrical actuation of the pin. This timer will have its own small power source in the form of a capacitor and is activated after deployment of the canister. This capacitor will be connect to the Electrical Power Subsystem via wireless contact to ensure maximum charge just before deployment.

As stated in Section 16.4.2, the main chute has a packed volume of a cylinder with a diameter of 9.9 cm and a height of 6.2 cm. This design leaves enough volume for the drogue chute inside the canister which in turn fits within 1 U. The canister is made out of UV-resistant material to minimise radiation damage to the parachute. A small pressure vessel with a valve is used to supply the necessary pressure to launch the canister.

16.4.4. System Testing and Costs

Extensive wind tunnel testing is required to ensure that the parachute and deployment mechanism function as intended. The wireless charging contact for the timer capacitor should be tested specifically with a vibration test. The deployment test will be performed in a low speed wind tunnel. This is estimated to cost EUR 8 k for 16 hours of testing. The total subsystem cost of the deployment system is broken down in Table 16.4.

Table 16.4: Recovery Subsystem Cost Breakdown

	Cost [EUR]	**Weight [kg]**
Deployment	7000	0.72
Parachutes	370	0.35
Testing	8000	-
Total	16000	1.2

16.5. Future Recommendations

Due to the vital decision to drop the heat shield after re-entry, there are several implications to the system that must be addressed in the future.

Firstly, by jettisoning both the side panel, and the heat shield in an uncontrolled manner it means that a system must be created to ensure a safe landing of the shield. For this reason, it is recommended in the future that a deceleration device be made for the heat shield. Since the shield will not have scientific importance like Delfi-C3, this means it can have a higher impact velocity, and loading. This means the parachute would not be as large, nor as complicated compared to the one needed for Delfi-REAL. It is recommended to look into a small parachute system that can be stored inside the shield, which can be deployed after a significant distance between Delfi-REAL is made.

Furthermore, the heat shield was initially planned to act as a damping system for Delfi-REAL during impact. As it will no longer be part of Delfi-REAL during impact, it is recommended to put more resources into impact testing of Delfi-REAL.

Furthermore, when known, it is recommended to take into account the vibrational analysis of the system to ensure the stability of the parachute. Each parachute has an angle of oscillation, and once it is known how stable the descent must be, the parachute choice can be further analysed for the system.

Lastly, it is recommended to do testing into the C_d of the specific annular parachute chosen for the system. If the C_d is 2.2 as the company suggests, this would significantly reduce the impact speed of Delfi-REAL from 6.7 $m\,s^{-1}$ to 4.3 $m\,s^{-1}$. This means further reductions to the parachute size would be possible, or the heat shield would not need to be jettisoned in order to bring Delfi-REAL to a safe impact speed.

17
Structures Subsystem

To ensure that Delfi-REAL's mission will succeed, all the subsystems must be housed in or on a structure that will allow them to function to the required performance without interference. Therefore, a structure must be designed for the mission. In this chapter the function of the structure subsystem for this mission will be introduced in Section 17.1. Following the definition of the functions to be carried out, the requirements for the subsystem will be presented in Section 17.2. Following the requirements, a primary structure will be selected in Section 17.3. Afterwards a trade-off will be carried out for the payload bay door mechanism in Section 17.4. Following the trade-off, the final design of the subsystem will be presented in Section 17.5. The verification and validation carried out during the design process will be discussed in Section 17.6. Finally, the recommendations for the continuation of the project are given in Section 17.7.

17.1. Subsystem Function

The structure is responsible for the housing and integration of all spacecraft subsystems. It must allow for the proper functioning of all systems throughout the mission. To comply with this responsibility the structure must be able to withstand all the loads and environments the spacecraft experiences throughout the mission.

The primary structure will be a Commercial Off-The-Shelf (COTS) cubesat structure, so the material type and layout are dictated by the manufacturer. There are no different primary structure concepts, but different available COTS structures. Being COTS, these structures are already rated for launch loads and have been designed using validated models. Furthermore, Delfi-C3 is also composed of a COTS cubesat structure, so its loading limits are similar and the loads throughout the re-entry mission phase can not surpass Delfi-C3's limits of 15 g steady acceleration and the vibrational load profile of the Polar Satellite Launch Vehicle (PSLV). The structure will thus not need to be sized according to the mission loading profile, but the Delfi-REAL will need to comply with the launcher requirements and the requirements imposed by the stakeholders.

The most important secondary structures are the payload bay doors and their deployment mechanism. The payload bay doors will need to open and adapt their orientation to fulfil their function as bearer of solar arrays. The payload bay doors will need to keep the same orientation with respect to the sun as explained in Section 11.5. This results in a speed of $3.75\,^{\circ}\,\mathrm{min}^{-1}$. To ensure the survival of Delfi-C3 during re-entry their second function will be to cover and restrain Delfi-C3. The attachments and components of the doors will thus need to withstand loads when closed as well as in open position. The mechanism must assure that Delfi-C3's Thin Film Solar Cells (TFSC) are not damaged when closing and during re-entry. Once the doors have restrained and covered Delfi-C3 they must not be able to open to prevent Delfi-C3 from being lost during re-entry. During re-entry the solar panels shall not generate power, so the mechanism relies on battery stored power once closed. The deployment and clamping mechanism are however of critical importance for mission success, thus the design options will be examined in detail.

To restrain Delfi-C3 and protect the TFSC's, two of the payload bay doors will have two small panels folded upon each other at the tip. These panels are indicated as panels B and C in Figure 17.1. The other two doors will have one small panel folded onto the door at the tip. They will thus consist of only of panels A and B shown in the figure. The clamp will fold two of Delfi-C3's solar panels but the other two will remain open. Due to Delfi-C3's panels being installed at 35° and their length of 325 mm, the TFSC of the remaining open panels will be sticking out of Delfi-REAL's side. If the payload bay doors were to close then the TFSC would likely be damaged or break as they would be the first contact point. To preserve the TFSCs one of the payload bay doors with panels B and C will thus have two levers, labelled as D in the figure, responsible for pre folding Delfi-C3's solar panels. The closing procedure will thus go as follows:

Step 1-The two doors consisting of panels A, B and C on the side of the closed panels will release the panels B and C on their tip.

Step 2-The two doors will close, with panel B laying flat against the TFSC at the top of Delfi-C3. Panel C will cover the top of Delfi-C3.

Step 3- Levers D on panel C, located on top of Delfi-C3 will be actuated to deflect the unfolded solar panels by a minimum of 17°, so that the TFSC will be within Delfi-REAL's edges.

Step 4-The other two payload bay doors will release their folded panel on their tip.

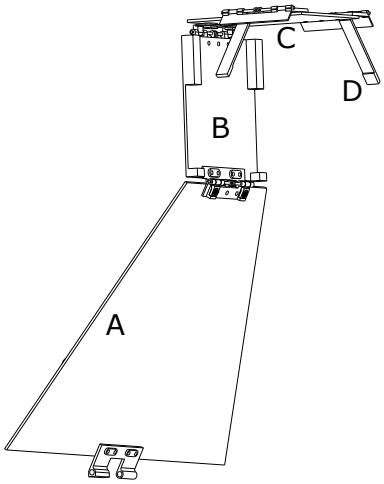

Figure 17.1: Payload bay doors concept.

Step 5- The remaining two doors will then close and fold Delfi-C3's solar panels the remaining 17°. Panels B of these doors will then lie flat against the top of the solar panel

17.2. Subsystem Requirements

The requirements found from the subsystem analysis are presented below. The STR label stands for structure.

RQ-STR-01	The structure shall have a mass lower or equal to 4.5 kg.
RQ-STR-02	The structure shall withstand the launch loads.
RQ-STR-02.01	The structure shall withstand 6.2 g steady longitudinal acceleration.
RQ-STR-02.02	The structure shall withstand 4 g dynamic longitudinal acceleration.
RQ-STR-02.03	The structure shall withstand 0.6 g steady lateral acceleration.
RQ-STR-02.04	The structure shall withstand 0.5 g dynamic lateral acceleration.
RQ-STR-02.05	The structure shall withstand the launcher-specified vibration test.
RQ-STR-03	The spacecraft shall comply with the separation mechanism.
RQ-STR-03.01	The spacecraft shall have 3 mounting points on a plane.
RQ-STR-03.02	The 3 mounting points will be on a diameter of [TBD] mm.
RQ-STR-03.03	The centre of gravity of the spacecraft will not be lower than 800 mm.
RQ-STR-04	The structure shall comply with the launcher limitations.
RQ-STR-04.02	The structure shall not exceed 12 U in size.
RQ-STR-05	The structure shall not interfere with functioning of other subsystems.
RQ-STR-05.02	The payload bay door hinges shall withstand 10 g when deployed.
RQ-STR-05.03	The payload bay doors shall remain closed, when carrying Delfi-C3, up to 10 g in acceleration.
RQ-STR-05.04	The packaging of components will not interfere with their performance.
RQ-STR-06	The structure shall withstand re-entry loads.
RQ-STR-06.01	The structure shall withstand 10 g longitudinal acceleration.
RQ-STR-07	The structure shall keep Delfi-C3 intact when landing.
RQ-STR-08	The payload bay doors deployment mechanism shall be able to open, close and restrain Delfi-C3.
RQ-STR-08.01	The payload bay doors mechanism shall allow the panels to fold flat on top of the satellite.
RQ-STR-08.03	The restraining mechanism shall not use power to maintain restrainment of Delfi-C3.
RQ-STR-08.04	The payload bay doors will not damage the TFSC during closing and clamping.
RQ-STR-08.05	The payload bay doors should not be able to open during re-entry.
RQ-STR-08.06	The payload bay doors shall be able to be rotate at 3.75 $^{\circ}\,\mathrm{min}^{-1}$.

17.3. Main Structure Selection

The main spacecraft concept dictates the need for a 9 U cubesat structure. From research it became evident that the 9U size is not a standard size. Innovative Solutions In Space (ISIS) is the only company with proven flight heritage that also offers custom solutions. All of ISIS's structures are rated for up to 15 g longitudinal acceleration and are delivered with functional, vibrational, mechanical shock, thermal cycling and thermal vacuum qualification testing for launch. This means that the structure will meet all the launch and re-entry loading requirements. The specifications of the ISIS custom 9 U cube-sat structure extrapolated form 3D models of their standard structures are presented in Table 17.1.

Table 17.1: 9U cubesat structure

Component	Width [mm]	Length [mm]	Height [mm]	Mass [g]	Cost [EUR]
9 U structure	340.5	342	100	1900	90 000

The mass of the structure was extrapolated from the masses of ISIS's 1, 3, 6, 8, 12 and 16 U structures. The cost was estimated through guidelines provided by ISIS, stating that the cost of every custom U module is approximately five times the normal price.

17.4. Payload Bay Doors Mechanism Trade-off

The payload bay door opening and closing mechanism is not a COTS available system so a trade off was carried out to determine the most adequate solution.

17.4.1. Design Option Tree

There are a few possible concepts for the deployment and restraining mechanism of the payload bay doors. The opening and closing of the doors can be done by means of springs, electrical and hydraulic actuators. Furthermore, it is possible to use the same mechanism to open and close the doors or to use a different mechanism. Delfi-C3 can be restrained through magnets, springs, electric actuators or hydraulic pistons. Lastly, the payload bay doors can be locked in place through a locking pin or the closing and clamping mechanism can keep the doors closed. The design option tree for the mechanism is presented in Figure 17.2.

17.4.2. Design Option Elimination

To decrease the number of concepts to bring into the trade-off all the options that were deemed unfeasible or didn't comply with requirements were eliminated. This is illustrated in the design option tree through red crosses. The reasoning behind these eliminations is explained in this section.

As the angle of the payload bay doors needs to be controlled during orbit all mechanical options are discarded for the opening and closing of the doors. Furthermore, the use of multiple electronic mechanisms to open and close the doors are discarded as it would add unnecessary mass and complexity when a single electronic device would suffice. The hydraulic options were eliminated as the spacecraft will already have an Electric Power System (EPS) on board. Adding a hydraulic system would take up too much volume and add unnecessary mass. Furthermore, hydraulic pistons are linear and in order to rotate the panels 180 deg they can not be placed in manner that would allow the doors to fold on top of each other as they would need to attach along the doors. Thus, this will also exclude electric linear actuators and springs for the opening and closing off the doors. Linear actuators and springs were also discarded for the unfolding of panels B and C as they would require levers and more space to carry out the task. Considering that the doors need to fold on top of each other, this would add unnecessary volume and complexity to the packaging of the doors. Furthermore, the folding of Delfi-C3's solar panels and the unfolding of the small panels B and C in space will not require much force, so the advantage of the high stiffness of linear springs is diminished.

The options that require electricity to maintain Delfi-C3 restrained are also discarded based on the requirements. Solenoids are also discarded for the opening and closing mechanism as they are binary actuators so they will not be investigated separately. Due to the doors being open first and then closed, a spring-loaded pin will not be feasible without actuation. This means the only locking pin option is an actuated pin. Also, as the doors should not be able to open during re-entry the use of no locking pin is also excluded. Lastly due to Delfi-C3 not being magnetic and the risk of affecting its electronics, the use of magnets to restrain Delfi-C3 is also unfeasible. The use of magnets is also discarded as it would hinder the opening of the payload bay doors.

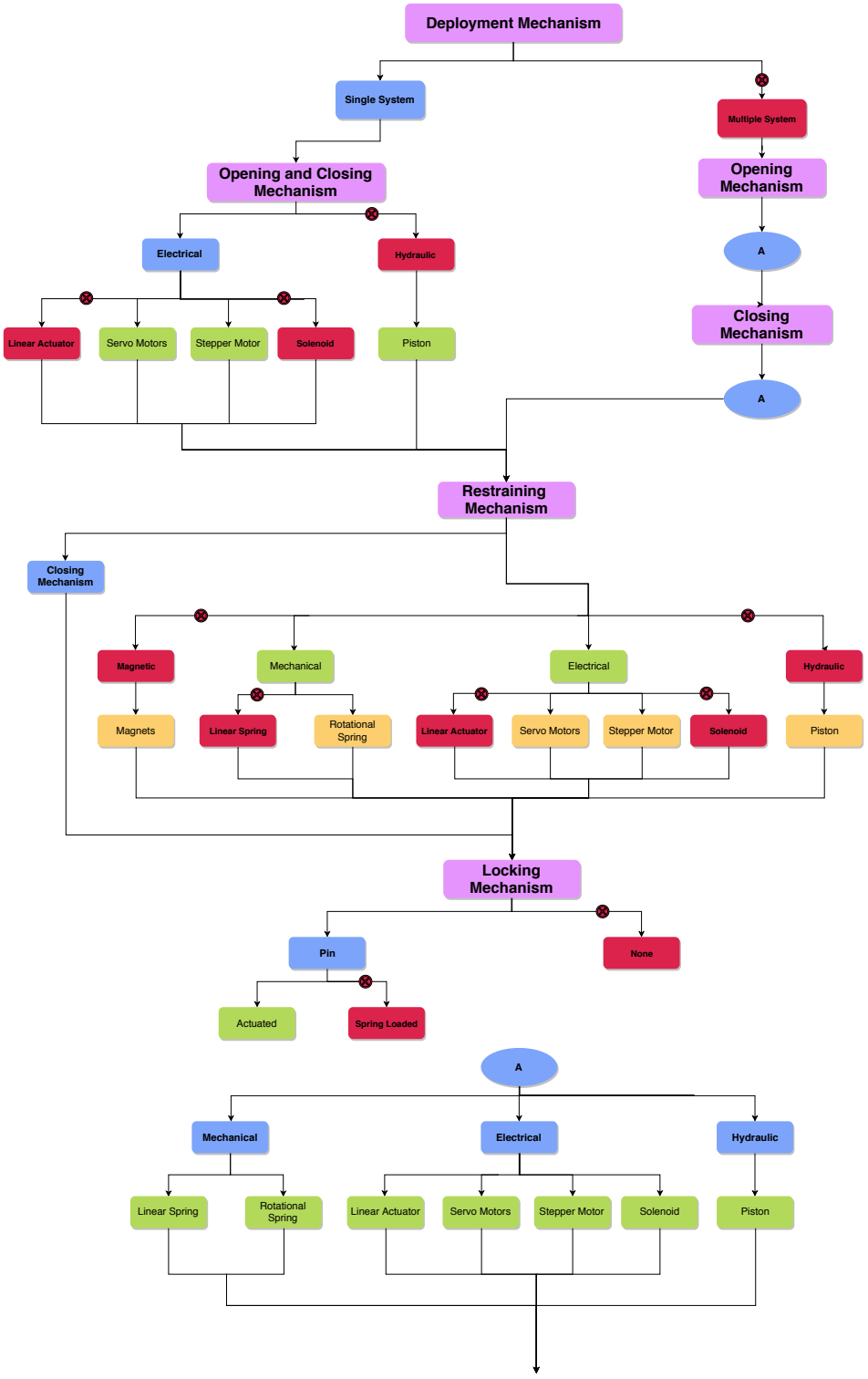

Figure 17.2: Payload bay doors deployment mechanism Design option tree.

The remaining feasible options could be split up into 2 main concept decisions in order to end up with a final design. These are presented below:

- **1- Servo for payload bay door hinge** - The remaining options to open, close and rotate the doors were a Direct Current (DC) motor and a stepper motor.
- **2-Mechanism for the panels B/C and lever D on the payload bay doors** - Panels B and C, and lever D could be actuated by means of 3 options. The options were spring-loaded hinges, DC motors, stepper motors and solenoids.

17.4.3. Component Selection

In this section the requirements for the components available are refined. With more refined requirements, a decision will be made regarding the most adequate solution for the servo for the payload bay doors and the unfolding mechanism of the restraining panels.

Servo's for doors

The two springs in parallel in the hinges of Delfi-C3's solar panel have a total stiffness of 0.29 N/ deg with an arm of 10 mm. Using this information and the free body diagram shown in Figure 17.3, the torque required on the payload bay door hinge was determined. From Figure 17.3, it is clear that the reaction force in the hinge is equal and opposite to the force applied on the solar panel.

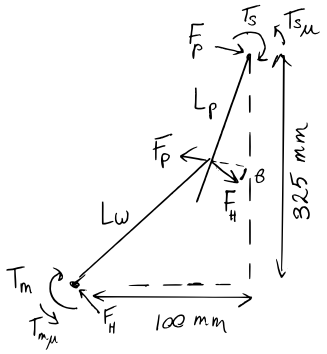

Figure 17.3: Free Body Diagram for stepper motor sizing

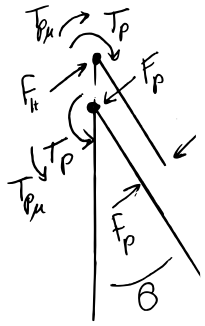

Figure 17.4: Free Body Diagram for restraining panel hinge

It was assumed that the hinge would be coated in Polytetrafluoroethylene (PTFE) or have PTFE bushing, resulting in a kinetic frictional coefficient of 0.2.[1] Delfi-C3's hinges are made of bronze with a steel axle. The friction coefficient is assumed to be equal to the dry kinetic frictional coefficient between brass and steel, 0.34. The maximum torque will occur when the angle in between the force vectors shown in Figure 17.3 is largest. This will occur in motion thus the kinetic frictional coefficient was used. This resulted in a maximum required torque of 460 mN m for the servos. The lever D responsible for deflecting Delfi-C3's solar panels from the top will also exert a torque on the panels until they are closed. This means the required torque is actually lower. Nevertheless, the servos were still sized disregarding the lever. This ensures that in the case of failure of the levers, Delfi-C3 will still be able to be enclosed, at the cost of two or one of the TFSC's.

Servo size generally scales with torque, so servos in combination with gear heads were examined to minimise size. From the torque requirement it became clear that DC motors were not a suitable option due to their high running speeds. The operating speed of a DC motor should be at least half the zero load speed for reliable operation. The DC motor with the lowest zero load speed for the required torque would require an operating speed of 35 RPM, which is too high for the requirement of 3.75 $\frac{\text{deg}}{\text{min}}$ set by the Electrical Power System (EPS). The feasible space grade stepper motors and gear head combination found are presented in Table 17.2.

Table 17.2: Stepper Motor and Gear Head Combinations

Motor-Gear Head	Nom T [mN m]	Max T [mN m]	Nom Power [W]	Max Power [W]	Mass [g]	Step Size [°]	Size [mm]
AM1524-15/1	567	648	0.875	2.19	65	0.0625	15 × 45.9
AM1524-17/1	504	576	0.875	2.19	83	0.0625	17 × 50.3
AM2224-20/1	739	832	1.5	3.75	114	0.349	22 × 56.3

The stepper motors and gear head were sized according to the guidelines set by the manufacturer, Faullhaber.[2] These guidelines stated that a safety factor of 30 % should be applied to the required torque in order to guarantee reliability. This resulted in a required torque of 546 mN m , which is above the torque rating of the Series 15/1 gear head. The AM1524-15/1 stepper motor, gear head combination was therefore not a reliable option. The remaining two options can both deliver the required torque. However the AM2224-20/1 combination would require more power, mass and space. The most suitable combination was chosen to be the AM1524 stepper motor with the Series 17/1 4 stage planetary gear head.

[1] `https://www.engineeringtoolbox.com/friction-coefficients-d_778.html` accessed on 14 Jan. 2019
[2] `https://www.faulhaber.com/fileadmin/Import/Media/EN_TECHNICAL_INFORMATION.pdf` accessed on 14 Jan. 2019

The two payload bay doors that will close first will not need to deflect Delfi-C3's solar panels and thus require less torque. For these two doors, smaller stepper motors can be selected. This will allow the hinges to be smaller and facilitate the folding of the payload bay doors on top of each other. This is because without the spring, a lower torque is needed. A stepper motor and gear head combination was chosen that could deliver half the torque required for the other doors, 283 mN m, this is assumed to be sufficient. The AM1524-15/1 combination with a different 4 stage gear ratio fulfilled this requirement and its specifications are presented in Table 17.3.

Table 17.3: Stepper Motor and Gear Head for 283 mN m requirement

Motor-Gear Head	Nom T [mN m]	Max T [mN m]	Nom Power [W]	Max Power [W]	Mass [g]	Step Size [deg]	Size [mm]
AM1524-15/1	258	295	0.875	2.19	65	0.122	15 × 45.9

Restraining Panels actuators

The payload bay doors will all have a restraining panel, B, that will need to unfold, but two of the payload bay doors will have an extra panel, C, that will need to unfold. These panels require a lever, D, on it that will fold the Delfi-C3 solar panels by 18°. The unfolding of panels B and C will not require much torque as it will only need to overcome the static and kinetic friction of the joint.

The critical hinges will be the one responsible for deflecting Delfi-C3's solar panel by 18° through lever, D. The normal force in the hinges will be equivalent to the force applied on the panels. The friction coefficient for Delfi-C3's hinges was assumed to be static friction coefficient between brass and steel, which is 0.5. The coefficient for brass and steel was used as no data could be found for the static coefficient of bronze and steel. This static coefficient was used because Delfi-C3's solar panels will initially be static. The friction coefficient in Delfi-REAL's hinge was assumed to be the same as the one for the main payload bay door hinge.

To determine the required torque for the stepper motors and spring stiffness the same procedure was followed for the servos at the main hinge but now using the free body diagram in Figure 17.4. The maximum torque required will occur at the maximum spring deflection of 18°. The resulting required torque including the 30 % safety factor advised by Faullhaber is 120 mN m. The specifications of the lightest and smallest possible space grade stepper motor and gear head provided by Faullhaber are presented in Table 17.4. It is to be noted that a motor controller is included in the mass of the stepper motor which would need to be packaged in Delfi-REAL.

Table 17.4: Stepper Motor and Gear Head for small panel

Motor-Gear Head	Nom T [mN m]	Max T [mN m]	Nom Power [W]	Max Power [W]	Mass [g]	Step Size [deg]	Size [mm]
AM1020-10/1	184	192	0.5	1.25	37.5	0.07	10 × 34.9

The torque provided by a spring depends on the spring stiffness, arm length and undeflected angle. The undeflected angle was chosen to be 270°, meaning that the hinge will lie flat against the side of Delfi-C3 if not restrained. The arm length of the spring was chosen to be 10 mm as that is the same as Delfi-C3 and would fit within the same hinge design. This resulted in a spring stiffness of 0.668 N/ deg. Furthermore, the spring-loaded hinge would need to be restrained by means of Dacron thread which will be melted by a surface mounted resistor as used by Delfi-C3. Resistors weighing a few grams can produce up to 5 kΩ[3], which is able to melt a 10 mm piece of Polyethylene terephthalate (PET) of 3 mm diameter in a few seconds based on the head capacity equation shown below.

$$Q = m \cdot c \cdot \Delta T \tag{17.1}$$

The resistor will however be mounted to a PCB and needs to have an attachment to the wire, so the total mass is assumed to be three times that of the resistor. Resulting in a total mass of 15 g. The dimensions of the spring were based on using two springs in parallel as well as the same mean coil diameter as Delfi-C3. The spring dimensions are presented in Table 17.5.

It is clear from Table 17.4 and Table 17.5 that the use of a stepper motor would not only be heavier but it would present various problems in comparison to a spring-loaded hinge. In order to package the stepper motor in the hinge the spacing between the panels B and C would need to increase. This would increase the volume in which the payload bay doors can be folded upon each other. Furthermore there would be more mass increase due to bigger hinges and brackets needed to restrain the motors. The extra power required to use these motors would also

[3] `https://nl.mouser.com/Passive-Components/Resistors/SMD-Resistors-Chip-Resistors/_/N-7h7yu` accessed on 15 Jan. 2019

Table 17.5: Torsional Spring dimensions

Component	Wire diameter [mm]	Mean Coil diameter [mm]	N. of active coils [#]	Mass of single Spring [g]	Total Mass [g]
Torsion Spring	1.25	4	10	1.4	18

increase the mass of the EPS. The choice was thus made to make use of spring-loaded hinges actuated through surface mounted resistors.

17.5. Final Design

With the main structure, and the payload bay door mechanism components selected the whole subsystem design could be completed. A Computer-aided three-dimensional interactive application (CATIA) model of the structure and shell wall mechanism was built in order to determine the actual dimensions of the components. The model of the 9 U structure was built based on dimensions from available 3D models of ISIS's cubesat structures. The final design model of Delfi-C3 was used in order to determine the exact dimensions required for the payload bay door mechanism. Furthermore, available 3D models of the stepper motor and gear head combinations were also used to design the system to the correct dimensions and determine any problems to be resolved. In this section the sizing and integration of all the components will be explained.

17.5.1. Payload Bay Doors and Panels

The payload bay doors will function as solar arrays and a protective shell for Delfi-C3. They will have to withstand the all the loads experienced when folded, opened and closed. Their shape is dictated by the requirement to cover Delfi-C3. Delfi-REAL is 340 mm wide, Delfi-C3 is 100 mm wide and the top of Delfi-C3 will be 332 mm from the top of Delfi-REAL when the clamped. The available width for mounting is 326.3 mm in length and thus the mounting surface is not square, resulting in two different payload bay door dimensions. The top of the payload bay doors panels is made to rest below the attachment of the TFSC. The dimensions of the payload bay doors that will rest on Delfi-C3's solar panels folded by the clamp are shown in Figure 17.5, while the dimensions of the payload bay doors that will fold Delfi-C3's solar panels are shown in Figure 17.6.

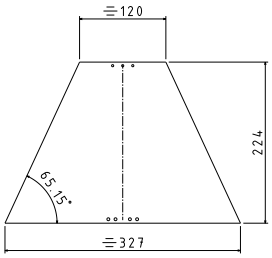

Figure 17.5: Payload bay door panel dimensions

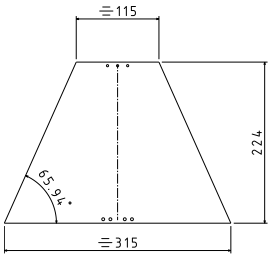

Figure 17.6: Payload bay door Panel for TFSC side dimensions

Figure 17.7: Dimension of the two Payload Bay Doors

The most critical loading for the payload bay doors will occur during re-entry. The payload bay doors must be able to withstand up to 10 g in longitudinal acceleration. The final maximum acceleration during reentry is 8.5 g but the panels were still sized for 10 g as a the time this refined value was not known yet. Two of the payload bay doors will undergo this acceleration together with the spring force of Delfi-C3's solar panels attempting to open them. The latter was examined as it is more severe. In order to determine a load from the acceleration, a thickness of 2 mm was used. This was based on the fact that Delfi-C3's panels were 1.5 mm thick. The panel was analysed separately and the 10 g was applied at the panels centre of gravity while the force generated by the spring of Delfi-C3's panels was applied at the contact point with Delfi-C3. The free body diagram for this static analysis is shown in Figure 17.9. The static analysis showed a maximum normal stress of 24 MPa and a maximum shear stress of 0.13 MPa.

The second critical loading scenario will occur during launch. The panel will undergo 6.2 g in longitudinal acceleration and 0.6 g lateral acceleration simultaneously. The panel was again analysed separately and the accelerations were applied at its centre of gravity. The free body diagram for this static analysis is shown in Figure 17.8. This loading scenario resulted in even lower stresses so the critical loading scenario was determined to be during re-entry. The resulting force required to restrain the panels during launch at the tip was 1 N. This low force will allow the use

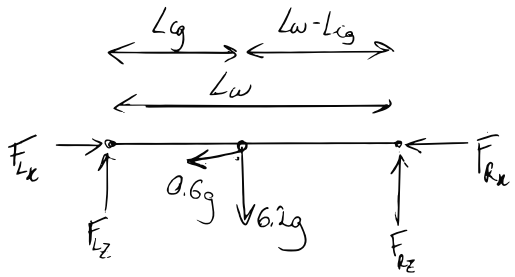

Figure 17.8: Free body diagram for launch loading

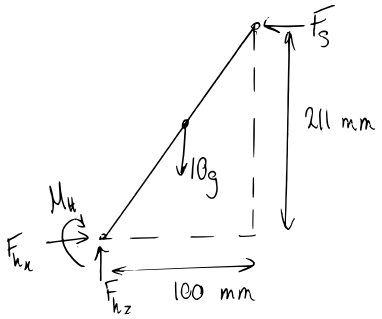

Figure 17.9: Free Body Diagram of Panel for re-entry loading

of dacron thread to restrain the panels during launch, which is then melted through surface mounted resistors as Delfi-C3 did.

The foldable panels will be used to cover Delfi-C3 and restrain its solar panels to prevent them from vibrating. They will however not carry other loads other than their own weight. The same holds for the panels covering the structure. As these panels will undergo less severe loading than the payload doors it was concluded that stresses would also not be a problem for them.

In conclusion, the static loads will not be the limiting factor for the payload bay doors. The critical factor will most likely be the vibrational loads during launch and re-entry. The yield stress of the material used will thus not be of importance , but the specific stiffness will be. The material selection for the payload bay doors was therefore, not based purely on strength but also on stiffness.

Material Selection

The materials being considered for the payload bay doors are Glass Fibre Reinforced Polymer (GFRP), Carbon Fiber Reinforced Polymer (CFRP), Aluminium 7075-T6, Steel and Grade 5 Titanium. The choice of material was based on the following criteria and their relative importance:

- **Specific Stiffness**-As examined, the loads for the payload bay doors will not be the critical factor, but stiffness will. Choosing a material with a high specific stiffness will produce a design with minimum weight for the same deformation or deflection. Due to the size of the payload bay doors, they will account for a significant mass of the structure. Thus choosing a material with high specific stiffness will substantially lower the subsystem mass. A lower system mass will have positive effects on the launch costs, propellant mass and the parachute.
- **Temperature Range**-The payload bay doors will function as solar panels and as a protective shell during re-entry. This means that they will be subjected to substantial heat. The higher the temperature range the less shielding material and insulation will need to be used on the payload bay doors. This will decrease the spacecraft mass. As for the specific stiffness, covering such relatively large area will cause an undesired increase in mass but not to the same extent as specific stiffness.
- **Cost**-The mission has a set limit on the cost of Delfi-REAL. Certain materials are considerably more expensive than others, so if possible one should try to minimise costs. The material costs of the payload bay doors and panels will be negligible compared to the costs of the main structure, which is 90 kEUR . This is because the production of a flat panel is very simple regardless of material and the small size of the panels will also not require the use of specialised machinery. Furthermore, the materials considered have associated costs, which are multiple orders of magnitude smaller than the main structure m. The effect on the total costs will thus be minimal.

The respective criteria for the possible materials are presented in Table 17.6. The flexural modulus for CFRP panels was found to be between 41 [45] and 200 [46] GPa, while the flexural modulus for GFRP panels was found to between 20 and 30 GPa [47]. The material costs were found through a quote of suppliers. [4] [5]

The chosen material for the payload bay doors and the other panels was CFRP laminate, as it is able to provide an extremely high specific stiffness in the bending direction compared to the other options. Its operating temperature range is not as high as the one provided by steel and titanium. However, the possible mass savings is deemed to compensate for this.

[4] `http://web.mit.edu/course/3/3.11/www/modules/props.pdf` accessed on 16 Jan. 2019
[5] `https://www.alibaba.com/showroom/` accessed on 16 Jan. 2019

Table 17.6: Material options for Payload Bay doors and Foldable Panels

Material	Specific Modulus E/ρ $[m^2 \cdot s^{-2}]$	Temperature Range [°]	Cost $\left[\frac{\text{EUR}}{\text{kg}}\right]$
GFRP	11 to 17	−22 to 149	3.4
CFRP	33 to 130	−50 to 250	105.6
7075-T6	25.6	−40 to 80	2.64
Steel	24.8	−40 to 500	0.7
Grade 5 Ti6al4V	26.6	−40 to 400	26.4

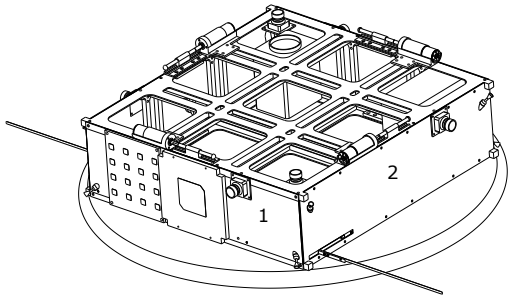

Figure 17.10: Isometric view of Delfi-REAL's structure with some components

The choice of CFRP resulted in the following mass and costs for the payload bay doors and panels presented in Table 17.7. The dimension of the panels were determined from the CATIA model of Delfi-REAL. The given dimensions for the payload bay doors, Panel C and Side Structure Panel 2, are the equivalent width and height, as these panels are not normal rectangles. The payload bay doors dimensions are shown in Figure 17.7. Side panel structure 2 has four cutouts on the edges to account for nubbins of the main structure, as seen in Figure 17.10. Lastly the top covering panel has a cutout in the middle for the clamp to move through.

Table 17.7: Final dimensions and specifications of remaining panels.

Panel	Amount	Width [mm]	Height [mm]	Thickness [mm]	Mass [g]	Material Cost [EUR]	Production Costs [EUR]
TFSC Door Panel	2	315	224	2	156	16.46	160
Door Panel	2	327	224	2	160	16.9	160
Restraining Panel B	4	100	104.5	1.5	25.1	2.64	160
Top Covering Panel C	2	83	100	1.5	21	2.21	NA
Side Structure Panel 1	2	342	100	1.5	82.08	8.67	160
Side Structure Panel 2	2	325	100	1.5	78	8.24	160
Top Cover Panel	326	2	342	1.5	252	26.6	NA

The production costs for laminating were based on an employee being payed EUR 80 per hour to laminate and post process the laminates. The required labour hours were approximated through contact with the dream teams of Formula Student Team Delft and Delft Aerospace Rocket Engineering (DARE). The smaller panels of the same thickness can be produced together and cut to size.

17.5.2. Hinges

The payload bay door mechanism is comprised of four different hinges. The main door hinges, that connect the payload bay doors to the main structure, which are rotated using stepper motors. The spring-loaded hinges responsible for unfolding panels B, the hinges responsible for unfolding panels C and finally the hinges mounted responsible for actuating lever D, as can be seen in Figure 17.12. These hinges must all withstand the loads throughout the entire mission and they all , except the one responsible for deflecting Delfi-C3's solar panels, must be able to lock in place once Delfi-C3 is enclosed.

Main Payload Bay Door Hinge- These hinges must not only withstand all the loads transferred through them but also allow for the proper functioning of the payload bay door mechanism. In order to allow the AM1524-17/1 stepper motor and gear head to rotate the door, the hinge must have the right dimensions to accommodate the mounting of the motor and the full rotation of the doors without clashing and be able to lock in place. The CATIA models of

Delfi-REAL and Delfi-C3 were used to size and design the hinge. The resulting design of the hinge and motor bracket is shown in Figure 17.11.

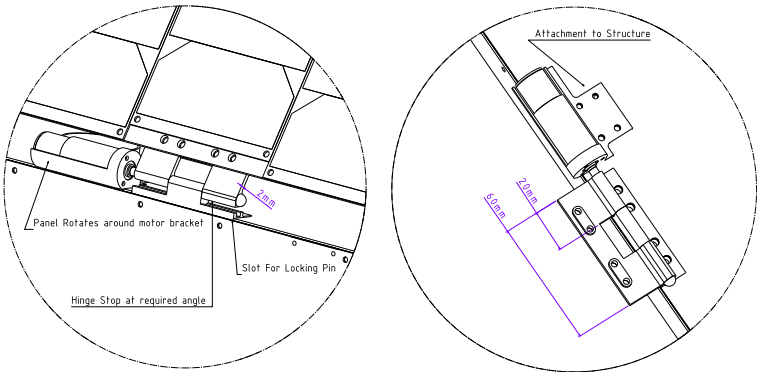

Figure 17.11: Payload bay doors hinge design

The design allows for the stepper motor to mount directly into the hinge and a set screw can be used to fix the motor axle to the moving part of the hinge as can be . The lower part of the hinge has a slot, in which the locking pin can be inserted by an actuator or a spring-loaded pin held in place by dacron thread. The hinge will not be able to move due to the flat face on the part of the hinge attached to the door. The motor bracket will likely be made out of aluminium to minimise mass, as yield stress, hardness and frictional coefficient are not of importance for the attachment bracket. There is also enough space to add thickness in case stiffness becomes a problem.

Spring-Loaded Hinges- The spring-loaded hinges responsible for unfolding the restraining and top cover panel had to be designed in order to lock in place on Delfi-C3 is restrained. The locking hinges must allow the proper folding of the panels and hinges within each other. The spring-loaded hinge used to actuate lever D did not have to lock as the payload bay doors will eventually restrain it against Delfi-C3. Once restrained the payload bay doors will lock themselves in place so there is no need for this hinge to also lock in place. Furthermore, it was chosen to place the non locking hinges on the same top covering panel, C, as to not torque these relative small panels. The design chosen was based on the design of Delfi-C3's hinges, as it possessed a very compact locking mechanism within the hinge. The hinges and panels were designed in CATIA and the resulting design is shown in Figure 17.12.

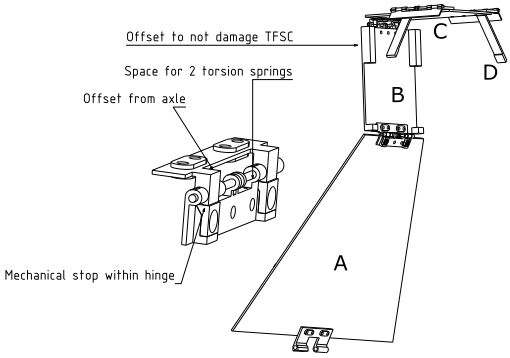

Figure 17.12: Spring-Loaded hinges design.

The offset from the hinge axle allows enough space for the panels to fold within each other, while the flat surfaces on both sides of the hinge assure that the hinge can not rotate further than the desired angle. Two small holes in the base of the hinges together with space around the axle allow for the instalment of two torsional springs per hinge. Furthermore the restraining panel,B, has an offset incorporated on the edges to make sure it leans against Delfi-C3's structure and not the TFSC's ro solar panels.

Material Choice

The most severe loading scenario for the hinge will be the same as for the payload bay doors, illustrated by the free body diagram as shown in Figure 17.9. The maximum stress caused by the deceleration and the torque of Delfi-C3's solar panels is 29 MPa. This occurs at the thinnest part of the hinge, according to the dimensions shown. The spring-loaded hinges are of similar dimensions and the torque experienced by them is more than half of that experienced by the main payload bay door hinge as explained in Section 17.4.3. The choice in material for all the hinges will not be limited by yield stress.

The materials examined for hinges were aluminium, titanium, steel and bronze. These are all relatively strong and stiff materials. The choice was based on a few criteria, which were the following:

Mass-Due to the constraints imposed by the panels having to fold within each other, the hinges can not decrease much in size. Therefore the current mass of one spring-loaded hinge will be compared with different materials. It is important to choose a material that will allow for a lightweight design.

Specific Stiffness-As for the payload bay doors and panels, strength will not be an issue for the hinges. It is however important that the hinges are stiff to assure Delfi-C3 is well restrained during re-entry. A material with a high specific stiffness will provide stiffness at the cost of little mass gain, which is important for the spacecraft.

Hardness- The spring-loaded hinges will impact on the hinge stop when released. Due to the space environment the hinge will keep accelerating until the stop is hit. A soft material might deform and thus change the locked angle of the panels. For the reliability of the mission it is important Delfi-C3 is well constrained and the hinges do not deform.

The comparison of the material for the hinges is presented in Table 17.8. From these results it was decided to use 7075-T6 aluminium for the hinges as it provides a great combination of specific stiffness with a very low mass for the current design size. With 12 hinges used for the mechanism it will be around 50 g lighter than titanium for almost the same specific stiffness. The performance difference in hardness could be accounted for by hard anodising the outside of the hinges. By doing so the axle surfaces can still be coated in Teflon to decrease the friction in the joints.

Table 17.8: Material options for Payload Bay doors Panel Hinges

Material	**Mass** [g]	**Specific Modulus E/ρ** $[m^2 \cdot s^{-2}]$	**Brinell Hardness** $[\mathrm{kgf\,mm^{-2}}]$
7075-T6	8.36	25.5	150
Steel	24.9	24.8	200
Grade 5 Ti6al4V	13.9	26.4	379
Bronze	25.6	13.3	42

With the choice made to use aluminium the relative masses and cost of all the hinges were calculated and is presented in Table 17.9. The production costs were calculated based on a Computer Numerical Control (CNC) machinist charging EUR 80 per hour. The number of hours were based on experience with milling and CNCing. Two hours of programming and three hours of machining was deemed to be a conservative estimate for the brackets.

Table 17.9: Final components specifications for payload bay door mechanism hinges.

Hinge	Amount	Mass [g]	Material Cost [EUR]	Production Cost [EUR]
Door Hinge	4	21	0.06	400
Spring-Loaded Hinges	8	8.36	0.02	400
Springs	8	3	3.4	NA
Motor Bracket	4	10.8	0.75	400
AM1524-17/1	2	83	760	NA
AM1524-15/1	2	65	660	NA

Total System Mass And Costs The total mass of the structure subsystem is currently 3.8 kg and the total costs is 103 kEUR .

17.6. Verification and Validation

The chosen cubesat structure is a COTS product based on a validated design. The structure was therefore not verified for launch loads and vibrations. This is also because the structure is tested before delivery as mentioned in Section 17.4.3. Two models were used to design the structure subsystem. The first is a Matlab model to determine all the required torques for the hinges and servos of the payload bay doors mechanisms. Matlab was used to solve the static analysis for all the required angles at once. The model was verified by calculating the analysis by hand. As mentioned in Section 17.5 a CATIA model was used to design the structure subsystem. The model was mainly used to fine-tune dimensions and to package the payload bay door mechanism. The model was verified by carrying out trigonometry calculations by hand to assure that the model was correct. Verification was done by determining the initial dimensions for the components by hand and then build them in CATIA. If components did not fit as expected,

the position and dimension of components like Delfi-C3 in the model were double checked before changing the design.

17.7. Recommendations

Due to the nature of the project, the final design presented is still far from being complete. There are various recommendations to be carried out to determine if the developed solution is feasible. The main structure is rated for the steady, dynamic and vibrational loads of the launcher. During the design of the payload bay door mechanism it became clear that steady loading was not going to be the limiting factor. The dynamic loading and vibrations during launch and re-entry were not analysed for the payload bay door mechanism. This means that Delfi-C3 could still come loose. Unfortunately there was no time to carry out a vibrational analysis of the system. It is imperative for mission success that resources be placed towards carrying out a vibrational analysis of the Delfi-REAL including Delfi-C3 during re-entry.

Furthermore, the payload bay doors were designed to cover Delfi-C3 but it is not a fully airtight and closed system. This means that during re-entry enough radiative heat could enter through these openings to damage Delfi-C3. To guarantee the validity of this design an analysis should be done to determine the amount of radiative heat caused by the ionized air during re-entry. If the radiation proves too be significant then the structural and thermal design of the payload bay doors should be adapted. The final payload bay door mechanism should then be tested to ensure the return of Delfi-C3.

All the selected components of the subsystems were included in the CATIA model inside the structure. The attachments, wires and propellant lines were not included in the model, but space was reserved for them. Attachments such as the required detachable heat shield or the parachute deployment mechanism are critical to the mission and they have not been analysed in detailed. To guarantee that all the required components fit in the structure it is advised to continue refining the CATIA model until fully complete and analyse those systems to more detail. If designed those systems should also be tested before flight.

The payload bay doors will require an actuator. The actuated locking pin and its bracket for the payload bay door hinge has not been designed yet and will require a design and analysis if the mechanism is to work. Lastly, Delfi-REAL will need to attach to a separation mechanism for launch. This interface has not been designed or analysed and resources should be assigned to it for future development.

18
Configuration and Layout

With all the subsystem trade offs having been carried out, the first iteration of the Delfi-REAL's components were identified. In this chapter the established configuration and layout of Delfi-REAL's components will be presented.

18.1. Layout

The final layout of the components in Delfi-REAL is presented from a top view in Figure 18.1 and from a side view in Figure 18.2. The side view is the side facing the positive x-direction. It is opposite of the star sensor.

To determine the most adequate configuration to optimise the performance of each subsystem, the components whose requirements imposed limitations on their positions were packaged first.

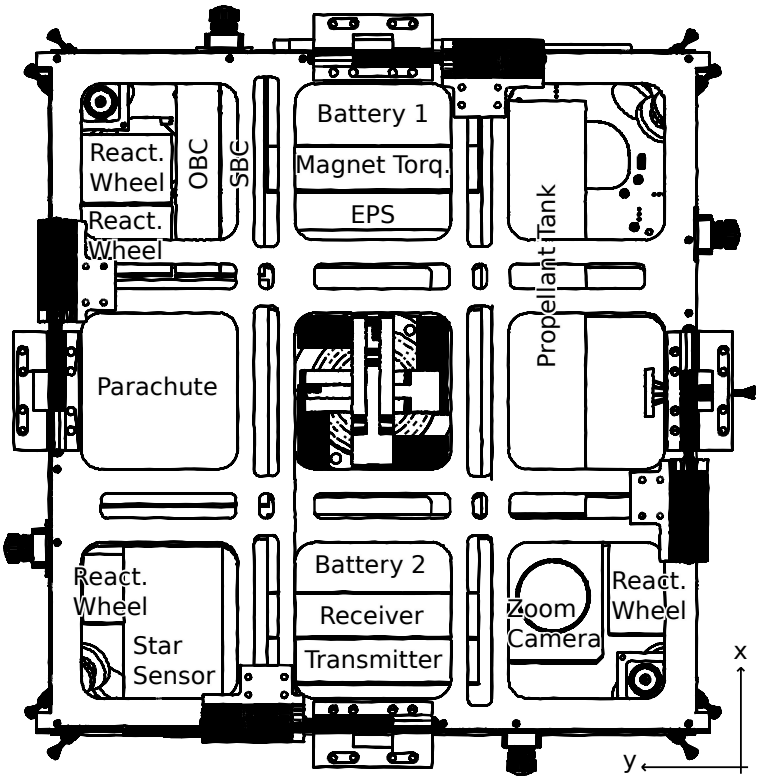

Figure 18.1: Internal Layout Top View

The concept dictates that Delfi-REAL will have a heat shield at the bottom for re-entry. Furthermore, the concept also dictates the clamp to be positioned in the middle of the 9 U structure and thus the 1 U module in the center of Delfi-REAL was taken up by the clamp. To be able to carry out the required orbit manoeuvres, a thruster had to be placed through the center of Delfi-REAL. This is based on the limitations imposed by the Attitude Determination and Control System (ADCS) for a maximum misalignment of the center-of-gravity form the thrusting axis.

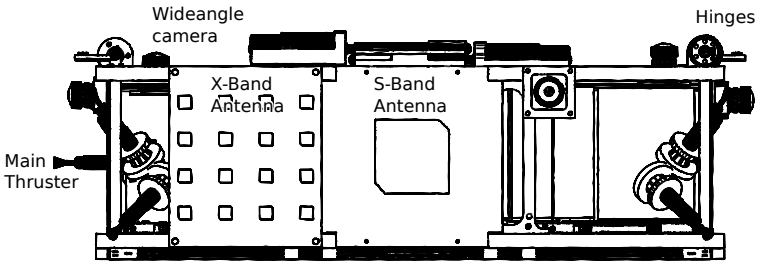

Figure 18.2: Internal Layout Side View

Having placed the orbit manoeuvring thrusters, it was decided to place the parachute opposite of the main thruster. This is because the large mass of the parachute would assist in keeping the center-of-gravity in line with the thruster. For the same reason the propellant tank and zoom camera were placed symmetrically to the parachute. Due to the thrusters, the wide angle cameras were placed slightly off center on each side of the structure to prevent any problems with heat. This allows the thrusters to be able to attach to the main structural stringers. The remaining two wide angled cameras were placed diagonally facing upwards as far away from the center as possible to improve their depth perception.

The S-Band antenna had to be placed on one of the perpendicular sides to the main thruster so that it is able to point to earth while thrusting. The sun sensor and star tracker had to be placed at opposite sides of the S Band antenna and X band phase antenna array so that when the antennas point towards the earth the star tracker and sun sensor will point towards the stars. The two dipole antennae were placed on the bottom in the top right and top left modules.

Two free modules remained above and below the clamp. One battery, the magnetorquer board and EPS control module were placed in the module above, while the other battery, receiver and transmitter were placed in the module below. This was done to keep the center-of-gravity close to the center. The remaining components were the four reaction wheels and the two On-Board Computers (OBC). Two reaction wheels had to be placed parallel in one direction. These were placed parallel to the main thruster direction in the top left module. The other two then had to be placed perpendicular to each other in a perpendicular direction to the main thrusting direction. One was placed flat on the bottom on the bottom right module and the other one vertically in the bottom left corner. Finally the only place left for the OBCs was in the right half of the top left module. Alternatives to the placement described are possible if the placement of the power cables and propellant lines dictates it.

With the components placed in and on the structure, the center-of-gravity of Delfi-REAL was calculated for the various in flight configurations. The datum point for the calculation was taken to be the bottom corner of the main structure left of the main thruster as indicated in Figure 18.1. The various centers-of-gravity are presented in Table 18.1.

Table 18.1: Center-of-gravity for different configurations

Configuration	**X coordinate** [mm]	**Y component** [mm]	**Z component** [mm]
Launch & Open Payload Bay Doors	179.5	172.5	42.3
Extended Clamp	179.5	172.5	46
Captured Delfi-C3	178.4	172.2	73.8
Enclosed Delfi-C3	178.4	172.2	94.75

Delfi-REAL, in its open payload bay door configuration, is shown in Figure 18.3. The closed system configuration is shown in Figure 18.4.

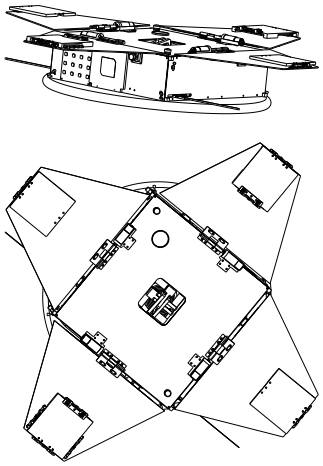

Figure 18.3: Side and top view of Delfi-REAL with open payload bay doors

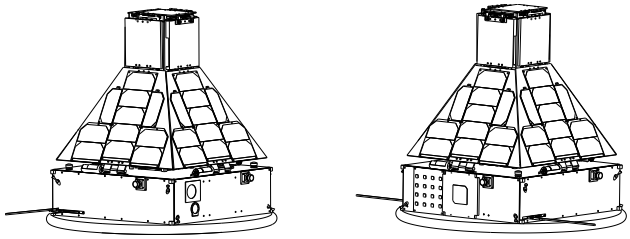

Figure 18.4: Front and side view of Delfi-REAL with closed payload bay doors

19
Sustainable Development Strategy

In this chapter, the sustainability analysis of Delfi-REAL is discussed. It starts with the sustainability strategy in Section 19.1. The strategy is followed by the subsystem sustainability of Delfi-REAL found in Section 19.2. Lastly, the adaptations and future potential of Delfi-REAL and its technology can be found in Section 19.3.

19.1. Sustainability Strategy

At the beginning of the mission design of Delfi-REAL, sustainability goals were put into place to try to find the balance between an optimised design and limiting the negative effects. This meant looking for solutions that limit the effects on society, economy and environment in the short term, while offering long term benefits. At the beginning of the design, the following system requirements were put into place, with SUS referring to sustainability:

RQ-SUS-01	The system shall not cause space debris.
RQ-SUS-01.01	The system shall not leave remains of Delfi-C3 in orbit that will not burn up in the atmosphere within 10 years.
RQ-SUS-01.02	The system shall not leave remains of itself in orbit that will not burn up in the atmosphere within 10 years.
RQ-SUS-01.03	The system shall initiate a de-orbit procedure in case of failure.
RQ-SUS-01.04	In case of failure the system shall not leave parts in orbit that are smaller than 10 cm in diameter.

A specific focus was laid on limiting the creation of space debris, as this was deemed the largest sustainability risk of the mission. To ensure that no space debris will be created, Delfi-REAL was designed to ensure high reliability and hence, mission success. Furthermore, the system requirements also limit the components to off-the-shelf options. This will mean less resources will be needed to produce and test all the components.

During the main trade-off in the midterm report, sustainability criteria were implemented into the main system criteria [1]. This was done to ensure that the overall design of the system would be sustainable, but that it would not hinder the overall design. This was done because overall, due to Delfi-REAL's potential to be applied to many more missions, the benefit of having a system that can complete the entire mission profile would outweigh the minor benefits of a more "green" choice that could not.

19.2. Sustainable Subsystem Design Choices

In the subsystem phase, the main goal was to limit over-designing the systems. With this goal in mind, the subsystems will lead to the lowest volume, and a propellant decrease from the initial estimate. Specific aspects that make the systems more environmentally sustainable are pointed out. In the remaining sub-systems the use of off-the-shelf components were used to limit the production costs.

Clamp - The clamp is designed in such a way that it is a simple design. This means material usage is kept low, development time and resources used for development are low, cost is low and assembly and testing takes less time than other design options. The number of motors needed in the design is kept to a minimum without compromising in reliability and redundancy. This also means that the clamp uses little power, and the power usage is not all at once. This is beneficial for the EPS since it has to generate and store less power. The clamp is also reusable if the mission is chosen to only de-orbit the satellites. It can be used to capture multiple satellites, one after each other, and not return them back to Earth. The clamp can also be scaled up or down to be able to catch larger or smaller satellites. Another option is to mount two clamps on a spacecraft to capture larger objects or objects which are difficult to grab onto with one clamp. The clamp can also be adapted to work with only two clamp arms instead of four, or even mount different clamp arms for different capture scenarios. All of this together makes the clamp design more sustainable.

Telemetry, Tracking and Communication - All components chosen are off-the-shelf. This eliminates the need to test the components individually. Furthermore, the validation procedure limits to testing the subsystem when it is built. This means the environmental impact due to testing will be as small as possible. Finally, the subsystem uses antennae, which will break off and burn up during re-entry. To reduce the impact, only two antennae for

telecommands are used which stick out and will be destroyed. The S band antenna for downlink is a patch and will not break off.

Propulsion - To successfully complete the mission and satisfy all the requirements with the current state of technology the use of a chemical propulsion system is unavoidable. However, the choice was made to use LMS-103S, a non-toxic propellant. Research was done on the use of drag sails but could not be used as they would not allow reliable control of the spacecraft re-entry angle. For future iterations of this design they could prove to be useful however. More information on the use of drag sails and their place in future designs can be found in Chapters 13 and 23 respectively.

Launch and trajectory - A launch usually is the most unsustainable part of any space mission. In the case of Delfi-REAL however, the launch will be as a secondary payload to another satellite. This means that the exhaust of greenhouse gasses is significantly lower than with an individual launch. During the trajectory, sustainability is also taken into account. The short 10 s burns at apogee ensure that the optimal burn efficiency if achieved, thus reducing the propellant required.

19.3. Future Potential

As explained in the baseline report, Delfi-REAL has the potential to positively impact space in several applications [3]. There is a heavy reliance on space for everyday life such as communications, banking, and national security. Thus, keeping satellites operational, and decluttering orbits to allow for further developments is in society's best interest [48].

Currently there are over 250 non-operational nano-satellites, and more larger satellites orbiting in 2 primary orbits, many of which with no active de-orbit systems.[1] As satellites are constantly being launched into these two orbits, the likelihood of in-orbit collisions increase due to the Kessler effect.[2] The kessler effect says that high speed collisions of space objects will break into many more smaller pieces in orbit and will consequentially collide with more objects. This means the orbits will become even more dangerous, and the complexity of launching the new satellites will increase. In order to keep the benefits of space technology for everyone, it is important to tackle this problem.

As Delfi-REAL is currently designed, it can be used to benefit society in several applications. Delfi-REAL has the ability to attach to a 1U base, and with the re-sizing of the clamp system could be adapted for other sizes of nano-satellites. Delfi-REAL can re-enter these nano-satellites for de-cluttering, and scientific purposes. Although nano-satellite re-entry will be a niche market likely for scientific purposes, Delfi-REAL can be a tool to gather useful information to improve future mission success. This can help in the sophistication of nano-satellite technology and can be a useful, accessible tool to learn more about the effects of space.

Furthermore, Delfi-REAL without the re-entry and recovery subsystems can act as an active de-orbiting system to send nano-satellites at end-of-life to burn up in the atmosphere. This application will mean the likelihood of in-orbit collisions will be decreased.

Delfi-REAL can also be adapted to accommodate for both larger nano-satellites and micro-satellites as shown in the market analysis in Section 23.1.2. Using a net capturing system instead of the clamp lowers the required accuracy, as the system does not have to match the rotation of the satellite. This lowers required propellant, and makes the system more applicable to a wide variety of satellites. This change will also lower the cost.

Additionally, Delfi-REAL's imaging system can be used as a tool for all sizes of satellites and spacecraft. With the rendez-vous and imaging technology, it means inspection of large satellites is now possible. This means that companies will no longer rely on gathering statistics from multiple subsequent launches of identical satellites when one fails. This is a common practice in the industry. This is mostly applicable to large and expensive satellites, where the cost of Delfi-REAL is much lower than the cost of the failing satellite. This opens the door to collect knowledge, for example of degradation effects, which can be used to increase reliability and scientific value of future missions.

Lastly, the building of Delfi-REAL shows the market that a nano-sat can rendez-vous, capture images, and even re-enter. It provides new technology that can be incorporated in future missions. For example, using our rendez-vous and capturing technology, a satellite for in-orbit repairs may become possible. Furthermore, Delfi-REAL also shows that for future satellites, re-entry technology can be included to limit the amount of out-of-service satellites in orbit in the future.

[1] `https://www.nanosats.eu/img/fig/Nanosats_orbits_2018-10-28_2.pdf` accessed on 20 Nov. 2018

[2] `https://www.esa.int/Our_Activities/Space_Engineering_Technology/The_Kessler_Effect_and_how_to_stop_it` accessed on 20 Nov. 2018

20
Reliability, Availability, and Safety

This chapter discusses the Reliability, Availability and Safety of the satellite in Section 20.1. Firstly, the safety will be discussed. The reliability will entail a rough estimate of the reliability of Delfi-REAL. Furthermore it will discuss the redundancy philosophy followed for the subsystems. Finally, the availability following from the reliability of the system is described.

20.1. Reliability, Availability, and Safety

The Reliability, Availability and Safety (RAS) characteristics include, a list of safety critical functions, the redundancy philosophy applied, and the expected reliability and availability. A definition has to be established for safety critical functions. According to the European Cooperation for Space Standardisation (ECSS)[1], it is a function that, if lost or degraded, or as a result of incorrect or inadvertent operation, can result in catastrophic or critical consequences. These critical consequences include: serious harm to people, severe damage to equipment or property, and environmental harm.

Safety

To list the safety critical functions, a Fault Tree Analysis (FTA) is created. The Fault Tree Analysis will only identify these faults that follow the definition of safety critical functions. Furthermore, the FTA has the added benefit of identifying the hardware which could lead to these faults.

Figure 20.1 shows the FTA for destructive re-entry. The following safety critical functions can be identified from the tree.

- Correct determination of Delta-V decrease needed by the On Board Computer (OBC), to get to the re-entry angle required.
- The proper functioning of the primary thruster to ensure the amount of Delta-V decrease needed is reached.
- Fluent movement of the arm of the clamp to ensure the arm can be retracted after clamping Delfi-C3.

From Figure 20.2, the safety critical functions for the prevention of destructive collision with Delfi-C3 are found.

- The Attitude Determination & Control System (ADCS) pointing correctly, to avoid collision with Delfi-C3.
- The proper determination by the OBC, to ensure the thrust vector is correct.

Finally, Figure 20.3 shows faults which lead to destructive landing. Safety critical functions from the FTA are found to be:

- Correct functioning of the altimeter, which measures when the parachute has to deploy.
- The OBC giving the proper signal to the parachute to deploy.
- The correct functioning of the opening mechanism of the parachute.

Reliability and Availability

In order to quantify the reliability of subsystems, the complexity and technological readiness will be analysed. The reliability will be roughly based on these parameters. Furthermore, instead of only giving the total reliability of Delfi-REAL, reliability per mission phase will be discussed.

- **Attitude Determination and Control System-** ADCS is critical until the re-entry phase. It will ensure that Delfi-REAL will be oriented properly and will counteract rotation when the thruster is on. The ADCS is low in complexity since the amount of components is low. Furthermore, the subsystem uses components which are space tested. The reliability of the ADCS components is high. Furthermore, there is redundancy in the sensors and reaction wheels. Therefore, the reliability of the entire subsystem is considered high.

[1] https://ecss.nl/glossary/safety-critical-function/ accessed on 16 Jan. 2019

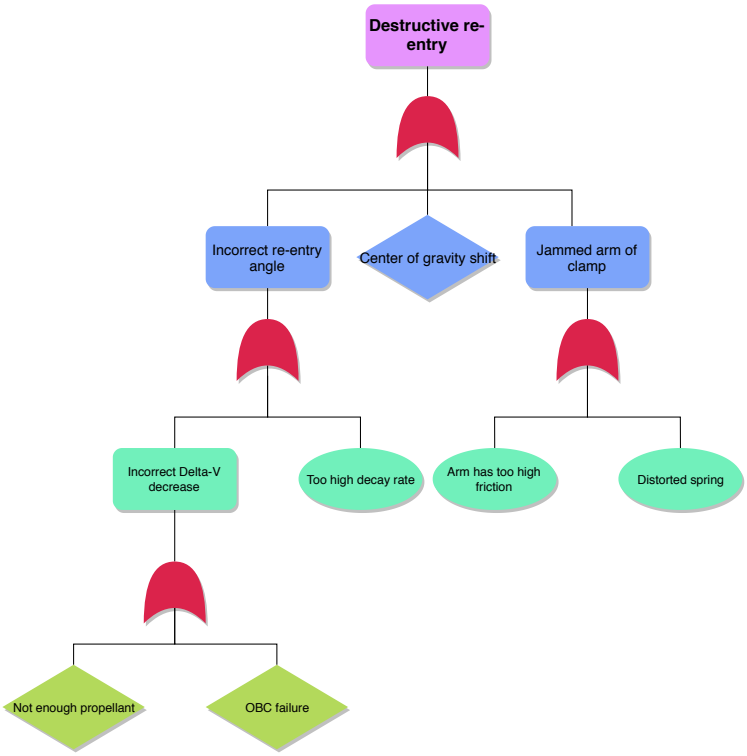

Figure 20.1: Fault Tree Analysis for destructive re-entry

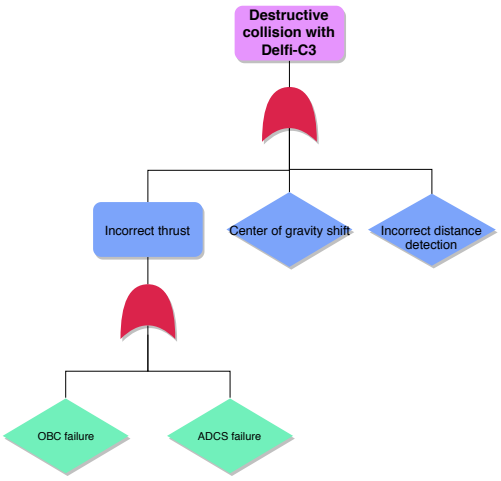

Figure 20.2: Fault Tree Analysis for destructive collision with Delfi-C3

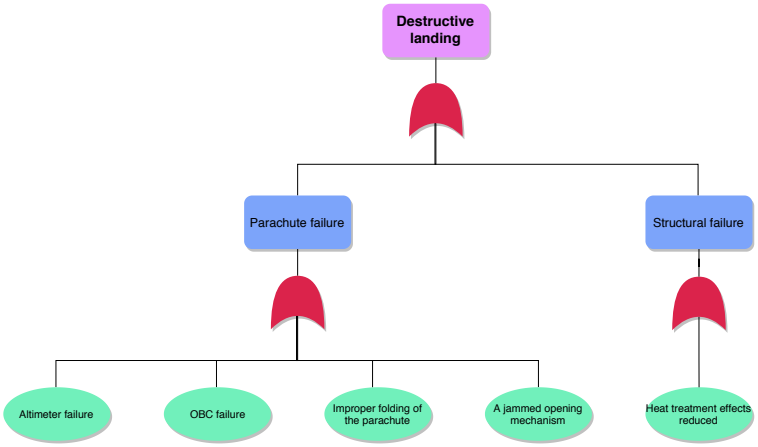

Figure 20.3: Fault Tree Analysis for destructive landing

- **Detection System-** This system is used to detect Delfi-C3 to determine the approach. The detection system is comprised of both space tested and non-space tested components. The complexity is also non-trivial. Several components work together to detect Delfi-C3. The reliability of the space tested components is considered high. This includes the phased antenna array and high resolution camera. The 360° camera's are not space tested. However, there are six of these camera's ensuring that the detection subsystem will function even if a few fail. The reliability of the 360° camera's is moderate. The reliability of the subsystem is considered high.
- **Clamping Enclosing System-** The clamp is only used to clamp Delfi-C3. The complexity is simple. Few components are used and the interactions between these components are limited. The components themselves are tested for space. However, the subsystem is designed specifically for Delfi-REAL. Therefore, the subsystem is considered experimental. The clamp also has a redundant motor. The reliability is considered high.
- **Telemetry, Tracking & Communication-** TT&C is critical throughout the entire mission. The components are space tested and the complexity of the subsystem is low. There is no redundancy. However, the reliability of the TT&C subsystem is high.
- **Command and Data Handling-** The command and data handling subsystem is used during all phases of

the mission. The primary OBC is connected to all the subsystems except for the detection subsystem. The primary OBC is space tested. Therefore, it is considered to be high reliability. The secondary OBC is used for the detection and encoding. It is not tested for space. The reliability of the secondary OBC is moderate. The reliability of the entire subsystem is considered moderate. Placing a second secondary OBC would increase the overall reliability of the subsystem.

- **Electrical Power System-** Power is used by all subsystems. This means that the power subsystem is needed throughout the entire mission. The components are all space tested. However, the subsystem has moderate complexity due to the fact that many components are involved. The reliability of the subsystem is considered high.
- **Structure-** The 9 U Structure is verified and validated by ISIS, which ensures high reliability. Furthermore, the 9 U structure has low complexity due to the modular design. The panels all consists of space-tested components which are highly reliable. The combination of the 9 U structure and the panels raises the complexity. This decreases the overall reliability to moderate.
- **Propulsion-** The propulsion subsystem is used until Delfi-REAL has a re-entry trajectory. All components of the propulsion subsystem have been space tested. The subsystem does not have many components. Therefore, the complexity is low. Finally, the subsystem is semi-redundant. The valves are redundant and the main thruster can be replaced by two secondary thrusters. The reliability of the subsystem is high.
- **Re-Entry-** The re-entry subsystem consists of a heat shield. The heat shield is an experimental design. The complexity of the subsystem is low. Not many parts are used. Furthermore, a high safety factor has been used during the design of the heat shield. Due to the experimental nature of the subsystem, the reliability is considered moderate. However, by extensive testing, the reliability will be high.
- **Descent and Landing-** The descent and landing subsystem consists of a parachute and an altimeter. The parachute and altimeter are not space tested. The parachute however is tested for use on earth and will be contained in a canister during the space part of the mission. The complexity of the subsystem is low. However, no redundancy is present to ensure the subsystem has a fail safe. The reliability of the subsystem is moderate. It can be increased by creating redundancy in the parachute deployment mechanism or the parachute itself.
- **Thermal Control-** Thermal control entails the control of heat during orbit. The thermal control of Delfi-REAL is passive. This means that some isolation is applied during production. However, no active components are used. Therefore, the reliability of the subsystem is not considered.

The reliability of the system is considered high for the reconnaissance phase of the mission. The reliability during the capturing phase of Delfi-C3 and the re-entry phase would be lower. However, by extensively testing the experimental parts, a high reliability can be guaranteed. In Sections 8.8 and 15.4 testing methods are discussed for these subsystems which will increase the reliability. Finally, the availability of Delfi-REAL is designed to be 100 %. The system is designed to ensure it does not need maintenance during the entire mission.

20.2. Requirements

Further requirements for Safety and Reliability were determined to ensure that the design of Delfi-REAL meets the overarching mission objective.

RQ-SAR-01-SH	The system shall not damage Delfi-C3 in case of a malfunction or abortion of the system.
RQ-SAR-01.01	The system shall have an abort procedure.
RQ-SAR-01.02	The system shall have a malfunction safe mode procedure.
RQ-SAR-02-SH	The system shall not endanger people.
RQ-SAR-02.01	The system shall not contain highly radioactive materials.
RQ-SAR-02.04	The system shall burn up in the atmosphere during mission abort.
RQ-SAR-03-SH	The system shall not endanger property.
RQ-SAR-03.01	The system shall not damage the launcher.
RQ-SAR-03.02	The system shall not damage the launch mechanism.
RQ-SAR-03.04	The system shall not land within 90 km of a built up area.

21 Technical Risk Assessment

Provided that the primary design options have already been defined for the final system, technical risk assessment aims to determine overlooked subsystems and interfaces that could potentially lead to mission failure. Risk identification and ranking is performed in Section 21.1 based off their likelihood of occurrence and impact on the mission. The mitigation procedures for each major risk are detailed in Section 21.2 and lastly, the treated risks are again analysed in Section 21.3 after mitigation has been applied to them.

21.1. Technical Risk Identifying and Ranking

Different mission phases employ and stress different subsystems and their components over a determined period of time. These subsystems have been considered individually as it enables a more detailed view at core issues rather than examining the system as a whole. Each risk has been evaluated relative to its likelihood of occurrence as well as its impact on the mission. The likelihood of occurrence is judged based on the maturity of the technology used and the complexity of the subsystem/components. Likelihood ranges from rare for a proven subsystem with flight heritage to very likely for new or purely theoretical concepts. The impact of the risk is evaluated from negligible to critical. The negligible impact implies no reduction in technical performance whilst critical impact suggests a failure to achieve mission objectives. The identified risks are listed in Table 21.1 and shown in the risk map Figure 21.1.

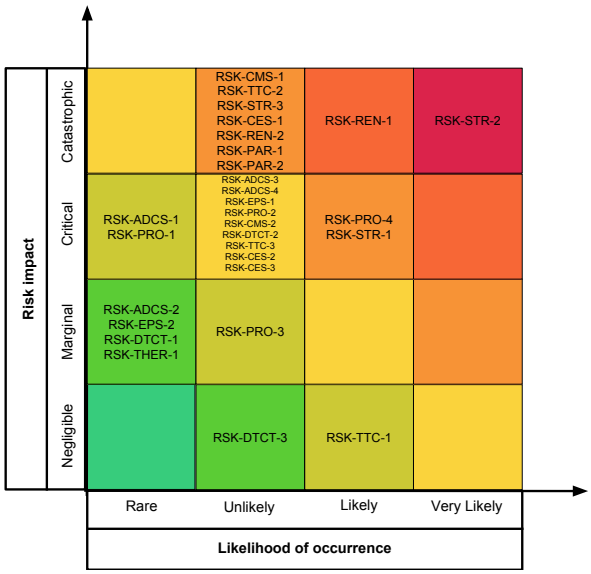

Figure 21.1: Technical Subsystem Risk Assessment Map

21.2. Risk Mitigation

The goal of this section is to treat risks found in the orange to red zone in Figure 21.1 by decreasing their likelihood of occurrence or their severity of impact on the mission. The following approaches can be used to mitigate risks:

1. **Mitigation 1**-Early initiation of development activities
2. **Mitigation 2**-Initiation of parallel developments
3. **Mitigation 3**-Implementation of extensive analysis and testing

The first two mitigation procedures focus on controlling schedule risks that could arise from technical risks. At the same time, these activities lead to higher costs. The risk of making incorrect critical design decisions mitigated using extensive analysis and testing via Mitigation 3, which requires time and capital allocation [49] as well. These considerations are applied to the unacceptable risk and the chosen mitigations are shown in Table 21.2. The necessity of implementing the mitigation ranges from 'Not required' (1) to 'Big necessity' (4) The mitigation procedures for each risk are added based off their numerical correspondence, enabling the observation of the most resource intensive

risks. It is relevant to note that the Table 21.2 presents the cumulative total resource allocation per subsystem. The following analysis assumes that singular risks can be avoided, controlled, or transferred, which enables them to be put in the acceptable risk category found on the yellow region in Figure 21.1 or to the left of it.

From Table 21.2 it is possible to observe that the most resource intensive risks involve the Structure subsystem/components. This subsystem contains no redundancies. The payload bay doors of Delfi-REAL represent a considerable engineering challenge given the fact that they are meant to open to capture Delfi-C3 and to withstand re-entry loads. The re-entry phase also subjects the structure to high thermal loads which are considered in RSK-STR-1 via existing gaps in the structure which enable heat to pass through. This could lead to weakened structural integrity or in a more severe scenario, destructive re-entry. Hence, a vibrational analysis for re-entry as well as further development of a locking mechanism for the payload bay doors is to be performed.

The components responsible for re-entry also need a considerable amount of resources in order to ensure that their likelihood of failure is decreased. In order to avoid burnup during re-entry, the angle at which Delfi-REAL approaches Earth's atmosphere needs to lie in a given accuracy range. Extensive analysis into ADCS and Propulsion subsystem configuration for the manoeuvre are required. Misalignment could be addressed by using remaining propellant to correct the approach angle. However subsequently all flammable propellants should be dumped before re-entry to avoid ignition due the high temperatures during re-entry. The centre of gravity shift could be evaluated through modelling or measurement in controlled conditions.

The Parachute subsystem does not provide a redundancy mechanism. The unfolding procedure involves one pin unlocking which is controlled by the OBC. The mitigation procedures aim to ensure that this is done properly, mostly via early start of development activities and testing. RSK-PAR-2 is mitigated via similar methods which aim to contain sufficient mass margin for the system. The proper functioning of the OBC is critical for mission success. Software development controlling each subsystem should be initiated as soon as possible, having specific considerations for the needs of each subsystem. Lastly, extensive testing during integration will be implemented.

The Clamp subsystem requires to be developed from an early stage and extensively tested, similarly to what the Propulsion subsystem needs. Notably the clamp subsystem requires more resources for Mitigation 1 given that it is customised for the mission with a configuration that has never been used in space. Lastly, the failure of the S-band antenna would prevent Delfi-REAL from communicating with the ground station as transmission of data is no longer possible. Provided that the antenna is Technological Readiness Level (TRL) 9 and space tested, the reliability is considered relatively high. In the event of a failure a destructive de-orbit manoeuvre could be initiated.

21.3. Technical Risk Ranking after Mitigation

After handling the possible uncertainties in Section 21.2, the likelihood of the most important risks has been reduced as well as their impact of occurrence. The mitigations applied change the placement of risks in the risk map. This results in a new risk map as shown in Figure 21.2. This new risk map shows there are no longer any risks that are likely or very likely to occur and have critical or catastrophic consequences.

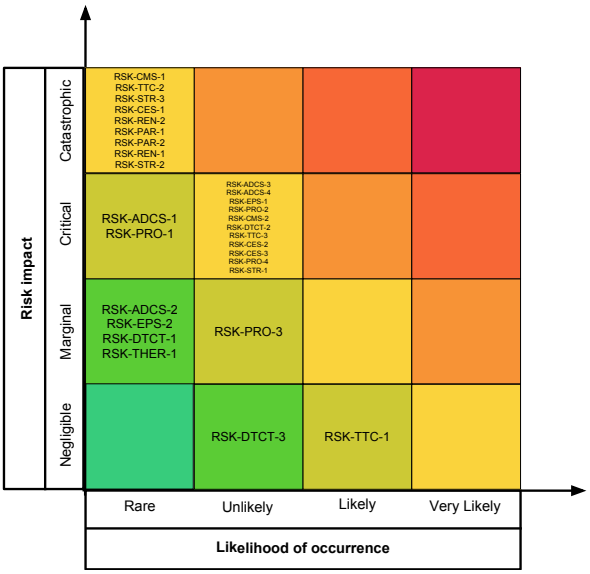

Figure 21.2: Technical Subsystem Risk Assessment Map after Mitigation

Table 21.1: Risk Identification Table.

Risk ID	Effect	Likehood	Impact
	Attitude Determination and Control		
RSK-ADCS-1	Reaction wheel failure	Rare	Critical
RSK-ADCS-2	Star or sun sensor failure	Rare	Marginal
RSK-ADCS-3	Magnetometer failure	Unlikely	Critical
RSK-ADCS-4	Magnetorquer failure	Unlikely	Critical
	Power		
RSK-EPS-1	Battery failure	Unlikely	Critical
RSK-EPS-2	Solar arrays hit by small space debris	Rare	Marginal
	Propulsion		
RSK-PRO-1	Failure of main thruster	Rare	Critical
RSK-PRO-2	Fuel tank leakage	Unlikely	Critical
RSK-PRO-3	Main thruster not going through the centre of gravity	Unlikely	Marginal
RSK-PRO-4	Fuel tank partially filled during re-entry	Likely	Critical
	On Board Computer		
RSK-CMS-1	Killer Software bug	Unlikely	Catastrophic
RSK-CMS-2	Electronics destroyed by radiation effects	Unlikely	Critical
	Cameras		
RSK-DTCT-1	Phased antenna array failure	Rare	Marginal
RSK-DTCT-2	Zoom camera failure	Unlikely	Critical
RSK-DTCT-3	360° camera failure	Unlikely	Negligible
	Telemetry, Tracking and Communication		
RSK-TTC-1	Interference due to other satellites transmitting/receiving data	Likely	Negligible
RSK-TTC-2	Failure of S-band antenna	Unlikely	Catastrophic
RSK-TTC-3	Failure of VHF or UHF antenna	Unlikely	Critical
	Structure		
RSK-STR-1	Unable to withstand heat loading during re-entry	Likely	Critical
RSK-STR-2	Unable to withstand mission vibrations	V. Likely	Catastrophic
RSK-STR-3	Weakened link with attached heat shield during re-entry	Unlikely	Catastrophic
	Clamp		
RSK-CES-1	Spring snap	Unlikely	Catastrophic
RSK-CES-2	Motor failure of clamp hands	Unlikely	Critical
RSK-CES-3	Extendable arm jammed	Unlikely	Critical
	Thermal Control		
RSK-THER-1	Incorrect isolation between solar panels and main body	Rare	Marginal
	Re-entry		
RSK-REN-1	Incorrect re-entry angle	Likely	Catastrophic
RSK-REN-2	Improper centre of gravity shift impacting aerodynamic properties	Unlikely	Catastrophic
	Parachute		
RSK-PAR-1	Failure of unlocking mechanism	Unlikely	Catastrophic
RSK-PAR-2	Breaking due to sudden deceleration	Unlikely	Catastrophic

Table 21.2: Resource Allocation for Risk Mitigation.

Risk	Mitigation 1	Mitigation 2	Mitigation 3	Total
RSK-STR-1	Big (4)	Medium (3)	Big (4)	11
RSK-STR-2	Big (4)	Big (4)	Big (4)	23
RSK-STR-3	Small (2)	Medium(3)	Big (4)	32
RSK-REN-1	Small (2)	Medium (3)	Big (4)	9
RSK-REN-2	Medium (3)	Medium (3)	Medium (3)	18
RSK-PAR-1	Medium (3)	No (1)	Small (2)	7
RSK-PAR-2	Big (4)	No (1)	Medium (3)	15
RSK-CMS-1	Big (4)	Big (4)	Big (4)	12
RSK-CES-1	Big (4)	No (1)	Big (4)	9
RSK-PRO-4	Small (2)	No (1)	Big (4)	7
RSK-TTC-2	Small (2)	No (1)	Medium (3)	6

22

Technical Performance Measurement

Throughout the entire design process it is necessary to track the Technical Performance Measurement (TPM) parameters in order to end up with a design that fulfils the top level and stakeholder requirements. These parameters are the Actual, Current, Target and Specification Value. The Actual value is the latest iteration without contingencies, the Current value is equal to the Actual value including contingencies. The Specification value is derived from the top level requirements and finally the Target value is equal to the Specification value minus the pre-planned contingency [49]. The tracking process of these parameters during the design is discussed in Section 22.1. In Section 22.2 the values of these parameters during the design process are shown.

22.1. Tracking process

At the start of the design process TPM parameters were established and both specification and target values were assigned to each of these parameters based on the requirements [3]. The specification value for the satellite cost was determined by subtracting the recovery, transport, insurance and testing costs from the total system costs. The costs for these mission components were estimated by contacting companies such as Hyperion and Innovative Solutions In Space.

Using initial sizing these parameters were broken down into individual subsystem specification values [1]. During the final design phase the distribution of these specification values were changed. The allowed cost of the Communication and Command Data Handling was increased. Part of the mass and cost allocated to the sensor and capture systems was shifted to the parachute, structure and communication systems. In order to successfully capture Delfi-C3 the maximal size of the capture system was increased. To sustain power demand during eclipse, larger batteries were needed than initially anticipated. Therefore, the specification size of the Power system was increased accordingly. Finally, the Attitude Determination and Control System was allowed to use more power as other subsystems turned out to use less than expected. Furthermore, a passive heat shield was chosen, which does not require any power. Table 22.1 shows the old and new specification values, the changes are highlighted.

Table 22.1: Change of specification value of the subsystems, changes are highlighted

	Old				**New**			
	Mass [kg]	Cost [kEUR]	Size [U]	Power [W]	Mass [kg]	Cost [kEUR]	Size [U]	Power [W]
Structure	4.5	29	0	0	4.5	129	0	2.3
Comms	1.0	53	1	31	1.0	103.2	1	31
Parachute	2.1	121	0.8	0	2.5	121	0.8	0
Heat Shield	6.2	242	3.4	6.8	6.2	242	3.4	0
Capture	2.5	15	0.5	16	2.5	14.5	1.2	15.2
Propulsion	2.1	97	1.7	19	2.6	97	1.7	19
ADCS	1.5	186	1.2	2.7	2.5	186	1.2	9.4
Sensors	2.9	348	3.4	4.7	1.9	198	1.7	4.7
Power	1.2	169	0.1	0	1.2	169	1.7	1
Total	25	1260	12	80.5	25	1260	12	80.5

It is important to note that although their relative distribution changed, the total value of the parameters remained the same. These specification values were used with a contingency factor to design the specific subsystems. The contingency percentages decreased as the design matured. At the start of the detailed design phase it was at fifteen percent and every week it was reduced resulting in a final contingency of five percent. Any lower than that would require actual measurement qualification hardware or actual measurement flight hardware [50].

Throughout the design phase the parameters, as discussed above, were logged every Friday. An overview of the dates of these logs and their corresponding contingency percentages can be found in Table 22.2. The contingency percentage of eleven was used for the sensitivity analysis for the individual subsystems as this was done in that corresponding week.

Table 22.2: Contingency percentage variation over time

Date	**7-12-18**	**13-12-18**	**21-12-18**	**11-01-19**	**18-1-19**	**25-1-19**
Contingency	20%	15%	11%	8%	6%	5%

22.2. Parameter values

Apart from the four main TPM parameters, the following other parameters were tracked throughout the design: the Delta-V budget, the link budget, the propellant mass and the pointing accuracy. These parameters are tracked because they have a significant impact on the final design. However, there are no high level requirements on these properties. Therefore, no specification value will be computed for these parameters. The actual values as they were at the start of the final design phase and at the end are stated in Table 22.3.

Table 22.3: Important parameters and their actual values

	Delta-V [$\mathrm{m\,s^{-1}}$]	**Link Budget** E_b/N_o [dB]	**Propellant Mass** [kg]	**Pointing accuracy** deg
Old Value	183	14	0.9	0.1
New Value	236	9.57	1.3	0.1

As can be seen the Delta-V increased by 28 % and therefore the propellant mass increased as well. This is not seen as a cause for concern as this increase was mainly due to the results obtained from the simulation software. However, as recommended in Chapter 14, the flight controller could be optimised further and would decrease the required Delta-V and Propellant Mass. The ratio of energy per bit and spectral noise density E_b/N_o decreased by 32 %. This is not an issue since, the Telemetry, Tracking & Communication subsystem will encode the signal, which decreases the required E_b/N_o by 8 dB as discussed in Section 9.3.

Graphs were made to visualise the TPM process, this is shown in Figures 22.1 to 22.4. As stated earlier, the process tracks four values; the target, current, actual and specification value. As can be seen, for all these parameters the actual values are below their targets and the current values are all below their specification values. This means all four main parameters will be well within their required values and no major design changes have to be made.

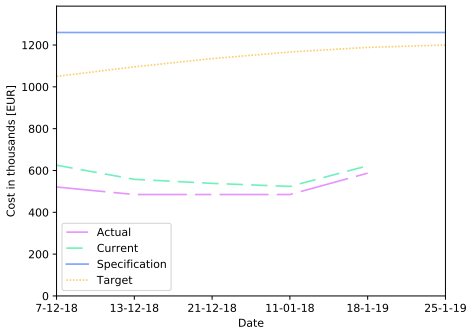

Figure 22.1: TPM overview for cost

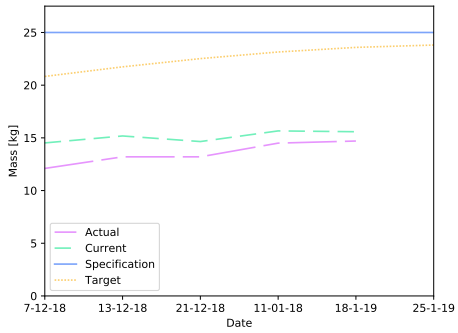

Figure 22.2: TPM overview for Mass

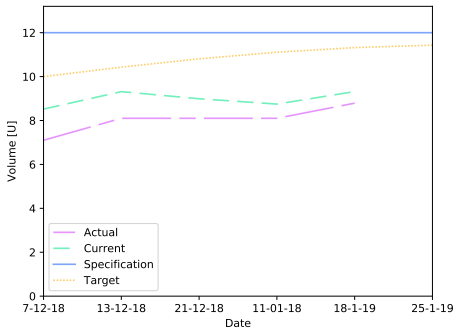

Figure 22.3: TPM overview for size

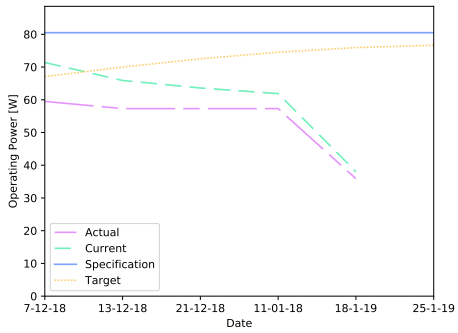

Figure 22.4: TPM overview for power

A breakdown of these parameters can be found below in Table 22.4. More detail of the cost for each individual component of each subsystem can be found in Table 23.3 in Section 23.3 of the Market Analysis. A more in-depth discussion and explanation of the mass, volume and operating power can be found in each subsystems chapter respectively.

Table 22.4: Delfi-REAL actual budget breakdown

Subsystem	**Mass [kg]**	**Cost in thousands [EUR]**	**Size [U]**	**Operating Power [W]**
Structure	3.8	98.6	2.29	0
Comms+CDH	0.68	55.6	0.75	10.7
Parachute	1.9	16	0.34	0
Heat Shield	3.0	194	2.4	0
Capture	0.57	23	1.0	3.6
Propulsion	2	86	1.24	10.2
ADCS	1.3	76	0.79	6.2
Sensors	0.42	15	0.38	2.4
Power	1.0	57	1.4	0.51
Total	14.7	621	10	35.9

23
Market Analysis

Market analysis is performed in order to establish the possible volume of the market and to determine the competitive cost of a product. The global nano-satellite industry is discussed in Section 23.1, as this is the market segment the product will mainly focus on. The state of the competitors is analysed in Section 23.2. In Section 23.3, an overview of the product is given as well as a SWOT analysis and a cost breakdown structure. The Return on Investment is described in Section 23.4. Finally, recommendations for possible revenue generating alterations and their potential buyers are given in Section 23.5.

23.1. The Nano-satellite Industry

In order to get an estimation of the market share of the product, the nano-satellite industry was analysed. This was done by researching the current market and attempting to predict its future growth. There are three sides to this industry: the companies and organisations using them, the ones that are developing the satellites and the ones launching them. In this section, special focus is put on the organisations using nano-satellites as they are potential, future buyers of the system developed by the design team.

23.1.1. Current State

In 2017, more than 275 nano-satellites were launched, which was an increase of 205% compared to 2016. It is estimated that there are currently 524 of them in orbit, with the majority being 3 U sized Cubesats. [1]

Most of the satellites are used for either Earth observation, remote sensing, or other scientific purposes. A large amount of satellites are owned and operated by Planet Labs Inc., who are responsible for roughly one-third of all nano-satellites launched to date [51].

23.1.2. Future Predictions

The four biggest sectors in the coming years are likely to be global internet, telecommunications, and Earth Observation and Remote Sensing (EO/RS), as can be seen in Figure 23.1. All these different sectors benefit from using nano-satellite constellations, which will therefore greatly increase the use of these products. For each of these sectors, big upcoming companies are examined in the descriptions provided below.

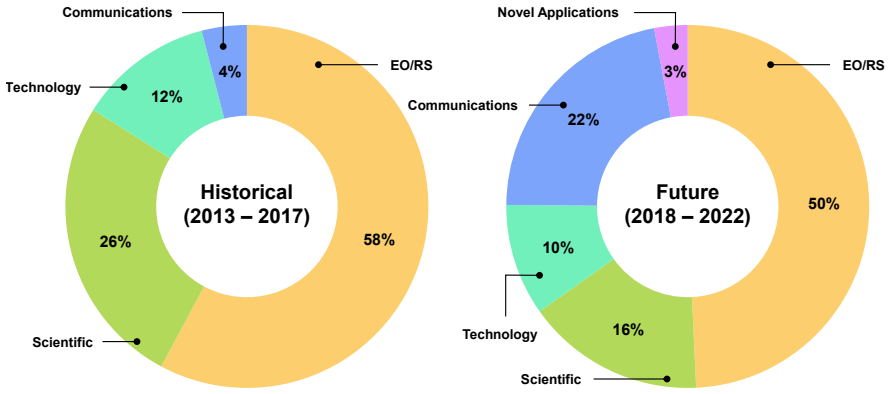

Figure 23.1: Nano-Satellite trends by application. Adapted from [51]

Furthermore, there are a many companies working on small satellite launch vehicles resulting in lower prices per kilogram and thus making getting to space cheaper and more accessible. Overall, an enormous increase in the use of nano-satellites is to be expected with predictions that up to 2,600 of them will be launched over the next 5 years, as shown in Figure 23.2.

- **Global Internet** - There are several companies working towards providing a worldwide wireless network infrastructure. The availability of such an internet connection could facilitate many new use-cases. Examples

[1] `https://www.space-track.org/` accessed 19 November 2018

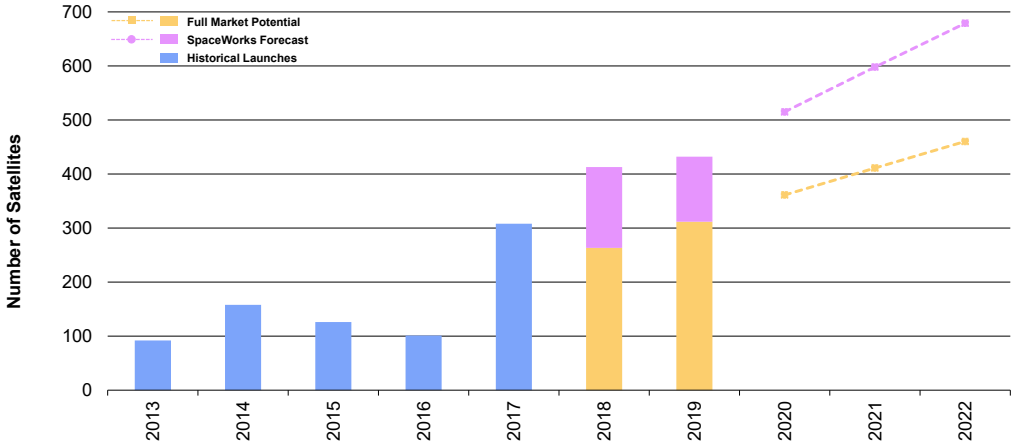

Figure 23.2: Nano-satellite launch number prediction. Adapted from [51]

of this are the General Electric (GE) Health Cloud and the John Deere Augmented Farm. The GE Health Cloud intends to connect 500 000 medical devices in hospitals around the world, to centralise the analysis of medical data through smart algorithms on the cloud [52]. The John Deere Augmented Farm intends to use this global internet connection to directly link the automated agricultural production machines such that they are informed in real-time, of the needs arising at other locations in the production chain. Together with global navigation systems, this allows for a significant increase in production efficiency and automation.

- **Telecommunications** - The telecommunications segment is expected to have the biggest growth and is expected to constitute of more than 20% of the market in the coming years as shown in Figure 23.1. This growth is caused by an increase in demand for data collection and transfer, as well as the ability to connect remote areas of the planet to the global communication network. Sky and Space Global has 200 nano-satellite launches planned while Kepler Communications and Fleet Space will both have a constellation of 100 satellites.[1]
- **Earth Observation** - Multiple mapping constellations are in the process of being created or being deployed, and will result in high frequency updated satellite maps of the surface of the Earth. These constellations are often employing large numbers of low flying nano-satellites. Planet Labs is a subscription service based planet imagery company and has launched a total of 298 nano-satellites and currently has 150 of them in orbit [51].
- **Remote Sensing** - Aside from visual mapping, surveillance of the Earth or some sub-regions are of interest for other purposes as well. For example, the monitoring of ships and aircraft, weather forecasting, mass-surveillance and location tracking of large populations of mobile-phone users. One of the companies involved is Hiber, a Dutch satellite constellation company. Hiber is planning to launch 48 satellites and is involved with projects regarding the tracking of the Indonesian fishing fleet for regulatory purposes, and a project in Tanzania connecting over 370 000 soil and water sensors. In order to provide accurate weather forecasting, Orora Tech is currently developing a constellation and is planning to launch 100 satellites in the coming years.

23.2. State of Competitors

In the present day, there are no companies providing a system with the same capabilities as Delfi-REAL. Furthermore, no companies have publicly stated that they are currently working on development of such a system. However, some companies and projects were found that were researching and developing systems that either partially fulfilled the requirements or were aiming to achieve similar results. Specifically, a lot of companies and research aimed at the prevention and removal of space debris was found. These were researched as they could potentially pivot to the use cases of the project or contain valuable information. A brief overview of these projects is divided below into two sections: the projects aimed at re-entry and the projects aimed at de-orbiting systems.

23.2.1. Re-entry

There have been no nano-satellites brought back to Earth by controlled re-entry. However, two projects have been found that are aiming to perform such task.

- **Spaceflight** - Andrews Space, now renamed to Spaceflight Industries, were developing a cubesat de-orbit and

recovery system. It is a 1 U sized module which can attach to a standard 2 U module. The re-entry is done by an inflatable tension cone with a small heatshield attached to it. It is designed to survive impact by having a integrated crushable structure and transmitting its location, found using Global Positioning System (GPS), after landing [53].

- **Qarman** - The 3 U sized QubeSat for Aerothermodynamic Research and Measurements on Ablation (QARMAN) is a project developed by the von Karman Institute and aims to demonstrate the use of non-powered rendezvous by chasing a target satellite by controlling the surface exposed to the residual atmosphere. It will demonstrate the use of passive de-orbiting as well as the ability of surviving re-entry. The spacecraft is currently still in development and there have been no launches yet [54].

23.2.2. Space Debris

In the last few years a lot of institutions, agencies and companies have started research and development to prevent or remove space debris. A selection of these projects is shown below.

- **Swiss Federal Institute of Technology** - The Swiss Federal Institute of Technology is currently developing CleanSpace One. Motivated by advancing technological readiness levels and removing debris from orbit, its objective is to de-orbit SwissCube, a small 1 U sized cubesat launched in 2009. It is aiming to locate the SwissCube by the means of an optical camera and signal analysis. Different capture devices were researched and finally a conical net was decided upon. The project is currently in a funding consolidation phase and launch is currently predicted to be in 2020 [55].
- **Astroscale** - Astroscale is a company aimed at removing space debris and is currently developing the End-of-Life Service by Astroscale demonstration (ELSA-d). Elsa-d is scheduled to launch in early 2020 and will consist of two spacecraft, a Chaser and a Target launched together. It will demonstrate target finding, rendezvous and capture [56].
- **D-Orbit** - D-Orbit is developing D3, a decommissioning device aimed to quickly and safely de-orbit a satellite at its end-of-life. It is an autonomous and independent module which can be added to a spacecraft design. On October 10th 2017, after 3.5 months in space, the D-Sat with a D3 device onboard has ended its mission.[2] The technology in space was validated, however, a controlled and direct decommissioning was not achieved.
- **ESA** - The European Space Agency (ESA) is working on the project e.Deorbit. It is studying an active debris removal mission which would remove an ESA owned non-functional satellite in low-Earth-orbit. It is currently considering a net or robotic arm as a capture device and is projected to launch in 2023 [3].

23.3. Product

In this section first a description of the product is given. After that the strengths, weaknesses, opportunities and threats are identified and discussed. Finally a cost breakdown is given of the spacecraft itself and the mission in total.

23.3.1. Product Description

The current iteration of the product is designed to observe and bring back 3U cubesats from low Earth orbit back to Earth. As stated earlier there are currently many 3U cubesats in orbit and many more are planned to be launched in isolation or in a constellation. In case of malfunction or total failure of one of these satellites Delfi-REAL could provide in-orbit inspection and if required for further research de-orbit and land the malfunctioning satellite. Just inspection could be done for larger satellites as well, providing a much needed troubleshooting tool for just a fraction of the development and launch cost for these larger satellites.

Ideas, descriptions and recommendations on possible future iterations of this product can be found in Section 23.5.

23.3.2. Strength, Weaknesses, Opportunities and Threats

A Strength, Weaknesses, Opportunities and Threats (SWOT) analysis was done to better understand the current place and possibilities of the product.

[2] `https://directory.eoportal.org/web/eoportal/satellite-missions/content/-/article/d-sat` accessed 19 November 2018
[3] `http://www.esa.int/Our_Activities/Space_Engineering_Technology/Clean_Space/e.Deorbit` accessed 19 November 2018

Table 23.1: SWOT Diagram for the product and market combination.

Strengths • First satellite able to return satellites to Earth • First satellite designed for damage observation • Provides possibility for companies to protect their investment through verification or mission life extension • Can observe any type and size of spacecraft	**Weaknesses** • Not a proven product • Return low mass spacecraft only • Amount of missions for which companies will be able to pay for the product is hard to predict. • A lot of different functions to fulfil
Opportunities • First product on the market available for these services and no competitors foreseen who can combine these services • Establish service for consultancy and information on new technology • Establish product as standard for this service and create brand • With orbit cluttering in the future possible services could expand • Great opportunity in the intelligence gathering market for observation of satellites	**Threats** • Failure to complete first mission will delay time for market to build confidence • Potential destruction of satellite could cause space debris and damage a lot of equipment on the orbit. • The use of de-orbiting modules will increase in the industry so the market for destructive de-orbiting might diminish with time • Few potential missions which will require return to Earth of nano-satellite • Possible involvement in military market could cause potential customers to decrease due to ethical reasons.

From the SWOT analysis found above, certain conclusions were drawn. Firstly, the product will be the first and only product to provide satellite inspection and de-orbiting services, allowing the company to establish a strong brand name and a customer base. The main risks for the product are the fact that it is not a proven product, so there will be scepticism in the market towards it. Furthermore, an incident during capturing could results in a whole orbit becoming unsafe to operate in. Lastly if the supplier of the product chooses to enter the military market, it might cause some other companies to withdraw if they do not want to be involved with companies involved in that market.

23.3.3. Cost Breakdown

In order to determine the feasibility and possible return on investment the total cost of the mission needs to be estimated. This was done by looking at the spacecraft cost, launch cost and operational cost.

Spacecraft Cost

For each of the subsystems estimations were made on the cost. This includes the commercially available hardware itself as well as integration and testing. For the components that have to be manufactured in-house, labour and material costs have been taken into account. The costs associated to labour and testing can be found in Table 23.2. These values were obtained by contact with companies such as Hyperion and Innovative Solutions in Space as well as student teams that regularly use these facilities such as the Formula Student Team Delft and Delft Aerospace Rocket Engineering.

Table 23.2: Standardised estimated costs

Type	Cost per hour [EUR]
Windtunnel testing	500
Vacuum chamber testing	1000
Manual Labour	80
CNC Machining	80

It is important to note that TU Delft has all of these facilities available for research and development itself, so the actual cost of using these facilities may be significantly lower or even totally free of charge. However for this cost breakdown it was assumed that that was not the case as this would provide a more conservative estimation. Using these values and estimations on how long certain parts need to be tested or take to manufacture, a detailed cost estimation was made. This detailed cost breakdown of the spacecraft can be found in Table 23.3.

Table 23.3: Spacecraft cost breakdown in thousands [EUR]

Subsystem	Component	Quantity	Cost per part	Total cost
Propulsion				86
	Thruster HPGP 0.1N	9	8	72
	Propellant tank	1	2	2
	Thruster valve	9	0.5	4.5
	Latch valve	5	0.2	1
	Drain valve	1	0.25	0.25
	Propellant			5
	Pipes			1
Power				57
	Azurspace 3G30C	22	2	44
	Electrical PCB	1	3	3
	Battery	2	5	10
Structure				99
	9U Structure	1	90	90
	Side Panel	4	0.65	2.6
	Top Panel	4	0.975	3.9
	Main Hinge	4	0.1	0.4
	Wall	4	0.21	0.84
	Clamping Wall	4	0.04	0.16
	Motor and Gear Head	4	0.25	1
	Motor Bracket	4	0.63	2.5
	Bolts and springs, small hinges			0.8
Heat Shield				194
	Heat shield	1	24	154
	Shield structure	1	10	40
CDH				8.6
	Primary OBC	1	4.4	4.4
	High Performance OBC	1	4.2	4.2
Payload				15
	Wide angle camera	6	0.7	4.2
	Zoom Camera	1	4.2	4.2
	Phased Antenna Array	1	6.5	6.5
ADCS				76
	Sun Sensor	1	12	12
	Magnetorquer Board	1	80	8
	Star Tracker	1	0.3	30
	Reaction Wheels	4	6.5	26
Telemetry				47
	Transmitter	1	30	30
	Receiver	1	8.5	8.5
	Rx and Tx antenna	1	6	6
Landing				16
	Drogue parachute	1	0.4	2.4
	Main parachute	1	0.4	6.4
	Parachute housing	2	0.5	1
	Pyrotechnique bolts	6	1	6
	Sensors	3	0.05	0.15
Clamp				23
	Arm motors + gearbox	4	1	4
	Telescopic arm	1	1	1
	Telescopic motor + gearbox	1	1	1
	Winch and rope	1	0.1	0.1
	Clamp base + arms	1	4	4
	Motion controllers	5	0.1	0.5
	Spring	1	0.1	0.1
	Assembly and testing	80	0.15	12
Spacecraft Cost				621

Launch Cost

The launch cost of a satellite is directly related to its mass. To be able to launch as fast as possible multiple launcher options are kept open. An overview of available and upcoming launcher options together with their costs is shown in Table 23.4

Table 23.4: Launcher costs [51] [57]

Launcher	Cost per kilogram in thousands [EUR/kg]
PSLV	45
Vega	23.3
Falcon 9	27.8
Electron	33
Kuaizhou 1A	57
LauncherOne	40
Small Satellite Launch Vehicle	12
Vector-R	54
Arion 2	38

As can be seen these cost vary quite a bit and most of these prices are negotiable. Furthermore, a lot of the launchers provide heavy discounts or even free rides for educational satellites. These lower prices per kilogram are usually for heavier spacecraft. Therefore, a cost per kilogram of EUR 55 000 was assumed, resulting in a total launch cost of EUR 800 000 .

Operational Cost

By making use of the groundstation already in place in Delft as well as radio amateurs from all over the world, the ground station operational costs were assumed to be zero.

After landing the spacecraft needs to be retrieved. As stated in Chapter 4 Kazakhstan was chosen, as it has a low population density and is frequently used for the landing of the Soyuz module, so the required procedures are known. For this retrieval EUR 500 000 was allocated.

Furthermore, the transportation to and the handling on the launch site is estimated to cost an additional EUR 50 000 .

Licensing and insurance

To be allowed to get launched and to operate a spacecraft a license must be obtained from the Radiocommunications Agency Netherlands.[4] In order to get this license the spacecraft must be insured, the costs for insuring Delfi-C3 are EUR 10 thousand.[5] Since Delfi-REAL will use a propulsion system it is expected that the insurance will be significantly more expensive and therefore a insurance cost of EUR 50 thousand is assumed.

Total Mission Cost

Combining spacecraft, operational and launch costs the total mission cost was determined, this can be found in Table 23.5

Table 23.5: Total Mission Cost [EUR]

Type	Cost in thousands [EUR]
Spacecraft	621
Launch	800
Operational	550
Licensing and insurance	50
Total	2021

[4] `https://www.agentschaptelecom.nl/onderwerpen/ruimtevaart` accessed 29 Jan. 2019
[5] J. Bouwmeester, personal communication, Nov. 11, 2018

23.4. Return on Investment

Now that the total cost of the mission has been determined the return of investment can be estimated. This is the ratio between the net profit and the cost of the investment. As the retrieval of TU Delft's own Delfi-C3 by Delfi-REAL is a unique mission, it brings not just monetary value but also prestige, brand awareness and provides educational and research opportunities to the university staff and students.

Therefore the current iteration of this project is not supposed to provide sustainable profits, but should be seen as a one time only mission, aiming to provide research and development opportunities. All while keeping cost low by getting partnerships and sponsors from interested companies. However, with only some small modifications, future variants of Delfi-REAL could be turned into a profitable product. These variants and their possible market share are discussed in Section 23.5.

23.4.1. Companies

Multiple companies were involved with the development of Delfi-C3 and would have an interest in it's retrieval for research. These companies include Airbus Defence & Space, TNO and SystematIC BV. Airbus Defence & Space by itself spends almost EUR 300 million on research and development [58]. Together with grants from research institutions and the government these companies are expected to finance the majority of the mission.

23.4.2. TU Delft

As stated earlier, a big part of the return on investment comes from the research and educational opportunities it brings. Delfi-REAL would provide a platform for interfaculty cooperation and development on state-of-the-art technology. Bringing together staff and students from Electrical Engineering, Mathematics & Computer Science, Aerospace Engineering and Mechanical, Maritime and Materials Engineering.

The marketing and communications department of Aerospace Engineering at TU Delft was contacted to determine the value of the media attention this project would generate. They kept track of the media attention the Delfi-N3xt launch got, which were six TV items on different broadcasting networks, four radio interviews, multiple online articles and items in the Volkskrant, Telegraaf, NRC Handelsblad, NRC Next and three local papers in Delft.[6] It was established that although it definitely contributes to the university's reputation and brand value, it is difficult to actually quantify that contribution. Some companies use advertising rates to determine the value of a news item but it is not used at TU Delft since it is unclear if that is a proper measurement.

To verify if people actually read, understood, remembered and liked the article and therefore the brand an effect study can be done. However this is also not used by TU Delft as this is very expensive. Furthermore, Aerospace Engineering has more applications than they have capacity so as a form of student recruitment it is not needed.

23.5. Recommendations

In this section recommendations are made to transform the current iteration of the project, tailored specifically to the capture and retrieval of Delfi-C3, to a commercially viable product.

23.5.1. Concepts

The design of Delfi-REAL accomplishes three primary functional objectives. Observing a target satellite, capturing the target satellite and recovering the target. Small changes to the clamp shape would provide opportunities to inspect, capture and land other 3U sized satellites as well.

However, the market analysis has shown that the most value lies in the inspection or de-orbit of a satellite. Three other satellite concepts were created that could provide sustainable profitability in the future. These concepts reuse most of the systems of Delfi-REAL, while dropping others to achieve a lighter, more specialised and more cost effective solution to address the needs of customers.

The first two concepts are directly aimed at reducing and preventing Space Debris. The first concept is to remove the ability to land and retrieve the satellite and to focus on destructive de-orbit. Without the need of protecting the satellite from the atmosphere and a high impact landing, the heat shield and parachute system as well as the protective panels can be removed. The design still maintains the clamp to capture the target. Furthermore, by

[6] I. Boneschansker, personal communication, Jan. 17, 2019

adding drag sails the required propellant can be reduced for the system. A sketch of this design in shown in Figure 23.3. The process of rotation matching and clamping a rotating target is very propellant expensive. The design can be further optimised by instead of a clamp using a net to capture the target as shown in Figure 23.4. This could also be used to capture even larger satellites.

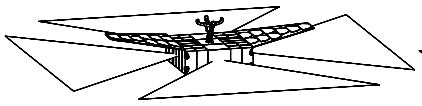

Figure 23.3: Concept 1: Clamp, capture and de-orbit

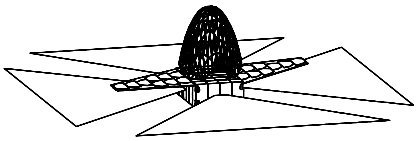

Figure 23.4: Concept 2: Net, capture, and de-orbit

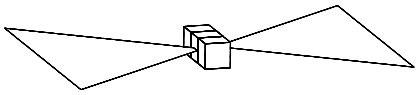

Figure 23.5: Concept 3: Observation satellite

Not needing the heat shield and protection panels means a standard 2 U*3 U structure can be used. Having a significant lower mass results in less required propellant which in turn means a lower mass and costs. In total this would result in a 6 U sized spacecraft.

Finally if capture is not required at all, a reconnaissance satellite would be possible with even less mass and complexity. It would still be able to de-orbit itself after completion of the observation mission using drag sails. This small 1 U*3 U sized reconnaissance concept is shown in Figure 23.5.

An overview of the estimated costs for these variants together with the current design is shown in Table 23.6. Although the development and production of the net based capture would be slightly more expensive it would also be able to generate more revenue as it allows the capture of larger satellites and pieces of space debris. Furthermore, it can be seen that the observation satellite would be by far the cheapest option. At a total mission cost of EUR 310 000 it allows inspection and troubleshooting of a malfunctioning satellite at only a fraction of the original's cost.

Table 23.6: Concepts estimated spacecraft and launch cost

System	Spacecraft cost in thousands [EUR]	Launch cost in thousands [EUR]
0. Delfi-REAL; Clamp, capture and landing	621	800
1. Clamp, capture and de-orbit	220	300
2. Net, capture and de-orbit	280	300
3. Observation	160	150

23.5.2. Potential Buyers

After having examined the current and future state of the nano-satellite market and defined the services that the future product will be able to provide, the potential buyers were identified. The potential buyers for each of the four designs are presented below.

- **Nano-satellite Recovery** - Companies or institutions that carry out projects with large investments, that suffer unexplained failures, will be willing to pay a relatively small cost to protect the economical or educational investment previously made.
- **Capture and de-orbit** - Due to space debris the amount of potential buyers will increase significantly in the future. There will be companies who would want to keep the orbit they are using safe, and minimise the risk of collision and loss of satellites. Similarly, in the future, institutes like National Aeronautics and Space Administration (NASA), ESA or even the United Nations (UN) could be interested in starting or funding an orbit cleaning program
- **Observation satellite** - Possible buyers could be the owners and operators of future satellite projects as described in Section 23.1.2. For instance, SpaceX will be sending thousands of micro-satellites to space for their constellation [59]. It is a project with hundreds of millions of dollars of investment and if one of their initial satellites were to prematurely fail, their investment would be at risk. Likewise, if a technology demonstration satellite fails in orbit, there is scientific and monetary value attached to determining the cause and extent of the failure. If a company is not able to determine why a certain component failed on an expensive satellite on their own, the investment would be at risk. Finally, the military would have interest in the observation of foreign technology in space.

In conclusion, it is possible to classify the potential buyers for the product. These buyers are mostly defined by the largely expanding satellite market which has introduced the space debris and orbit cluttering hazard as well as the

large amount of investment in new projects.

The first class of potential buyers are companies or private entities responsible for nano-satellite missions with large amount of investment. When their satellites suffer unexplained failures that can impact the quality of their product or mission and thus require their system to be returned to Earth. Such potential buyers are Planet Labs and TU Delft. Furthermore, institutions or private entities which require damaging and non-damaging observation of other satellites. Such potential buyers are SpaceX and the military.

Finally, the second class of potential buyers are companies, institution or private entities which will be affected by orbit cluttering and require a de-orbiting service. Such potential buyers are ESA and OneWeb.

24
Sensitivity Analysis

In the sensitivity analysis multiple scenarios which could lead to a mission failure are investigated. It is determined if it is still possible to correct for these changes and whether the mission will still be a success.

24.1. Orbit insertion correction

For the sensitivity analyses it is analysed by how much the insertion orbit of Delfi-REAL can vary without leading to a mission failure. In this section this is discussed.

In Section 13.2.1 the Delta-V budget is discussed. In this budget $16\,\mathrm{m\,s^{-1}}$ is allocated for insertion compensation of 35 km and $10\,\mathrm{m\,s^{-1}}$ for an inclination compensation of 0.2°. Furthermore a margin of 5 % is used, $11\,\mathrm{m\,s^{-1}}$. This margin can, in a worst case scenario, be used for an altitude compensation, an inclination compensation or a combination of these two. If the inaccuracy to high that it would lead to a mission failure, half of the Delta-V for the De-Orbit can be freed to correct the insertion orbit, this amounts to $55\,\mathrm{m\,s^{-1}}$. This would mean that it would take more time to de-orbit, but Delfi-REAL would still return to Earth.

Altogether this would lead to a Delta-V of $92\,\mathrm{m\,s^{-1}}$. If this is used for an altitude correction, the height inaccuracy could be at most 201 km. If it is used for an inclination correction, the maximum deviation can be 0.7°. A combination of these two parameters is also possible to correct for.

24.2. Storm at the landing zone

If a storm at the landing zone occurs during the re-entry, it leads to extra risk in damaging or losing Delfi-C3 and Delfi-REAL. The option to avoid the storm by skipping on the atmosphere and land a certain distance away from the storm is very difficult. There is no actuation and no propulsion to steer Delfi-REAL during re-entry. It is therefore almost impossible to change the trajectory during re-entry. The other problem is that the landing zone is not really big. Which means if there is a storm of for instance 200 km in diameter the complete landing zone is covered. Landing outside the landing zone is dangerous since these areas are populated. To counter these risks, the weather forecast has to be monitored to determine if the conditions to re-enter and land are safe. If it turns out not to be safe, Delfi-REAL could be kept in orbit longer using the propellant margin of 5 %. Therefore, a storm over the landing zone does not directly lead to a mission failure.

24.3. Damaged Delfi-C3

In the case that Delfi-C3 is damaged, by for instance micro meteorites, it could mean that there are extra difficulties in capturing Delfi-C3. If for instance the solar panels are severely damaged or the hinge is blocked from moving, it could mean that it is not possible to capture Delfi-C3. This cannot be solved in space and would mean that Delfi-C3 cannot be brought back with Delfi-REAL.

24.4. Launch expedited

If Delfi-C3 has to be brought back at a shorter notice than Delfi-REAL is designed for, it would mean that the production time has to be shorter and the detailed design has to be done in a short amount of time. This means the cost of the development and production would go up. Since the total cost is now EUR 2 M and the estimated cost was EUR 3.5 M, as can be found in Section 22.1 and from the Budget requirements found in Appendix A, there is space to increase the cost to launch Delfi-REAL earlier.

24.5. Higher spinning rate of Delfi-C3

Delfi-REAL is designed to be able to match Delfi-C3's rotation up to 4° per minute on each axis. This is already higher than the anticipated actual rotation rate. However the simulation software shows it is capable of matching it to 6° per minute. This could be improved even more by further developing the flight controller used.

24.6. Higher power consumption

If Delfi-REAL uses more power during the mission than it was designed for, it could have fatal consequences for the mission. In the Electrical Power System(EPS) there is a Power margin of 8 W. This margin could be used in case some instruments draw more power than normal. Furthermore it could be used when extra instruments have to be turned on when it was not anticipated to be on at that time. If this power of 8 W is not enough to solve the problem some subsystems have to be shut off to save power. One of the subsystems which can be shut off is the Onboard Computer(OBC). It cannot be shut off completely but the data processing can be reduced which lowers the power consumption of the OBC by 5 W. The consequences of reducing the data processing is that less pictures can be processed and less data can be sent to the ground station. However, the mission can still proceed and Delfi-C3 can still be captured and brought back to Earth.

25
Recommendations and Future Development

To ensure mission success, further steps need to be taken to finalise design and development of Delfi-REAL. Recommendations with respect to future design strategies are given in Section 25.1. In Section 25.2 a timeline is suggested for the continuation of the project.

25.1. Recommendations

Due to limited development time, the design of Delfi-REAL is not yet detailed enough for production. In this section, some recommendations are made on what should be done to ensure Delfi-REAL is capable of fulfilling its mission and do so optimally.

Firstly, the Signal Board Computer (SBC) selection was based on a preliminary estimation of processing workload. To ensure that the selected SBC is the correct choice, the SBS selection should be reiterated when its workload it known to a higher accuracy. The high performance needs of the OBC correspond to a high power usage as well. The thermal analysis is recommended to be improved by including high energy point sources like the OBC CPU. Which might require the design of a thermal sink to conduct the heat generated by the chips to be dissipated by the structure.

Secondly, in the design of the power subsystem the bus voltages and switches were not modelled. It is thus recommended to carry out further modelling of the solar array and batteries to ensure no over voltages or over currents will occur during mission phases.

It is also recommended to optimise the rendezvous and approach manoeuvres by designing a new flight controller. The simulation built for the design was a proof of concept simulation. To ensure a smooth and reliable approach a flight controller should be designed and tested.

Re-entry is the most critical and complex mission phase. The conditions during re-entry should be analysed in further detail, especially regarding the loading and thermal conditions. The clamping and restraining mechanism have not been analysed for vibrational and dynamic loads. Once these loads are determined these mechanisms should be further analysed to ensure they will withstand these loads. Furthermore, once the thermal loading from the super heated ionised air around Delfi-REAL is known, the design of the encapsulating mechanism and thermal protection should be reiterated if needed.

Furthermore, once a more detailed representation of the re-entry loads is known, a last iteration in the parachute calculations should be performed. Furthermore, the due to limited resources, is not fully worked out in this report. This option is to discard the heat shield once the satellite has reached subsonic velocity, just before the pilot chute is deployed. This results in a parachute which can be sized for approximately 3 kg less than the current value. In order to finish this design, a deceleration system to ensure a safe landing of the heat shield should be designed as well as a release mechanism.

25.2. Future Development

Besides an approach to finalise design of Delfi-REAL, the development of the system also needs to be planned. Therefore, a chronological timeline of future design and develop stages is depicted in Figure 25.1. In this figure, a clear distinction can be made within the stages. First the design will need to be analysed in a higher level of detail, as mentioned in Section 25.1. After a more detailed analysis of some critical design stages, a final design iteration for all subsystems need to be performed. The brackets which will fit all the components inside the structure, have to be designed. The parachute attachment and deployment has to be developed. Finally, the release mechanism of the heat shield needs to be designed.

After the design is finalised, the software required for the system needs to be written, as well as the acquisition of licences and requirements. After this, the components needed for manufacturing of subsystems and the off-the-shelf parts can be purchased. Next, the assembly and testing stage begins. Here the subsystems first need to be assembled and tested, before they can be integrated into the final product, which also needs to be tested. Finally, Delfi-REAL will be launched and the mission can be executed.

In Figure 25.2 the timeline for future development is shown in a Gantt chart. This also includes the dates all stages are planned to start and how long they will approximately take.

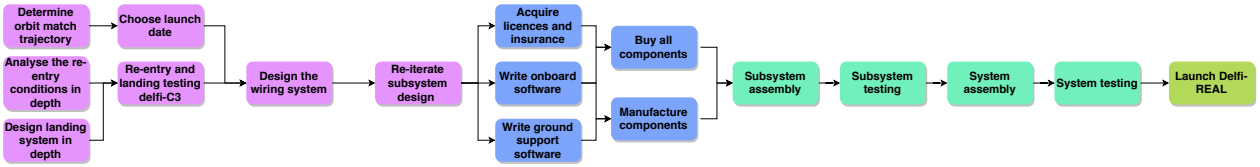

Figure 25.1: Design & development logic

ID	Task Mode	Task Name	Time	Start Date	End Date
1		**Design refinement**	**40 days?**	**Mon 4-2-19**	**Fri 29-3-19**
2		Analyse re-entry conditions	15 days	Mon 4-2-19	Fri 22-2-19
3		Detailed landing system design	15 days	Mon 25-2-19	Fri 15-3-19
4		Choose launh date	5 days	Mon 25-2-19	Fri 1-3-19
5		Trajectory refinement	10 days?	Mon 18-3-19	Fri 29-3-19
6		**Perform subsystem tests**	**45 days?**	**Mon 1-4-19**	**Fri 31-5-19**
7		Test re-entry system	22 days	Mon 1-4-19	Tue 30-4-19
8		Test parachute system	23 days	Wed 1-5-19	Fri 31-5-19
9		**Test deployment systems**	**45 days?**	**Mon 1-4-19**	**Fri 31-5-19**
10		Test antenna deployment	11 days?	Mon 1-4-19	Mon 15-4-19
11		Test solar panel deployment	11 days?	Mon 15-4-19	Mon 29-4-19
12		Test payload bay door deployment	11 days?	Mon 29-4-19	Mon 13-5-19
13		Test clamping system	15 days?	Mon 13-5-19	Fri 31-5-19
14		**Refine system assembly**	**10 days?**	**Mon 3-6-19**	**Fri 14-6-19**
15		Determine wiring placement	3 days	Mon 3-6-19	Wed 5-6-19
16		refine small part budget	2 days	Thu 6-6-19	Fri 7-6-19
17		Make more accurate 3D model	5 days	Mon 10-6-19	Fri 14-6-19
18		Acquire permits and insurance	105 days	Mon 4-2-19	Fri 28-6-19
19		**Order parts**	**36 days?**	**Fri 14-6-19**	**Fri 2-8-19**
20		**Buy custom components**	**36 days?**	**Fri 14-6-19**	**Fri 2-8-19**
21		Deliver high detail part drawings	11 days	Fri 14-6-19	Fri 28-6-19
22		Assemble costum parts	25 days	Mon 1-7-19	Fri 2-8-19
23		Buy COTS components	36 days	Fri 14-6-19	Fri 2-8-19
24		**Perform system assembly**	**101 days?**	**Fri 2-8-19**	**Fri 20-12-19**
25		Put all bus subsystems in place	21 days	Fri 2-8-19	Fri 30-8-19
26		Put clamp in place	20 days	Mon 2-9-19	Fri 27-9-19
27		Attach payload bay doors	25 days	Mon 30-9-19	Fri 1-11-19
28		Attach heat shield	35 days	Mon 4-11-19	Fri 20-12-19
29		**Perform system testing**	**105 days**	**Mon 6-1-20**	**Fri 29-5-20**
30		Perform re-entry heat test	20 days	Mon 6-1-20	Fri 31-1-20
31		Perform vibration test	10 days	Mon 3-2-20	Fri 14-2-20
32		Perform radiation test	20 days	Mon 17-2-20	Fri 13-3-20
33		test communication system	10 days	Mon 16-3-20	Fri 27-3-20
34		Test integrated parachute deployment	15 days	Mon 30-3-20	Fri 17-4-20
35		Test camera detection system	15 days	Mon 20-4-20	Fri 8-5-20
36		Perform 0g deployment test	15 days	Mon 11-5-20	Fri 29-5-20
37		**Launch Delfi-REAL**	**30 days?**	**Mon 1-6-20**	**Fri 10-7-20**
38		Rollout of Delfi-REAL	5 days	Mon 1-6-20	Fri 5-6-20
39		Transport to launch site	16 days	Mon 8-6-20	Sat 27-6-20
40		Insert Delfi-REAL into the launcher	5 days	Mon 29-6-20	Fri 3-7-20
41		Launch	5 days	Mon 6-7-20	Fri 10-7-20

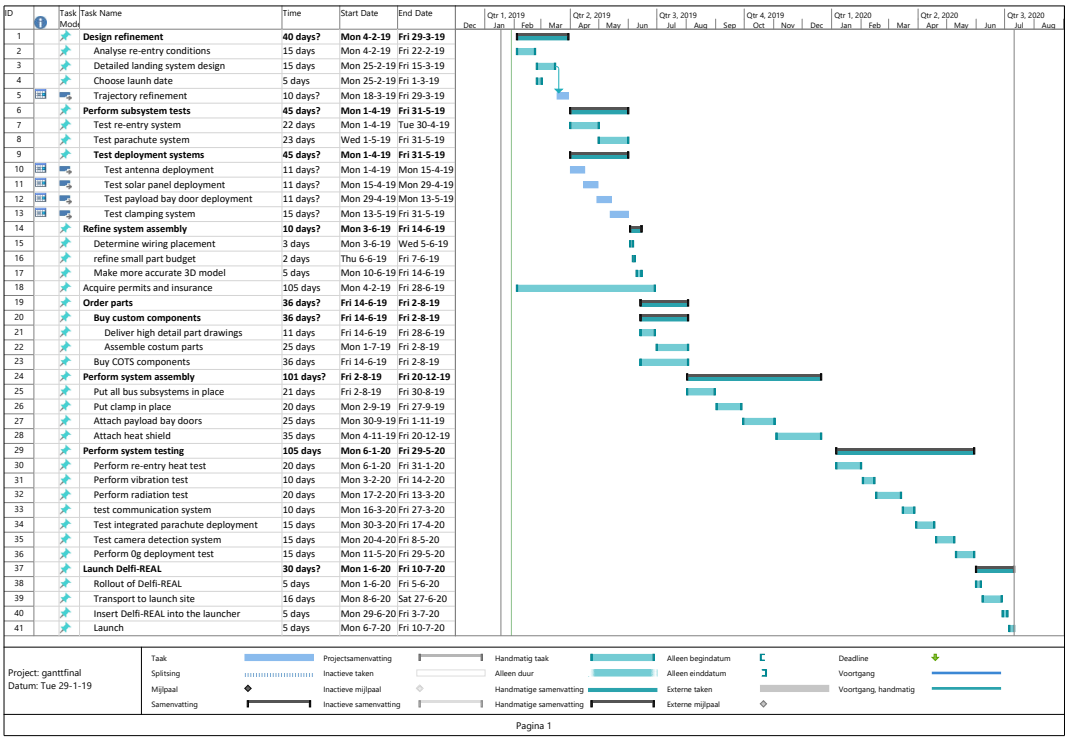

Figure 25.2: Gantt chart for future development

26
Conclusion

The final design of Delfi-REAL is capable of doing reconnaissance, capture of Delfi-C3 and re-entry with successful recovery. It is possible to build a system that can achieve the mission goal. This will be done by means of a satellite which will be able to manoeuvre towards Delfi-C3 from a starting orbit. After which, the damage of Delfi-C3 will be assessed, and it will be clamped. Finally, Delfi-REAL will reduce its velocity until the point that it has a sufficient re-entry angle, which ensures that Delfi-C3 will be recovered without causing damage. In this way, the deaf radio receiver and the increase in current consumption of the On-Board Computer can be analysed. Furthermore, the experimental Thin Film Solar Cells used will be recovered, which will make it possible to research the ablation on the cells. The research done on Delfi-C3, and specifically the solar cells, will increase the understanding of degradation in space. This in combination with the development of both hardware and software of Delfi-REAL, will ensure that the knowledge gain compensates for the mission cost. The mission will cost approximately EUR 2 M of which, EUR 600 k for the the spacecraft, EUR 800 k for the launch, and EUR 550 k operational cost.

The satellite itself consists mostly of commercial off-the-shelf components, which will ensure the system will have a high reliability of success. Exception to this condition are the heat shield and the clamping system which are specific parts of Delfi-REAL which are going to be custom-designed to perform the mission successfully. In order to increase reliability, the heat shield has been designed with a safety factor of five for the heat loading, and the clamp has been designed to be as simple as possible. Furthermore, the material used for the heat shield is off-the-shelf available. The overarching design philosophy used for Delfi-REAL is to guarantee mission success.

Delfi-REAL fulfills all the stakeholder requirements to ensure proper functioning during every mission phase. Furthermore, it possesses low-mass, has a low-cost design with good reliability and low complexity. Finally, Delfi-REAL can be used as a stepping stone for sustainable projects in space, a market which is likely to increase in size over the years. Despite being focused on returning Delfi-C3 back to Earth, Delfi-REAL's functions could be used to perform reconnaissance, capture and re-entry separately. These variants could be adapted to fulfil the demand of these growing market sectors.

A

Subsystem Requirements

The compliance matrix is displayed in the following pages. ✓ indicates a requirement that is met. ~ indicates a requirement for which it cannot be stated if it is met or not. There is one requirement with a ✗; this requirement was too stringent but does not break the subsystem. Further explanation is given in Chapter 9 on page 41.

	Requirement	Actual Value	Meets Requirement
Compatibility			
RQ-COM-01	The system shall be compatible with nano-satellite standards.	-	✓
RQ-COM-01.02	The system shall be launched from a nano-satellite cassette.	-	✓
RQ-COM-01.03	The system shall be able to withstand the load as specified in the launcher manual.	-	✓
RQ-COM-01.04	The system shall operate on a standard nano-satellite I^2C bus.	-	✓
RQ-COM-02	The system shall be compatible with nano-satellite procedures.	-	✓
RQ-COM-02.01	The system shall be launched as a secondary payload.	-	✓
RQ-COM-03	The system shall be able to withstand the environmental conditions for the mission lifetime.	-	✓
Budget			
RQ-BUD-01	The system shall not exceed a total cost of EUR 2 M.	EUR 621 k	✓
RQ-BUD-02	The capture and re-entry system shall not exceed a total cost of EUR 300 k.	EUR 227 k	✓
RQ-BUD-03	The system launch cost shall not exceed EUR 800 k.	EUR 800 k	✓
RQ-BUD-04	The system shall have a mass of at most 20 kg.	14.7 kg	✓
RQ-BUD-05	The system shall have an operation cost which is comparable to that of a nano-satellite.	EUR 550 k	✓
RQ-BUD-06	The system shall provide its own power for the duration of the mission.	-	✓
RQ-BUD-07	The system shall be ready for operation before the launch date.	Launch Date Mid 2020	✓
RQ-BUD-07.01	The system design shall be finished by December 2019.	-	✓
RQ-BUD-07.02	Production of the system shall be finished 6 months before the launch date.	-	✓

	Requirement	Actual Value	Meets Requirement
ADCS			
RQ-ADCS-01	The ADCS shall be able to determine the attitude of Delfi-REAL.	-	✓
RQ-ADCS-01.01	The ADCS shall have a determination accuracy of 0.1° during daylight.	0.1°	✓
RQ-ADCS-01.02	The ADCS shall have a determination accuracy of 1° during eclipse.	1°	✓
RQ-ADCS-01.03	The ADCS shall have a determination range in all directions	all directions	✓
RQ-ADCS-02	The ADCS shall be able to control the attitude of Delfi-REAL	-	✓
RQ-ADCS-02.01	The ADCS shall have a control accuracy of 0.1°.	0.1°	✓
RQ-ADCS-02.02	The ADCS shall have a control range in all directions.	all directions	✓
RQ-ADCS-03	The ADCS shall have a mass no larger than 1.5 kg.	1.3 kg	✓
RQ-ADCS-04	The ADCS shall cost less than EUR 189 k.	EUR 76 k	✓
RQ-ADCS-05	The ADCS shall have a volume no larger than 1.2 U.	0.79 U	✓
RQ-ADCS-06	The ADCS shall have a maximum power consumption of less than 12 W.	11.8 W	✓
Propulsion			
RQ-PRO-01	The propulsion system shall provide all required Delta-V and thrust as needed for insertion inaccuracy compensation, rendezvous, reconnaissance, capture and de-orbit.	-	✓
RQ-PRO-01.01	The propulsion system shall provide a minimum total Delta-V of 225 $m\,s^{-1}$.	236 $m\,s^{-1}$	✓
RQ-PRO-01.02	The propulsion system shall have a minimal thrust of 0.1 N to complete the mission in the required mission time.	Max 0.3 N	✓
RQ-PRO-01.03	The propulsion system shall have a duty cycle of at least 10 000 cycles.	> 20000 cycles	✓
RQ-PRO-01.04	The propulsion system shall have a minimum impulse bit of at least 0.012 Ns.	0.005 N s	✓
RQ-PRO-01.05	The propulsion system shall have a minimum impulse frequency of 10 Hz.	20 Hz	✓
RQ-PRO-01.06	The propulsion system shall have a 3-axis thruster system to control translational movement.	9 Total Thrusters 4 Min. per axis	✓
RQ-PRO-02.01	A failure of one component of the propulsion system shall not cause failure of the entire system.	Redundant Components	✓
RQ-PRO-02.02	A failure of one component of the propulsion system shall not cause failure of another component.	Redundant Components	✓
RQ-PRO-03	The propulsion system mass shall not exceed 2.6 kg.	2.06 kg	✓
RQ-PRO-04	The propulsion system shall have a nominal power usage lower or equal to 19 W.	10.2 W	✓
RQ-PRO-05	The propulsion system shall have a total volume lower or equal to 1.7 U.	1.2 U	✓

	Requirement	Actual Value	Meets Requirement
Power			
RQ-EPS-01	The EPS shall distribute power for all spacecraft components, their duty cycles and special operating modes.	-	✓
RQ-EPS-02	The EPS shall generate power via solar arrays.	-	✓
RQ-EPS-02.01	The solar arrays shall use a maximum area of 1328 cm^2.	1328 cm^2	✓
RQ-EPS-02.02	Solar array configuration shall be body-mounted.	-	✓
RQ-EPS-02.03	The peak power shall be 50 W minimum.	77.02 W	✓
RQ-EPS-03	The system shall use at least two batteries for energy storage and sufficient redundancy.	-	✓
RQ-EPS-03.01	The batteries shall provide a stable voltage for all operating conditions during the mission life.	-	✓
RQ-EPS-03.02	The number of duty cycles (discharge and charge cycles) shall be 5510 times per year.	5510	✓
RQ-EPS-03.03	The secondary battery shall have a maximal depth-of-discharge of 25 %.	20 %	✓
RQ-EPS-04	The EPS shall distribute power within the specified voltage band to all bus and payload equipment.	-	✓
RQ-EPS-04.01	Power distribution shall be provided to busses of different voltages using direct current.	3.3 V,5 V and 12 V	✓
Capture			
RQ-CES-01	The clamp shall exert a minimal force on the side of Delfi-C3 of 1 N.	3.2 N maximum	✓
RQ-CES-02	The clamp shall be able to extend itself in the direction of Delfi-C3 by a minimum of 15 cm.	15.2 cm	✓
RQ-CES-03	The clamp shall be locked into it's lowest position after capturing Delfi-C3.	-	✓
RQ-CES-06	The clamp shall exert a minimal force on the solar panels of Delfi-C3 of 2.26 N at 45 mm from the hinge.	3.2 N maximum	✓
RQ-CES-07	The clamp arms shall have a length in folded position of maximum 7.5 cm.	7.4 cm	✓
RQ-CES-08	The clamp shall have a maximum height in folded position of 10.6 cm.	10.5 cm	✓
RQ-CES-08-01	The clamp extension base plus arms shall be lower than 4.6 cm in folded position.	4.5 cm	✓
RQ-CES-08-02	The extendable arm of the clamp shall have a maximum height of 6 cm.	6 cm	✓
RQ-CES-09	The clamp shall not use more than 10 W during operation.	5 W	✓
RQ-CES-10	The clamp shall be locked into it's lowest position during the mission phases before capture.	-	✓
RQ-CES-11	The clamp shall be less than 8.9 cm wide.	8.8 cm	✓
RQ-CES-12	The clamp shall be less than 8.9 cm long.	8.8 cm	✓
RQ-CES-13	The extending part of the clamp shall not be larger than 8 cm × 8 cm.	7.8 cm × 7.5 cm	✓

	Requirement	Actual Value	Meets Requirement
Thermal			
RQ-THER-01	The system shall only use passive thermal control.	-	✓
RQ-THER-02	The system main body shall not exceed an internal temperature of 50 °C.	24.4 °C	✓
RQ-THER-03	The system main body shall not have an internal temperature of less then 0 °C.	11.1 °C	✓
RQ-THER-04	The solar cells shall not exceed an internal temperature of 150 °C.	55.0 °C	✓
RQ-THER-05	The solar cells shall not have an internal temperature of less then −120 °C.	−16.4 °C	✓
Detection			
RQ-DTCT-01	The system shall not fully eclipse Delfi-C3.	-	✓
RQ-DTCT-02	The system shall be able detect Delfi-C3 visually using cameras when closer than 200 m.	-	✓
RQ-DTCT-03	The system shall be able to detect Delfi-C3 still when eclipsed.	-	✓
RQ-DTCT-04	The system shall do docking only when Delfi-C3 is illuminated to allow high accuracy visual position detection.	-	✓
RQ-DTCT-05	The system shall match a 3d model to the picture of Delfi-C3 to determine both distance and rotation per camera.	-	✓
RQ-DTCT-06	The system shall use the combination of the individual camera measurements and known camera position to triangulate position with increased accuracy.	-	✓
RQ-DTCT-07	The system shall interpolate position measurements overtime to create an iteratively refined position prediction.	-	✓
RQ-DTCT-08	The OBC needs to perform real-time analysis and object detection using up to 4 4k 360° camera feeds with at least 20 fps.	20 fps	✓
RQ-DTCT-09	The capture procedure shall only be execute while Delfi-C3 is illuminated by the Sun.	-	✓
TT&C			
RQ-TTC-01	The TT&C subsystem shall have an antenna to transmit payload data to amateur ground stations and the Delft University of Technology (TU Delft) ground station.	-	✓
RQ-TTC-01.01	The TT&C subsystem shall be able to transmit payload data with a minimum bit rate of 3 Mbit s^{-1}.	3.4 Mbit s^{-1}	✓
RQ-TTC-01.02	The TT&C subsystem shall have a bit error rate of maximum 8×10^{-9} during the transmission of payload data.	8.55×10^{-9}	✓
RQ-TTC-02	The TT&C subsystem shall have an antenna to transmit health and status telemetry to the TU Delft ground station.	-	✓
RQ-TTC-02.01	The TT&C subsystem shall be able to transmit health and status telemetry with a minimum bit rate of 80 kbit s^{-1}.	3.4 Mbit s^{-1}	✓
RQ-TTC-02.02	The TT&C subsystem shall have a bit error rate of maximum 10×10^{-8} during the transmission of health and status telemetry.	8.55×10^{-9}	✓
RQ-TTC-03	The TT&C subsystem shall have an antenna to receive telecommands from the TU Delft ground station.	-	✓
RQ-TTC-03.01	The TT&C subsystem shall be able to receive telecommands with a minimum bit rate of 16 kbit s^{-1}.	9.6 kbit s^{-1}	✗
RQ-TTC-03.02	The TT&C subsystem shall have a bit error rate of maximum 10×10^{-8} while receiving telecommands.	-	✓
RQ-TTC-04	The TT&C subsystem shall transmit a signal after landing back on Earth.	-	✓

	Requirement	Actual Value	Meets Requirement
Command			
RQ-CMS-01	Commands shall be encrypted during uplink.	-	✓
RQ-CMS-02	The system shall be commandable to start recording a video.	-	✓
RQ-CMS-03	The OBC shall be able to encode video in real-time at 20 fps.	20 fps	✓
RQ-CMS-04	The docking manoeuvre shall be recorded on video.	-	
RQ-CMS-05	The compression encoding and bit-rate settings shall be changeable from the ground station using commands.	-	✓
RQ-CMS-06	Each video frame shall have a time stamp associated with it.	-	✓
RQ-CMS-08	Any electronic devices currently not needed shall not be powered.	-	✓
RQ-CMS-09	Over current protection shall be added to protect critical hardware from exceeding their design voltage.	-	✓
RQ-CMS-10	The OBC shall have a memory size of 128 GB.	128 GB	✓
Structures			
RQ-STR-01	The structure shall have a mass lower or equal to 4.5 kg.	4.4 kg	✓
RQ-STR-02	The structure shall withstand launch loads.	-	✓
RQ-STR-02.01	The structure shall withstand 6.2 g steady longitudinal acceleration.	15 g	✓
RQ-STR-02.02	The structure shall withstand 4 g dynamic longitudinal acceleration.	-	~
RQ-STR-02.03	The structure shall withstand 0.6 g steady lateral acceleration.	1.4 g	✓
RQ-STR-02.04	The structure shall withstand 0.5 g dynamic lateral acceleration.	-	~
RQ-STR-02.05	The structure shall withstand the launcher-specified vibration test.	-	~
RQ-STR-03	The spacecraft shall comply with the separation mechanism.	-	~
RQ-STR-04	The structure shall comply with the launcher limitations.	-	✓
RQ-STR-04.02	The structure shall not exceed 12 U in size.	9 U	✓
RQ-STR-05	The structure shall not interfere with functioning of other subsystems.	-	✓
RQ-STR-05.02	The structure shall not interfere with functioning of other subsystems.	-	✓
RQ-STR-05.03	The shell walls shall remained closed, when carrying Delfi-C3, up to 10 g in acceleration.	-	✓
RQ-STR-05.04	The packaging of components will not interfere with their performance.	-	✓
RQ-STR-06	The structure shall withstand re-entry loads.	-	✓
RQ-STR-06.01	The structure shall withstand 10 g longitudinal deceleration.	15 g	✓
RQ-STR-07	The structure shall keep Delfi-C3 intact when landing.	-	✓
RQ-STR-08	The shell walls deployment mechanism shall be able to open, close and restrain Delfi-C3.	-	✓
RQ-STR-08.01	The shell wall mechanism shall allow the panels to fold flat on top of the satellite.	-	✓
RQ-STR-08.03	The clamping mechanism shall not use power to mantain restrainment of Delfi-C3.	-	✓
RQ-STR-08.04	The shell walls will not damage the TFSC during closing and clamping.	-	✓
RQ-STR-08.05	The shell walls should not be able to open during re-entry.	-	✓
RQ-STR-08.06	The payload bay doors shall be able to be rotate at 3.75 °min^{-1}	3.75 °min^{-1}	✓

	Requirement	Actual Value	Meets Requirement
Re-entry			
RQ-REN-05	The deceleration during re-entry shall not exceed 15 g.	8.5 g	✓
RQ-REN-06	The system shall have a thermal protection system.	-	✓
RQ-REN-07	The thermal protection system shall be able to protect the system from the total heat load experienced during re-entry.	-	✓
RQ-REN-09	The parachute shall be deployed when the system's velocity is subsonic.	Mach 0.3	✓
RQ-REN-10	The impact acceleration of the system shall not exceed 15 g.	13.6 g	✓
RQ-REN-11	The impact velocity of the system shall not exceed 7 $m\,s^{-1}$	6.7 $m\,s^{-1}$	✓
RQ-REN-12	The leeward side of the thermal protection system shall have a maximum temperature of 80 °C.	80 °C	✓
RQ-REN-13	The thermal protection system mass shall not exceed 3 kg.	3 kg	✓
Reliability			
RQ-SAR-01	The system shall not damage Delfi-C3 in case of a malfunction or abortion of the system.	-	✓
RQ-SAR-01.01	The system shall have an abort procedure.	-	✓
RQ-SAR-01.02	The system shall have a malfunction safe mode procedure.	-	✓
RQ-SAR-02	The system shall not endanger people.	-	✓
RQ-SAR-02.01	The system shall not contain highly radioactive materials.	-	✓
RQ-SAR-02.04	The system shall burn up in the atmosphere during mission abort.	-	✓
RQ-SAR-03	The system shall not endanger property.	-	✓
RQ-SAR-03.01	The system shall not damage the launcher.	-	✓
RQ-SAR-03.02	The system shall not damage the launch mechanism.	-	✓
RQ-SAR-03.04	The system shall not land within 90 km of a built up area.	90 km	✓
Sustainability			
RQ-SUS-01	The system shall not cause space debris.	-	✓
RQ-SUS-01.01	The system shall not leave remains of Delfi-C3 in orbit that will not burn up in the atmosphere within 10 years.	-	✓
RQ-SUS-01.02	The system shall not leave remains of itself in orbit that will not burn up in the atmosphere within 10 years.	-	✓
RQ-SUS-01.03	The system shall initiate a de-orbit procedure in case of failure.	-	✓
RQ-SUS-01.04	In case of failure the system shall not leave parts in orbit that are smaller than 10 cm in diameter.	-	✓

Bibliography

[1] Bosman, B., Fricano, T., Kraijema, J., Mikirtumov, V., Sachs, M., Schild, M., Schutten, H., Segeren, M., Villé, T., de Vries, J., and de Vries, R. J., "The Return of the Queen - Midterm Report," Tech. rep., Delft University of Technology, 2018.

[2] "Sale Price Drives Potential Effects on DOD and Commercial Launch Providers," GAO, 2017.

[3] Bosman, B., Fricano, T., Kraijema, J., Mikirtumov, V., Sachs, M., Schild, M., Schutten, H., Segeren, M., Villé, T., de Vries, J., and de Vries, R. J., "The Return of the Queen - Baseline Report," Tech. rep., TU Delft, 2018.

[4] "Space Technology Game Changing Development ADEPT SR-1 Flight Experiment," NASA Ames research center, 2018.

[5] SpaceWorks, "Nano/Microsatellite Market Forecast," Tech. rep., Space Works, 2017.

[6] ISRO, *PSLV User's Manual*, issue 3 ed., May 1996.

[7] Wertz, J. R., and Larson, W. J., *Space Mission Analysis and Design*, Microcosm, Hawthorne, CA, 2010.

[8] Defense, A., and Space, *ARIANE 5 User's Manual*, issue 4, revision 0 ed., November 2004.

[9] KU Leuven, D. o. M. E., "KU Leuven Star Tracker," Tech. rep., KU Leuven, Department of Mechanical Engineering, 2016.

[10] Ltd., N. S. P., "Sun Sensor NFSS - 411," Tech. rep., NewSpace Systems (Pty) Ltd., 2007.

[11] B.V., I. I. S. I. S., "Magnetorquer Board (iMTQ)," Tech. rep., ISIS - Innovative Solutions In Space B.V., 2013.

[12] CubeSpace, "CubeWheel - Reaction/Momentum Wheel," Tech. rep., CubeSpace, 2008.

[13] Speretta, S., "Satellite Communication Systems," Technical University of Delft, 2018.

[14] ISIS, *Ground Station Datasheet*, issue 2, revision 2 ed., 2016.

[15] Cakaj, S., Kamo, B., Kolici, V., and Shurdi, O., "The Range and Horizon Plane Simulation for Ground Stations of Low Earth Orbiting (LEO) Satellites," Tech. rep., Polytechnic University of Tirana, 2011.

[16] Daeri, A. M., Elfituri, M., and Zerea, A. R., "Quadrature Phase Shift Keying and Offset Quadrature Phase Shift Keying BER Performance Comparison," Tech. rep., Zawia University, 2016.

[17] Wertz, J. R., and Larson, W. J., *Space Mission Analysis and Design*, Microcosm, Torrance, CA, 1995.

[18] Pierre, T., "Design and Implementation of On-board Electrical Power Supply of Student Nanosatellite OUFTI-1 of University of Liège." Tech. rep., Applied Science Faculty of the University of Liège, 2008.

[19] Nimal, N., Regina, L., and Hugh, C., "Characterization of Lithium-Polymer batteries for CubeSat applications," Tech. rep., Acta Astronautica, 2011.

[20] Robert, B., "Distributed Electrical Power System in Cubesat Applications," Tech. rep., Utah State University, 2011.

[21] Valdez, J., and Becker, J., "Understanding the I2C Bus," Tech. rep., Texas Instruments, 2015.

[22] Graça, R., "Low Earth Orbit Nano Satellite Electrical Power System Design," Tech. rep., Instituto Superior Técnico, 2014.

[23] ecaps, B., "Flight-Proven High Performance Green Propulsion," , 2017.

[24] Sheldalh, "Product Bullitin ITO," , 2018.

[25] NASA, "Spacecraft Thermal Control Coatings References," , 2005.

[26] SpaceX, *Falcon 9 Launch Vehicle: Payload User's Guide*, revision 2 ed., October 2015.

[27] Roscosmos, *SOYUZ User's Manual*, issue 2 ed., June 1997.

[28] Roscosmos, *SOYUZ User's Manual*, issue 3 ed., April 2001.

[29] NASA, "State of the Art of Small Spacecraft Technology," Tech. rep., NASA, 2019.

[30] Fortescure, P., Swinerd, G., and Stark, J., *Space Systems Engineering*, John Wiley And Sons Ltd, 2011.

[31] Boning, G., Hiemstra, J., Sears, T., and Zee, R., "The CanX-7 Drag Sail demonstration Mission," UTIAS, 2013.

[32] Georgevic, R. M., "The Solar Radiation Pressure Forces and Torques Model," NASA JPL, 1971.

[33] Johnson, S. M., "Thermal Protection Materials and Systems: Past, Present, and Future," Entry Systems and Technology Division NASA Ames Research Center, 2013.

[34] Pulci, G., Tirillò, J., Marra, F., Fossati, F., Bartuli, C., and Valente, T., "Carbon–phenolic ablative materials for re-entry space vehicles: Manufacturing and properties," *Composites: Part A*, Vol. 41, 2010, p. 1483–1490.

doi:10.1016/j.compositesa.2010.06.010.

[35] Sikharulidze, Y. G., Moraes Jr., P., and Korchagin, A. N., "Analysis of Accuracy at Ballistic Re-Entry in the Earth Atmosphere," Tech. rep., Centro Técnico Aeroespaciale, 1998.

[36] Foreest van, A., Gülhan, A., Esser, B., Sippel, M., Ambrosius, B. A. C., and Sudmeijer, K., "Transpiration Cooling Using Liquid Water," *AIAA Thermophysics Conference*, Vol. 39, 2007, pp. 1–14. doi:10.2514/6.2007-4034.

[37] Hillje, E. R., "Entry Flight Aerodynamics form Apollo Mission AS-202," Tech. rep., NASA Manned Spacecraft Center, 1967.

[38] International Civil Aviation Organization, *Manual of the ICAO Standard Atmosphere*, 3rd ed., January 1993.

[39] Pepermans, L., Rozemeijer, M., Gurumoorthy, R., Menting, E., Suard, N., Khurana, S., Britting, T., and Serman, M., "Flight Simulations of the Stratos III Parachute Recovery System," Tech. rep., Delft Aerospace Rocket Engineering, 2018.

[40] Ley, W., Wittmann, K., and Hallmann, W., *Handbook of Space Technology*, Wiley, 2009.

[41] Hong, C., Han, J., Zhang, X., David, H., Li, W., Chen, Y., and Du, S., "Novel phenolic impregnated 3-D Fine-woven pierced carbon fabric composites: Microstructure and ablation behavior," *Composites: Part B*, Vol. 43, 2011, pp. 2389–2394. doi:10.1016/j.compositesb.2011.12.001.

[42] Knacke, T. W., *Parachute Recovery Systems Design Manual*, Para Publishing, Santa Barbara, CA, 1992.

[43] Deweese, J., and Schultz, L., "Recovery Systems Design Guide," Tech. rep., US Department of Commerce, 1978.

[44] NASA, "Orion's Parachute System," Tech. rep., NASA, 2017.

[45] Farooq, U., and Myler, P., "Efficient Determination of Mechanical Properties of Carbon Fibre-Reinforced Laminated Composite Panels," Tech. rep., University of Bolton, 2017.

[46] Petrescu, I., Mohora, C., and Ispas, C., "The Determination of Young Modulus for CFRP Using Three Point Bending Tests at Different Span Lengths," Tech. rep., University Politehnica of Budapest, 2013.

[47] Ephraim, M. E., and Adetiloye, A., "Mechanical Properties of Glass Fiber Reinforced Polymer Basen on Resin from Recycled Plastic," Tech. rep., Rivers State University of Science and Technology, 2015.

[48] Wilson, K., "Space Sustainability, a Practical Guide," Tech. rep., Secure World Foundation, 2014.

[49] Hamann, R. J., and van Tooren, M. J. L., *Systems Engineering & Technical Management Techniques Part I*, Delft University of Technology, 2006.

[50] Hamann, R. J., and van Tooren, M. J. L., *Systems engineering & Technical Management Techniques Part III*, Delft University of Technology, 2006.

[51] SpaceWorks, "Nano/Microsatellite Market Forecast," Tech. rep., Space Works, 2018.

[52] Smith, S., "GE Healthcare to Connect 500,000 Imaging Machines with Announcement of GE Health Cloud and Apps," , nov 2015.

[53] Andrews, J., Watry, K., and Brown, K., "Nanosat Deorbit and Recovery system to enable new missions," Andrews Space, 2011.

[54] Sakraker, I., Umit, E., Scholz, T., Testani, P., Baillet, G., and Van der Haegen, V., "QARMAN: An atmospheric entry experiment on cubesat platform," Von Karman Institute for Fluid Dynamics, 2015.

[55] Richard, M., Kronig, L., Belloni, F., Rossi, S., Gass, V., Paccolat, C., Thiran, J., Araomi, S., Gavrilovich, I., and Shea, H., "Uncooperative Rendezvous and Docking for MicroSats," Swiss Federal Institute of Technology, 2013.

[56] Bonnal, C., "Active Debris Removal: current status of activities in CNES," CNES, 2013.

[57] Crisp, N., Smith, K., and Hollingsworth, P., "Small satellite launch to LEO: a review of current and future launch systems," , 2014.

[58] Airbus, "Interim IFRS Consolidated Financial Information," Tech. rep., Airbus SE, 2017.

[59] Dortch, M. H., "FCC-18-38A1," , 2018.